UNIVERSITÀ DEGLI STUDI DI TRIESTE

XXVIII CICLO DEL DOTTORATO DI RICERCA IN SCIENZE E TECNOLOGIE CHIMICHE E FARMACEUTICHE

TOWARDS NEW PHOTODYNAMIC THERAPY AGENTS: SYNTHESIS, BIOLOGICAL EVALUATION AND TARGETING TO TUMOR CELLS

Settore scientifico-disciplinare: **CHIM/08**

DOTTORANDA
GIULIANA MION

COORDINATORE
PROF. MAURO STENER

SUPERVISORE DI TESI
Dr. TERESA GIANFERRARA

ANNO ACCADEMICO 2014 / 2015

For the people who survived to cancer,

for those that did not

and for the people that are still fighting cancer.

RIASSUNTO

In questa tesi di dottorato sono riportati la sintesi e lo studio della fototossicità e dell'interazione con il DNA di due nuove porfirine e dei corrispondenti renio(I) coniugati. Inoltre è riportato anche uno studio di targeting di cellule tumorali.

La tesi è divisa in due sessioni. Nella prima è descritta la sintesi di due nuove porfirine solubili in acqua: una porfirina neutra e simmetrica e una porfirina carica e asimmetrica in cui, rispettivamente, uno o quattro chelanti [1,4,7]-triazaciclononano (TACN) sono legati al macrociclo attraverso uno o quattro linker idrofobici. Sono inoltre descritti anche i corrispondenti renio(I) coniugati. Il metallo renio(I) è stato inserito nella periferia del macrociclo sia per ottenere una molecola con un possibile effetto terapeutico che con una funzione diagnostica. Infatti, grazie alle simili proprietà del renio e del ^{99m}Tc radioattivo, i coniugati radioattivi del ^{99m}Tc(I) possono essere sintetizzati a partire dai corrispondenti Re(I) coniugati. I composti sintetizzati sono stati valutati come fotosensibilizzatori (PS) per la terapia fotodinamica (PDT). Gli studi in vitro di foto-tossicità sono stati eseguiti sulle cellule HeLa (cellule del carcinoma della cervice uterina), H460M2 (cellule del carcinoma polmonare a non-piccole cellule) e HBL-100 (cellule epiteliali non tumorali). Tre di questi composti non si sono dimostrati tossici al buio fino a 100 µM e, in seguito alla coordinazione del Re(I), è stato osservato un aumento della fototossicità solo per la porfirina carica e simmetrica. La localizzazione cellulare dei composti è stata studiata sulle cellule HeLa usando la microscopia a fluorescenza. Nonostante la loro scarsa localizzazione nucleare, i composti sono stati studiati per valutarne la capacità di legare il DNA, sia quadruplex che duplex, e il risultato di questi studi ha dimostrato una significativa selettività delle porfirine asimmetriche per il G-quadruplex.

Nella seconda parte è descritto uno studio preliminare di targeting di una porfirina carica e asimmetrica sulle cellule tumorali. É noto infatti che l'accumulo delle porfirine nel tessuto tumorale è preferenziale ma non selettivo. L'aumento della selettività del fotosensibilizzatore può essere migliorata attraverso l'uso di peptidi. L'idea del progetto nasce dalla volontà di sintetizzare una molecola che possa essere un fotosensibilizzatore in PDT, che possa trasportare nel tessuto tumorale il Re(I) e che possa, grazie alla presenza del peptide, accumularsi in un specifico tessuto tumorale. Per questo è stata sintetizzata una molecola contenente una porfirina asimmetrica

solubile in acqua, il chelante TACN e la bombesina BN[7-14] come peptide, allo scopo di aumentare la sua selettività per il tumore alla prostata. La sintesi è stata svolta sia in soluzione sia in fase solida usando diversi approcci sintetici. Durante la sintesi multistadio, sono stati riscontrati alcuni problemi inerenti al legame con la porfirina. Per questo motivo solo una piccola quantità del composto finale è stata ottenuta e il corrispondente Re(I) coniugato non è stato sintetizzato. Infine, si è provato a sostituire la porfirina con un fullerene[60], essendo nota anche in questo caso la capacitá di agire come fotosensibilizzatore. Il corrispondente derivato contenente il fullerene, il peptide BN[7-14] e il chelante TACN è stato perciò sintetizzato. Così come nel caso precedente, la bassa resa e i problemi di purificazione non hanno consentito la sintesi del corrispondente Re(I) coniugato.

I risultati di questa tesi di dottorato mostrano che una porfirina neutra e simmetrica e una porfirina carica e asimmetrica possono coordinare il frammento metallico *fac*-$\{Re(CO)_3\}^+$ in buone rese. Considerando i risultati biologici, c'è quindi la possibilità di ottenere il corrispondente ^{99m}Tc coniugato. Inoltre sono state sintetizzate una nuova porfirina e un nuovo fullerene entrambi leganti una peptide e un chelante. Per ovviare ai problemi riscontrati, sarà però necessario sviluppare una nuova strategia sintetica al fine di unire in una singola molecola una porfirina asimmetrica, un frammento di Re(I) ed il peptide BN[7-14] per il targeting del tumore alla prostata.

ABSTRACT

This PhD thesis reports the synthesis, the phototoxic activity, the DNA interactions of new porphyrins and their Re(I) conjugates and a first study to the targeting of porphyrins to tumor cells.

The thesis is divided in to two sections. In the first one the synthesis of two new water soluble porphyrins, a neutral fourfold-symmetric compound and a +3-charged tris-methylpyridinium derivatives, in which either one or four [1,4,7]-triazacyclononane (TACN) units are connected to the porphyrin macrocycle through a hydrophilic linker, is described. The correspondent Re(I) conjugates are also reported. The Re(I) metal was inserted at the periphery of the macrocycle both to provide a possible additive therapeutic effect and to obtain a molecule with diagnostic feature. In fact, since the properties of the "cold" Re and of the "hot" ^{99m}Tc complexes are assumed to be very similar, the hot ^{99m}Tc(I) conjugate can be synthesized from the correspondent cold Re(I) conjugate. These compounds were evaluated as photosensitizers for photodynamic therapy (PDT). The in vitro (photo)toxic effects were evaluated towards the human cell lines HeLa (cervical cancer), H460M2 (non-small-cell lung carcinoma), and HBL-100 (non-tumorigenic epithelial cells). Three of the compounds were not cytotoxic in the dark up to 100 μM and upon Re(I) coordination an enhancement in the phototoxicity activity was observed only for the fourfold-symmetric compound. The intracellular localization of these compounds was studied on HeLa cells by confocal fluorescence microscopy. Although low nuclear localization was observed for some of them, it still prompted us to investigate their capacity to bind both quadruplex and duplex DNA and a significant selectivity in the tris-methylpyridinium derivates for G-quadruplex was observed. In the second section a preliminary study on the targeting of photosensitizers towards cancer cells is described. Indeed, it is well known that the accumulation of porphyrins in the tumor tissues is only preferential and not selective. For this reason the use of targeting peptides is very promising in order to increase the tumor selectivity of the photosensitizer. The fundamental concept of the project was to synthesize a molecule that could be a good photosensitizer in PDT treatment, delivery into the tumor a Re(I) fragment and finally accumulate in a specific tumor. A molecule containing a water soluble +3-charged tris-methylpyridinium porphyrin, a [1,4,7]-triazacyclononane (TACN) unit and the targeting peptide bombesin BN[7-14] was

synthesized in order to increase the selectivity on prostate cancer cells. The synthesis was performed both in solution and in solid phase using different approaches. Unfortunately, several synthetic problems were found concerning the reaction with the porphyrin unit. For this reason a really small amount of the final compound was obtained and the correspondent Re(I) conjugate was not synthesized. Since fullerene derivatives are good photosensitizers the correspondent molecule containing a fullerene unit, the BN[7-14] and the chelator TACN was synthesized, but also in this case the yield was very low and the product was difficult to purify.

The results of this PhD thesis show that a neutral fourfold-symmetric and a +3-charged tris-methylpyridiniumporphyrins can bind the *fac*-$\{Re(CO)_3\}^+$ fragment in good yields. Considering the biological evaluations, the possibility of obtaining the correspondent ^{99m}Tc conjugates, these results are interesting in order to develop new therapeutic agents. Furthermore, a new targeted porphyrin and fullerene containing a TACN unit, as a chelator for Re(I) metal fragments, were synthesized. A new synthetic strategy to obtain a single molecule able to target the charged tris-methylpyridinium porphyrin and a Re(I) fragment to prostate cancer cell is still to be discovered in order to overcome low yield and hard purification procedures.

LIST OF ABBREVIATIONS

AEEA	8-amino-3,6-dioxaoctanoic acid
ACN	Acetonitrile
ALA	δ-aminolevulinic acid
ANOVA	Analysis of variance and Tukey-Kramer
BFC	Bifunctional chelator
Boc	*t*-Butyloxycarbonyl
BN	Bombesin
COSY	Correlation spectroscopy
CPP	Cell-penetrating peptides
CuAAC	Copper catalyzed azide-alkyne cycloaddition reaction
DIPEA	N-etil-diisopropilammina
DMA	9,10-dimethylanthracene
DMAP	Dimethylaminopyridine
DMF	N,N-dimethylformamide
DMSO	Dimetyl sulfoxide
DTPA	Diethylene triamine pentaacetic acid
EDCI	N-(3-dimethylaminopropyl)-N'-ethylcarbodiimide hydrochloride
EDTA	Ethylenediaminetetraacetic acid; en, ethane - 1,2-diamine
EHIDA	2,6-diethylphenylcarbamoylmethyliminodiacetic acid
ESI	Electrospray ionisation
ER	Endoplasmic reticulum
Fmoc	9-Fluorenylmethoxycarbonyl
GPCR	G-protein-coupled receptor
GRP	Gastrin-releasing peptide
GRP-R	Gastrin-releasing peptide receptor
HDL	High-density lipoprotein
HOBt	1-hydroxybenzotriazole
HPLC	High performance liquid chromatography
HSQC	Heteronuclear Single Quantum Coherence
IR	Infrared
LDL	Low-density lipoprotein

LED	Light-emitting diodes
MALDI-Tof	Matrix-assisted laser desorption/ionization time of fight
MLS	Mitochondrial localization signal
MTT	Thiazolyl blue tetrazoliumbromide
MS	Mass spectrometry
Mtt	4-Methyltrityl
NLS	Nuclear localization signal
NMB	Neuromedin-B
NMP	1-metil-2-pirrolidone
NMR	Nuclear magnetic resonance
OTf	Triflate
PBS	Phosphate-buffered saline
PDT	Photodynamic therapy
PEG	*Poly*-ethylene glycol
PI	Photo index
PpIX	Protoporphyrin IX
PS	Photosensitizer
Re	Rhenium
RP-UPLC	Reverse phase ultra performance liquid chromatography
RNS	Reactive nitrogen species
ROS	Reactive oxygen species
rt	Room temperature
rt	Retention time
SP	Solid-phase
sp	Side product
SPPS	Solid-phase peptide synthesis
TACN	[1,4,7]-triazacyclononane
TBTU	O-(Benzotriazol-1-yl)-N,N,N',N'-tetramethyluronium tetrafluoroborate
Tc	Thechetium
TCPP	*Meso*-4'-tetracarboxyphenylporphyrin
TEA	Trietylamine
TFA	Trifluoroacetic acid
THF	Tetrahydrofuran
TLC	Thin layer chromatography
UV-vis	Ultraviolet visible

TABLE OF CONTENENTS

1. Introduction

Photodynamic Therapy and Porphyrins

1.1 Photodynamic Therapy 1

1.1.1. History of the development of photodynamic therapy 1

1.1.2. Mechanism of action of photodynamic therapy 1

1.1.3. The role of light in photodynamic therapy 3

1.1.4. The role of the photosensitizer in photodynamic therapy 4

1.2. Porphyrins 6

1.2.1. General information about porphyrins 6

1.2.1. Mechanism of action/damage and subcellular targets 8

2. New water soluble porphyrins and their correspondent rhenium (I) conjugates

2.1. Porphyrins and radiopharmaceuticals 11

2.2. DNA interactions of porphyrins 13

2.3. Strategies for the development of new rhenium porphyrins 14

2.4. Synthesis and characterization of new porphyrins 17

2.5. Biological evaluations of new rhenium porphyrins 39

2.5.1. (Photo) toxicity studies 39

2.5.2. Determination of singlet oxygen quantum yields (Φ_{Δ}) 41

2.5.3. Cellular localization studies 42

2.5.4. DNA binding studies 43

2.5.5. DNA photocleavage 47

2.6. Conclusions 48

2.7. Experimental part 49

3. Synthesis of peptide-photosensitizers to target prostate cancer cells

3.1. Targeting cancer cells 72

3.2. Strategies for the development of new photosensitizers 77

3.3. Click chemistry approach for the synthesis of BN[7-14]- porphyrin 78

3.3.1. First strategy for the synthesis of the final molecule 78
3.3.2. Synthesis of the alkyne-porphyrin and the azido peptide 80
3.3.3. Click chemistry reaction 89
3.4. Coupling reaction approach for the synthesis of the BN[7-14]-porphyrin 99
3.4.1. Second strategy for the synthesis of the final molecule 99
3.4.2. Synthesis of the BN[7-14]-porphyrin 100
3.4.3. Synthesis of a BN[7-14]-fullerene 112
3.5. Conclusions 114
3.6. Experimental part 115

4. **Bibliography** 130

1.

INTRODUCTION:

PHOTODYNAMIC THERAPY AND PORPHYRINS

1.1. PHOTODYNAMIC THERAPY

1.1.1. HISTORY OF THE DEVELOPMENT OF PHOTODYNAMIC THERAPY

Cancer is one of the deadly diseases of our time and researchers from all over the world are actively involved in fighting it by developing new antitumor drugs. Several treatments are used such as surgery, radiation and chemotherapy. Unfortunately these treatments have important side effects: nausea, vomiting, in some cases depression of the immune system and loss of the normal organ functions. In addition, radiations give damage to the epithelial surfaces, infertility and swelling of soft tissues of the patients [1]. Nowadays photodynamic therapy (PDT) is used to treat several tumors such as skin, lung, gall bladder, esophagus, endo-bronchial, breast, stomach, oral cavity head and neck cancer and also skin's premalignant lesions [2-4]. PDT is a minimally invasive treatment that destroys target cells in the presence of oxygen when the light irradiates a molecule generating highly reactive singlet oxygen (ROS). The origin of PDT goes back to the Egyptians as they first used sunlight to bleach fabrics. At the beginning of the nineties Finsen discovered that light treatment could control skin manifestations of tuberculosis. Later on Raab, Jesionek and Von Tappeiner discovered a relationship between the light activation of a dye and the therapeutic effect. Finally in the second half of the twentieth century Dougherty demonstrated that the topical administration of hematoporphyrin IX and red light eradicated mammary and bladder tumors in mice [5,6].

1.1.2. MECHANISM OF ACTION OF PHOTODYNAMIC THERAPY

The PDT treatment consists in several steps. First a non-toxic drug (named photosensitizer, PS) is administrated intravenously or topically to the patient. The so-called time delay corresponds to the time that elapses between the PS's administration and the illumination of the tumor tissue. During this incubation period the maximum drug uptake in the tumor is reached. The tumor is then irradiated usually with red light, thus the PS is converted from its low energy ground singlet state (S0) into a short-lived higher energy excited state (S1). The activated PS can transfer its energy or electrons to produce reactive oxygen species (ROS) or singlet oxygen ($^1O_2$). The activated PS causes apoptosis and/or necrosis, which appears in two or three days, with two types of mechanisms [7-10] (Figure 1).

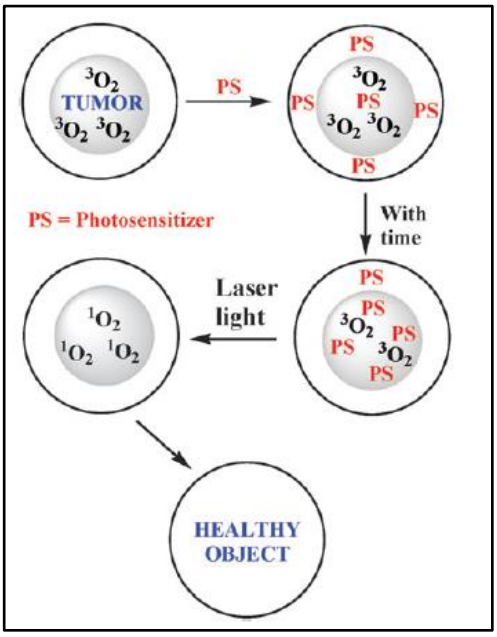

Figure 1: General mechanism of PDT [1]

More in detail: *i*) the activated PS can react directly with a biological substrate (for example lipids, proteins and nucleic acids) to form free radicals which, after interaction with the molecular ground triplet state oxygen ($^3O_2$), can produce ROS ($O_2^{-\bullet}$, $OH^\bullet$, H_2O_2); *ii*) the activated PS can transfer its energy directly to oxygen converting $^3O_2$ to singlet oxygen $^1O_2$. Singlet oxygen is a non-radical, highly reactive species, with a short lifetime in biological systems (< 0.04 µs). The damage caused by singlet oxygen is highly localized. For all these reasons singlet oxygen is considered a potent cytotoxic agent [1, 11, 12] (Figure 2).

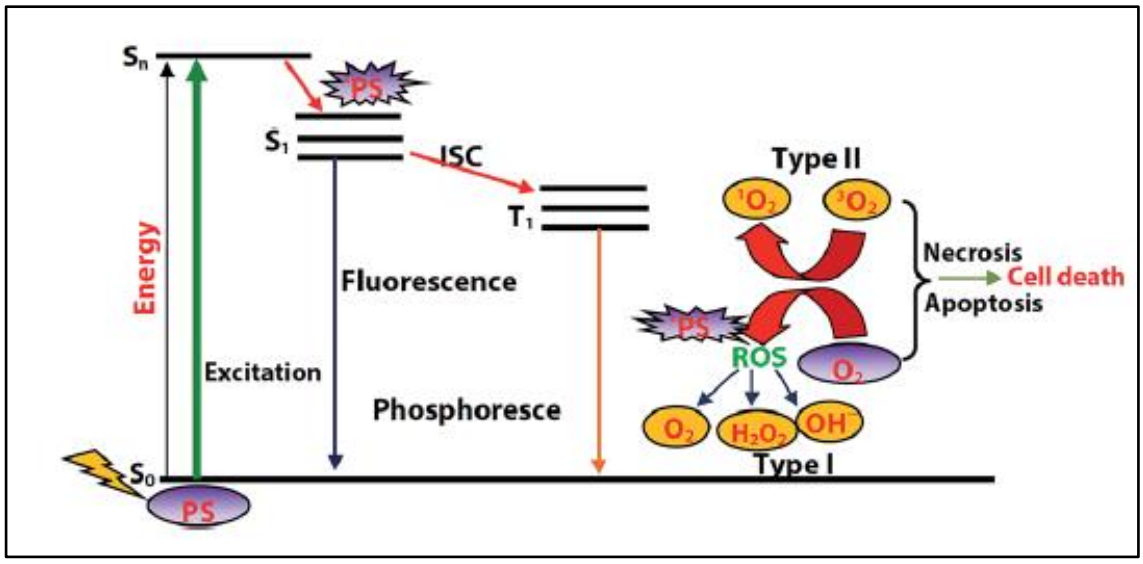

Figure 2: Simplified Jablonski energy level diagram for PDT [11]

Besides the apoptosis and/or necrosis tumor death, the PS can cause cell death by damaging the blood vessels surrounding the tumor cells, thus preventing the cancer from receiving necessary nutrients and oxygen, and by activating the immune mediators against tumor cells [7,10,13].

1.1.3. THE ROLE OF LIGHT IN PHOTODYNAMIC THERAPY

Besides the presence of oxygen in the tumor tissue, also the light has an important role in PDT [14]. Upon interaction with a tissue surface, light can be reflected, scattered, transmitted or absorbed depending on the optical features of the tissue and on the light properties [15]. The features that the light source should have a total optical power (measured in Watts, W) at the appropriate wavelength to activate the PS and an optimal penetration in the tumor tissue [16]. In phototherapy light is used in the phototherapeutic window, the wavelength range between 600 and 900 nm [17]. Penetration of light into deeper tissues is only possible for wavelength >700 nm. For this reason the ideal PS would be activated at wavelength > 700 nm, but most of the PSs currently used are excited at lower wavelengths. The penetration in tissue of wavelengths < 600 nm is about 0.5 cm, while wavelengths >600 nm can double tissue penetration to 1 cm.

The total light dose administrated during PDT depends on the type and size of the tumor and usually its fluence rate should not exceed 100 mW/cm^2 to avoid thermal effects that can damage the cells.

The choice of the type of light source depends on *i*) the location of the tumor; *ii*) the light dose delivered and *iii*) the choice of the PS. Lasers are the sources of light usually used in PDT treatment. An advantage of lasers is the ability to easily convey this light into fiber optics that allows the delivery of the activating photons directly to the target tissue [16]. With the laser the tumors located both internally and superficially can be irradiated. The standard source for clinical PDT is the argon/dye laser that can irradiate at 630 nm with a power from 1 to 7 W. In the past few years the research has also focused on the improvement of LEDs (light-emitting diodes) in order to use them in PDT. The advantages of this challenging instrument are: low price, versatility, less hazard, thermal nondestructive and readily availability. A very important feature of LEDs is the emission wavelengths that ranges from UVA to the near infrared (350 nm-1100 nm) and the power that can reach up to 150 mW/cm^2 over a 3 cm x 3 cm area [13, 18, 19].

1.1.4. The Role of the Photosensitizer in Photodynamic Therapy

Several groups of molecules are used as PSs in PDT. To be considered a good PS a molecule should have the following characteristics: *i*) strongly absorb in the 600-800 nm range; *ii*) produce singlet oxygen and cause the desired biological response; *iii*) be chemically pure; *iv*) have minimal dark toxicity and be cytotoxic only in the presence of light; *v*) be selectively uptaken by cancer cells prior to light activation; *vi*) be rapidly excreted from the body; *vii*) be easily administrated though various routes [6,13]. Basically three generations of PSs have been developed (Table 1).

Category	Example	Area of localization	Molecular target	Application
Porphyrins (First generation photosensitizers) (1970)	Photofrin®	Golgi, plasma membrane	Vascular damage and ischemic tumor cell necrosis	Esophageal (including Barrett's) and bronchial cancer.
	Hemoporfin® (hematoporphyrin monomethyl ether, HMME)	---	Vascular damage and blood vessel occlusion	ocular as well as anti-tumor
Porphyrins (Second generation photosensitizers) (1980)	Tookad®	Vasculature	Vascular damage	In phase II/III clinical trials for prostate cancer.
	Foscan® (Mesotetra hydroxy phenyl chlorin)	Endoplasmic reticulum (ER), mitochondria	Vascular damage, tumor cytotoxicity	Head and neck cancer.
	Purlytin	Mitochondria, lysosomes	Tumor cytotoxicity	---
	Lutrin	Lysosome	Vascular damage, tumor cytotoxicity	---
	NPe6	Lysosome, endosome	Vascular stasis, tumor cytotoxicity	---
	Photosens®		Tissue penetration	Choroid and epibulbar melanoma
	Metvix® (Methyl ester of 5-ALA)	Mitochondria, cytosol, membranes	Tumor cytotoxicity	---
	Visudyne®	--		Age-related macular degeneration (AMD)
	Photoclor®	---	Poorer lymphatic drainage of the tumours, higher proliferation rates of tumour cells or leaky vasculature	In clinical trials for esophageal (including Barretts) and bronchial cancer
Chlorophyll-based photosensitizer	Chalcogenopyrylium dyes	Lysosome	Tumor cell cytotoxicity	---
Dyes	Phenothiazinium dye (Toluidine Blue)	ER, Golgi bodies	Tumor cell cytotoxicity	---
	Phenothiazinium dye (Nile blue and derivatives)	Lysosomes	Tumor cell cytotoxicity	---
	Cyanines	Mitochondria, plasma membrane	Tumor cell cytotoxicity	---
	ADPM06	ER, mitochondria	Vascular-targeted	---
Prodrugs	Levulan® (Aminolevulinic acid ; ALA)	Mitochondria, Cytosol, membranes	Tumor cytotoxicity	Skin cancers such as basal skin carcinoma and Bowen's disease
	Metvix® (Methyl ester of 5-ALA)	Mitochondria, cytosol, membranes	Tumor cytotoxicity	Actinic keratosis and basal cell carcinoma
Antibody conjugates (photoimmuno conjugates)(Third generation photosensitizers)	#Mylotarg® (drug-linked monoclonal antibody)	---	---	Cutaneous malignancies and AMD
LDL-complexed photosensitizers	Benzoporphyrin derivative monoacid A (BPD-MA) complexed with LDL	----	----	---

Table 1: Examples of photosensitizers [6]

The first generation includes porphyrins that were discovered in the 1970s and 1980s, for example Photofrin (Figure 4). The second generation of photosensitizers refers to the porphyrin derivates synthetized from the late 1980. The δ-aminolevulinic acid (ALA) belongs to this class and is already authorized in European Union for fluorescence-guided resection. ALA is the biosynthetic precursor of heme since it can generate protoporphyrin IX (PpIX). Exogenous administration of 5-ALA can lead to an intracellular accumulation of PpIX (Figure 3) [1, 5, 10, 20-22].

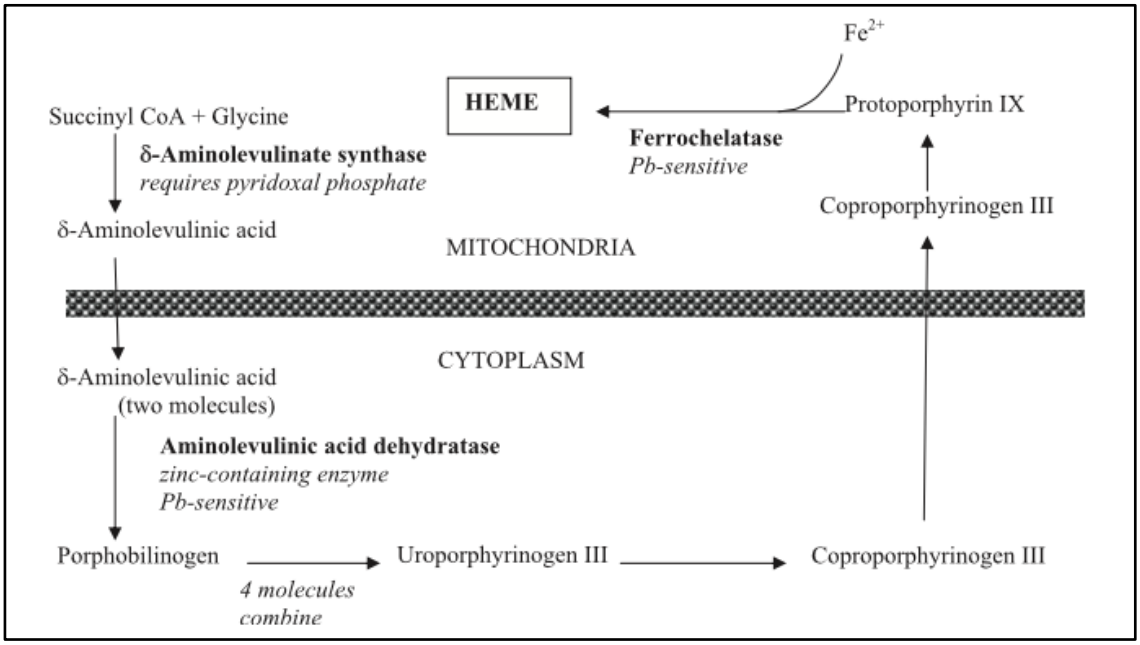

Figure 3: Heme synthesis pathway [23]

The third generation of photosensitizers includes drugs that are modified for example with antibodies in order to obtain a PS more tumor specific [5].

Also non-porphyrin (such as dyes) can be used as PSs. Rose bengal, eosin, methylene blue are good PSs as they can generate $^1O_2$. Rose Bengal is frequently used as PS thanks to its high solubility in water, high singlet oxygen quantum yield and low rate of photobleaching (Figure 4) [12, 13, 24, 25].

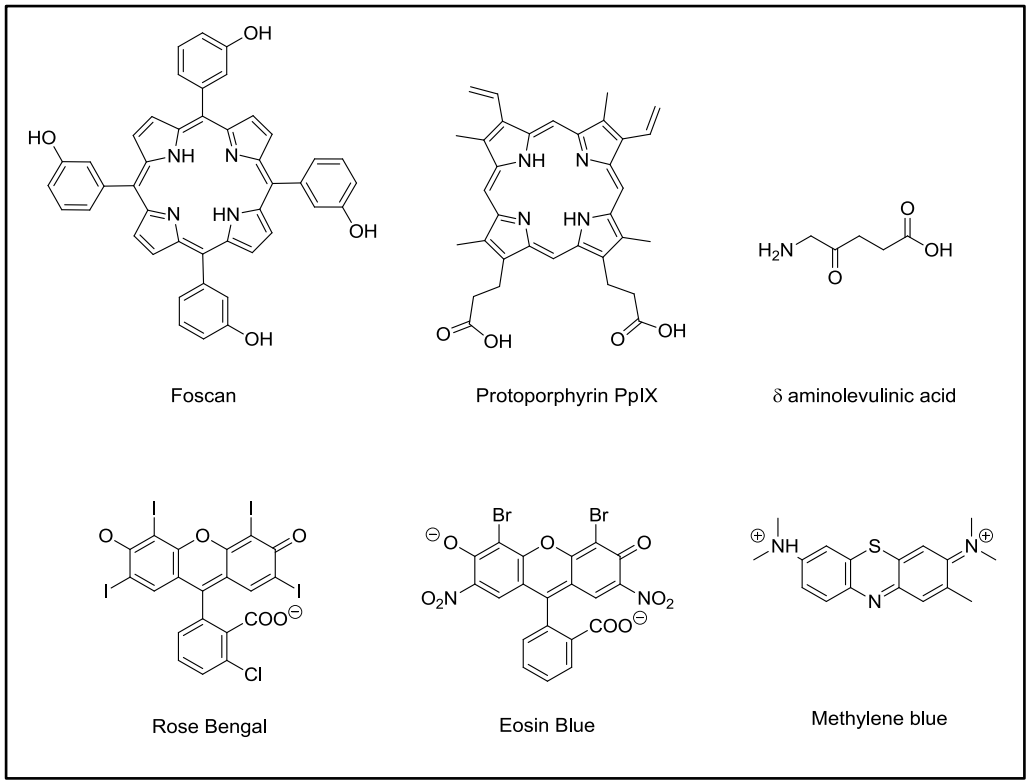

Figure 4: Structure of photosensitizers

1.2. PORPHYRINS

1.2.1. GENERAL INFORMATION ABOUT PORPHYRIN

Porphyrins are often found in nature since they play several roles in a large number of biological processes such as photosynthesis and transport of oxygen in the blood. Indeed all the heme proteins (such as hemoglobin, cytochrome b and c and cytochrome P450) contain in their structure a molecule of porphyrin. Also other biomolecules as chlorophylls, phaeophytins and vitamin B_{12} have a porphyrin related structure [26].

Porphyrins are a versatile class of π-conjugated macrocycles that have in their structure a cyclic tetrapyrrole in which the pyrrole rings are linked through their α carbon atoms by methine bridges (–CH=) (Figure 5).

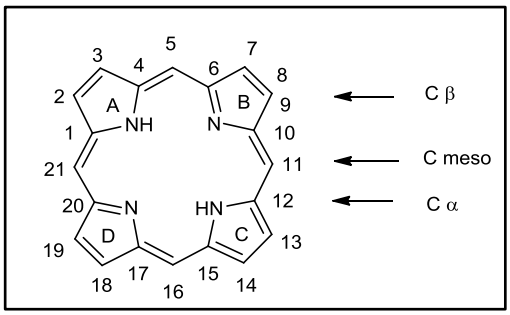

Figure 5: Porphyrin structure

The tetrapyrrole defines a cavity of dimension nearly perfect to coordinate a large number of metals usually Fe(III), Fe(II), Zn(II), Cu(II) and Co(II) giving rise to metalloporphyrins. Only diamagnetic metals (Zn, Pd, In, Sn, Lu) allow the tetradentate macrocycle to retain its photosensitizing ability, while paramagnetic (Fe, Cu, Gd) do not [27]. The macrocycle is highly conjugated, planar, rigid, aromatic, and chemically stable. Its low reactivity is the reason why reactions can be performed in the peripheral positions without modifying the central core. Another important feature for chemical applications is the stability of the porphyrin ring in strong acid and basic conditions. Porphyrins are amphoteric compounds having properties of both acids and bases in solution. The two nitrogen atoms that have an unpaired electron doublet ($pK_b \approx 9$) can be protonated by strong acids as TFA with formation of mono- and deprotonated species MP and DP (Figure 6). Furthermore strong bases, such as alkoxide, can remove the protons present on the nitrogen atoms ($pK_a \approx 16$) of the pyrroles giving a dianion [10].

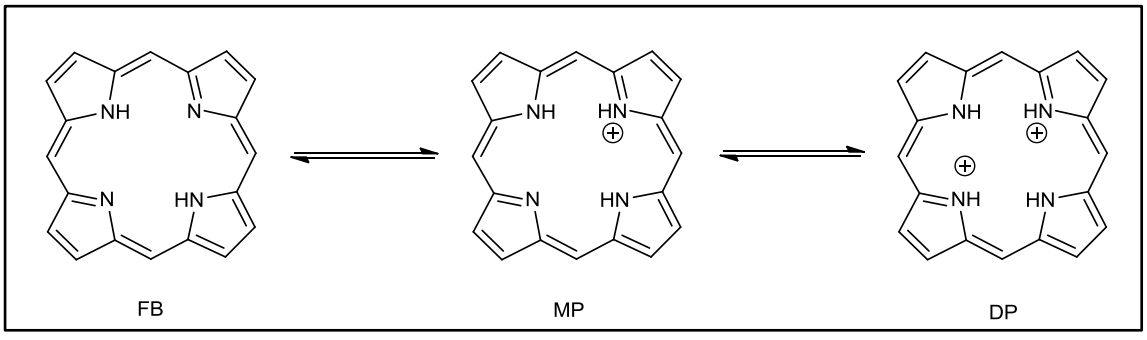

Figure 6: Mono- and diprotonated species MP and DP.

Many synthetic porphyrins bear phenyl rings in the *meso* positions. Besides their applications in biological field (in particular as antitumor agents for PDT, and antibacterial and antimicrobial agents) these compounds can be used in analytical chemistry, in organic solar cells as energy transfer systems, in oxidation catalysis, and in agriculture (as potential photoactivable herbicides, pesticides, insecticides) [28, 29].

Furthermore, they could be also useful as tools for the detection of early-stage tumors exploiting their fluorescence properties. Porphyrins emit intense red fluorescence on irradiation with light of wavelength near 400 nm. Indeed as a consequence of the extensive electron delocalization, the electronic absorption spectrum of a typical porphyrin is very characteristic: it consists of the intense Soret band at ≈ 400 nm (strong transition to the second excited state, S_0 -> S_2) and four Q bands of lower intensity from 500 nm to 700 nm (weak transition to the first excited state, S_0 -> S_1) (Figure 7).

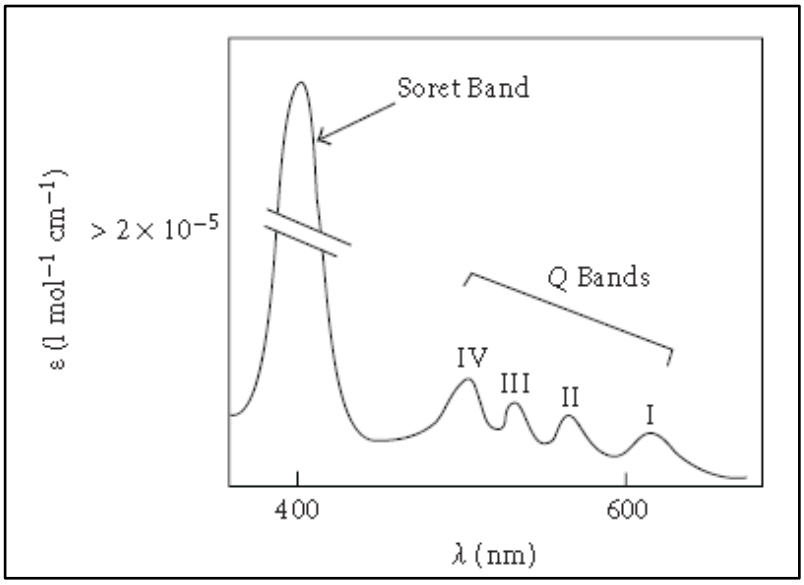

Figure 7: UV-vis spectrum of a porphyrin.

1.2.2. MECHANISM OF ACTION/DAMAGE AND SUBCELLULAR TARGETS

It is well known that porphyrins selectively accumulate in the tumor tissue, but the mechanism is still not fully understood. Dolmans et al. postulate that porphyrin accumulation in tumors is due to the high vascular permeability of the agents, as well as their affinity for proliferating endothelium and the lack of lymphatic drainage in tumors. For this reason research is currently working to enhance selective tissue localization, using targeting strategies such as antibodies, peptides or nanoparticles [30].

Several factors are involved in the accumulation of porphyrins in the tumor tissue. In aqueous media porphyrin derivates show a strong tendency to form aggregated species and for this reason several porphyrins, once systemically injected into the bloodstream, become readily associated with hydrophobic regions of the specific plasma proteins, such as low-density lipoprotein (LDL) and high-density lipoprotein

(HDL) [31]. Besides the blood proteins transport several factors are involved in accumulation of porphyrins in the tumor tissues, such as: *i*) structure that determinates its molecular weight; *ii*) electronic charge; *iii*) hydrophobic nature; *iv*) affinity for biological ligands and *v*) type of formulation [32]. Moreover, other factors are determined by the characteristics of the tumor tissue [33-35]: *i*) the increased vascular permeability and the ineffective lymphatic clearance might cause the build-up of porphyrins in the interstitial spaces; *ii*) the decreased intratumoral pH may affect the ionization of derivative porphyrins; *iii*) the increase number of LDL receptors: it is known that porphyrins with a high level of lipophilicity have more affinity for LDL, instead the ones with a high level of hydrophilicity prefer either HDL or albumin. [36-38]. Because of the high reactivity and short half-life of singlet oxygen and hydroxyl radicals, only molecules and structures that are proximal to the area of their production are directly involved in PDT and for this reason the damage depends on the subcellular localization of the PS. The PDT effects are different according to the cell type, consequently the degree of damage changes [20].

Focusing on the subcellular level, PDT interest membranes, cell surfaces, lysosomes, endoplasmic reticulum (ER), mitochondria and other cells organelles [39]. The ROS and the singlet oxygen molecules can produce oxidation and cycloadditions reactions. Indeed important targets are amino acids residues in proteins, such as cysteine, methionine, tyrosine, histidine and tryptophan [26, 40, 41]. Also unsaturated lipids such as cholesterol, undergo reactions to give lipid hydroperoxides [26] Since lipids and proteins are part of the biological membranes, the reaction between $^1O_2$ and the components of the membrane causes alteration of the permeability of the membrane that leads to cytolysis, swelling, blistering on the cell membrane, release of vesicles containing enzymes, inhibition of enzymes of membranes such as Na^+/K^+-ATPase, destruction of the calcium channels [42-43]. In the mitochondria these events can lead to the release of cytochrome C and the rapid induction of apoptosis [44-46].

Also DNA is a target of PDT, since it can be oxidative damaged at both the pyrimidine and purine bases (especially guanine) and at apurinic/apyrimidinic (abasis) sites such as the sugar moieties causing DNA damage, mutations and carcinogenesis to the tumor cells. As a result of PDT also single-strand (SSBs) and doublet-strand breaks (DSBs), and a directly inhibition of the DNA and RNA polymerase can be observed [26, 47, 48]. Besides the effects of cell damages also the vascular damages are responsible of the tumor cell death. The vascular effects of PDT consist in inflammation processes, change of the vascular permeability and conformation, and finally vessel occlusion..

Indeed PDT causes the invasion of leukocyte, lymphocytes, neutrophils, macrophages, cytokines, interleukin IL-6 and IL-1 [49] and this was observe during PDT with Photofrin on mouse EMT6 tumors. PDT changes the endothelium of the vases and this leads to the change of the permeability and structure of blood vessels. In fact after irradiation there is a cascade of biological responses such as the accumulation of macrophages and plates, release of cytokines and prostaglandins, and the plates aggregation causes thrombus formation [7, 20, 50].

2.

NEW WATER SOLUBLE PORPHYRINS AND THEIR CORRESPONDENT RHENIUM (I)-CONJUGATES

2.1. PORPHYRINS AND RADIOPHARMACEUTICALS

In recent times research has focused on the preparation of multifunctional agents that might combine in a single molecule both imagining and treatment properties. For this purpose we took in consideration rhenium compounds. So far relatively few rhenium complexes have been explored as potential anticancer agents, although they possess excellent properties for developing a novel class of antineoplastic drugs [51-54]. Notably, certain organometallic rhenium complexes have been found to have interesting luminescence properties which allow their intracellular distribution as well as their mechanism of action to be followed by emission microscopy [55]. In Figure 8 two rhenium complexes are shown and their IC_{50} values are compared to the one of cisplatin [56].

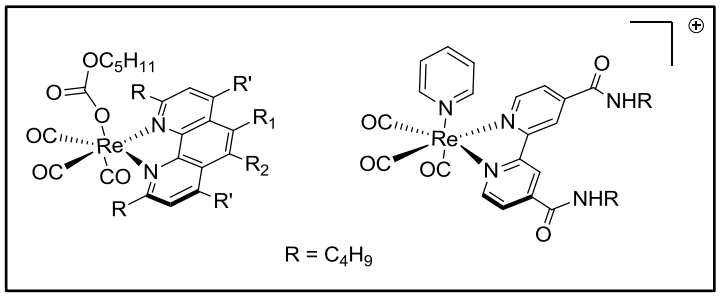

Figure 8: a) IC_{50} (µM) on MDA-MB- 468 cell line: Re compound 4.0 ± 6.5 and cisplatin 5.0 ± 2.5 b) IC_{50} (µM) on HeLa cell line: Re compound 7.7 ± 1.0, cisplatin 25.6 ± 2.3

The most attractive property of rhenium is that its chemistry is similar to that of the hot technetium, and for this reason it is frequently used as nonradioactive surrogate for the characterization of ^{99m}Tc complexes [57]. ^{99m}Tc radiopharmaceuticals play an important role in widespread applications of nuclear medicine. ^{99m}Tc complexes themselves represent the first generation of radiopharmaceuticals, and several chelators have been studied for the coordination of this radioactive element. For example ^{99m}Tc-DTPA and ^{99m}Tc-EHIDA derivate are used in radiodiagnostic respectively for the kidney and liver scintigraphy (Figure 9) [58].

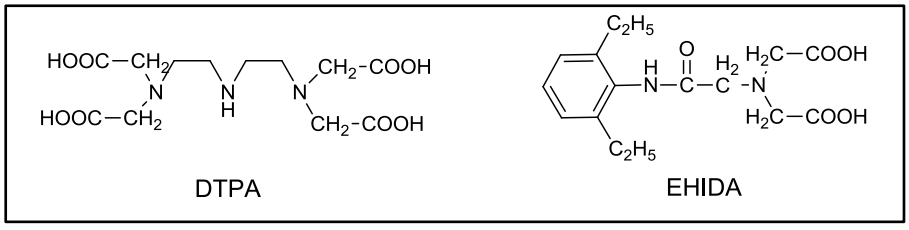

Figure 9: DTPA and EHIDA chelators for ^{99m}Tc

In the second generation of radiopharmaceuticals the radionuclide is delivered in the tumor tissue by a targeting molecule. Two approaches have been studied for this purpose: *i*) an integrated design where the ^{99m}Tc unit is incorporated into the bioactive molecule; *ii*) a bifunctional approach, which couples a receptor-binding organic molecule to a metal chelate via a spacer [58, 59]. These latter molecules are made of a targeting molecule and a bifunctional chelator (BFC) (Figure 10). Indeed the chelator must be able both to coordinate the radioactive element and to connect it to the targeting molecule. The spacer is important since it both influences the lipo- or hydrophilicity of the radiopharmaceutical and separates the bioactive part from the metal-complex, thus minimizing steric effects [60-62].

Many biomolecules, including monoclonal antibodies and small peptides, have been studied as "carriers" for radionuclides and several molecules are under development, for example Neotec1 (^{99m}Tc-Arcitumomab), where the carrier is a monoclonal antibody, to target colorectal cancer cells [63]. An alternative approach has been proposed by our research group. We selected a water soluble porphyrin to act as targeting molecule: besides being highly fluorescent, it might behave as carrier ligand for the active transport of metal compounds, including radiotracers, into cancer cells (Figure 10). In fact this macrocycle typically shows preferential uptake by tumor tissues, as already discussed.

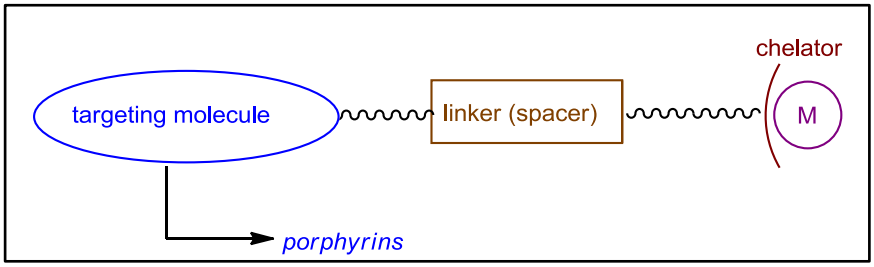

Figure 10: Structure of second generation radiopharmaceuticals using BFC

^{99m}Tc/Re-porphyrins are very interesting since, by applying the matched pair paradigm, the ^{99m}Tc/Re-porphyrin conjugates may act as multifunctional agents endowed either with diagnostic (^{99m}Tc) or with therapeutic properties (Re) [64]. In principle, radioimagining performed on a labeled ^{99m}Tc(I)-porphyrin might allow noninvasive, in vivo localization of the corresponding PDT active cold Re conjugate. There are however relatively few examples of water-soluble ^{99m}Tc/Re-porphyrin adducts. More recently, we described the preparation and characterization of two novel water-soluble porphyrins bearing three *meso*-pyridyl rings and one peripheral chelator, which was

either a diethylenetriamine unit (Figure 11, a) or a bipyridyl fragment (Figure 11, c). Both chelators were suitable for complexation of the $\{^{99m}Tc/Re(CO)_3\}^+$ moieties (Figure 11, b and d) [65, 66].

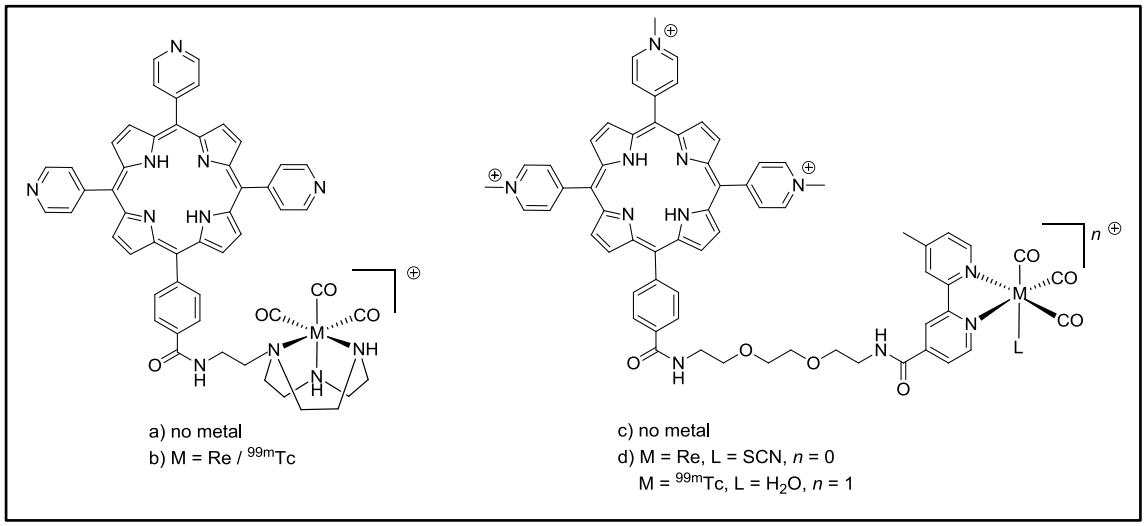

Figure 11: Structure of monofunctionalized Re/^{99m}Tc-porphyrin conjugates

2.2. DNA INTERACTIONS OF PORPHYRINS

The ability of cationic porphyrins and their metal complexes to interact with nucleic acids is well documented [67-71], and one of the most extensively investigated compound is *meso*-tetrakis-(4-N-methylpyridiniumyl)porphyrin (TMPyP) (Figure 5). The original studies of Fiel and coworkers on the interactions of TMPyP with DNA was aimed at developing DNA-targeting photosensitizers, since selective photocleavage of DNA in tumor cells might result in lethal damage to the cells [68, 72, 73]. Furthermore, cationic porphyrins were recently exploited for selective recognition of non-canonical DNA structures called G-quadruplexes [74-78]. The formation of G-quadruplex DNA structures in vivo has been associated with a number of key biological processes such as regulation of gene expression and telomere maintenance. In general, cationic porphyrins with relatively long and flexible side-arms are better binders of G-quartets compared to TMPyP, presumably because they might permit the stacking of the aromatic porphyrin core on the G-tetrad minimizing steric clashes with the G-tetrad edges. In Figure 12 the structure of a Mn-porphyrin synthetized by Meunier and coworkers is shown. This porphyrin with four cationic and flexible peripheral

substituents is 10000 times more selective for G-quadruplex DNA respect to duplex DNA [76].

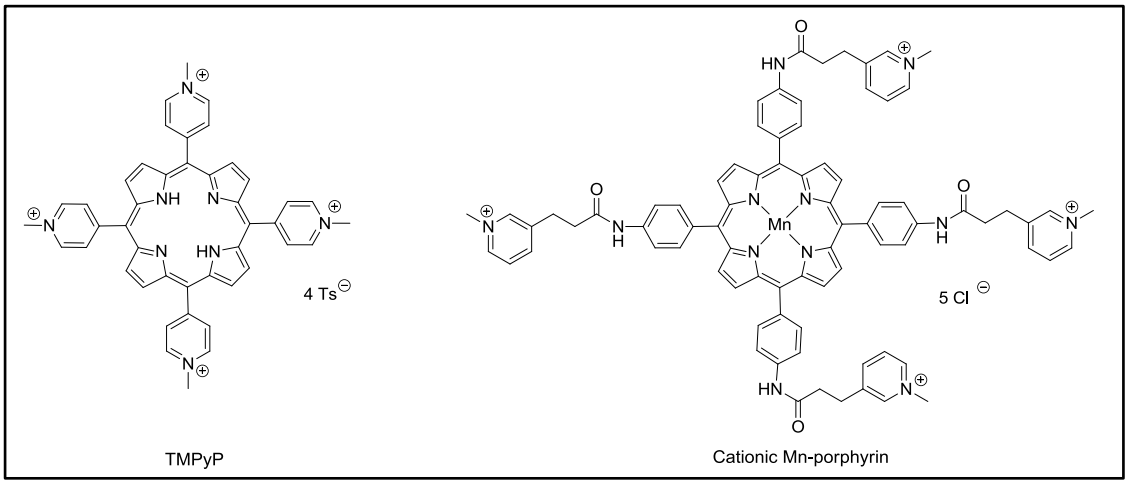

Figure 12: TMPyP and the Meunier's cationic Mn-porphyrin

Consequently, there is a mounting interest in synthetizing cationic porphyrins as G-quadruplex ligands, in particular to obtain molecules endowed with an increased affinity for the telomeric structures by virtue of additional interactions [29]. Due to the important biological roles associated to G-quadruplexes, they are potential targets for anticancer drug candidates [79-83]. Moreover, as was already described in the introduction, DNA can be damaged by exogenous and endogenous oxidative stress induced by reactive oxygen (ROS).

2.3. STRATEGIES FOR THE DEVELOPMENT OF NEW RHENIUM PORPHYRINS

For all the reasons detailed above, we decided to investigate tetrapyrrolic chromophores suitable for the conjugation with Re fragments to be potentially used both in therapy and diagnosis of cancer. Here we describe the synthesis, characterization, cellular localization, affinity evaluation for both quadruplex and duplex DNA, and the (photo)-toxic behavior of two novel porphyrins functionalized with either four or one [1,4,7]-triazacyclononane (TACN) peripheral units, the neutral **9** and the 3+ charged **16**, as well as of their corresponding tetracationic Re(I)-conjugates **20** and **21**. The bifunctional chelator is connect to the macrocycle through an hydrophilic 2,2'-

(ethylenedioxy)diethylamine linker (Figure 13 and 14) that, besides increasing the water solubility of the final molecule, also increase its flexibility.

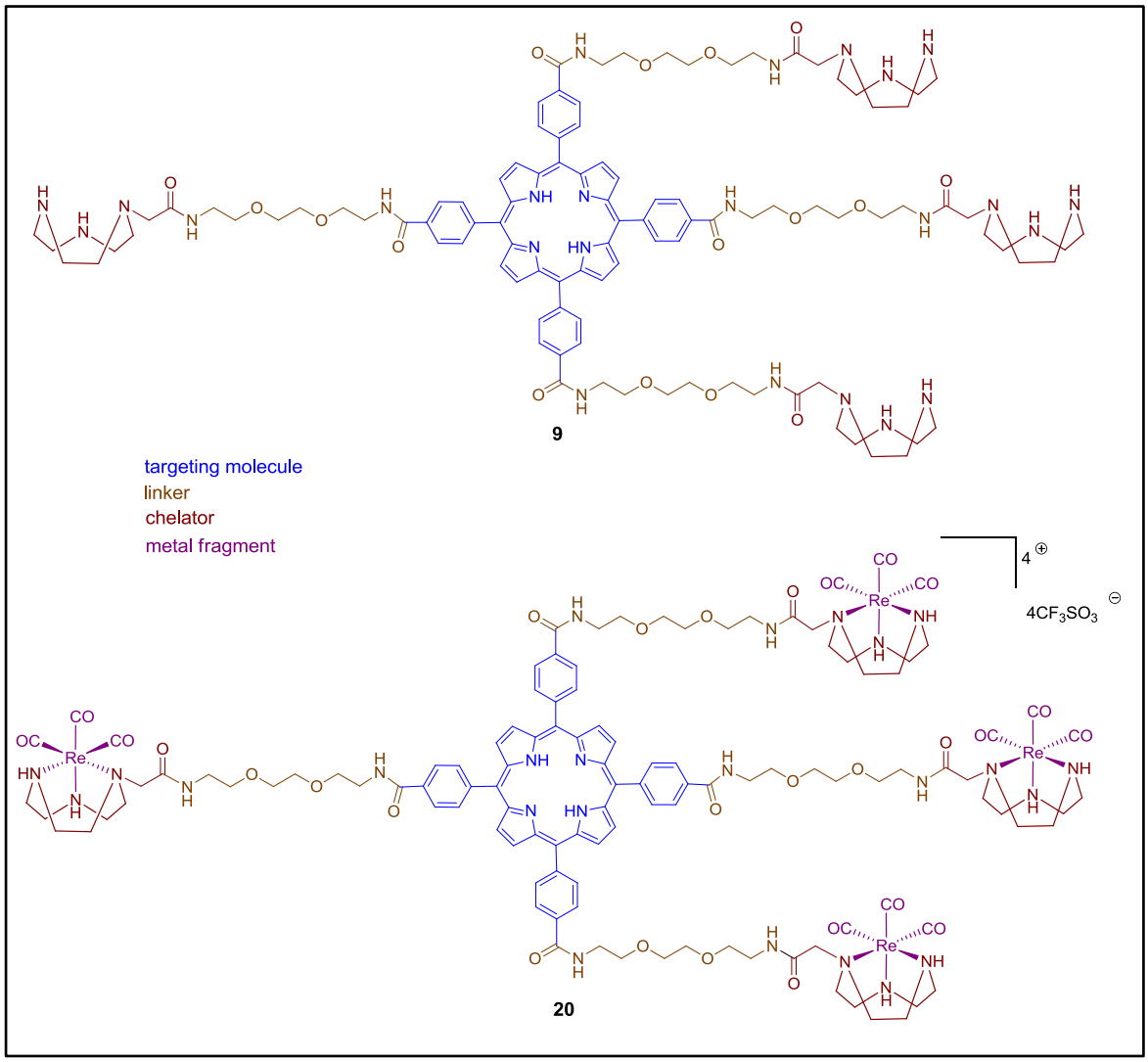

Figure 13: Structure of porphyrins **9** and **20**

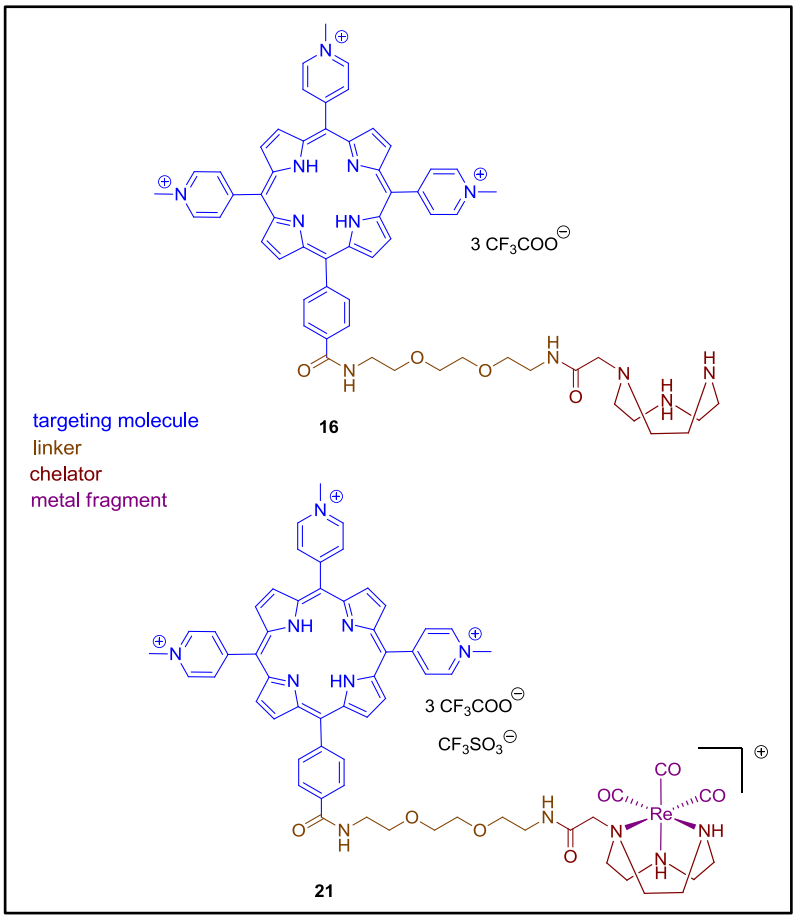

Figure 14: Structure of porphyrins **16** and **21**

Porphyrins **9** and **16** were specifically designed for binding a facial metal fragment such as Re/^{99m}Tc(CO)$_3$. In fact, the neutral TACN chelating unit matches the binding preferences of those metal fragments providing a relatively rigid set of three thermodynamically and kinetically stable bonds. Porphyrins **9** and **16** are an evolution of monofunctionalized porphyrins a and c shown in Figure 11 [65, 66]. Of note, the open-chain diethylenetriamine ligand has a worse geometrical match than TACN and, being flexible, is a less efficient binder than TACN. The bidentate bipyridyl ligand is hydrophobic in nature and leaves an hydrolysable position upon coordination with Re/Tc(CO)$_3$ fragment (Figure 11, d). The coordination chemistry of Re(I)/Tc(I) with TACN as a ligand is well documented, and a variety of complexes containing rhenium, as well as technetium, in the formal oxidation state (I) with TACN have been already reported [82-87].

2.4. SYNTHESIS AND CHARACTERIZATION OF NEW PORPHYRINS

In order to synthesize porphyrins **9** and **16**, a suitably functionalized TACN derivate, 2-(diBoc)TACN acetic acid (**4**), was synthesized in good yield by selective 1,4-bis-protection of the amino groups of the commercially available TACN (**1**) [88], followed by reaction with benzyl bromoacetate, affording **3** in good yield. After reductive deprotection with H_2 on Pd/C the functionalized chelator **4** was obtained (Scheme 1).

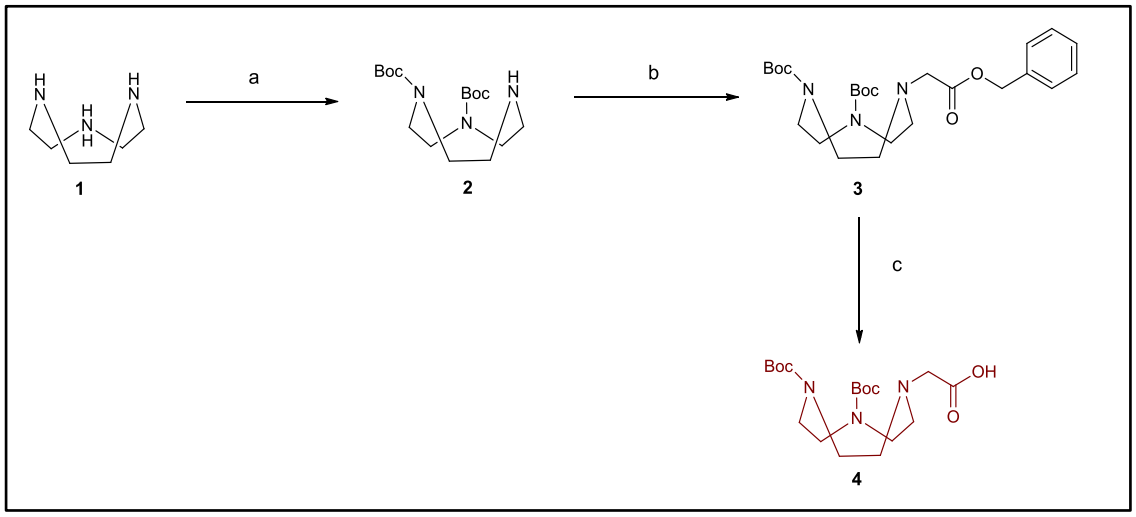

Scheme 1: Synthetic route for **4**. *Reagents and conditions*: a) TEA, $CHCl_3$, $(Boc)_2O$, $CHCl_3$, Ar, 12 h, rt, 56%; b) benzyl bromoacetate, TEA, $CHCl_3$, 0°C,1h, rt, 48 h, 89%; c) H_2, Pd/C, CH_3OH, 24 h, 91%

Concerning porphyrin **9** synthesis, the condensation of pyrrole and methyl 4-formyl benzoate [89] followed by hydrolysis in basic conditions in THF/MeOH, gave the *meso*-4'-tetracarboxyphenylporphyrin (TCPP) **5**.

The four carboxylic groups of **5** were activated with HOBt and coupled with the free amino group of the spacer N-Boc-2,2'-(ethylenedioxy)diethylamine **6**. After column chromatography porphyrin **7** was obtained in high yield and purity (Scheme 2).

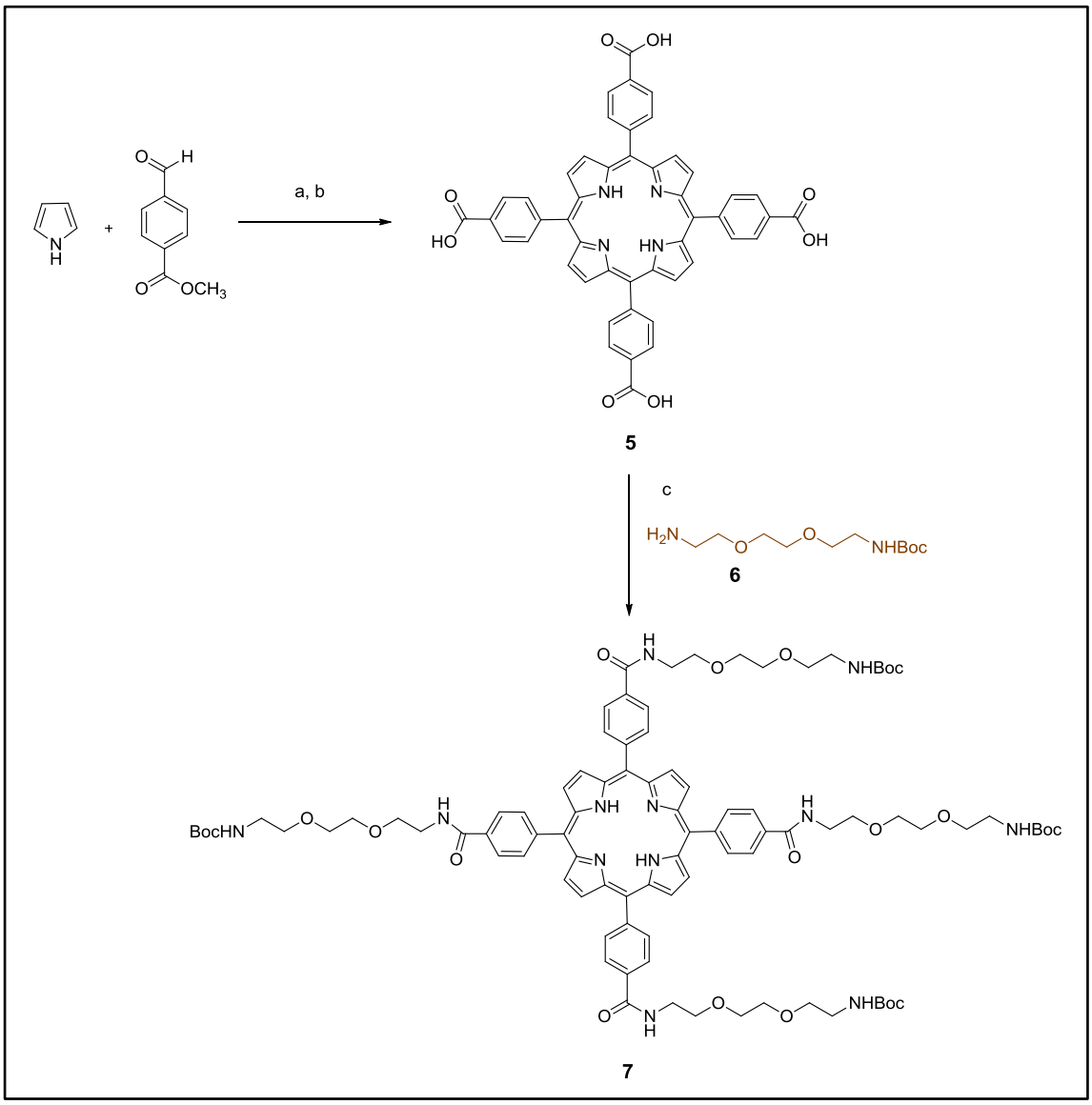

Scheme 2: Synthetic route for **5** and **7**. *Reagents and conditions*: a) propionic acid, reflux, 1,5 h, 21%; b) KOH aq 40%, THF/CH_3OH 2:1, 40°C, 30 min, 91.5 %; c) DMAP, EDCI, HOBt, DMF, 24 h rt, 74%

The Boc amino groups of **7** were then quantitatively deprotected using TFA in CH_2Cl_2 obtaining the intermediate as TFA salt that was used for the following step without purification. The coupling reaction between the hydroxybenzotriazole (HOBt) ester of **4** and the terminal amino groups of the porphyrin intermediate in anhydrous DMF gave after purification by column chromatography, the Boc-protected porphyrin **8** as a purple solid in high yield. The intermediate was quantitatively deprotected using TFA in CH_2Cl_2 and neutralized with TEA to give the neutral fourfold-symmetric porphyrin **9** (Scheme 3). As this compound is very hygroscopic it appears as a sticky purple semi-solid.

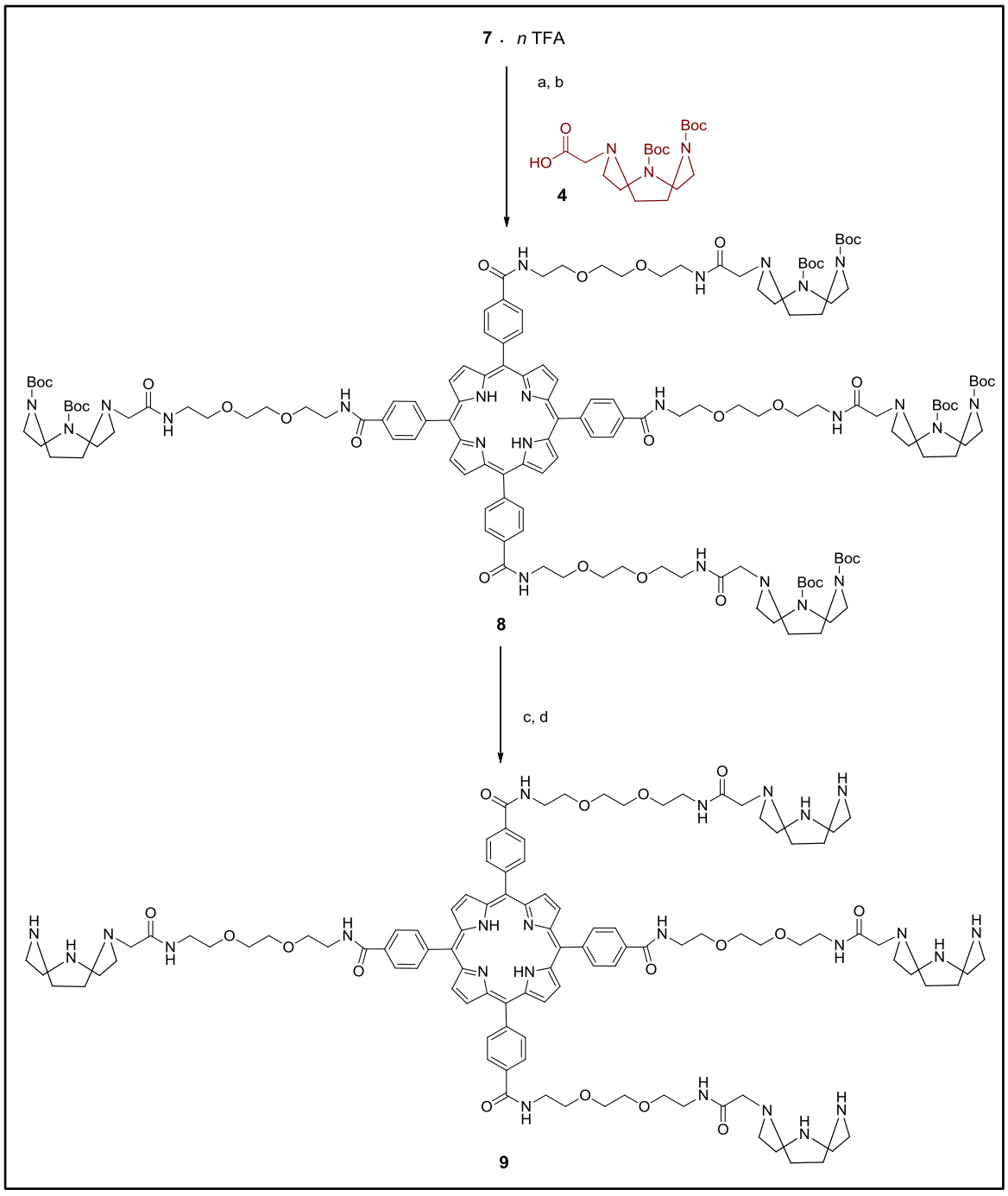

Scheme 3: Synthetic route for **8** and **9**. *Reagents and conditions:* a) TFA, CH_2Cl_2, 2 h, rt; b) DMAP, EDCI, HOBt, DMF, overnight, rt, 66%; c) TFA, CH_2Cl_2, 4 h, rt; d) CH_3OH, TEA, Et_2O, 97%.

The ^{1}H NMR spectrum of **9** in CD_3OD (Figure 15) shows in the downfield region a broad singlet at δ 8.88 of the 8 Hβ and at δ 8.34 two doublets of the 16 H of the phenyl rings. The spacer and TACN protons resonate in the upfield region of the spectrum as eight multiplets and the chemical shifts were assigned by means of the conventional 2D correlation spectra and by comparison with the intermediates previously synthesized and characterized. More in detail, the protons of the four CH_2O groups of

the spacer resonate as four multiplets between δ 3.83 and 3.64 and are bound to carbon atoms that resonate at δ 70 (Figure 16). The multiplet at δ 3.78 accounts both for the protons of one CH_2O and one CH_2NH of the spacer (cross peak respectively at δ 70 and 40 in the HSQC spectrum). The multiplet at δ 3.47 shows two correlation peaks in the HSQC spectrum, suggesting the superimposition of two resonaces: the multiplet of the CH_2NH protons of the spacer (cross peak at δ 39) and the singlet of Hd protons (cross peak at δ 57). The TACN protons resonate as three multiplets at δ 3.22, 3.04 and 2.86. The most upfield multiplet is attributed to the protons in a position and it correlates with a carbon atom at δ 50 in the HSQC spectrum. Since the H-H COSY spectrum shows the correlation between this resonance and the multiplet at δ 3.04, this signal was assigned to protons in b position, while the multiplet at δ 3.22 account for the protons in c position. It is noteworthy that the protons in b and c position correlate with carbon atoms (δ 44 and 45 respectively), bound to the same chemical function, a secondary amino group.

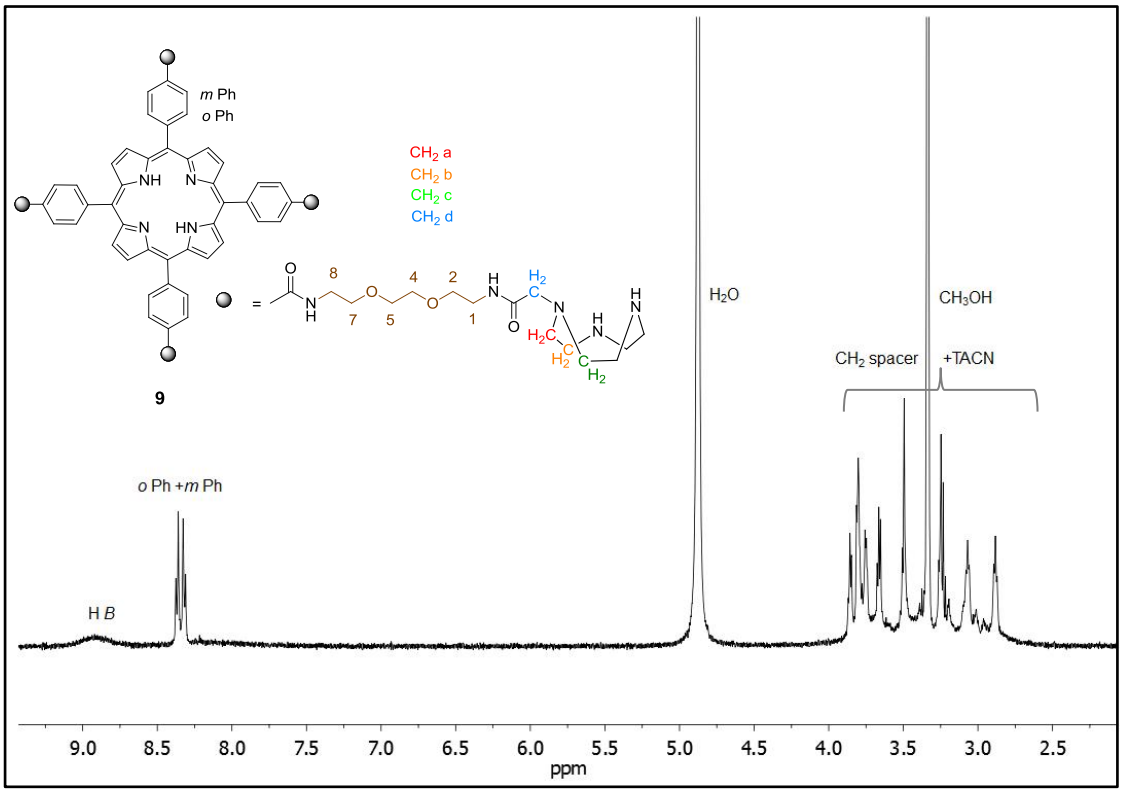

Figure 15: ^{1}H NMR (CD_3OD) of **9**

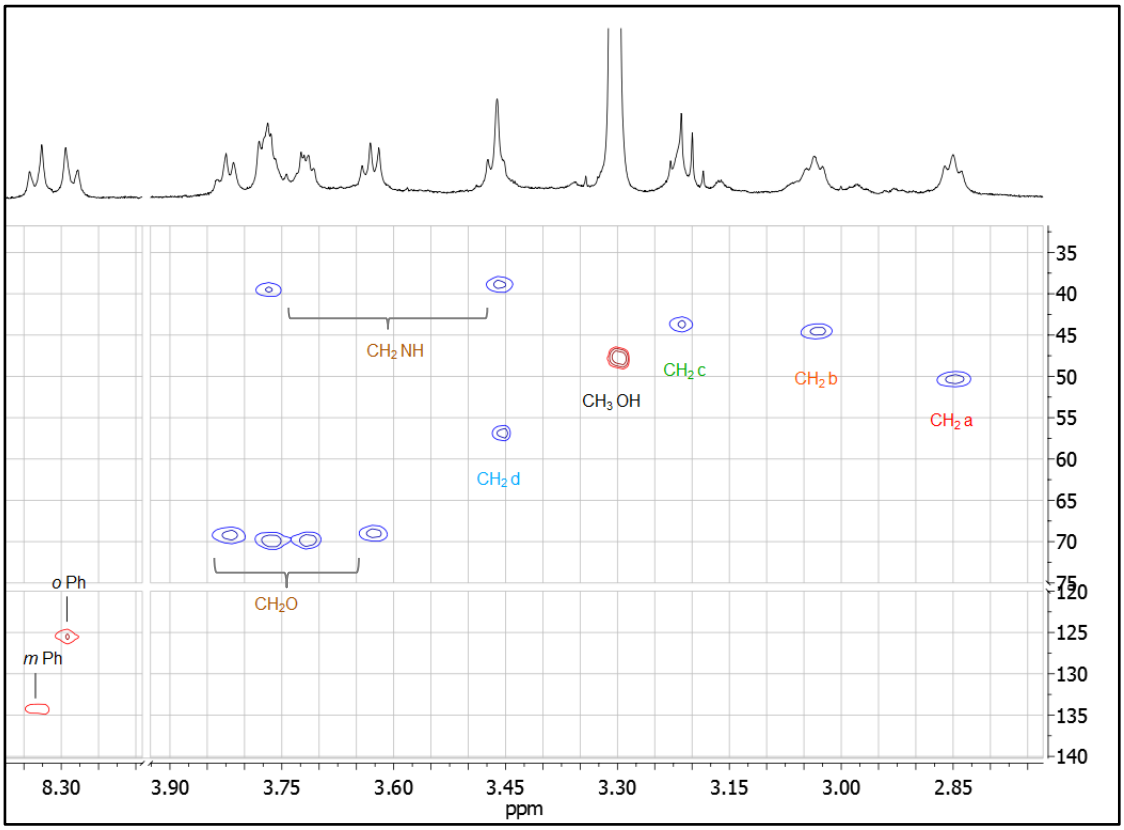

Figure 16: HSQC (CD_3OD) of **9**

Porphyrin 4'-TrPyMMeP (**10**) was synthesized starting from the condensation of 4-pyridylcarboxyaldehyde, methyl 4-formyl benzoate and pyrrole in a 3:1:4 molar ratio under Alder-Longo conditions, followed by accurate chromatographic separations of the statistic mixture of the isomeric porphyrins (Scheme 4) [89].

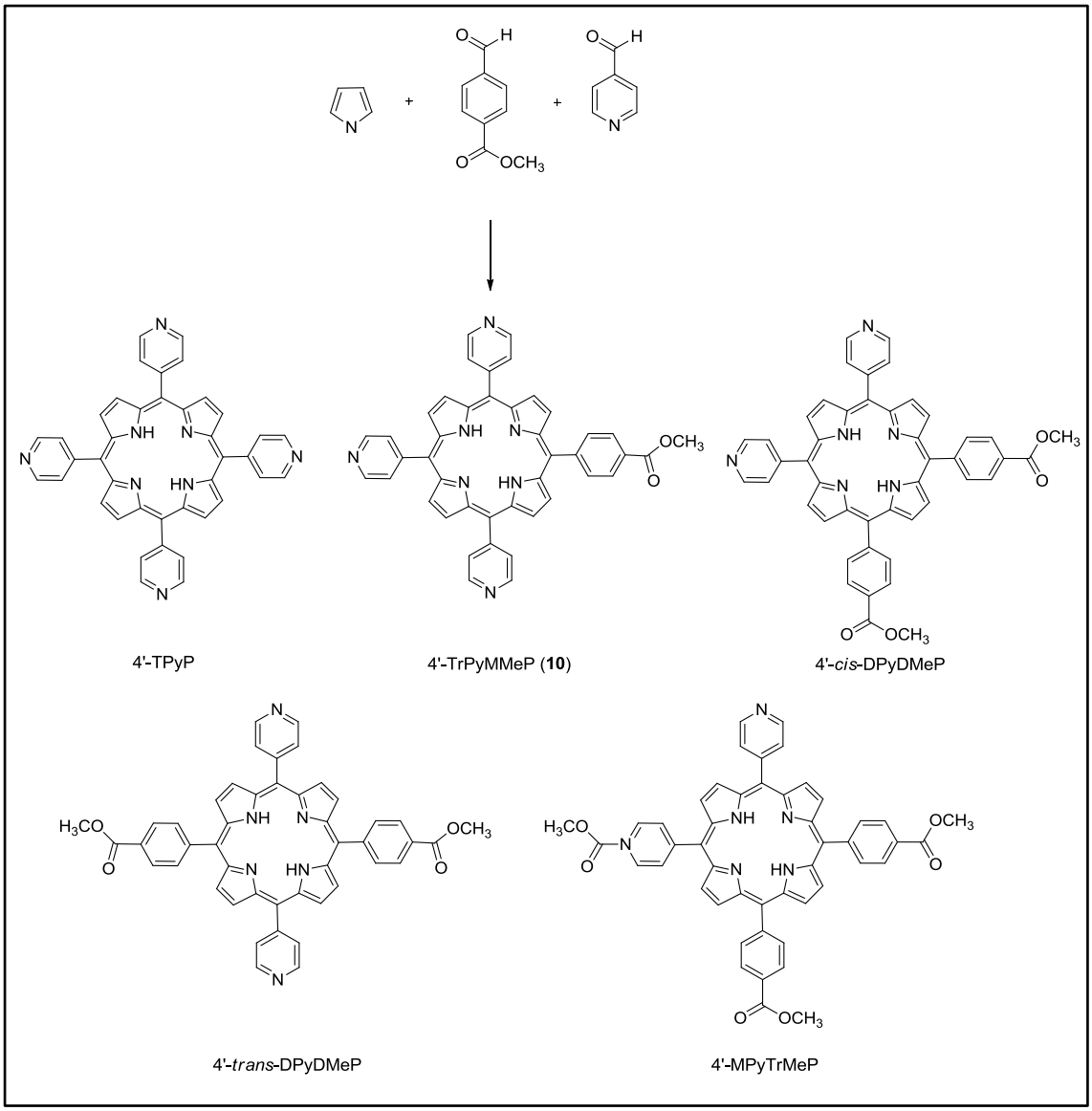

Scheme 4: Synthetic route for 4'-TrPyMMeP. *Reagents and conditions*: propionic acid, reflux, 2 h, CH_3OH/ $C_2H_6O_2$, 6.5% (absolute yield for **10**) , 45.5% (relative yield for **10**)

Hydrolysis of the ester of **10** in THF/CH_3OH under basic conditions gave porphyrin **11** (Scheme 5). The hydroxybenzotriazole (HOBt) ester of **11** was then coupled with the terminal amino group of **6** in anhydrous DMF and, after purification by column chromatography, the Boc-protected intermediate **12** was obtained as a purple solid in high yield. Methylation of this intermediate with excess of methyl iodide in anhydrous DMF gave the tricationic porphyrin **13** as iodide salt in almost quantitative yield. The intermediate **13** was deprotected in acidic conditions obtaining **14** as TFA salt (Scheme 5).

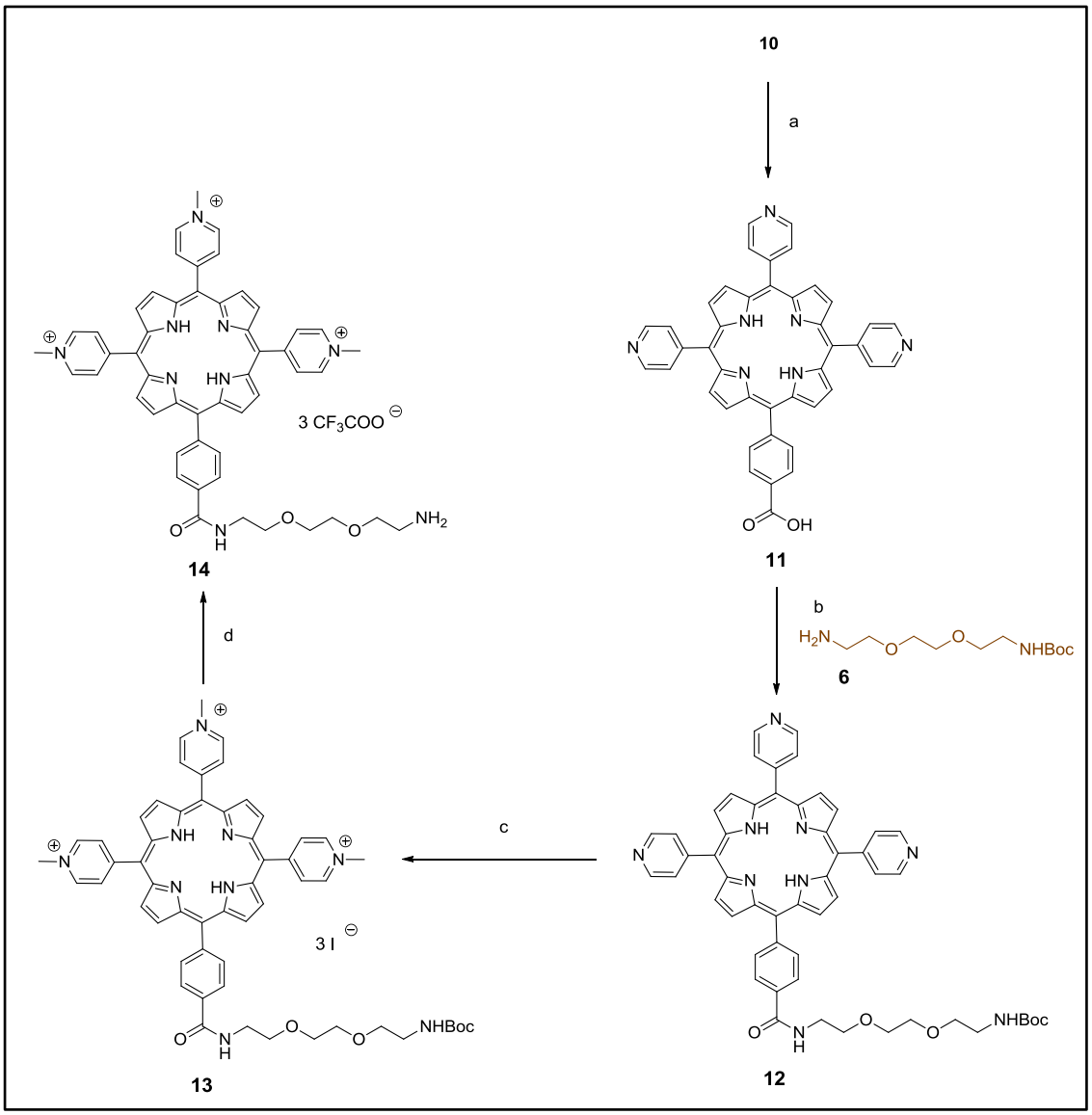

Scheme 5: Synthetic route for **11-14**. *Reagents and conditions*: a) KOH aq 40%, THF/CH_3OH 2:1, 40°C, 5 h, 100 %; b) DMAP, EDCI, HOBt, DMF, 20 h rt, 81%; c) CH_3I, DMF, 90°C, 3 h, 87%; d) TFA, CH_2Cl_2, 3 h, rt, 97%

From the HSQC spectrum in CD_3OD of **14** it was established that the CH_2 bound to the free amino group resonates as a multiplet at δ 3.18 (Figure 17).

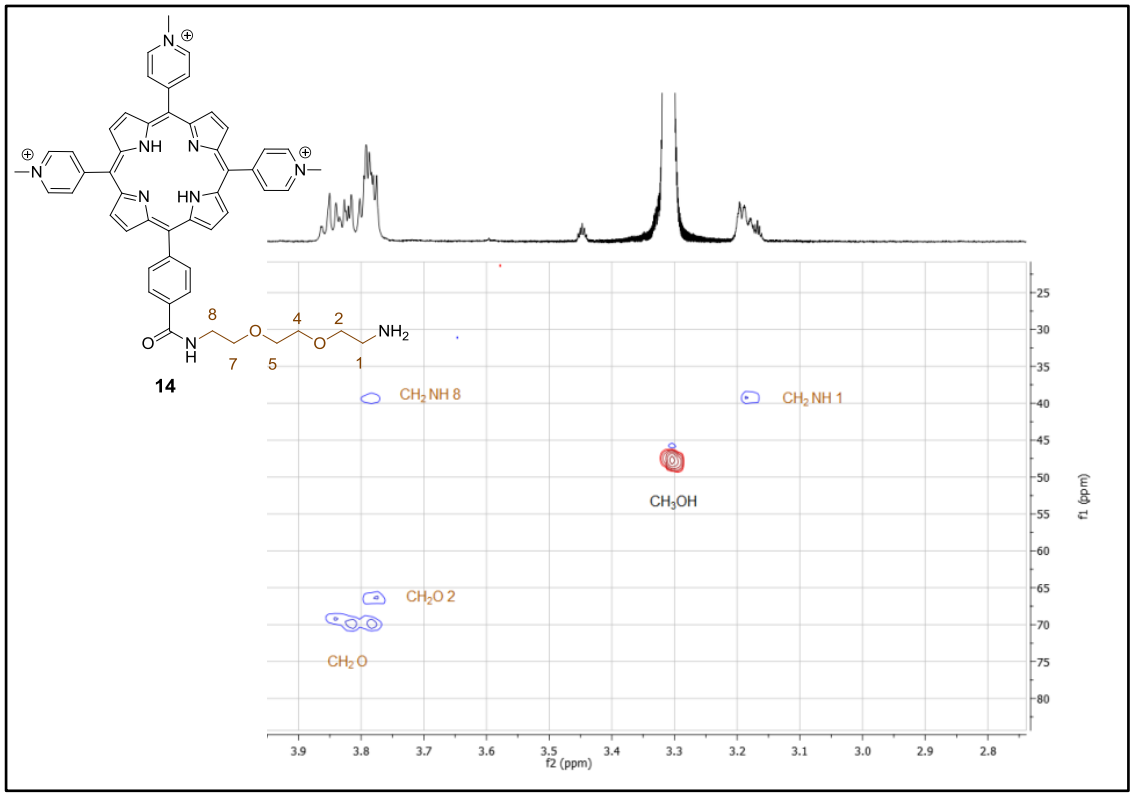

Figure 17: HSQC spectrum (CD_3OD) of **14**, upfield region.

The carboxylic group of **4** was then coupled with the amino group of **14** in anhydrous DMF using HOBt, EDCI and DMAP. The coupling reaction was performed in a microwave oven at 60 °C. This technique was used for it excellent results, since microwave-enhanced chemistry is based on the efficient heating of materials by microwave dielectric heating effects: specific material (solvent or reagent) are able to absorb microwave energy and convert it into heat. Microwave irradiation produces efficient internal heating by direct coupling of microwave energy with the molecules that are present in the reaction mixture [90]. In the coupling reaction to synthesize **15**, the microwave irradiation reduced the reaction time from 24 hours to 6 minutes and increased the yield from 54% to 66%. A higher reaction time and temperature were not used to avoid degradation phenomenon that was observed from the TLC analysis. Compound **15** was purified by several precipitations and washes with Et_2O and CH_2Cl_2. This intermediate was quantitatively deprotected using TFA and treated with TEA to give the +3-charged monofunctionalized porphyrin **16** (Scheme 6).

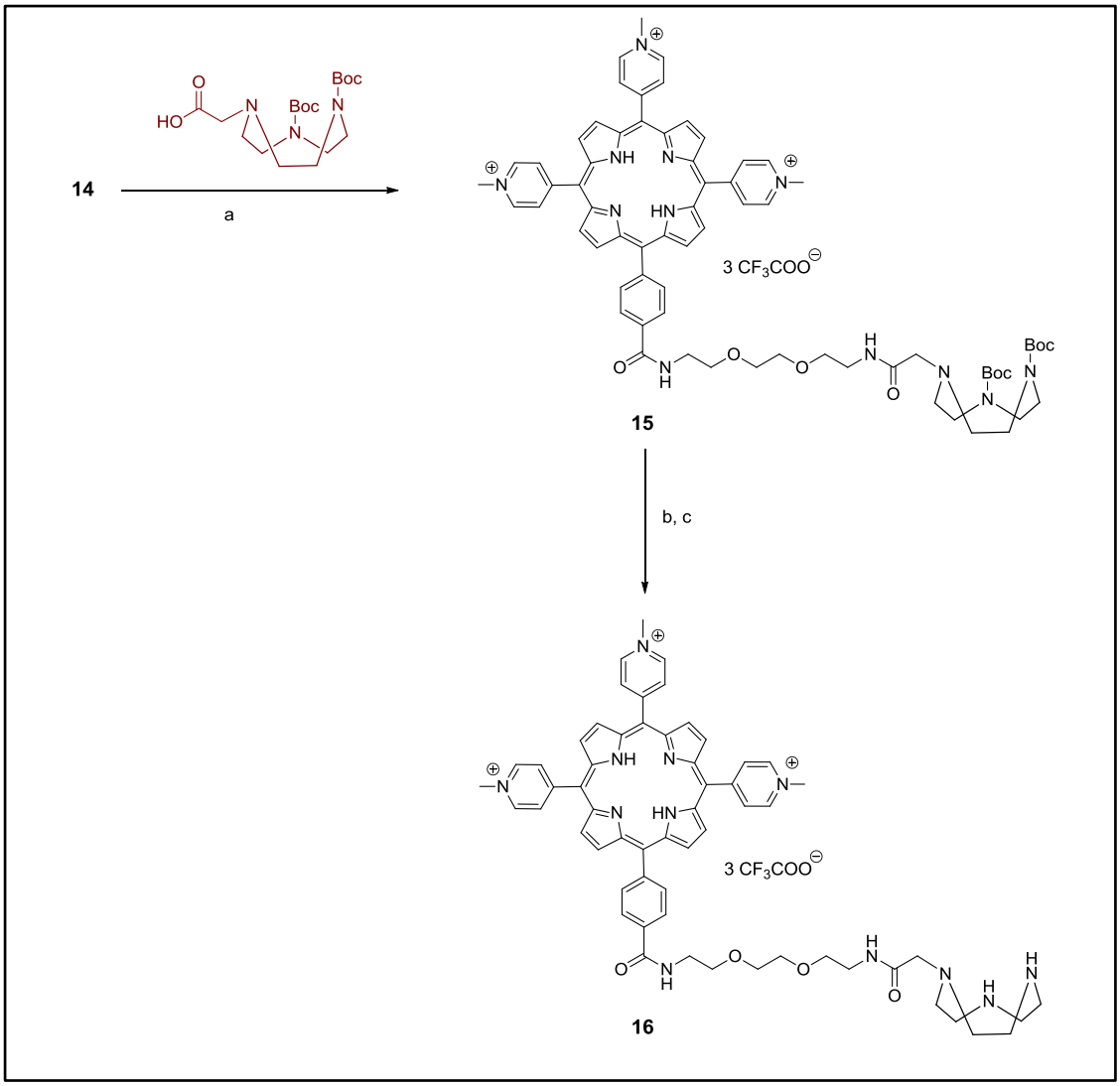

Scheme 6: Synthetic route for **15** and **16**. *Reagents and conditions:* a) DMAP, EDCI, HOBt, DMF, MW 6 min, 60 °C MW 66%; b) TFA, CH_3OH, 3 h, rt; c) CH_3OH, TEA, Et_2O, 98%

The ^{1}H NMR spectrum of porphyrin **16** in CD_3CN (Figure 18) shows in the downfield region two doublets for the pyridyl protons at δ 9.13 (2,6 py) and 8.83 (3,5 py). These protons are bound to carbon atoms that resonate respectively at δ 144 and 133 in the heterocorrelated spectrum (Figure 19). Two multiplets at δ 9.06 and 8.98 are observed for the 8 Hβ and at δ 8.30 the 4 H of the phenyl ring resonate as a multiplet. The resonances of the methyl groups of the pyridyl rings are observed as two singlets at δ 4.69 and 4.70 (cross peak at C48 in the HSQC spectrum, Figure 20). In the upfield region the protons of the spacer and of the chelator resonate between δ 3.79 and 2.82. The multiplets at δ 3.79, 3.72, 3.66 and 3.58 are attributed to the CH_2O groups (cross peaks at C70 in HSQC spectrum). The multiplet at 3.72 accounts also for the 2 H of CH_2NH (cross peak at C39 in HSQC spectrum). The multiplet at δ 3.38 accounts for

the 2H of the CH_2 d and for the 2H of the CH_2NH (cross peak respectively at C57 and C39 in HSQC spectrum). The TACN protons resonate at δ 3.29, 3.02, 2.82 (cross peak respectively at C43, C44, C49 in HSQC spectrum). The H-H COSY spectrum confirms these correlations (Figure 21).

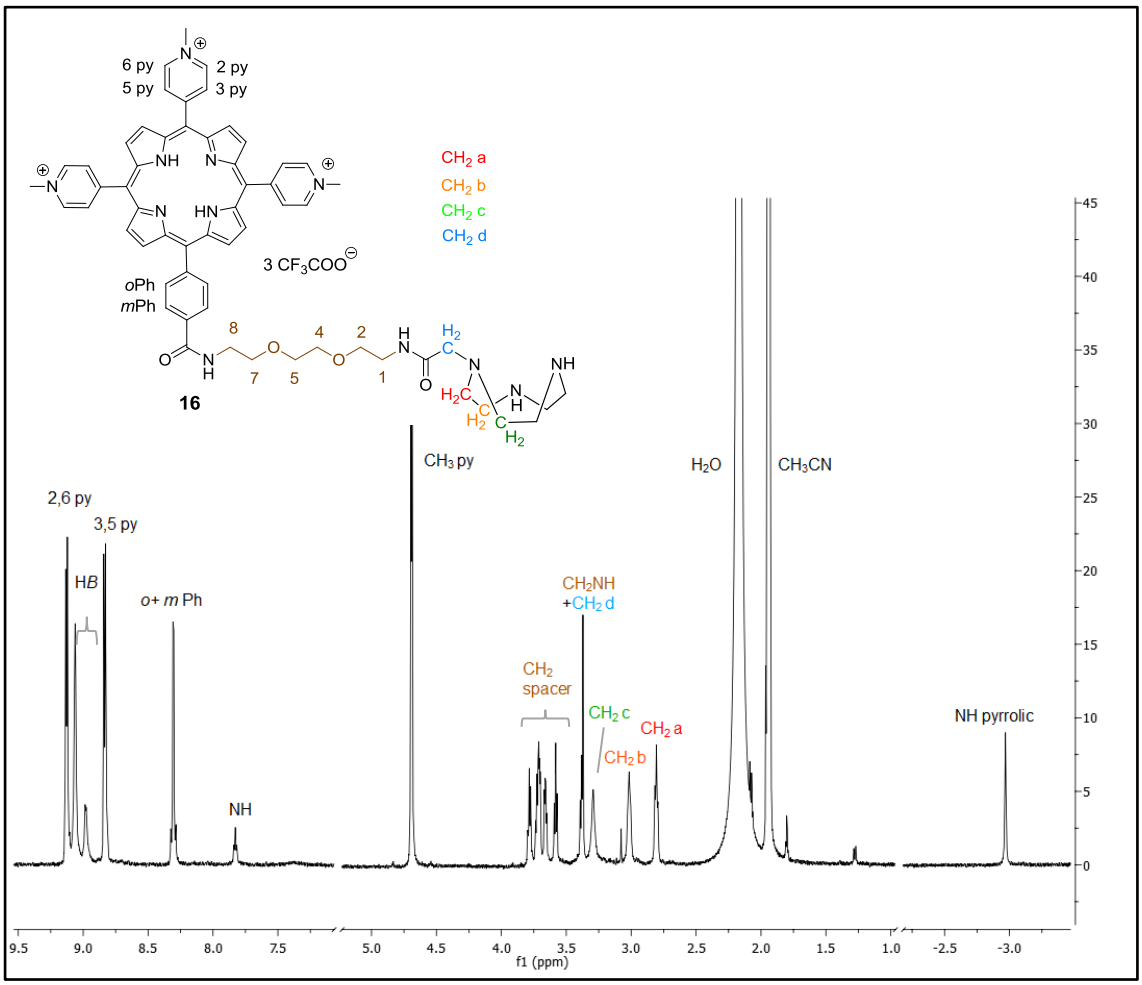

Figure 18: ^{1}H NMR spectrum (CD_3CN) of **16**

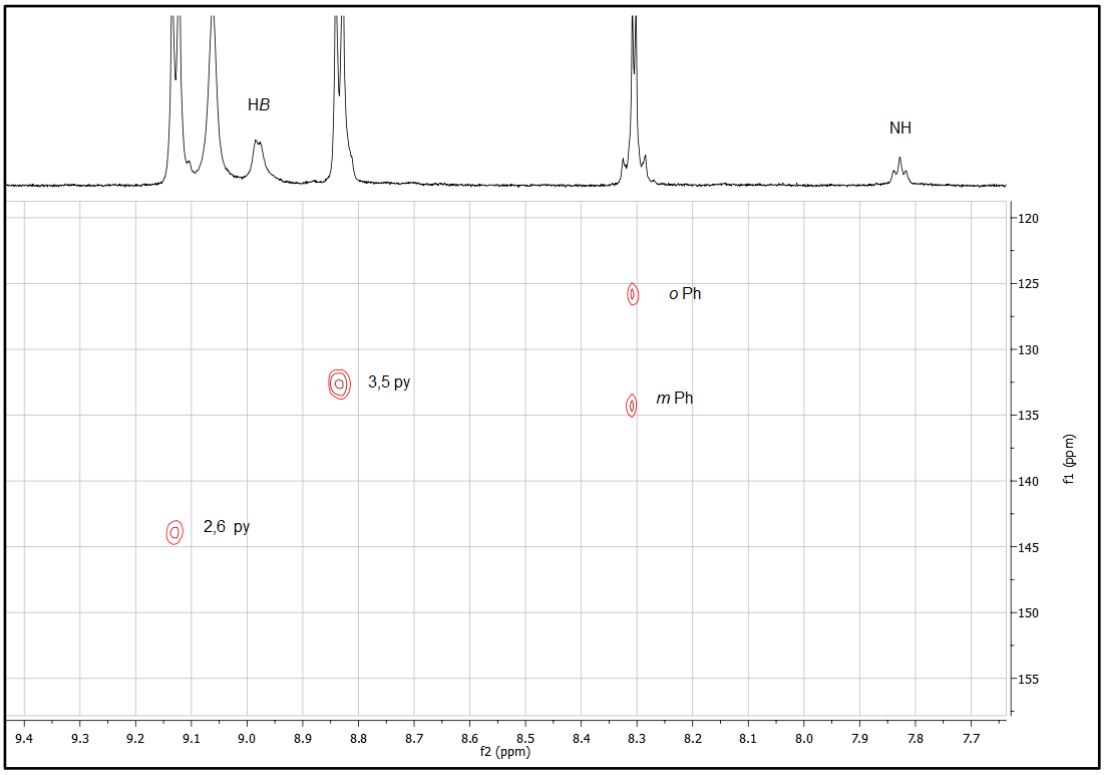

Figure 19: HSQC spectrum (CD_3CN) of **16**, downfield region

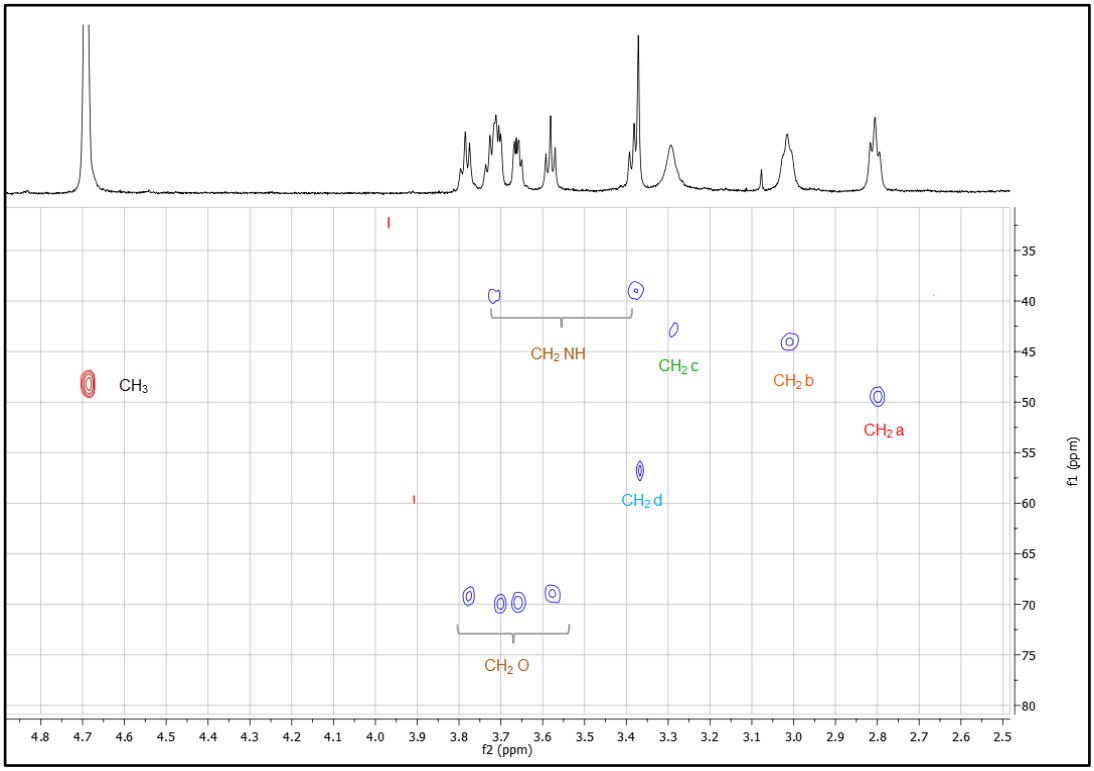

Figure 20: HSQC spectrum (CD_3CN) of **16**, upfield region

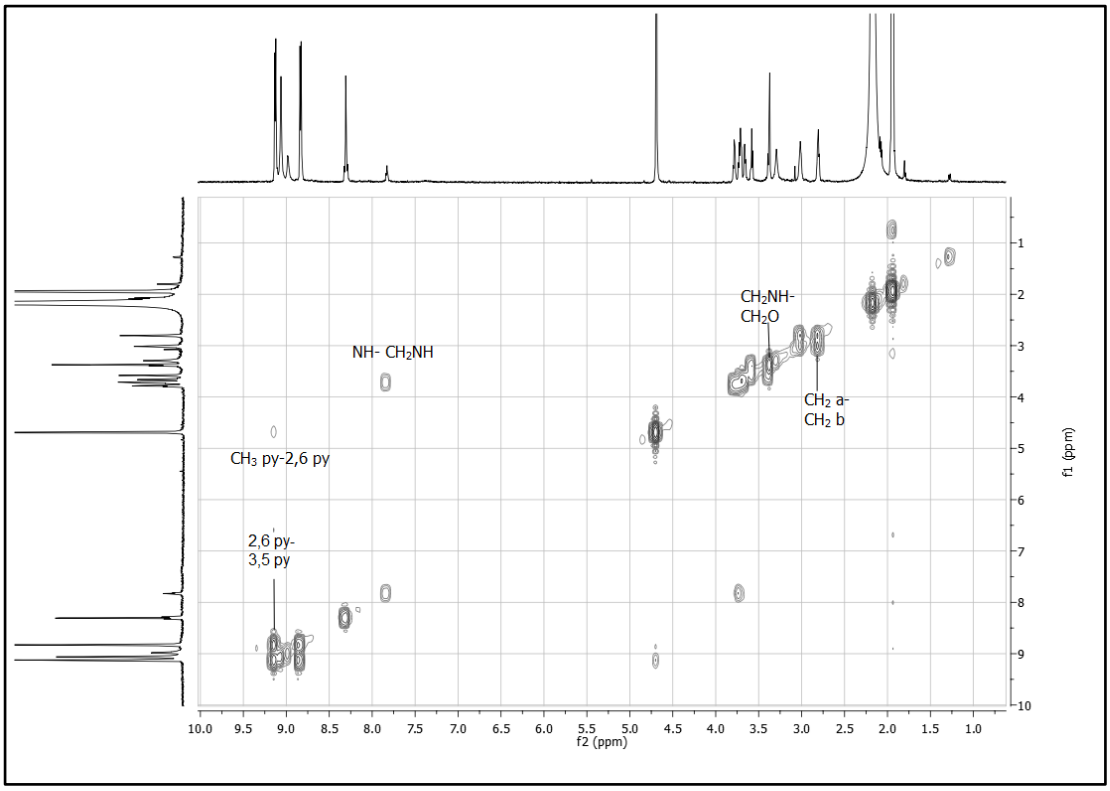

Figure 21: H-H COSY spectrum (CD_3CN) of **16**

Also tris-pyridinium porphyrin **19** was synthesized (Scheme 7). For this purpose the intermediate **12** was deprotected in TFA and neutralized with TEA to give porphyrin **17**. The upfield region of the ^1H NMR spectrum of **17** in CD_3OD was superimposable on the one of the +3-charged tris-methylpyridinium derivate **14**. In Figure 22 the ESI-MS of **17** is reported.

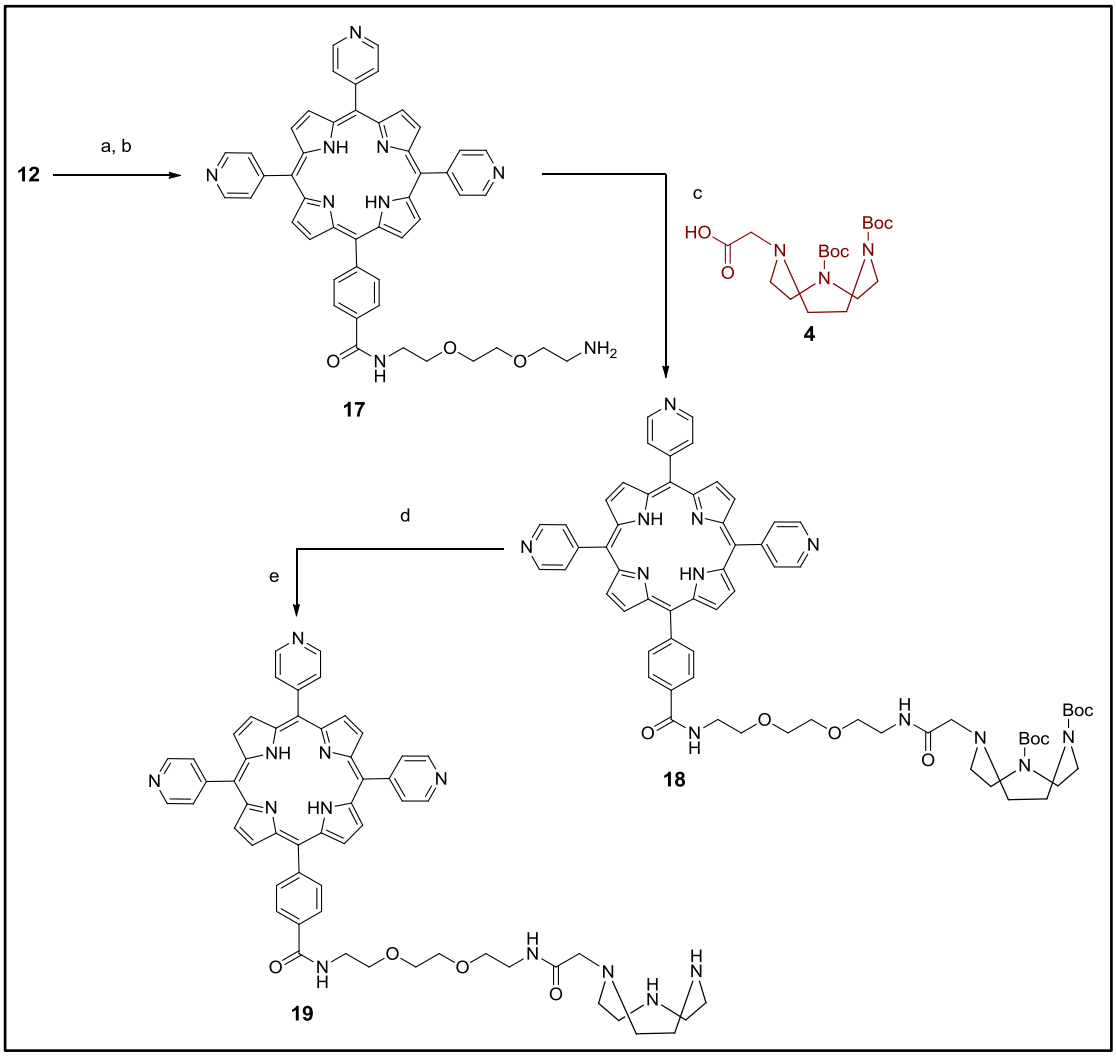

Scheme 7: Synthetic route for **17-19**. *Reagents and conditions*: a) TFA, CH_2Cl_2, 3 h, rt; b) CH_3OH, TEA, Et_2O, 100%; c) DMAP, EDCI, HOBt, DMF, MW 6 min 60°C, 70.5%; d) TFA, CH_2Cl_2, 3 h, rt; e) CH_3OH, TEA, Et_2O, 100%

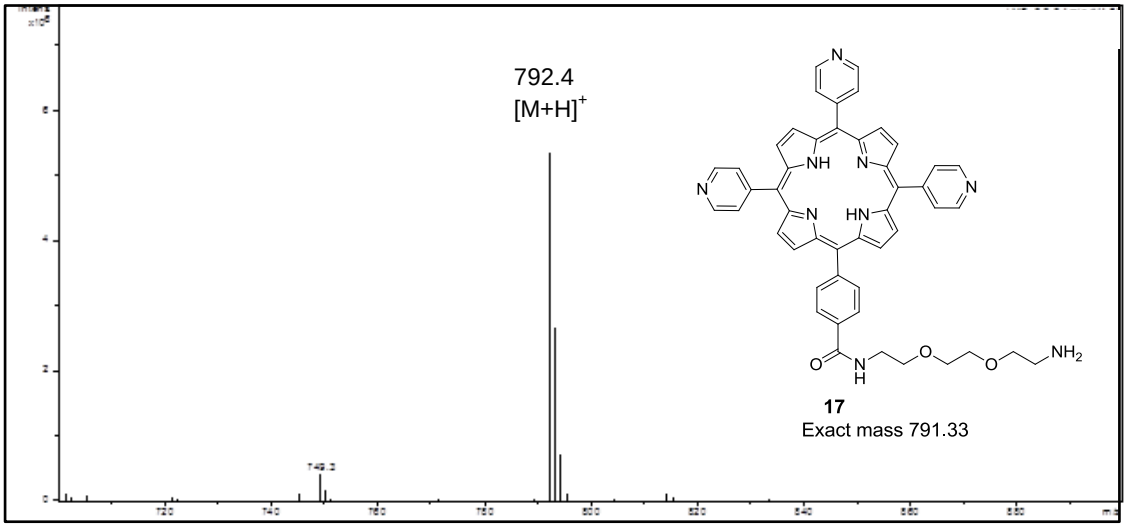

Figure 22: ESI-MS spectrum of **17**

The amino group of **17** was coupled with the carboxylic group of **4** (Scheme 8). The reaction occurred only using microwave heating and EDCI and HOBt as coupling reagents. The purification by column chromatography gave the Boc-protected intermediate **18**. After deprotection and neutralization the neutral tris-piridinium porphyrin **19** was obtained as a dark brown solid. This porphyrin is soluble in H_2O, DMSO, CH_3CN as the +3-charged tris-methylpirydinum porphyrin **16** but also in CH_3OH and CH_2Cl_2. In Figure 23 the HSQC spectrum in CD_3OD of **19** is reported.

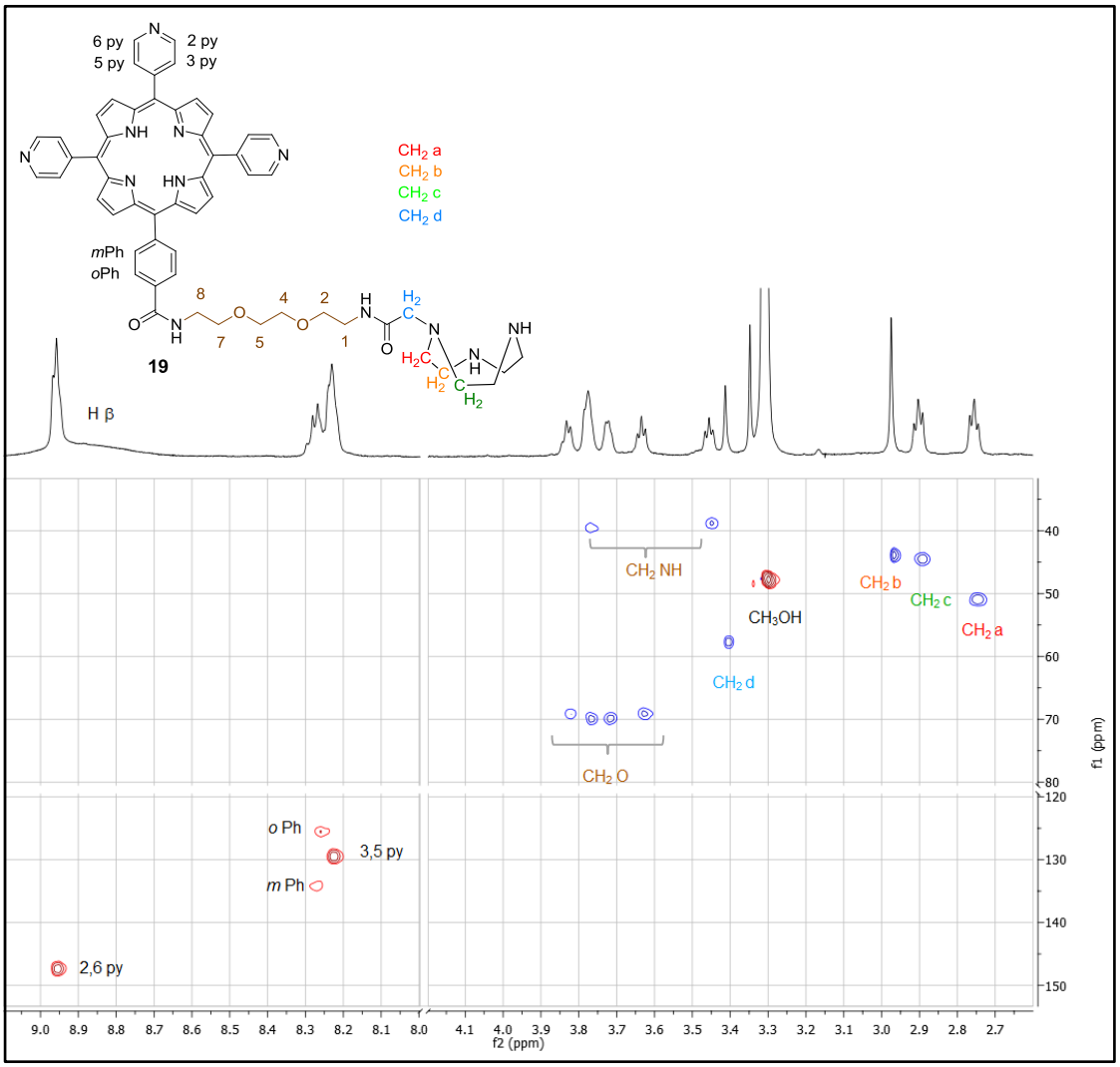

Figure 23: HSQC spectrum (CD_3OD) of **19**

The fourfold symmetric porphyrin **9**, the +3 charged tris-methylpyridinium porphyrin **16** and the neutral tris-pyridinium porphyrin **19** are very soluble in water and this makes them suitable for the labeling with ^{99m}Tc. For this reason it is interesting to synthesize their correspondent rhenium conjugates. We obtained the rhenium conjugates of

porphyrins **9** and **16** but surprisingly we were not able to synthetize the conjugate of the neutral tris-pyridinium porphyrin **19**.

To obtain the rhenium conjugates **20** and **21**, each porphyrin was reacted with the Re(I) precursor $[Re(CO)_3(dmso)_3](OTf)$ (Scheme 8). The rhenium conjugate of the neutral fourfold-symmetric porphyrin **20** was obtained at reflux in anhydrous CH_3OH in argon atmosphere, while the rhenium conjugate of the +3-charged tris-methylpyridinium porphyrin **21** required a microwave reaction. In order to find the experimental microwave conditions, a model coordination reaction of rhenium to the chelator TACN (**1**) was performed in a microwave reactor. After heating for 10 minutes at 110 °C the coordination reaction was complete and compound **22** was afforded in quantitative yield. The ^1H NMR spectrum in D_2O of **22** is reported in Figure 24.

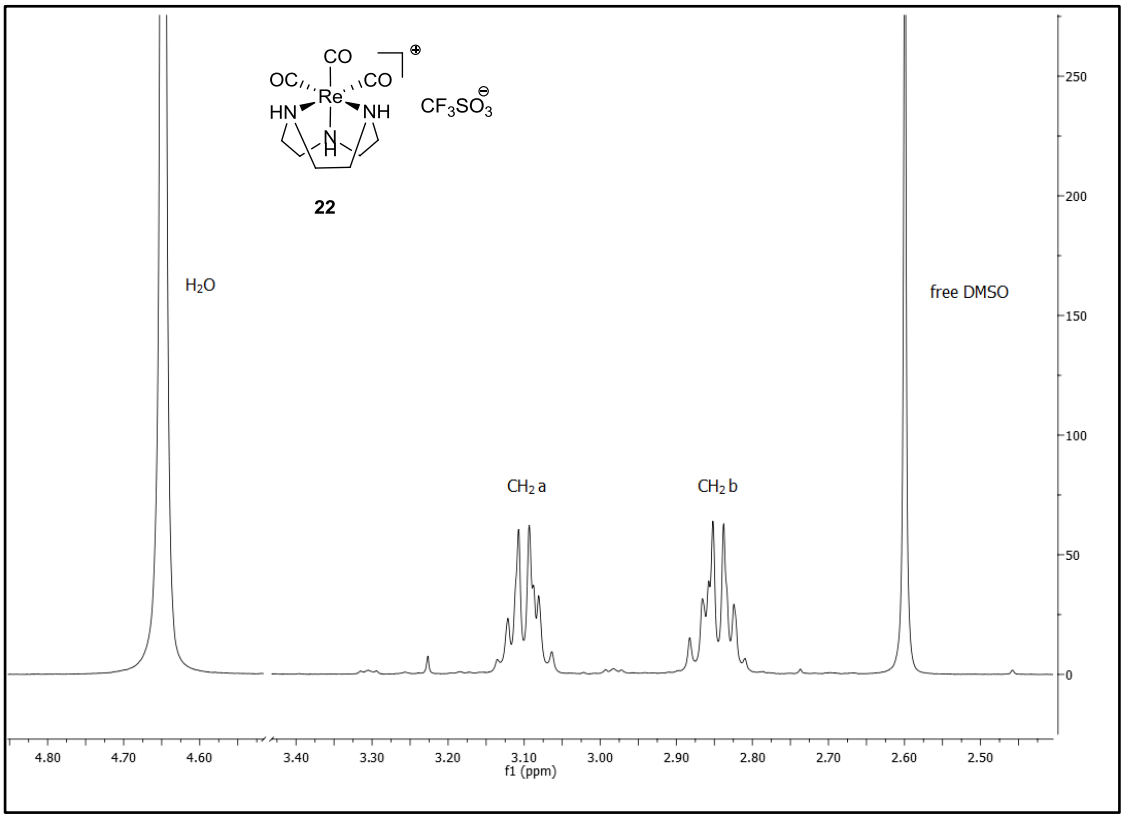

Figure 24: ^1H NMR spectra (D_2O) of **22**

Conjugates **20** and **21** were obtained in high yield and purity and both reactions were monitored by TLC and by recording ^1H NMR spectra of the reaction mixtures at time intervals (Figure 25 and 26).

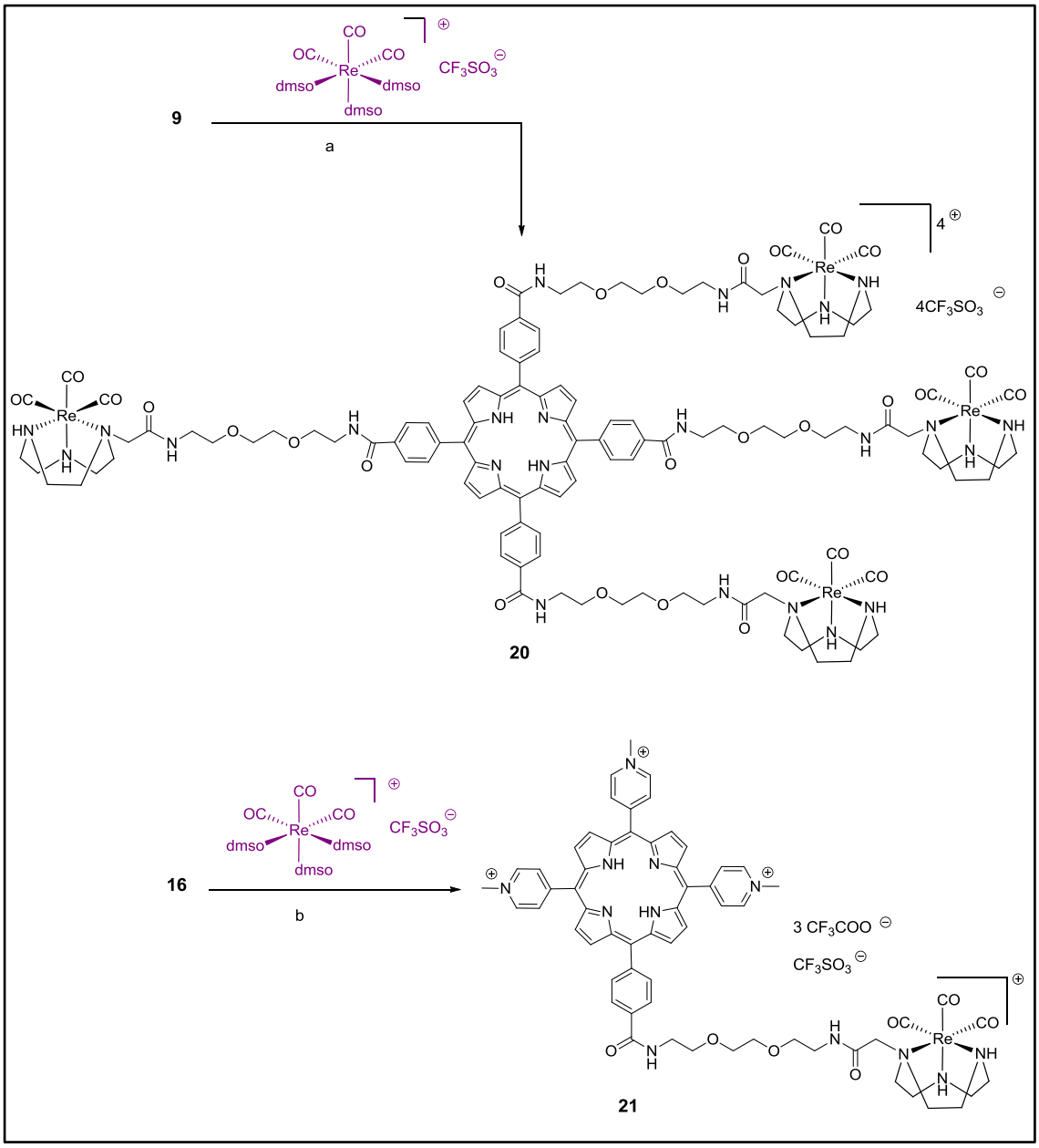

Scheme 8: Synthetic route for **20** and **21**. *Reagents and conditions*: a) anhydrous CH_3OH, 48 h, reflux, 65%; b) anhydrous CH_3OH, MW 10 min, 110 °C, 73%

As a result of the coordination reaction, the resonances of Hd and NH of TACN moved significantly downfield in the ^{1}H NMR spectra of **20** and **21**. These resonances are diagnostic of the product formation and their integration increases over time, as it can be observed for **20** in Figure 25.

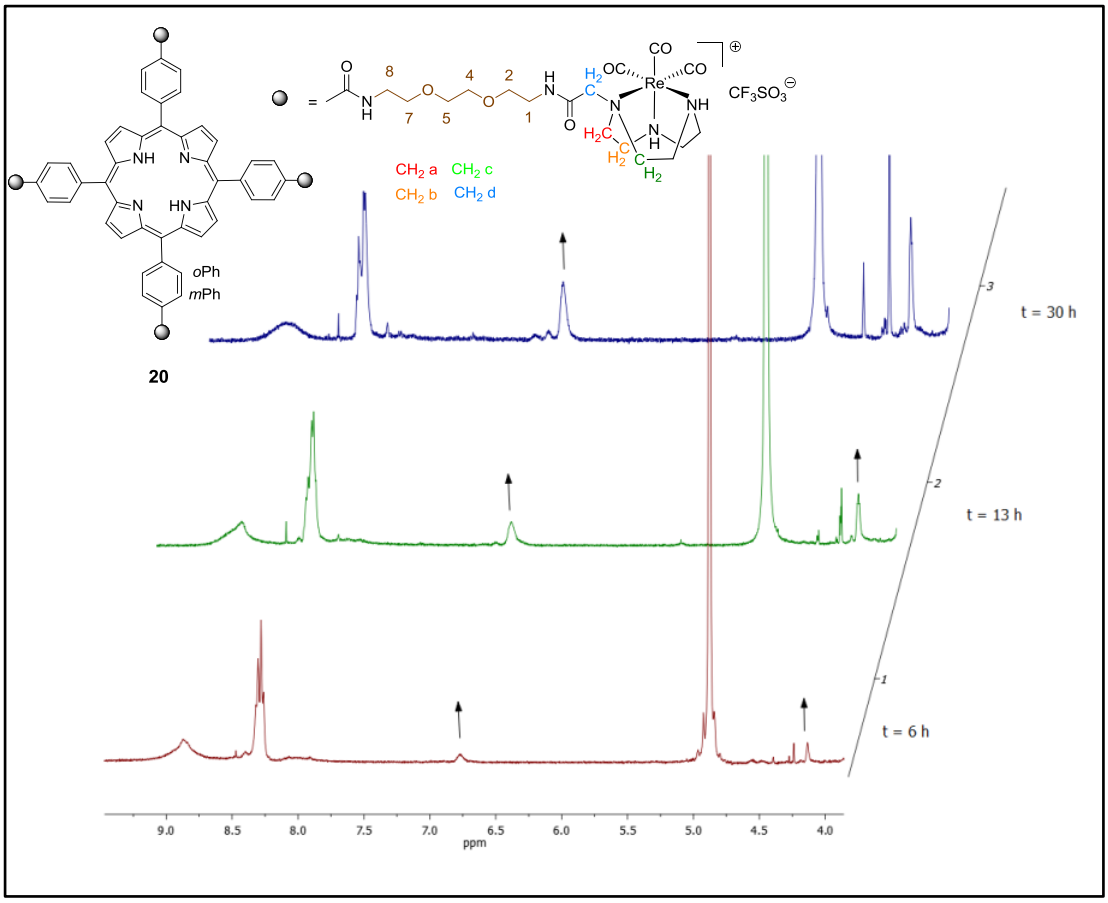

Figure 25: ^{1}H NMR spectra (CD_3OD) monitoring the formation of **20** after 6, 13 and 30 h

In the synthesis of Re-conjugate **21** the proton spectrum recorded after 20 minutes of MW irradiation time showed, besides the Hd singlet, several resonances between δ 4.0-4.3, and this could be due to the degradation of the product (Figure 26). For this reason the reaction was stopped after 10 minutes of irradiation at 110 °C as found in the model reaction.

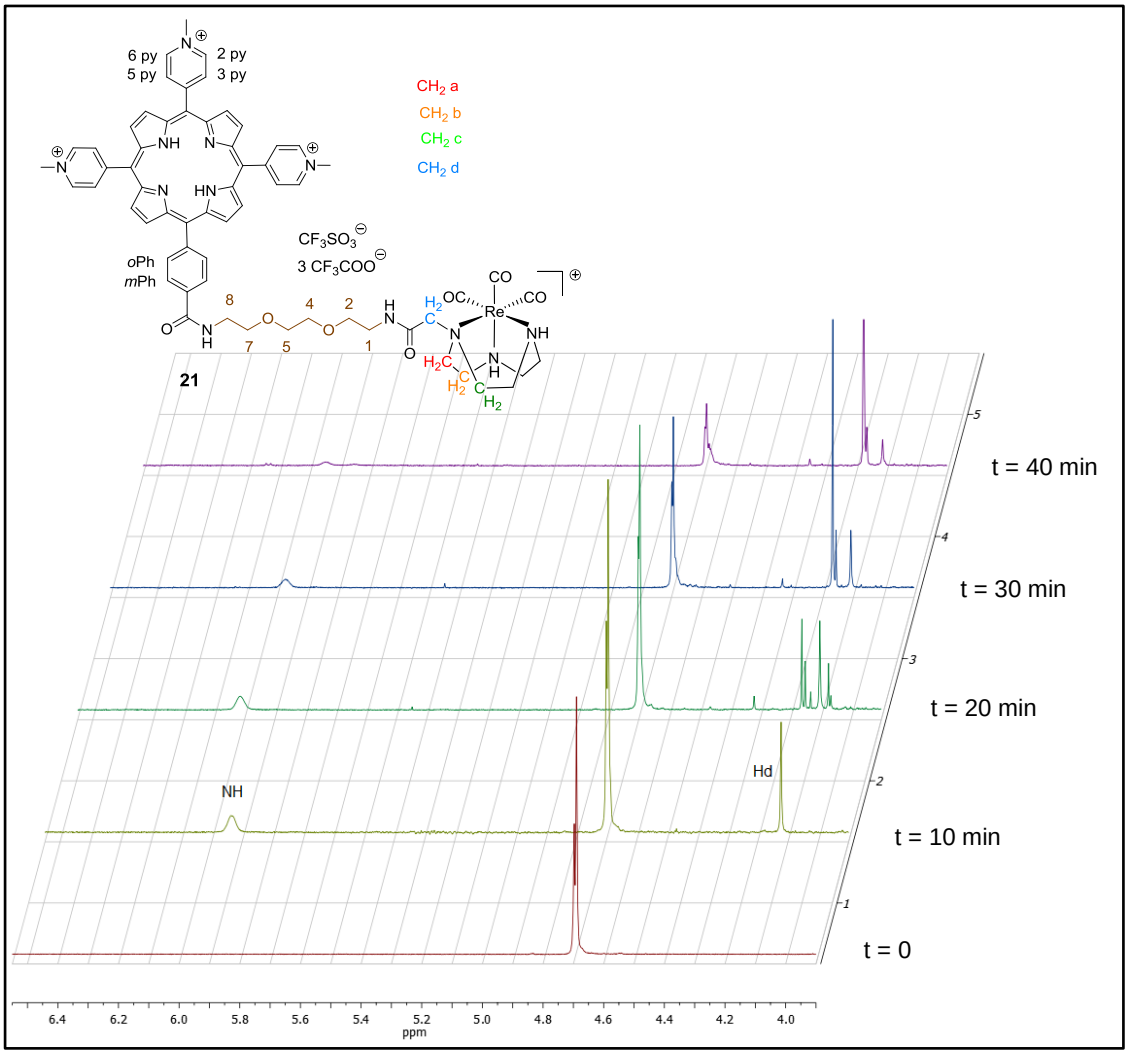

Figure 26. ^{1}H NMR spectra monitoring the formation of **21** in CD_3CN, after 10, 20, 30, 40 min of reaction time in a microwave reactor. Degradation is visible after 20 min of reaction

The rhenium conjugates **20** and **21** show similar mono- and bidimensional spectra. After the Re(I) coordination, the NH of TACN resonate at δ 6.83 and 5.90 respectively for **20** and **21** in the proton spectra . Surprisingly the position of the CH_2 protons of TACN is not substantially influenced upon Re(I) coordination and they resonate as a series of multiplets between δ 3.3 and 2.6. Instead, the resonance of Hd is the most affected since it moved downfield of ≈ 0.7 ppm for both the conjugates (Figure 27, 28).

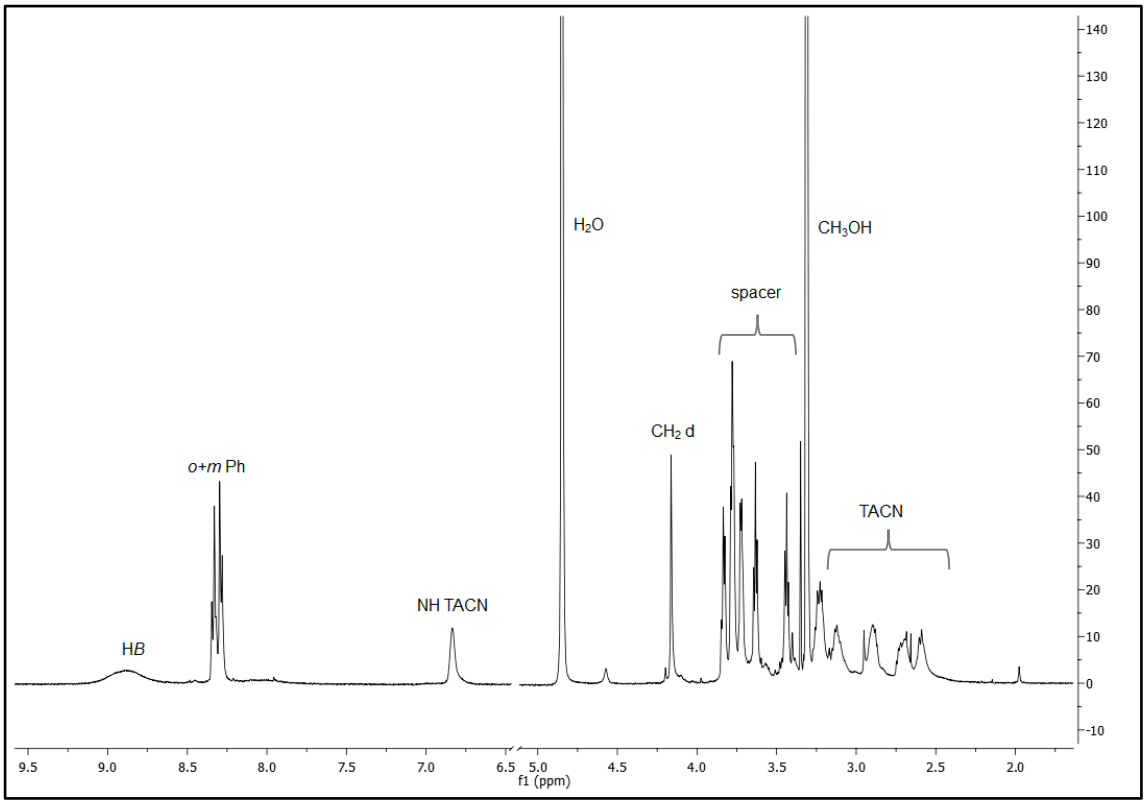

Figure 27: ^{1}H NMR spectrum (CD_3OD) of **20**

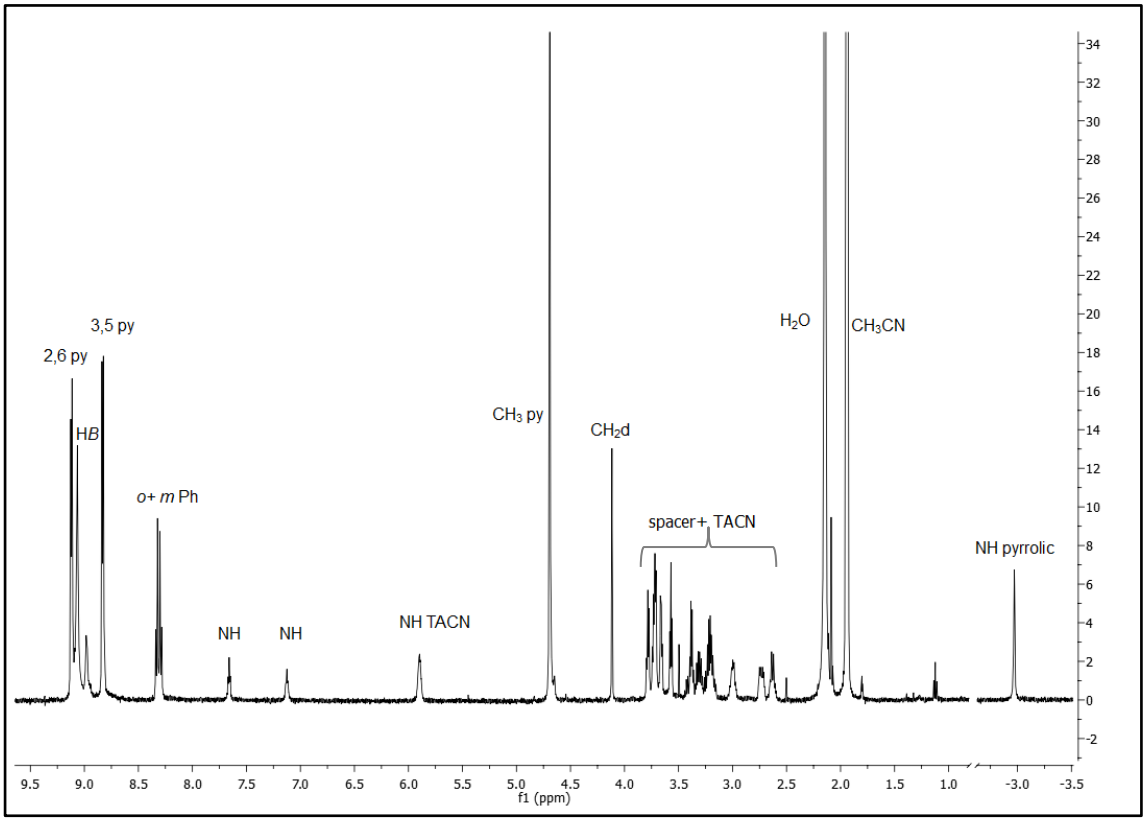

Figure 28: ^{1}H NMR spectrum (CD_3CN) of **21**

Another important feature is that the CH_2 groups of TACN are not anymore equivalent after the metal coordination, and for this reason in the HSQC spectra of both **20** and **21** two cross peaks are found for each methylene group at the same chemical shift of the carbon atom (C56 for Ha, C51 and C49 for Hb and Hc) (Figure 29 and 30).

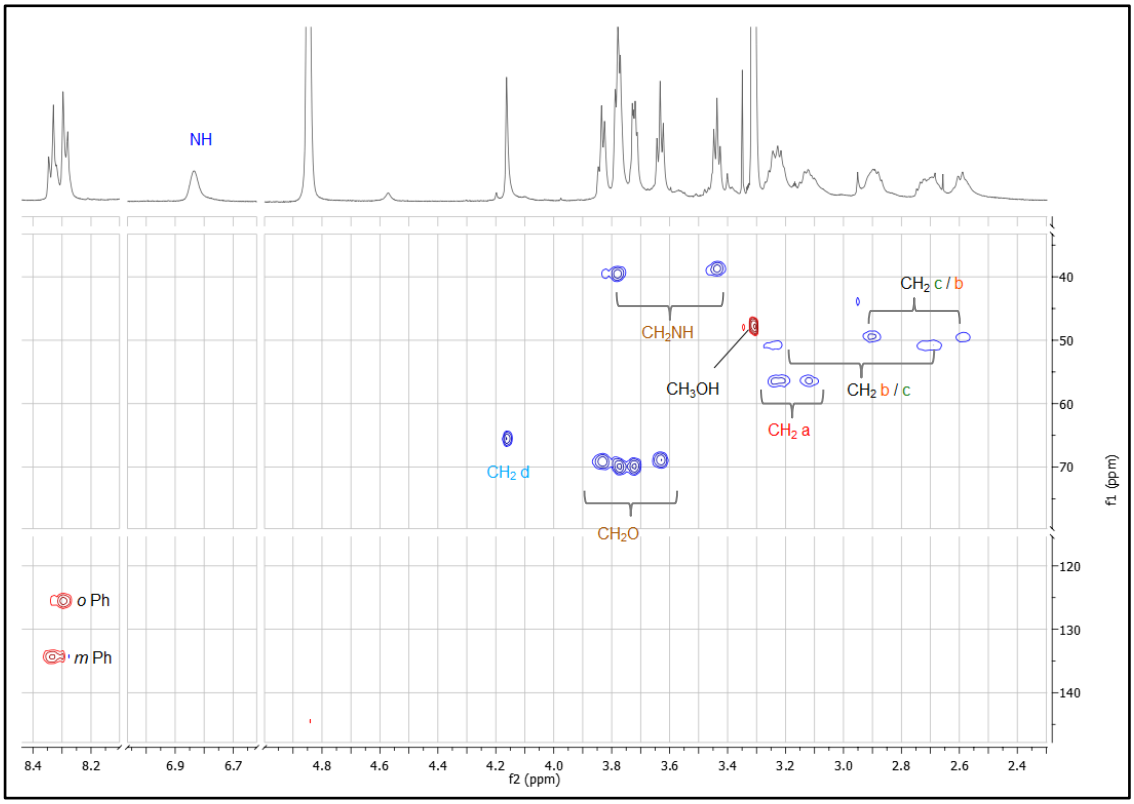

Figure 29: HSQC spectrum (CD_3OD) of **20**

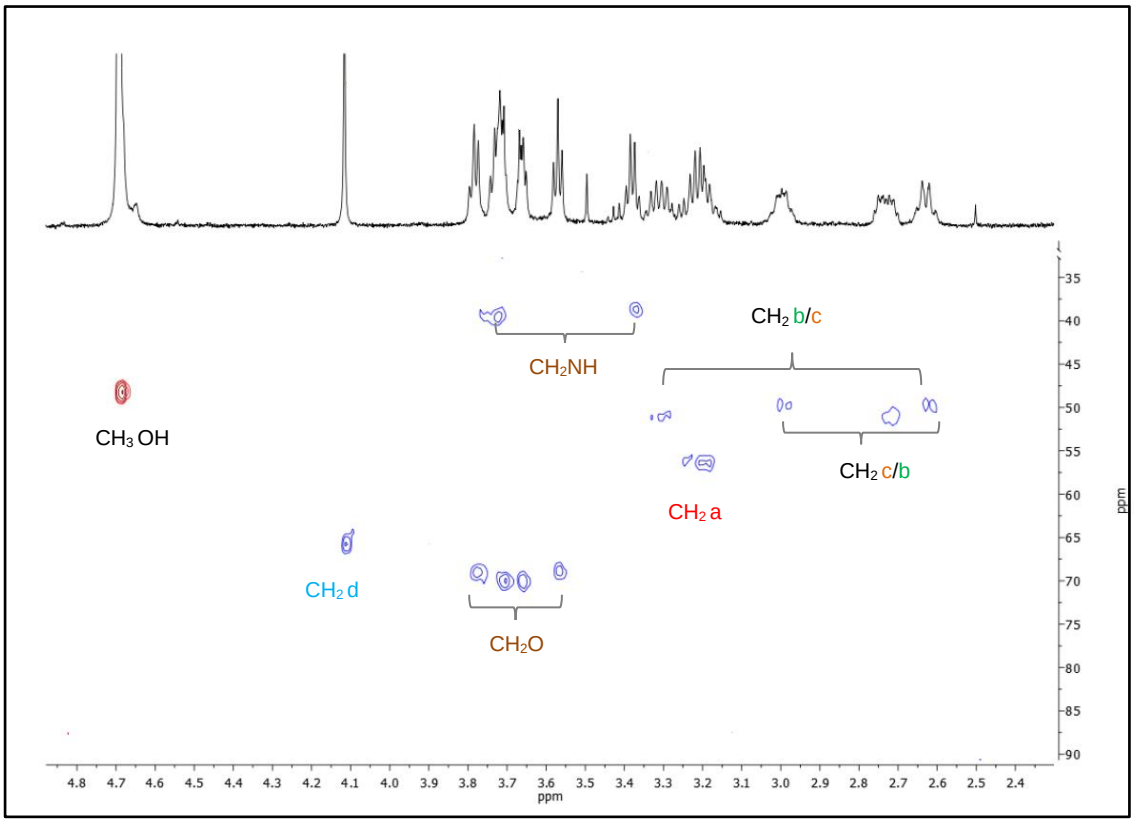

Figure 30: HSQC spectrum (CD_3CN) of **21**

For both conjugate **20** and **21** the Hb and Hc protons of TACN showed strong correlation in the H-H COSY spectrum with NH of TACN (Figure 31).

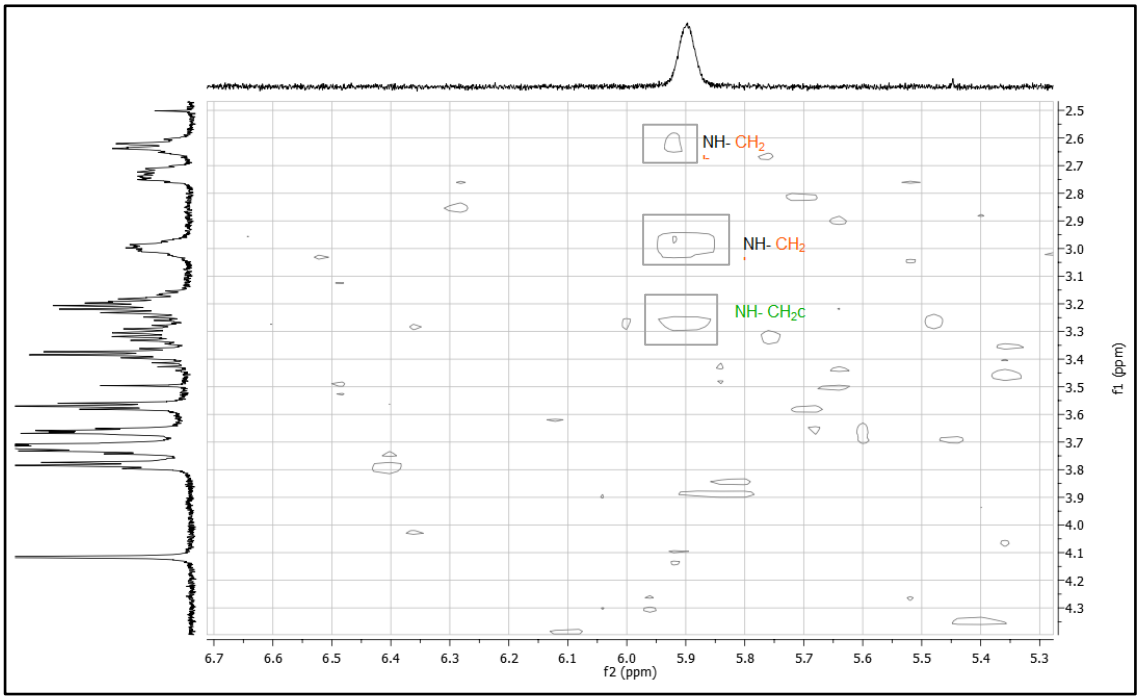

Figure 31: H-H COSY spectrum (CD_3CN) of **21**.

To confirm the coordination of $Re(CO)_3$ unit, an IR spectrum was recorded for both conjugates. The spectrum shows two bands for the stretching of the CO groups of the metal fragment for porphyrin **20** (at 1912 and 2027 cm^{-1}) and **21** (at 1977 and 2104 cm^{-1}). The ^{19}F NMR in CD_3CN of **21** (Figure 32) showed two resonances at δ -79.3 for the fluorine atoms of the triflate ($CF_3SO_3^-$) and at δ -75.4 for the ones of the trifluoroacetic (CF_3COO^-) in a 1:3 ratio. From this data we estimated that **21** contain three triflate and one trifluoroacetic as counter ions.

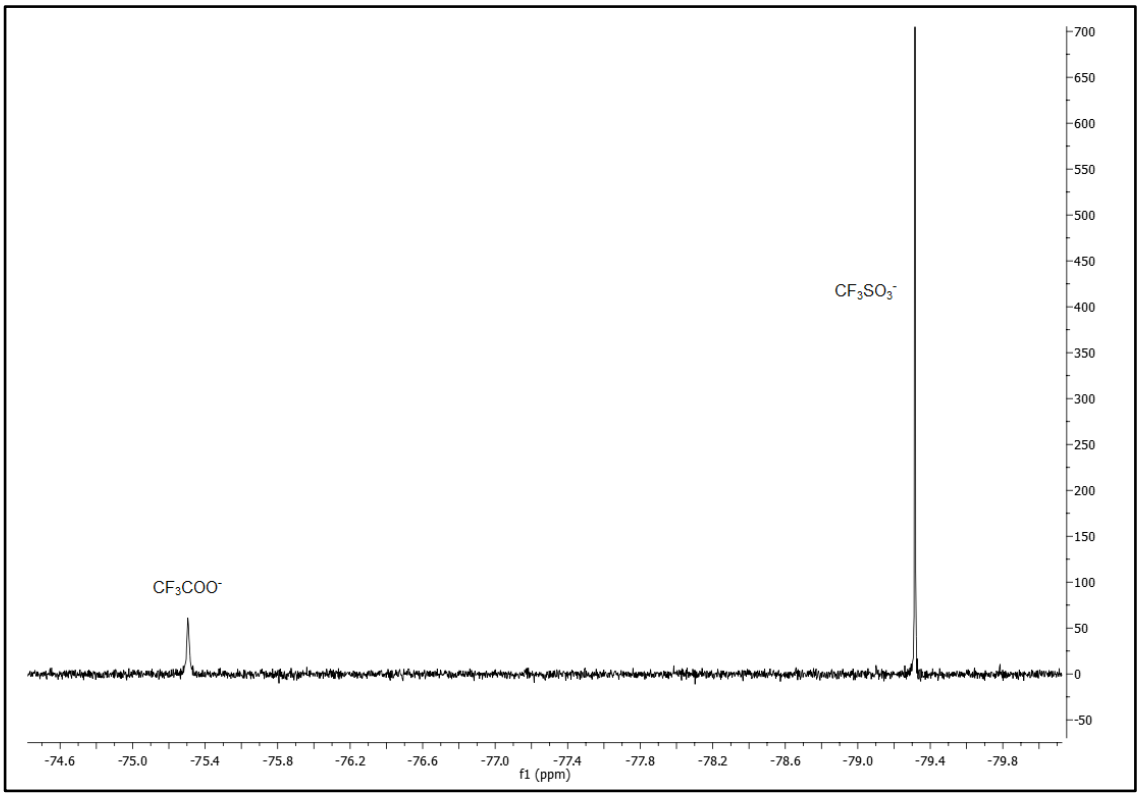

Figure 32: ^{19}F NMR spectrum (CD_3CN) of **21**

2.5. BIOLOGICAL EVALUATIONS OF NEW RHENIUM PORPHYRINS

We decided to evaluate porphyrin **9**, **16** and the Re(I) porphyrins **20** and **21** as potential PSs [39]. For this reason several experiments were performed in particular to assay their (photo)toxicity and their DNA interactions.

2.5.1. (PHOTO) TOXICITY STUDIES

This work was performed in collaboration with Professor Alberta Bergamo - Callerio Foundation Onlus, *Trieste*

The in vitro (photo)toxic effects of the compounds towards the human cell lines HeLa (cervical cancer), H460M2 (non small-cell lung carcinoma), and HBL-100 (non tumorigenic epithelial cells) were evaluated. The photoxicity of compounds **9** and **20** was found to increase upon to the total light dose used: by irradiating tumor cells at increasing total light doses from 1 to 10 Jcm^{-2}, the dose-response curve shifts to the left, and the IC_{50} values correspondingly decrease (Figure 33).

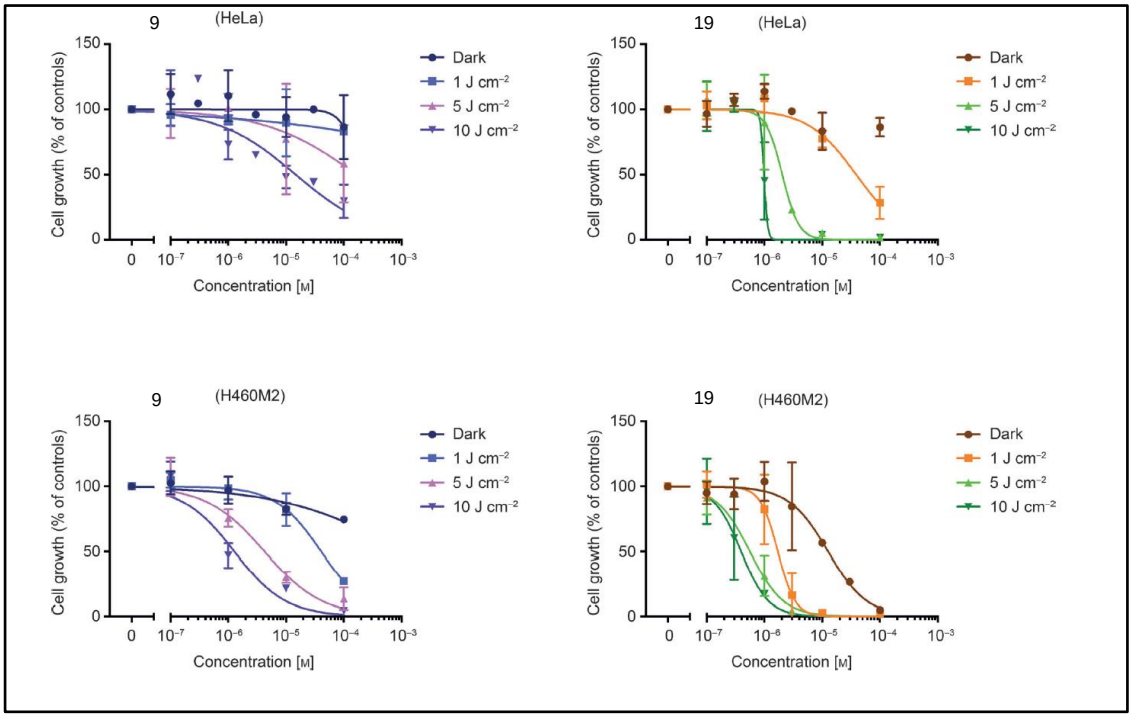

Figure 33: Light dose–effect curves for **9** and **20** as representative porphyrins. HeLa and H460M2 cells were exposed to doses from 0.1 to 100 mm for 24 h, then the cells were irradiated at λ=650 nm with a fluence rate of 14 mW cm^{-2} and total light doses ranging from 1 to 10 J cm^{-2}. Cell cytotoxicity was determined 24 h after the end of irradiation by MTT test.

As it can be observed from Table 2, all compounds were found to be non-cytotoxic in the dark, with the exception of **20**, which proved to be cytotoxic towards both H460M2 and HBL-100 cell lines, with IC_{50} values of 7.4 and 33.7 μM, respectively, but not towards HeLa cells at the maximum concentration used in our experimental settings. This result is consistent with the observations previously reported [55-57] that tetrasubstituted Ru(II)-porphyrin conjugates typically show remarkable cytotoxicity in the absence of light. The negligible dark cytotoxicity of **21** is consistent with the one found for monosubstitute Ru(II)-porphyrins- conjugate by several research groups [91-94].

After exposure to red light, the monofunctionalized compounds **16** and **21** were consistently less active than the tetrafunctionalized compounds **9** and **20** under the same experimental conditions. In particular **16** and **21** are not effective at the lowest light dose (1 J cm^{-2}) on all the cell lines (IC_{50} values >100 μM). Instead, an activity from mild to moderate was always observed at 10 J cm^{-2}, with a greater effectiveness of both porphyrins against the H460M2 tumor cell line (IC_{50}: 13 and 12 μM for **16** and **21**, respectively). A comparison between compound **9** and **20** reveals a greater phototoxic effect of the latter against the HeLa cell line at all light dose (e.g., PI at 10 J cm^{-2} >7.8 and >71.4, respectively). Conjugate **20** showed a PI value >38.5 upon irradiations at 5 J cm^{-2}, which is consistent with the PI of known PSs as photofrin and hypericin [95] (>10 and >43, respectively, at the same light dose) [96]. On the other hand **9** is 77-fold more active after irradiation at 10 J cm^{-2} on H460M2 cells, whereas **20** has much lower PI (>14.8 both at 5 and 10 J cm^{-2}). The cytotoxicity activity of **20** on H460M2 cells in the dark, with an IC_{50} value very close to that found after photo-irradiation indicates a different sensibility between the two cell lines. These results suggest that **20** is not suitable for non-small-cell lung cancers, but it could be used in PDT for other tumor types that similarly show a different sensitivity between dark and irradiated conditions. In compound **21** the rhenium fragment does not enhance the phototoxicity compared to **16**, suggesting that other features (hydrophilicity, permanent positive charges, one flexible arm etc.) might play a major role in determining their phototoxic properties.

		Dark	1 J/cm^2	PI[b]	5 J/cm^2	PI[b]	10	PI[b]
HeLa	**9**	>100	>100	ND[c]	>100	ND[c]	12.9± 3.0	>7.8
	20	>100	32.6±4.4	>3	2.6 ± 1.6	>38.5	1.4± 1.3	>71.4
	16	>100	>100	ND[c]	>100	ND[c]	100± 41	>1
	21	>100	>100	ND[c]	≥100	ND[c]	73 ± 19	>1.4
H460M2	**9**	>100	35.5± 7.7	>2.8	4.3 ± 1.3	>23.3	1.3± 0.6	>77
	20	7.4 ± 2.0	2.8 ± 1.4	>2.6	0.5 ± 0.2	>14.8	0.5± 0.2	>14.8
	16	>100	>100	ND[c]	≥100	ND[c]	13 ± 1	>7.7
	21	>100	>100	ND[c]	58 ± 9	>1.7	12 ± 5	>8.3
HBL-100	**9**	>100	82.0± 7.4	>1.2	4.8 ± 2.9	>20.8	1.4± 0.9	>71.4
	20	33.7±14.55	9.4 ± 3.4	>3.6	1.0 ± 0.3	>33.7	0.5± 0.1	>67.4
	16	>100	>100	ND[c]	76.6± 1.6	>1.3	23.4±2.0	>4.3
	21	>100	>100	ND[c]	75.4± 0.1	>1.3	42.8± 5.3	>2.3

Table 2: Cells were exposed for 24 h to each compound at concentrations 0.1, 1, 3, 10, 30 and 100 μM. Subsequently, cells were irradiated with red light (650 nm) with a fluence rate of 14 mW/cm^2 for increasing time intervals corresponding to total light doses of 1Jcm^{-2}, 5 Jcm^{-2} or 10 Jcm^{-2}. These light doses do not affect proliferation of untreated cells in control experiments. Cell cytotoxicity was determined using the MTT assay 24 h post-irradiation. Cells treated with the same concentrations of the test compounds, but kept in the dark, were used as controls. Statistics: ANOVA Analysis of variance and Tukey-Kramer post test. Statistical analysis is not reported in the table.

b: PI = IC_{50} in the dark/IC_50 upon irradiation.

c: ND = not determinable

2.5.2. DETERMINATION OF SINGLET OXYGEN QUANTUM YIELDS (Φ_Δ)

As it was already described, the main mechanism of action in PDT involves the generation of $^1O_2$ after photoexcitation of the PS. For this reason $^1O_2$ quantum yield (Φ_Δ) of the compounds was evaluated in DMSO. Tipically a clinically useful PS has Φ_Δ value of ~0.5 [97]. Among the investigated porphyrins, the best singlet oxygen generator was **9** (Φ_Δ = 0.63) while compounds **16**, **20** and **21** had lower values (Φ_Δ= 0.31, 0.20, 0.19 for **20**, **16** and **21** respectively). However, despite being the best $^1O_2$ generator, **9** showed lower potency than **20** in the phototoxicity assay, probably due to its low cellular uptake. Instead the low Φ_Δ value of **16** and **21** might be related to their low activity on all cell lines after light irradiation. Since the Φ_Δ values were determined in DMSO that is a different environment of the in vivo conditions, the phototoxic potencies of the compound are not predictable only on the basis of their Φ_Δ values.

2.5.3. CELLULAR LOCALIZATION STUDIES

This work was performed in collaboration with Dr. Vanessa Pierroz and Professor Gilles Gasser - Department of Chemistry, University of Zurich

The intracellular localization in HeLa cells of the compounds was determined using confocal fluorescence microscopy. After incubation for 2 h at 20 µM only compound **20** displayed a significant cellular internalization. These data are in agreement with the antiproliferative experiments. However, upon light irradiation compound **9** and **21** showed toxicity, indicative of probable uptake. Consequently, to investigate their localization we increased the treatment concentration to 100 µM. Porphyrin **9** displayed the lowest accumulation signal inside the cell, with red luminescent speckles localized in the cytoplasm (Figure 34, a). Compounds **20**, **16** and **21** showed a similar pattern with a diffused and more intense luminescence localized in the cytoplasm and to a very minor extent in the nucleoli (Figure 34, b,c, and d, white arrows), as indicated by comparison with DAPI staining. The intense red luminescence of **20** suggests that was more efficiently taken up inside the cell than the other three compounds used in this study.

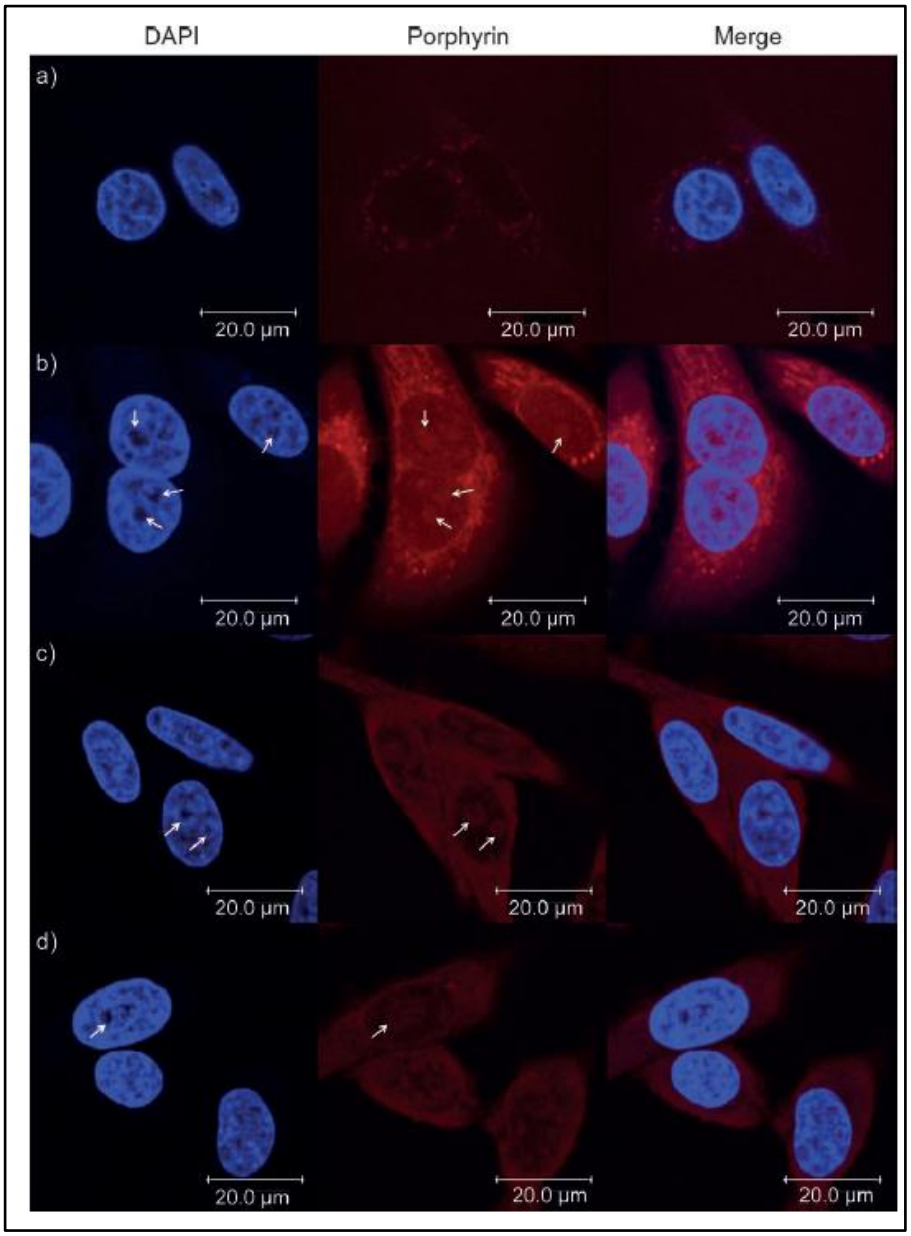

Figure 34: Fluorescence confocal microscopy images showing the pattern of HeLa cells incubated for 2 h with a) 100 µM **9**, b) 20 µM **20,** c) 100 µM **16**, and d) 100 µM **21**, fixed in formaldehyde and stained with mounting solution containing DAPI (Vectashield, 1.5 µg mL^{-1}). White arrows indicate the nucleoli.

2.5.4. DNA BINDING STUDIES

This work was performed in collaboration with Dr. Anna Leczkowska and Professor Ramon Vilar - Department of Chemistry, Imperial College London

Although low nuclear localization was observed for some of the porphyrins, it still promoted us to investigate their capacity to bind both quadruplex and duplex DNA. The ability of the compounds to recognize and bind to DNA structures such as quadruplex-

forming sequences (Myc22 and H-telo), and duplex (ds-26) was investigate using emission spectroscopy. In Figure 35 the excitation and emission spectra of the studied compounds in the absence of DNA are reported.

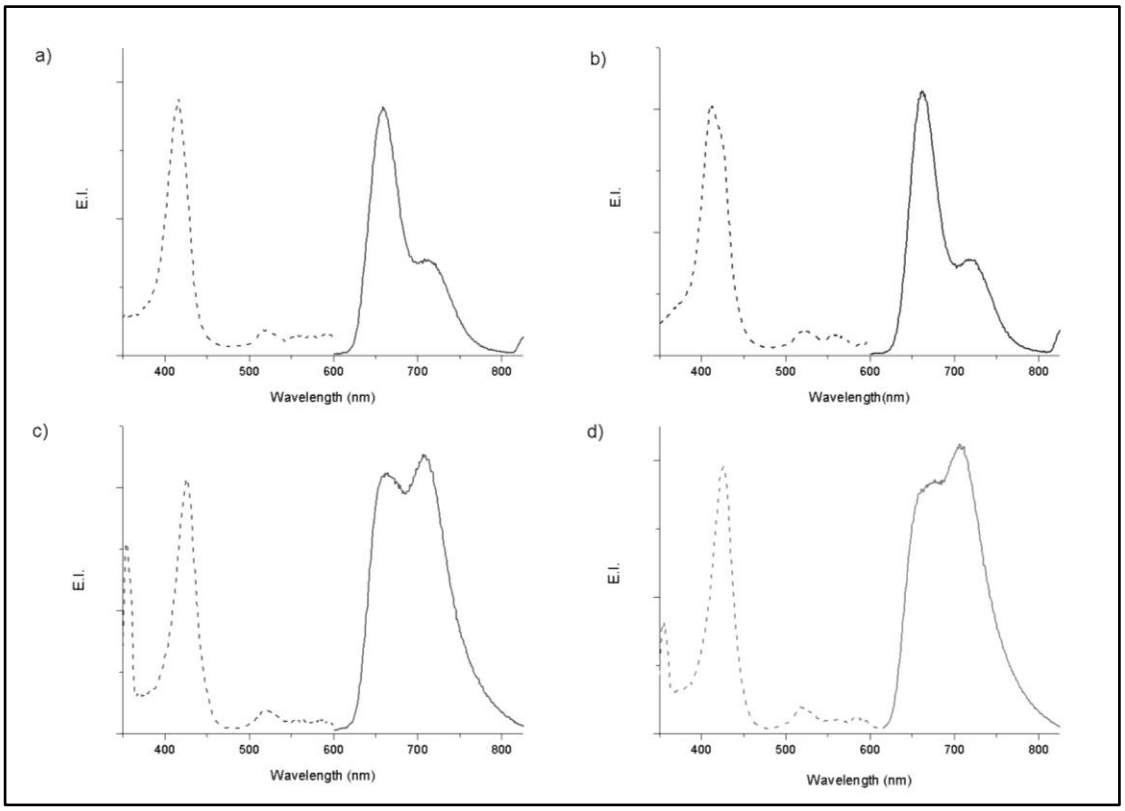

Figure 35: Excitation (dotted) and emission (solid) spectra of **9** (a), **20** (b), **16** (c), **21** (d) in the absence of DNA (the spectra are not on the same scales)

In all the cases the interaction with DNA causes red shifting of the excitation/absorption bands of each porphyrin, while different changes were observed in the emission spectra: no shifting for **9**, a blue shift for **20** and a red sift for **16** and **21**. The latter may be indicative of π - π stacking interactions (Figure 36).

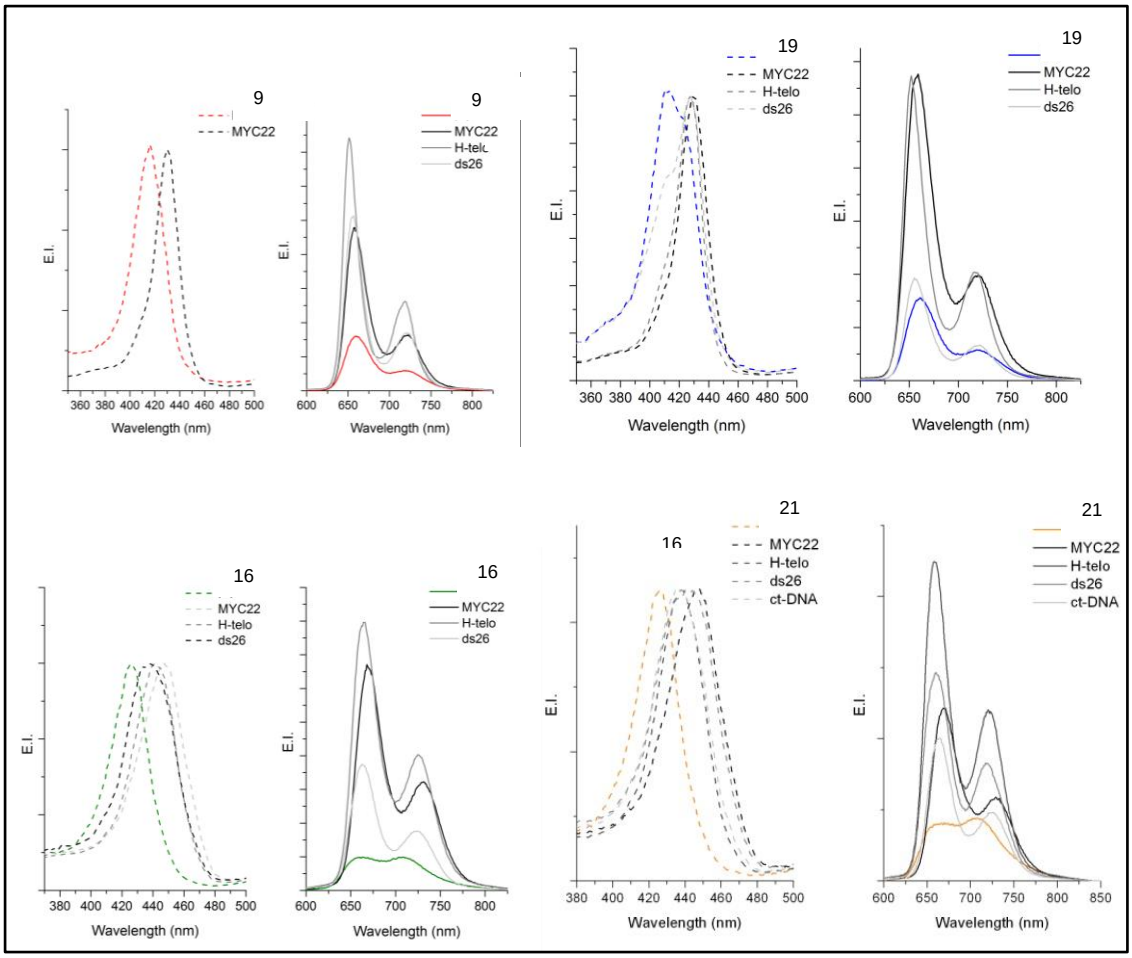

Figure 36: Excitation spectra (dotted) and emission (solid) of the studied compounds in the absence and presence of different DNA topologies; (from top) **9**, **20**, **16** and **21**. The intensity of the excitation spectra has been normalized for comparison purposes.

The compounds also display changes in emission intensity upon addition of different DNA sequences (Figure 37).

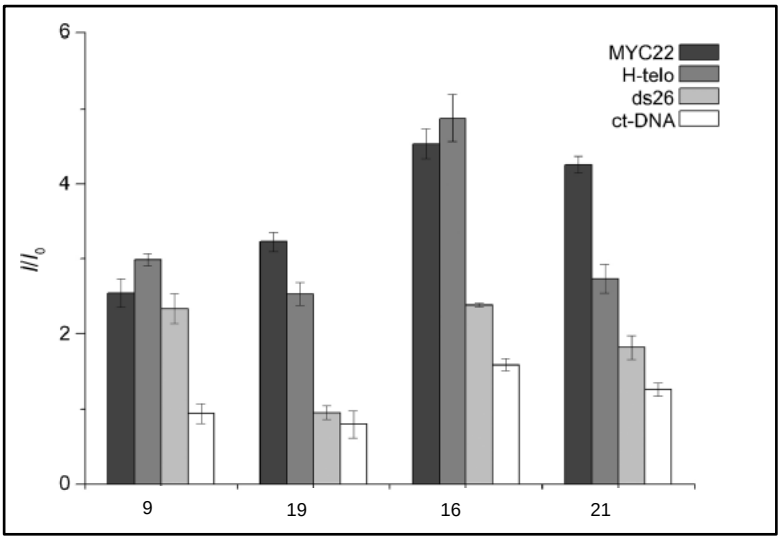

Figure 37: Bar chart showing changes in the emission intensity (determinate by integration of the emission between λ=600-850 nm) of the compounds (Tris/KCl buffer) upon addition of 20 equivalents of Myc22, H-telo,ds-26 and ct-DNA, λ_{ex}: 430 nm (**9**), 430 nm (**20**), 445 nm (**16**), 445 nm (**21**).

In the case of **20**, **16**, **21** the enhancement in the emission is more pronounced for the quadruplex DNA than ds26. In contrast, **9** do not display selectivity for the quadruplex sequences under study versus ds26. We also carried out studies using calf thymus (ct)-DNA. The four compounds showed greater enhancement of emission in the presence of quadruplex than with (ct)-DNA. The effect of the compounds on the thermal stability of Myc22 DNA was further investigated by using variable-temperature circular dichroism (CD). The experiments were carried out for Myc22 (5μM) alone and in the presence of two equivalents of each compound. Compounds **16** and **21** were found to have the greatest stabilization effect on Myc22 (ΔTm =19 and 20 °C for **16** and **21** respectively). Lower ΔTm was observed for **9** (6 °C) and surprisingly **20** showed no stabilization of Myc22. The apparent lack of DNA stabilization by this compound could be due to its lower solubility in aqueous media (Figure 38).

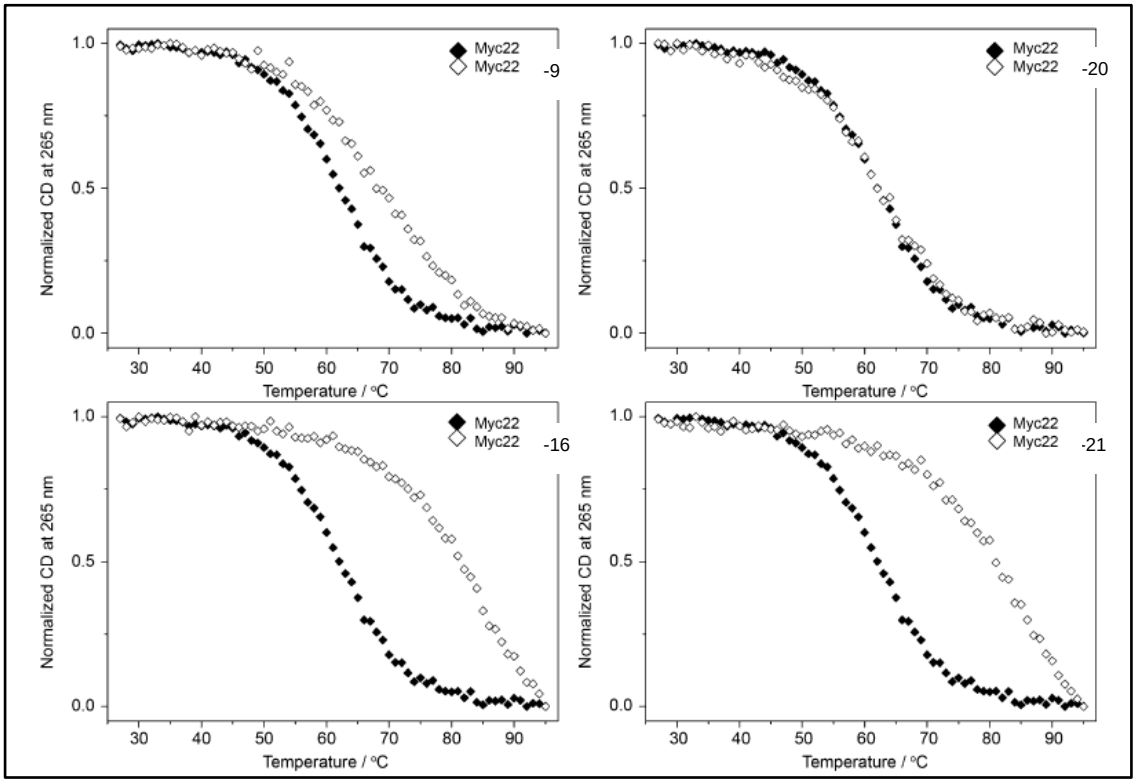

Figure 38: CD thermal denaturation profiles of Myc22 (5µM) alone and in the presence of 2 equivalents of **9**, **20**, **16** and **21**. All measurements were carried out in lithium cacodylate buffer (10 mM Li cacodylate, 99 mM LiCl, 1 mM KCl, pH 7.4); each experiment was performed in triplicate

2.5.5. DNA PHOTOCLEAVAGE

This work was performed in collaboration with Dr. Riccardo Rubbiani and Professor G. Gasser - Department of Chemistry, University of Zurich

Taking into account the favorable uptake into the nucleus, the interactions with different topologies of DNA, and the phototoxic activity of these compounds, we decided to investigate their effect on the plasmid DNA upon light irradiation. In these experiments, circular plasmid DNA was treated with the target porphyrins and then irradiated. If the compounds induce DNA-damage, a decrease in intensity of the supercoiled (intact form) band and the formation of single-strand breaks (nick form) or double-strand breaks (linear form) bands, which migrate slower in the gel, would be observed. Supercoiled pUC18 plasmid was treated with increasing concentrations of the porphyrins (0.5-10 µM) and incubated at room temperature for 20 minutes. Then, taking advantage of the intense Soret band, we irradiated the samples at 420 nm for 22 minutes to achieve the same light dose used in the phototoxicity experiments (10 Jcm^{-2}). A negative control of the plasmid treated with **9**, **20**, **16**, **21** (10 µM) in the dark was

used for comparative purpose. The complexes were all able to photocleave plasmid DNA in a concentration-dependent manner. Notably, **9** and **20** demonstrated a mild effect just at 10 μM with attenuation of the supercoiled band and an increase in intensity of the nicked band. **16** and **21** showed a marked photocleavage effect already at 0.5 μM. This is most likely due to the intercalative potential of the porphyrin core and the presence of the three positive charges, which are thought to maximize the DNA-complex interaction. DNA treated in the dark with the compounds (dark sample) did not show any significant alteration of the supercoiled form. Compound **20** showed a shift of the supercoiled and niked bands. This effect could be related to the interaction of the porphyrin with the plasmid DNA (Figure 39).

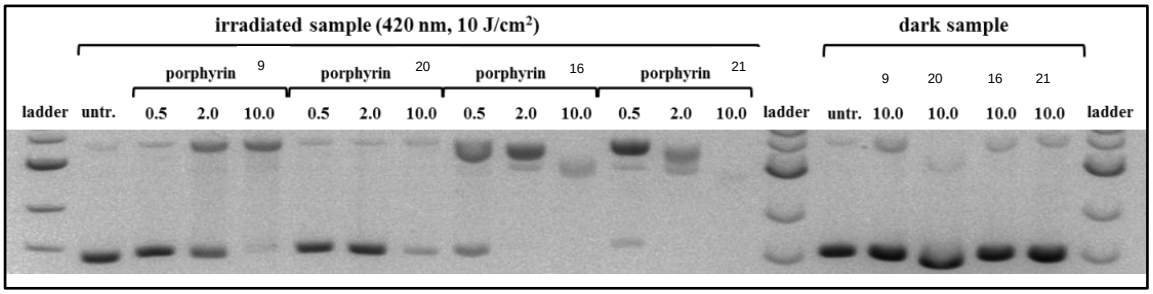

Figure 39: DNA photocleavage experiments of pUC18 plasmid treated with **9**, **20**, **16** and **21**, in the dark and upon light irradiation at 420 nm for 22 minutes (10 Jcm^{-2}); untr.= DNA untreated; concentration expressed in μM.

2.6. CONCLUSIONS

The results showed that a neutral fourfold-symmetric and a +3-charged tris-methylpyridiniumporphyrin can bind the *fac*-$\{Re(CO)_3\}^+$ fragment in good yields. The presence of one or four hydrophilic spacers containing the ethylendioxy groups, as well as the positive charges on the complexes contribute to the water solubility of compounds **9**, **16**, **20** and **21**. These compounds were evaluated as potential PSs. All the compounds are not toxic up to a concentration of 100 μM in the dark on the cell lines studied and upon irradiation **9** and **20** showed much better phototoxic properties than **16** and **21**. Upon Re coordination we observed an enhancement in the phototoxic activity of **9** but not for **16**. Compounds **16** and **21** were found to be more efficient than **9** and **20** at binding the DNA (with some selectivity for quadruplex versus duplex) as well as in DNA photocleavage. The possibility of obtaining the correspondent ^{99m}Tc conjugates in order to develop new therapeutic agents is very interesting.

2.7. EXPERIMENTAL PART

Mono and bidimensional (H-H COSY and HSQC) NMR spectra were recorded on a Bruker 400 or on a Varian 500 spectrometer (500 MHz for ^{1}H, 470 MHz for ^{19}F). All the spectra were run at ambient temperature and chemical shifts were referenced to the peak of residual non deuterated solvent (δ 7.26 for $CDCl_3$, 3.31 for CD_3OD, 2.50 for DMSO-d6, 1.94 for CD_3CN and 4.79 for D_2O). ^{19}F NMR shifts were referenced to $CFCl_3$ as internal standard. The UV-Vis spectra were performed at ambient temperature on a Jasco V-500 UV-vis spectrophotometer equipped with a Peltier temperature controller, using 1.0 cm path-length quartz cuvettes (3 mL). The IR spectra were recorded on a Perkin Elmer Spectrum RXI FTIR spectrophotometer. Electrospray mass spectra were performed on a Bruker Esquire ESI-MS instrument. ESI HRMS were obtained using a Brukner maXis instrument. Column chromatography was performed on silica gel 60 (Merck,230–400 mesh ASTM), eluting with CH_2Cl_2/CH_3OH mixtures as specified below. The reactions were monitored by TLC (silica gel/UV 254, 0.25 mm, glass or aluminum support). Re(I) precursor fac-[Re-$(CO)_3$(dmso-$O)_3$](CF_3SO_3) was prepared according to the published procedure [98]. All chemicals were purchased from Sigma–Aldrich and used without further purification unless otherwise specified. The porphyrins and their Re conjugates precipitate with variable amounts of crystallization solvent, depending on the batch. For this reason elemental analysis of such compounds did not afford reliable and reproducible results, and the values are not reported here (typically, some of the elemental analysis values, especially for C, differ from calculated values by >0.5 %). Nevertheless, the purity calculated from elemental analysis data was always >95%, and the proposed formulae are all consistent with NMR, ESI-MS and ESI HRMS spectra. Of note, the ^{13}C NMR spectra are not reported, as the solubility of the porphyrins and of their Re conjugates in CD_3OD at the maximum extent was insufficient to observe all the carbon resonances, especially of the quaternary carbons, even after an accumulation time of 72 h.

Di-*tert*-butyl-[1,4,7]-triazacyclononane-1,4-dicarboxylate (diBoc-TACN) (2)

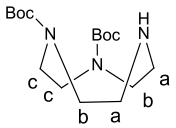

To a solution of [1,4,7]-triazacyclononane (TACN, **1**) (500.5 mg, 3.87 mmol) in $CHCl_3$ (10 mL) triethyl amine (TEA) (744 µL, 5.4 mmol, 1,4 equiv) was added. To this clear solution a solution of $(Boc)_2O$ (1.53 g, 7.00 mmol, 1.8 equiv) in $CHCl_3$ (20 mL) was added dropwise under an argon atmosphere in 4 h at room temperature, obtaining a suspension. The reaction mixture was stirred overnight under an argon atmosphere at rt. The reaction was monitored by TLC (EtOAc/EtOH 10:1, R_f = 0.3). The solvent was removed under reduced pressure to give the product as white oil. The product was dissolved in EtOAc (100 mL) and then washed first with 4% $NaHCO_3$ (100 mL) and with brine (100 mL×2). The organic phase was washed with 10% aqueous citric acid (100 mL×3) and the product moved in the water phase. NaOH 10% was added under ice-cooling until the water phase was adjusted to pH 10 and the product was extracted with CH_2Cl_2 (100 mL×3). The organic solution was dried over anhydrous Na_2SO_4 and the solvent was removed under reduced pressure to give the product as white oil.

Yield: 56% (718 mg).

^{1}H NMR ($CDCl_3$, δ): 3.49 (m, 2H, CH_2 c), 3.43 (m, 2H, CH_2 c) 3.31 (m, 2H, CH_2 b), 3.25 (m, 2H, CH_2 b), 2.94 (m, 4H, CH_2 a), 1.48 (s, 18H, CH_3 Boc).

ESI MS *m/z:* 330.2 $[M+H]^+$, 325.2 $[M+Na]^+$.

1,4-Bis(*tert*-butyloxycarbonyl)-1,4,7-triazacyclononane-7-benzylacetate (diBocTACNCbz) (3)

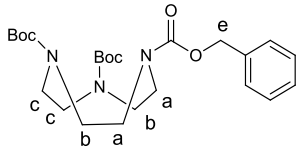

To a solution of **2** (718 mg, 2.18 mmol) and TEA (608 µL, 4.36 mmol, 2 equiv) in $CHCl_3$ (12 mL) a solution of benzyl bromoacetate (1.26 g, 5.50 mmol, 2.5 equiv) in $CHCl_3$ (23 mL) was added dropwise under ice-cooling in 1 h. The solution was stirred for 48 h at rt and the reaction was monitored by TLC (CH_2Cl_2/EtOH 95:5, R_f = 0.6). The solvent was removed under reduced pressure to give a yellow oil that was purified by silica gel

chromatography (CH_2Cl_2/EtOH 97:3 then 95:5) to afford the pure product as a yellow oil.

Yield: 89% (926 mg).

^{1}H NMR ($CDCl_3$, δ): 7.35 (m, 5H, H Ph), 5.13 (t, 2H, CH_2 e), 3.49 (s, 2H, CH_2 d), 3.45 (m, 4H, CH_2 c), 3.26 (m, 2H, CH_2 b), 3.20 (m, 2H, CH_2 b), 2.84 (m, 4H, CH_2 a), 1.46 (s, 9H, CH_3 Boc), 1.45 (s, 9H, CH_3 Boc).

ESI MS *m/z:* 478.3 $[M+H]^+$, 500.3 $[M+Na]^+$, 516.3 $[M+K]^+$.

1,4-Bis(*tert*-butyloxycarbonyl)-1,4,7-triazacyclononane-7-acetic acid (2-(diBoc)TACN acetic acid) (4)

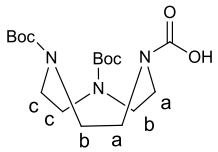

To a deoxygenated solution of **3** (926 mg, 1.94 mmol) in CH_3OH (25 mL) Pd/C was slowly added and then the reaction flask was purged with H_2 several times. After 24 h of reaction at rt the catalyst was removed by filtration over a celite pad and the solvent was evaporated under reduced pressure to give a white crystalline solid.

Yield: 91.3% (686 mg).

TLC: CH_2Cl_2/ EtOH 9:1, R_f = 0.3

^{1}H NMR ($CDCl_3$, δ): 3.56 ─ 3.18 (m, 8H, CH_2 b+CH_2 c), 3,39 (s, 2H, CH_2 d) 2.77─ 2.65 (m, 4H, CH_2 a) 1.48 (s, 9H, CH_3 BOC), 1.49 (s, 9H, CH_3 Boc).

UPLC t_r: 1.85 min.

ESI MS *m/z:* (negative mode) 386.1 $[M–H]^-$, (positive mode) 388.2 $[M+H]^+$, 410.2 $[M+Na]^+$.

meso-4'-Tetracarboxymethylphenylporphyrin (4'-TCMePP)

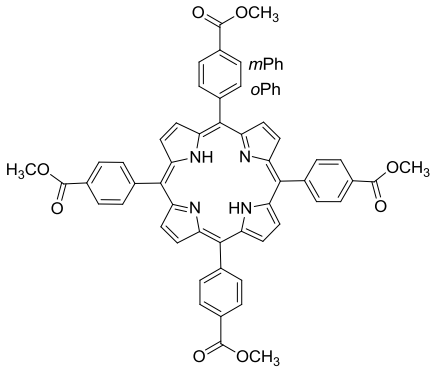

To a solution of methyl 4-formylbenzoate (2.30 g, 14 mmol) in propionic acid (50 mL) heated at 140 °C freshly distilled pyrrole (1 mL, 14 mmol, 1 equiv) was added in portions. The resulting solution was refluxed for 1.5 h and then cooled at rt and stored at -18°C for 12 h. The purple precipitate was removed by filtration, washed several times with cold CH_3OH and dried under vacuum.

Yield: 21% (0.63 g).

TLC: CH_2Cl_2/EtOH 95:5, R_f = 0.91.

^{1}H NMR ($CDCl_3$, δ): 8,85 (s, 8H, Hβ), , 8.48 (d, 8H, *m*Ph, *J* = 8.3 Hz), 8.32 (d, 8H, *o*Ph, *J* = 8.0 Hz), 4.14 (s, 12H, CH_3), -2.80 (br s, 2H, NH).

UV-Vis (CH_2Cl_2): λ_{max}, (relative intensity, %): 420 (100), 515 (4.0), 550 (2.0), 590 (1.4), 646 (1.0).

IR (KBr, cm^{-1}): *v* = 3313 (m, NH), 1723 (s, CO), 1276 (s, CO), 1020 (s, CO).

Porphyrin 5

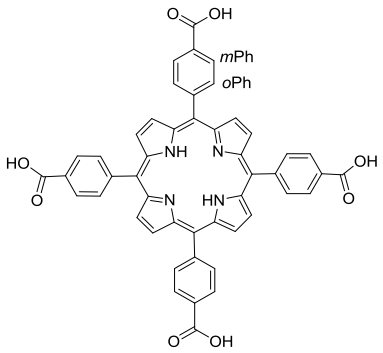

101 mg of 4'-TCMePP (0.12 mmol) were dissolved in a 2:1 THF/CH_3OH mixture (100 mL). 40% KOH solution (w/v) (4 mL) was added and the mixture warmed at 40 °C for 30 min under magnetic stirring. The reaction was monitored by TLC (CH_2Cl_2/CH_3OH 9:1, R_f = 0) until the complete disappearance of 4'-TCMePP. At reaction completion, the

mixture was acidified to pH 5 with conc HCl and extracted with CH_2Cl_2 (25 mL×3) after addition of water (40 mL). The joined organic fractions were washed with H_2O (20 mL×3) and dried over anhydrous Na_2SO_4. The solvent was removed under vacuum obtaining the product as a purple solid.

Yield: 91.5% (86.8 mg).

^{1}H NMR (DMSO-d_6, δ): 13.30 (s, 4H, COOH), 8.87 (s, 8H, βH), 8.38 (m, 16H, *o*+*m* Ph), -2.94 (s, 2H, NH).

UV-Vis (EtOH): λ_{max} (relative intensity, %): 416 (100), 513 (4.2), 548 (2.1), 590 (1.3), 646 (0.9).

_N_-Boc-2,2'-(ethylenedioxy)-diethylamine (6)

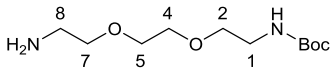

To a solution of ethylenedioxy-diethylamine (17.6 g, 0.12 mol, 2 equiv.) in CH_2Cl_2 (90 mL) di-*tert*-butyl dicarbonate (13.16 g 0.06 mol) in CH_2Cl_2 (90 mL) was added dropwise at 0 °C for 3.5 h, and the reaction mixture was left for other 24 h at rt. The reaction was monitored by TLC (CH_2Cl_2/CH_3OH 9:1, R_f = 0.33). The organic phase was concentrated and H_2O was added (150 mL). The water phase contains the mono protected ammine and was extracted with CH_2Cl_2 (20 mL x 7), instead the organic phase contains both the mono- and diprotected ammine. The mixture was purified by silica gel chromatography (CH_2Cl_2/CH_3OH, 90:10, then 85:15) to afford the pure mono-protected amine as a yellow oil.

Yield: 54% (8.04 g).

^{1}H NMR ($CDCl_3$, δ): 5.14 (br s, 1H, NHBoc), 3.62 (s, 4H, CH_2O), 3.53 (m, 4H, CH_2O) 3.32 (m, 2H, CH_2 1), 2.88 (t, 2H, CH_2 8),1.44 (s, 9H, CH_3 Boc).

Porphyrin 7

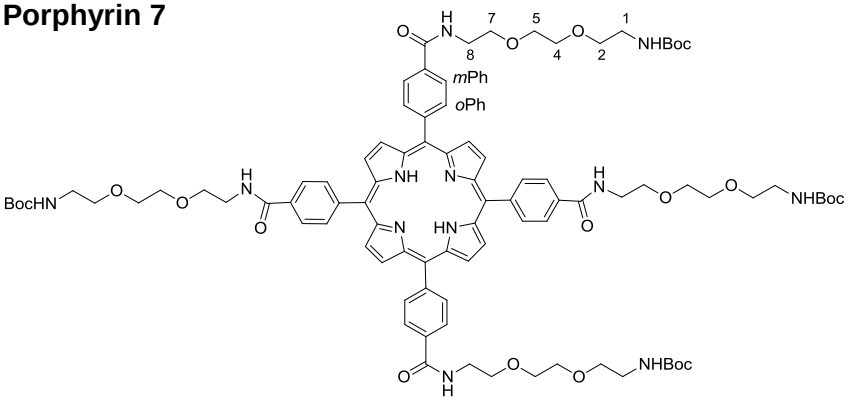

36.29 mg of EDCI (0.1893 mmol, 6 equiv) and 25.58 mg of HOBt (0.1893 mmol, 6 equiv) were added to a solution of **5** (25 mg, 0.0316 mmol) dissolved in 3 mL of anhydrous DMF. After stirring for 30 min, 30.35 mg (0.1222 mmol, 4 equiv) of **6** and 16.99 mg (0.1391 mmol, 4.4 equiv) of DMAP dissolved in 1 mL of anhydrous DMF were added. The reaction mixture was shielded from light and stirred at rt for 24 h, and then the solvent was removed on a rotary evaporator to yield a dark semisolid. 20 mL of H_2O were added and the product was extracted with THF/CH_2Cl_2 1:1 (3×17 mL). The organic fraction was evaporated to dryness under vacuum and the resulting solid was dried over P_2O_5. The product was purified by column chromatography (2×20 cm, silica gel, CH_2Cl_2/CH_3OH 95:5) obtaining the pure product as a purple solid.

Yield: 74% (40 mg).

TLC: CH_2Cl_2:CH_3OH=9:1, R_f = 0.59.

^{1}H NMR ($CDCl_3$, δ): 8.81 (s, 8H, βH), 8.24 (dd, 16H, 8H *m*Ph + 8H *o*Ph), 7.04 (br s, 4H, NHCO) 5.04 (br s, 4H, NHBoc), 3.84 (m, 16H, CH_2O), 3.73 (m, 16H, CH_2O) 3.61 (t, 8H,$CH_2$8) 3.35 (m, 8H,$CH_2$1), 1.38 (s, 36H, CH_3 Boc), -2.83 (br s, 2H, NH).

Porphyrin 7 · *n*TFA

Porphyrin **7** (30.5 mg, 0.018 mmol) was dissolved in CH_2Cl_2 (2 mL) obtaining a purple solution. To this solution TFA (2 mL) was added. The solution was stirred for 2 h shielded from light and then the solvent was completely removed under reduced pressure to give a blue solid as TFA salt. The reaction is quantitative and the product was used in the following step without further purification.

Porphyrin 7 as free base

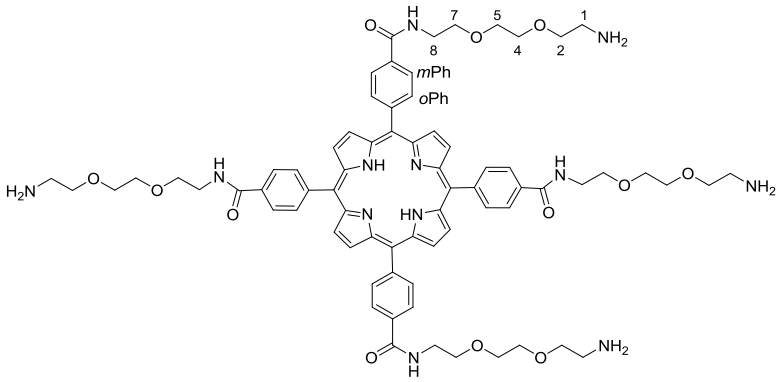

A small amount from the product as TFA salt (20 mg ca.) was dissolved in CH_3OH (2 mL) and neutralized with TEA (2 drops), then it was precipitated with Et_2O, filtered, and thoroughly washed with Et_2O for characterization.

^{1}H NMR (CD_3OD, δ): 3.17 (t, 8H, CH_2NH_2), 3.80 (m, 40H, CH_2O), 8.32 (dd, 16H, *m*Ph + *o*Ph), 8.90 (br s, 8H, βH).

UV-vis (CH_3OH): λ_{max} ($\varepsilon \times 10^{-3}$, $dm^3\ mol^{-1}cm^1$): 415 (479), 513 (20), 546 (11), 587 (7.1), 645 (5.9).

ESI MS *m/z*: 1312.7 $[M+2H]^+$, 1334.6 $[M+H+Na]^+$, 1350.6 $[M+H+K]^+$.

Porphyrin 8

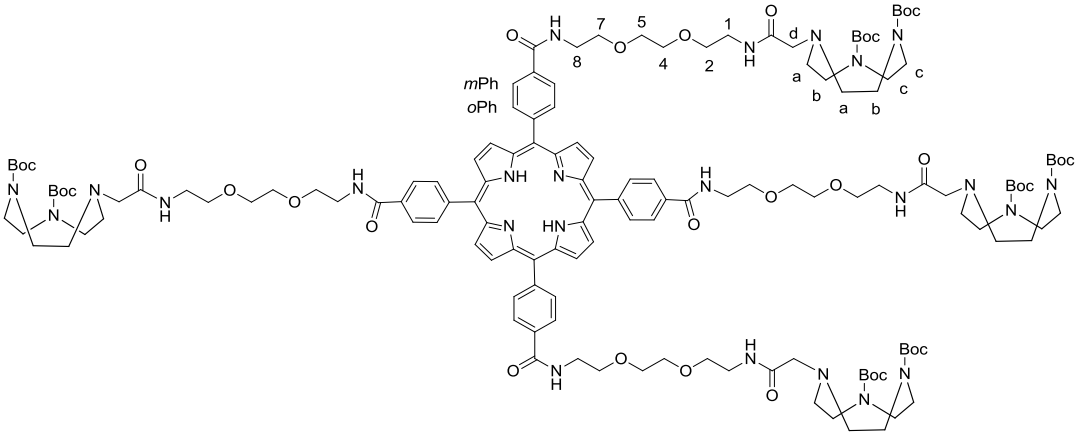

To a solution of **4** (54.44 mg, 0.14 mmol, 6 equiv) in anhydrous DMF (3 mL) HOBt (28.51 mg, 0.21 mmol, 9 equiv) and EDCI (40.6 mg, 0.21 mmol, 9 equiv) were added. The solution was stirred for 30 min, then a purple solution of the porphyrin **7**·*n*TFA (0.0234 mmol) and DMAP (28.80 mg, 0.23 mmol, 10 equiv) in anhydrous DMF (4 mL) was added. The reaction was monitored by TLC (CH_2Cl_2/EtOH 9:1, R_f = 0.3). The reaction solution was stirred overnight at rt and shielded from light. After removing the

solvent, the product was purified by column chromatography (4 x 15 cm, silica gel, CH_2Cl_2/EtOH 90:10 then 85:15) to obtain a purple solid.

Yield: 66.2% (43.2 mg).

^{1}H NMR ($CDCl_3$, δ): 8.83 (s, 8H, βH), 8.27 (dd, 16 H *m*Ph + *o*Ph), 7.74 (m, 2H, NHCO), 7.66 (m, 2H, NHCO), 7.38 (m, 4H, NHCO), 3.83 (m, 8H, CH_2NH + 8H, CH_2O), 3.72 (m, 16H, CH_2O), 3.62 (m, 8H, CH_2O), 3.50 (m, 16H, CH_2 c + CH_2 1), 3.35 (m, 16H, CH_2 b), 3.21 (m, 8H, CH_2 d), 2.67 (m, 16H, CH_2 a), 1.48, 1,46, 1.42 (s, 72H, CH_3 Boc), -2,78 (br s, 2H, NH).

UV-Vis (CH_2Cl_2): λ_{max}, (relative intensity, %): 419.5 (100), 515.2 (4.3), 550.2 (2.1), 590.2 (1.5), 645.9 (1.1).

Porphyrin 9

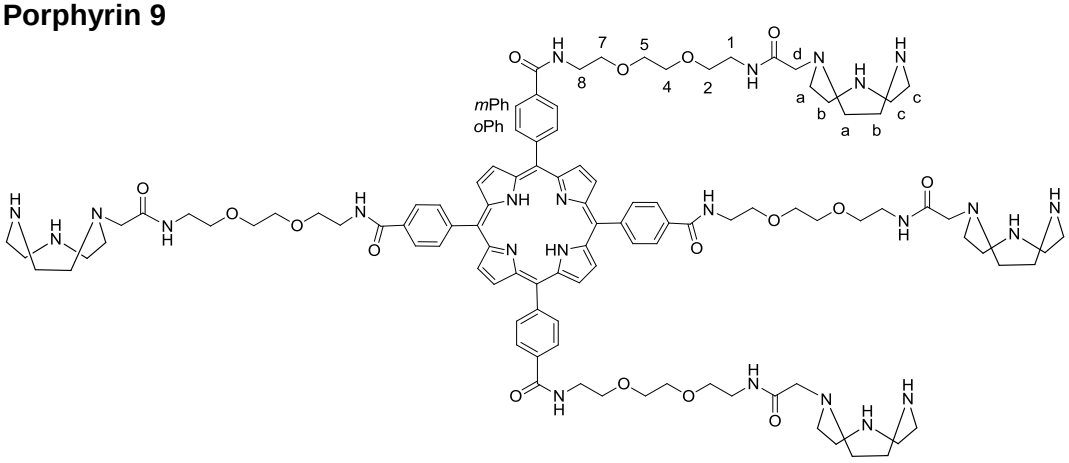

Porphyrin **8** (14.54 mg, 0.0052 mmol) was dissolved in CH_2Cl_2 (1.5 mL) to obtain a purple solution. To this solution TFA (1.5 mL) was added and the solution turned into deep green. The solution was stirred for 4h shielded from light, then the solvent and the excess of TFA were removed under reduced pressure to give a green-blue product. The porphyrin was dissolved in the minimum volume of CH_3OH obtaining a deep green solution. To this solution 30 µL (0.20 mmol) of TEA were added and the solution turned purple. The product was precipitated by adding Et_2O dropwise to the solution. The solid was extensively washed with Et_2O and dried under vacuum.

Yield: 97.4% (10 mg).

^{1}H NMR (CD_3OD, δ): 8.88 (br s, 8H, Hβ), 8.34 (d, 8H, H Ph, *J* = 8.2 Hz) 8.30 (d, 8H, H Ph, *J* = 8.2), 3.83 (m, 8H, CH_2O), 3.78 (m, 16H, CH_2O + CH_2NH), 3.73 (m, 8H, CH_2O), 3.64 (m, 8H, CH_2O), 3.47 (m, 16H, CH_2 d + CH_2NH), 3.22 (m, 16H, CH_2 c), 3.04 (m, 16H, CH_2 b), 2.86 (m, 16H, CH_2 a).

UV-Vis (CH_3OH): λ_{max} ($\varepsilon \times 10^{-3}$, $dm^3\ mol^{-1}\ cm^{-1}$): 416 (250), 513 (11), 547 (4.9), 590 (2.8), 645 (2.4).
ESI MS *m/z*: 1989.9 $[M+H]^+$.
ESI HRMS calcd for $[C_{104}H_{146}N_{24}O_{16}]/z$: $[M+3H]^{3+}$ 663.37829, found 663.71765; calcd for $[M+4H]^{4+}$ 497.78372, found 498.04085; calcd for $[M+5H]^{5+}$ 398.42697, found 398.63419.

meso-5-(4'-Methoxyphenyl)-10,15,20-tris(4'-pyridyl)porphyrins 10

To a solution of methyl-4-formylbenzoate (1.13 g, 6.88 mmol, 1 equiv) and pyridine 4-carboxaldehyde (2 mL, 20.65 mmol, 3 equiv) in propionic acid (120 mL) 2 mL of pyrrole (27.52 mmol, 4 equiv) were added dropwise. The resulting solution was refluxed at 140 °C for 2 h and then cooled at rt, then the solvent was partially distilled under reduced pressure to 40 mL. After the addition of a mixture of 1:2 ethylene glycol/ CH_3OH (60 mL), the solution it was stored at -4 °C for 72 h. The purple precipitate was removed by filtration, thoroughly washed with cold methanol, and dried under vacuum at rt. The TLC of the crude product (CH_2Cl_2/CH_3OH 98:2) showed to be a mixture of five possible porphyrin isomers: 4'-MPyTrMeP (R_f = 0.77), 4'-*trans*-DPyDMeP (R_f = 0.55), 4'-*cis*-DPyDMeP (R_f = 0.43), 4'-TrPyMMeP **10** (R_f = 0.33) and 4'-TPyP (R_f = 0.13). As only one equivalent of methylformylbenzoate was used, the 4'-TMeP isomer (R_f = 0.95) was not present in the crude product.

Chromatographic separation of the mixture of porphyrins

The isomers were separated by column chromatography. To isolate each isomer it was necessary to perform a series of chromatographic separations. After the first chromatography (6×20 cm, silica gel, CH_2Cl_2/CH_3OH 99:1 then 98:2) two mixtures (A and B) of the following composition were obtained: mixture A (4'-TrPyMMeP **10** and 4'-TPyP) and mixture B (4'-MPyTrMeP, 4'-*cis*- and 4'-*trans*-DPyDMeP and a small amount of 4'-TrPyMMeP). 4'-TMeP formed in a very small amount and it was not possible to isolate it.

Mixture A: the chromatographic separation (6 x 20 cm, silica gel, CH_2Cl_2/CH_3OH 98:2) gave two pure isomers: 300 mg of TrPyMMeP **10** (absolute yield 6.5%, relative yield 45.5%) and 110 mg of TPyP (absolute yield 2.2%, relative yield 15%).

Mixture B: several chromatographic separations were performed to separate the three porphyrins.

- 4'-TrPyMMeP **10**: obtained in pure form after a chromatographic column (5 x 15 cm, silica gel, CH_2Cl_2/CH_3OH 99:1 then 98:2). During the purification, a mixture made of 4'-*cis*- and 4'-*trans*- DPyDMeP 1:1 and a mixture made of 4'-MPyTrMeP, 4'-*trans*-DPyDMeP and 4'-*cis*- DPyDMeP were obtained.
- 4'-MPyTrMeP was separated from 4'-*trans*-DPyDMeP and 4'-*cis*- DPyDMeP by a column chromatography (6 x 20cm, silica gel, CH_2Cl_2 100% then CH_2Cl_2/CH_3OH 99:1, 98:2, 97:3).
- 4'-*cis*- and 4'-*trans*- DPyDMeP 1:1 were separated by column chromatography (5 x 12cm, silica gel, CH_2Cl_2 100% then CH_2Cl_2/CH_3OH 99:1, 98:2, 97:3).

Characterization

4'-TyP

^{1}H NMR 4'-TPyP ($CDCl_3$, δ): 9.07 (d, 6H, 2,6py), 8.87 (m, 8H, βH), 8.17 (d, 6H, 3,5py), - 2.93 (br s, NH, 2H).

4'-TrPyMMeP (**10**)

^{1}H NMR 4'-TrPyMMeP ($CDCl_3$, δ): 9.06 (d, 2,6py, 6H), 8.87 (m, βH, 8H),8.47 (d, Ph, 2H), 8.30 (d, Ph, 2H), 8.17 (d, 3,5py, 6H), 4.13 (s, CH_3, 3H), -2.89 (br s, NH, 2H).

4'-*cis*-DPyDMeP

^{1}H NMR ($CDCl_3$, δ): 9.04 (dd, 2,6py, 4H), 8.85 (m, βH, 8H), 8.48 (dd, Ph, 4H), 8.31 (dd, Ph, 4H), 8.18 (d, 3,5py, 4H), 4.12 (s, CH_3, 6H), -2.87 (br s, NH, 2H).

4'-MPyTrMeP

^{1}H NMR ($CDCl_3$, δ): 9.03 (m, 2H, 2,6py), 8.83 (m, 8H, βH), 8.41 (m, 8H, Ph), 8.27 (m, 8H, Ph), 8.15 (dd, 2H, 3,5py), 4.12 (s, CH_3, 9H), -2.85 (br s, NH, 2H).

Porphyrin 11

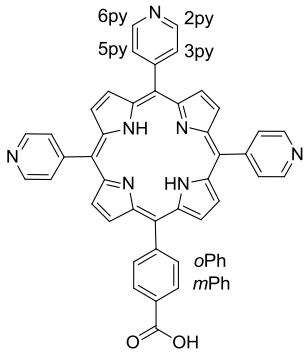

48.70 mg of 4'-TrPyMMeP **10** (0.0721 mmol) were dissolved in a 2:1 THF/CH_3OH mixture (30 mL). 40% KOH solution (w/v) (6 mL) was added and the mixture warmed at 40 °C for 5 h under magnetic stirring. The reaction was monitored by TLC (CH_2Cl_2/CH_3OH 9:1, R_f = 0) until the complete disappearance of 4'-TrPyMMeP. At

reaction completion, the mixture was acidified to pH 5 with conc HCl and extracted with CH_2Cl_2 after addition of H_2O. The joined organic fractions were washed with H_2O. The solvent was removed under vacuum and the product was washed with Et_2O and H_2O and then dried over anhydrous P_2O_5 obtaining purple-brown solid.

Yield: 100% (47.71 mg).

^{1}H NMR (DMSO-d_6, δ): 9.05 (d, 6H, 2,6py), 8.90 (m, 8H, βH), 8.37 (dd, 4H, *o*Ph+*m*Ph), 8.27 (d, 6H, 3,5py).

Porphyrin 12

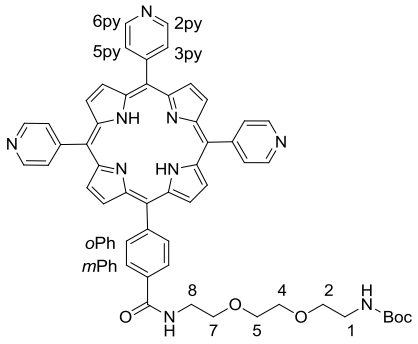

21.76 mg of EDCI (0.1135 mmol, 1.5 equiv) and a 15.80 mg of HOBt (0.1169 mmol, 1.5 equiv) were added to a solution of **11** (50.03 mg, 0.0756 mmol) dissolved in 6 mL of anhydrous DMF. To this solution, after stirring for 30 min, 28.16 mg (0.1134 mmol, 1.5 equiv) of **6** and 10.25 mg (0.0839 mmol, 1.1 equiv) of DMAP dissolved in 2 mL of anhydrous DMF were added. The reaction mixture was shielded from light and stirred at rt for 20 h and monitored by TLC (CH_2Cl_2/CH_3OH, R_f = 0.4). Then the solvent was removed on a rotary evaporator to yield a dark semisolid that was washed with H_2O and dried over P_2O_5. The solid was purified by column chromatography (3×15 cm, CH_2Cl_2/CH_3OH 97:3 then 95:5). The product was washed with Et_2O obtaining the pure product as a purple solid.

Yield: 81% (54.64 mg).

^{1}H NMR ($CDCl_3$, δ): 9.06 (m, 6H, 2,6py), 8.86 (m, 8H, Hβ), 8.26 (dd, 4H, *o*Ph + *m*Ph) 8.16 (m, 6H, 3,5py), 7.08 (br s, 1H, NHCO), 5.05 (br s, 1H, NHBoc), 3.87 (m, 4H, CH_2 8), 3.75 (m, 4H, CH_2O), 3.67 (m, 2H, CH_2O), 3.35 (m, 2H, CH_2 1), 1.40 (m, 9H, CH_3Boc).

UV-Vis (CH_3OH): λ_{max} (relative intensity, %) = 417 (100), 512 (6.1), 547 (1.8), 590 (1.7), 643 nm (0.7).

ESI MS *m/z*: 892.6 $[M+H]^+$, 914.5 $[M+Na]^+$, 930.4 $[M+K]^+$.

Porphyrin 13

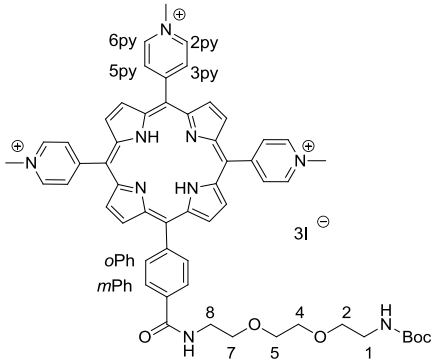

Porphyrin **12** (54.64 mg, 0.0612 mmol) was dissolved in DMF (5 mL). To this purple solution, CH_3I (190.81 µL, 3.065 mmol, 50 equivalents) was added and the solution was heated at 90 °C under magnetic stirring for 3 h and shielded from light. The reaction was monitored by TLC (CH_2Cl_2/CH_3OH, R_f = 0 and $CH_3CN/KNO_3/H_2O$ 4:0.3:1, R_f = 0.23). Then the solvent was removed under reduced pressure obtaining a solid that was washed with Et_2O and $CHCl_3$, and dried under vacuum to give the product as a purple solid.

Yield: 87% (70.12 mg).

^{1}H NMR (dmso-d_6, δ): 9.47 (d, 6H, 2,6py), 9.15 (m, 2H, Hβ), 9.05 (m, 4H, Hβ), 9.00 (m/t, 6+2H, 3,5py+Hβ), 8.93 (t, 1H, NHCO), 8.34 (dd, 4H, *o*Ph + *m*Ph) 6.80 (t, 1H, NHBoc), 4.72 (m/d, 9H, CH_3py), 3.73-3.55 (m, 3+1H, CH_2O+CH_2 8), 3.44 (t, 2H, CH_2 O), 3.11 (m, 2H, CH_2 1), 1.36 (m, 9H, CH_3Boc), -3.02 (br s, 2H, NH).

^{1}H NMR (CD_3OD, δ): 9.45 (d, 6H, 2,6py), 9.45-8.96 (brs, 8H, Hβ), 8.96 (d, 6H, 3,5py), 8.29 (dd, 4H, *o*Ph+*m*Ph), 4.81 (m, 9H, CH_3py), 3.82 (m, 2H, CH_2 spacer), 3.77 (m, 4H, CH_2 spacer), 3.72 (m, 2H, CH_2 spacer), 3.58 (m, 2H, CH_2 spacer), 3.20 (m, 2H, CH_2 spacer), 1.36 (m, 9H, CH_3Boc).

UV-Vis (CH_3OH): λ_{max} (relative intensity, %) = 424 (100), 516 (7.4), 553 (3.3), 590 (2.8), 647 nm (1.1).

ESI MS *m/z*: 936.4 $[M]^+$, 468.4 $[M]^{2+}$, 836.5 $[M(14)]^+$.

Porphyrin 14

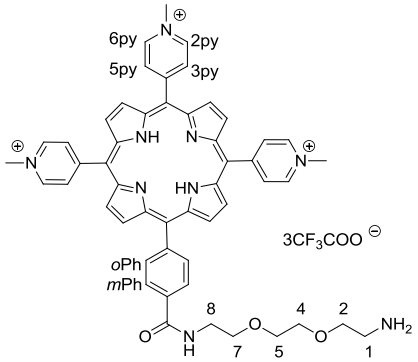

Porphyrin **13** (31.69 mg, 0.0240 mmol) was suspended in CH_2Cl_2 (3 mL) obtaining a brown-green mixture. To this solution TFA (120 µL) was added. The solution was stirred for 3 h shielded from light, then the solvent was completely removed under reduced pressure to give the product as TFA salt. The product was washed with Et_2O and 1:1 CH_2Cl_2/Et_2O obtaining a solid color brown-purple.

Yield: 97.4% (27.49 mg).

TLC: $CH_3CN/KNO_3sat/H_2O$ 4:0.3:1, R_f = 0.25.

^{1}H NMR (CH_3OD): δ= 9.39 (d, 6H, 2,6py), 9.35–9.01 (br s, 8H, Hβ), 8.97 (d, 6H, 3,5py), 8.34 (dd, 4H, *o*Ph+*m*Ph) 4.84 (m, 3H, CH_3py), 3.90–3.73 (m, 8+2H, CH_2O+CH_2 8), 3.18 (m, 2H, CH_2 1).

^{19}F NMR (CD_3CN, δ): -76.91 (CF_3COO^-).

UV-Vis (CH_3OH): λ_{max} (relative intensity, %)= 424 (100), 516 (7.4), 553 (3.3), 590 (2.8), 647 nm (1.1).

RP-UPLC t_r: 1.15 min.

ESI MS *m/z*: 836.4 $[M]^+$, 418.1 $[M]^{2+}$.

Porphyrin 15

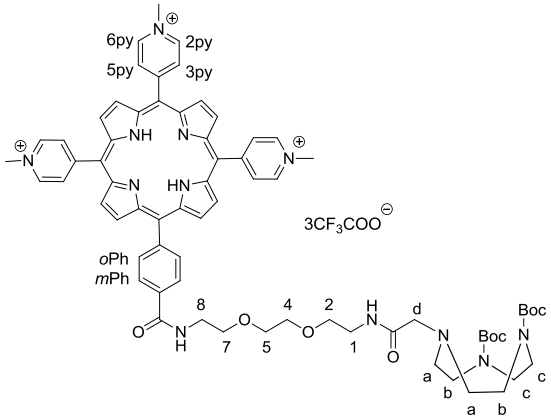

To a solution of **4** (14.34 mg, 0.0370 mmol, 1.44 equiv) in anhydrous DMF (1.5 mL) HOBt (7.52 mg, 0.0556 mmol, 2.17 equiv) and EDCI (10.64 mg, 0.0555 mmol, 2.17 equiv) were added and the resulting solution was stirred for 30 min. To this solution a purple solution of the porphyrin **14** (30.07 mg, 0.0256 mmol) and DMAP (7.65 mg, 0.0626 mmol, 2.44 equiv) in anhydrous DMF (1.5 mL) was added. The coupling was performed in a microwave oven reactor (ramp time: 10 s, hold time: 6 min, T 60 °C, P 1720 kPa, power 30 W). The reaction was monitored by TLC (CH_3CN/KNO_3sat/H_2O 4:0.3:1, R_f = 0.38). The charged porphyrin **15** was purified by repeated precipitation (CH_3OH/Et_2O and CH_3CN/Et_2O) and extensive washing with Et_2O and CH_2Cl_2 to remove the excess both of the reagents and of the ligand.

Yield: 66.4% (26.27 mg).

^{1}H NMR (CD_3CN, δ): 9.12 (m, 6H, 2,6py), 9.07 (m, 6H, βH), 8.95 (m, 2H, βH), 8.82 (m, 6H, 3,5py), 8.30 (dd, 4H, *o*Ph + *m*Ph), 4.70 (s, 3H, CH_3 py), 4.69 (s, 6H, CH_3 py), 3.75 (m, 2H, CH_2O), 3.70 (m, 4H, CH_2O+CH_2NH), 3.65 (m, 2H, CH_2O), 3.55 (t, 2H, CH_2O, J = 5.6 Hz), 3.37 (m, 6H, CH_2 NH + CH_2 c), 3.23 (m, 4H, CH_2 b), 3.09 (m, 2H, CH_2 d), 2.59 (m, 4H, CH_2 a), 1.43, 1.42, 1.36 (s, 18H, CH_3Boc), -2.96 (s, 2H, NH pyrrole).

UV-Vis (CH_3OH): λ_{max} (relative intensity, %)= 422 (100), 516 (8.3), 553 (3.9), 589 (3.3), 648 nm (1.3).

ESI MS *m/z*: 1205.7 $[M]^+$, 603.1 $[M]^{2+}$.

Porphyrin 16

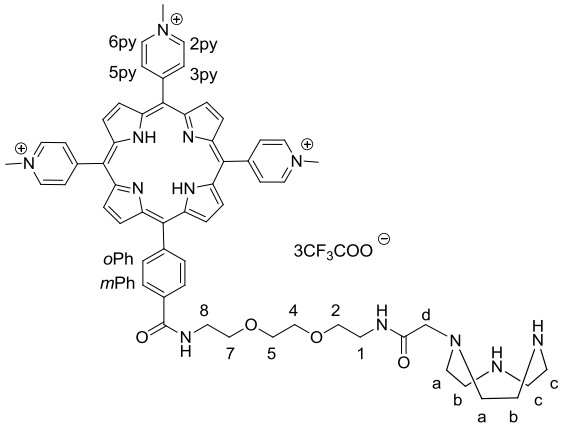

To a solution of porphyrin **15** was stirred for 3 h shielded from light, then the solvent was removed under reduced pressure until the complete elimination of TFA, to give the product as TFA salt. The deep green–brown solid was dissolved in CH_3OH (1 mL). To this solution TEA (10 µL) was added. The product was precipitated by adding Et_2O dropwise to the solution and was then extensively washed with Et_2O. The product was obtained as a purple solid.

Yield: 98% (21.83 mg).

TLC (CH_3CN/KNO_3 sat/H_2O 4:0.3:1, R_f = 0.6).

^{1}H NMR (CD_3CN, δ): 9.13 (d, 6H, 2,6py, J = 6.4 Hz), 9.06 (m, 6H, δH), 8.98 (m, 2H, bH), 8.83 (d, 6H, 3,5py, J = 6.5 Hz), 8.30 (dd, 4H, *o*Ph+*m*Ph), 7.83 (t, NHCO, 1H, J = 5.4 Hz), 4.69 (s, 3H, CH_3 py), 4.70 (s, 6H, CH_3 py), 3.79 (t, 2H, CH_2O, J = 5.4 Hz), 3.72 (m, 4H, CH_2O + CH_2NH), 3.66 (m, 2H, CH_2O), 3.58 (t, 2H, CH_2 2, J = 5.5 Hz), 3.37 (s, 2H, CH_2 d), 3.38 (m, 2H, CH_2NH), 3.29 (m, 4H, CH_2 b), 3.02 (m, 4H, CH_2 c), 2.82 (t, 4H, CH_2 a, J = 5.4 Hz).

^{19}F NMR (CD_3CN, δ): -75.62 (CF_3COO^-).

UV-Vis (CH_3CN): λ_{max} (ε x 10^{-3}, $dm^3\,mol^{-1}\,cm^{-1}$)= 423 (157), 517 (15), 553 (8.3), 590 (6.4), 646 nm (3.2).

ESI MS *m/z*: 1005.6 $[M]^+$, 502.8 $[M]^{2+}$.

ESI HRMS calcd for $[C_{59}H_{65}N_{12}O_4]/z$: $[M]^{3+}$ 335.17451, found 335.17451.

Porphyrin 17

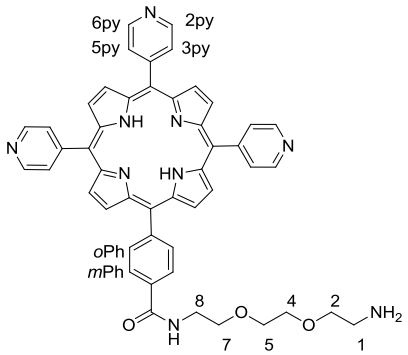

Porphyrin **12** (20 mg, 0.0224 mmol) was dissolved in CH_2Cl_2 (2 mL). To this solution TFA (500 µL) was added. The solution was stirred for 3 h shielded from light, then the solvent was completely removed under reduced pressure to give the product as TFA salt. The product was dissolved in CH_3OH (600 µL) and neutralized with TEA, precipitated and washed with Et_2O (3×10mL).

Yield 100% (17.74 mg)

TLC: $CH_3CN/KNO_3sat/H_2O$ 5:0.3:1, R_f = 0.30.

^1H NMR (CD_3OD, δ): 9.1-8.7 (br s, βH 8H), 8.98 (d, 6H, 2,6Py), 8.29 (m, 10H, HPh + 3,5 H Py), 3.87-3.75 (m, 10H, CH_2O + CH_2 8), 3.18 (t, 2H, $CH_2$1).

UV-Vis (CH_3OH): λ_{max} (relative intensity, %)= 413 (100), 511 (4.5), 545 (1.4), 588 (1.2), 642 nm (0.3).

ESI MS *m/z*: 792.4 $[M+H]^+$.

Porphyrin 18

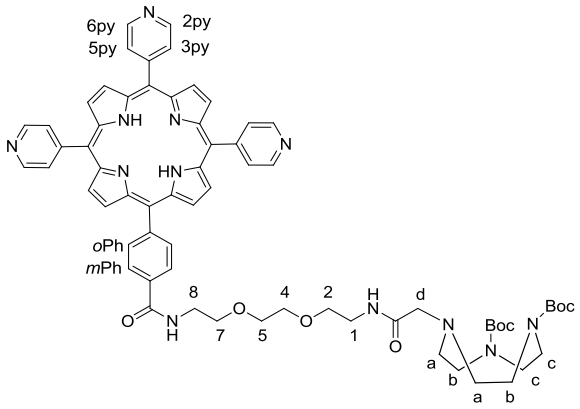

To a solution of **4** (9,36 mg, 0.024 mmol, 1.5 equiv) in anhydrous DMF (1 mL) HOBt (4.90 mg, 0.036 mmol, 2.25 equiv) and EDCI (0.036 mmol, 2.25 equiv) were added and the resulting solution was stirred for 30 min. To this solution a purple solution of the porphyrin **17** (12.75 mg, 0.0161 mmol) and DMAP (4.92 mg, 0.040 mmol, 2.5 equiv) in

anhydrous DMF (2 mL) was added. The coupling was performed in a microwave oven reactor (ramp time: 10 s, hold time: 6 min, T 60 °C, P 1720 kPa, power 30 W). The reaction was monitored by TLC ($CH_3CN/KNO_3sat/H_2O$ 4:0.3:1, R_f = 0.32). Porphyrin **18** was purified by column chromatography (2×10 cm, CH_2Cl_2/CH_3OH 95:5) obtaining the pure product as a purple solid.

Yield: 70.5 % (13.11 mg)

^{1}H NMR ($CDCl_3$, δ) 9.06 (d, 6H, 2,6py), 8.86 (m, 8H, βH), 8.28 (m, Ph, 4H), 8.16 (d, 6H, 3,5py), 7.51 (m, 2H, NHCO), 3.82 (m, 4H, CH_2O, CH_2NH), 3.71 (m, 4H, CH_2O), 3.63 (m, 4H, CH_2O), 3.49 (m, H, CH_2N, CH_2 TACN), 3.34 (m, 6H, CH_2 TACN), 3.20 (m, 2H, CH_2 d), 2.66 (m, 4H, CH_2 a), 1.46 (m, 9H, CH_3Boc).UV-Vis (CH_3OH): λ_{max} (relative intensity, %) = 417 (100), 513 (4.3), 547 (1.1), 589 (1.1), 643 nm (0.3).ESI MS *m/z*: 1183.6 $[M+Na]^+$, 1161.6 $[M+H]^+$.

Porphyrin 19

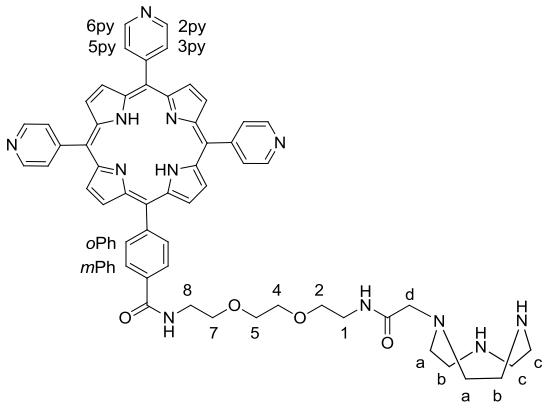

To a solution of porphyrin **18** (13.11 mg, 0.0113 mmol) in CH_2Cl_2 (1 mL) TFA (500 µL) was added. The solution was stirred at rt for 3 h shielded from light, and then the solvent was removed under reduced pressure until the complete elimination of TFA, to give the product as TFA salt. The solid was dissolved in CH_3OH (500 µL) and TEA (5 µL) was added. The product was precipitated by adding Et_2O dropwise to the solution and was then extensively washed with Et_2O. The product was obtained as a purple solid.

Yield: 100% (10.9 mg).

^{1}H NMR (CD_3OD, δ): 8.99 (m, 14H, 2,6py + Hβ), 8.29 (m, 10H, 3,5py + *o*Ph + *m*Ph), 3.82 (m, 2H, CH_2O), 3.78 (m, 4H, CH_2O + C*H*$_2$NH), 3.72 (m, 2H, CH_2O), 3.65 (t, 2H, CH_2O), 3.52 (m, 2H, CH_2O), 3.49 (t, 2H, C*H*$_2$NH), 3.42 (m, 2H, CH_2 d), 3.16 (m, 4H, CH_2 b), 2.95 (m, 4H, CH_2 a).

UV-Vis (CH_3OH): λ_{max} (relative intensity, %)= 413 (100), 510 (5.5), 543 (1.9), 588 (1.8), 643 nm (0.8).ESI MS *m/z*: 961.5 $[M+H]^+$.

Re(I)-conjugate 19

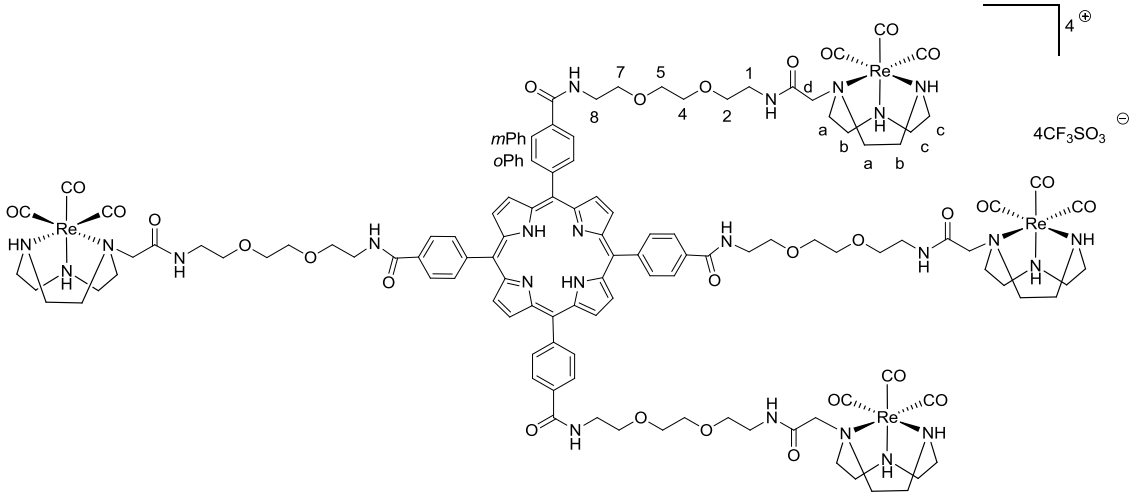

Porphyrin **9** (25.08 mg, 0.0126 mmol) was dissolved in anhydrous CH_3OH (20 mL). To this solution *fac*-$[Re(CO)_3(dmso)_3](CF_3SO_3)$ (49.91 mg, 0.0764 mmol, 6 equiv) was added. The stirred mixture was shielded from light and refluxed under argon for 48h. The reaction course was monitored by ^1H NMR spectroscopy at time intervals (6, 13 and 30 h) and by TLC ($CH_3CN/H_2O/KNO_3$, R_f = 0.46). After the solvent was removed under reduced pressure, the solid was dissolved in the minimum amount of CH_3OH and precipitated by adding Et_2O dropwise. The product was then extensively washed with Et_2O and CH_2Cl_2 to give a brown product.

Yield: 65% (30 mg).

^1H-NMR (CD_3OD, δ): 8.32 (dd, 16H, *o*+*m*Ph) 8.89 (br s, 8H, βH), 6.83 (s, 8H, NH TACN), 4.16 (s, 8H, CH_2 d), 3.83 (m, 8H, CH_2O), 3.78 (m, 16H, CH_2O+C*H*$_2$NHCO), 3.72 (m, 8H, CH_2O), 3.63 (t, 8H, CH_2O, *J* = 5.5 Hz), 3.44 (t, 8H, C*H*$_2$NHCO, *J* = 5.5 Hz), 3.23 (m, 16H, CH_2 a + CH_2 TACN), 3.13 (m, 8H, CH_2 a), 2.90 (m, 8H, CH_2 TACN), 2.70 (m, 8H, CH_2 TACN), 2.59 (m, 8H, CH_2 TACN).

UV-vis (CH_3OH): λ_{max} (ε × 10^{-3}, dm^3 mol^{-1} cm^1) 416 (217), 516 (10), 554 (5.0), 596 (3.1), 649 (2.3).

ESI HRMS calcd for $[C_{120}H_{170}N_{24}O_{28}Re_4]/z$: $[M]^{4+}$ 785.77116, found 785.77425.

IR (KBr, cm^{-1}): *v* =2028 (CO), 1910 (CO).

Re(I)-Conjugate 21

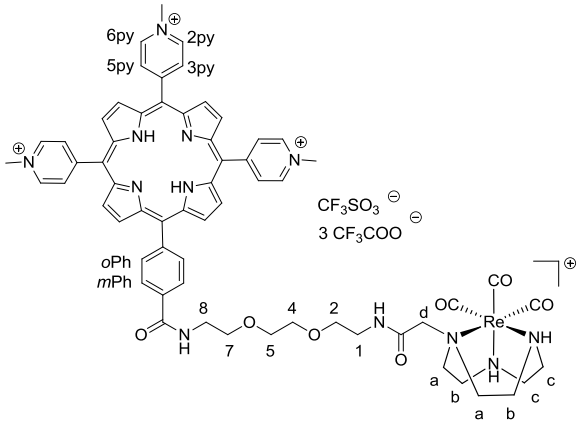

Porphyrin **16** (14.32 mg, 0.0106 mmol) was dissolved in anhydrous CH_3OH (5 mL). To this solution *fac*-[$Re(CO)_3$(dmso-$O)_3$](CF_3SO_3) (10.27 mg, 0.0157 mmol, 1.5 equiv) was added. The reaction was performed in a microwave oven reactor (first step: T = 65 °C, ramp time: 10 min, hold time: 30 s, P = 1720 kPa, power: 25 W; second step: T=110 °C, ramp time: 10 min, hold time: 10 min, P = 1720 kPa, power: 30 W). The reaction was monitored by TLC ($CH_3CN/KNO_3/H_2O$, 4:0.3:1, R_f = 0.32). The solvent was then removed under reduced pressure. The product was dissolved in the minimum volume of CH_3OH and precipitated with Et_2O, then washed with Et_2O and CH_2Cl_2 to remove the excess of the complex.

Yield: 73% (13.76 mg).

^{1}H NMR (CD_3CN, δ): 9.12 (d, 6H, 2,6py, *J* = 6.2 Hz), 9.06 (m, 6H, βH), 8.98 (m, 2H, βH), 8.83 (d, 6H, 3,5py, *J* = 6.5 Hz), 8.31 (dd, 4H, *o*Ph+*m*Ph), 7.66 (t, NHCO, 1H, *J* = 6.2 Hz), 7.12 (t, NHCO, 1H, *J* = 7.5 Hz), 5.90 (m, 2H, NH TACN), 4.96 (m, 9H, CH_3py), 4.12 (s, 2H, CH_2 d), 3.78 (t, 2H, CH_2O, *J* = 5.5 Hz), 3.72 (m, 4H, CH_2O+CH_2 8), 3.66 (m, 2H, CH_2O), 3.57 (t, 2H, CH_2 2 *J* = 5.5 Hz), 3.38 (m, 2H, CH_2 1), 3.31 (m, 2H, CH_2 c), 3.21 (m, 4H, CH_2 a), 3.00 (m, 2H, CH_2 b), 2.72 (m, 2H, CH_2 c), 2.63 (m, 2H,CH_2 b).

^{19}F NMR (CD_3CN, δ): -75.30 (CF_3COO^-), -79.28 ($CF_3SO_3^-$).

UV-Vis (CH_3CN): λ_{max} (ε x 10^{-3}, dm^3 mol^{-1} cm^{-1})= 424 (222), 517 (15), 553 (6.0), 590 (4.5), 646 nm (0.7).

ESI HRMS calcd for [$C_{63}H_{71}N_{12}O_7Re$]/z: $[M]^{4+}$ 323.62774, found 323.62772.

IR (KBr, cm^{-1}): *v* = 1977 (CO), 2104 (CO).

[Re(CO)$_3$TACN](CF$_3$SO$_3$) (22)

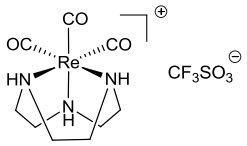

TACN (1.13 mg, 0.0087 mmol) was dissolved in anhydrous CH_3OH (2 mL). To this solution *fac*-[Re(CO)$_3$(dmso-O)$_3$](CF$_3$SO$_3$) (5.75 mg, 0.0085 mmol, 0.98 equiv) was added. The reaction was performed in a microwave oven reactor (first step: T 65 °C, ramp time: 10 min, hold time: 30 s, P 1720 kPa, power: 25 W; second step: T 110 °C, ramp time: 10 min, hold time: 10 min, P 1720 kPa, power 30 W). The solvent was then removed under reduced pressure to obtain the product as withe solid.
Yield: 100% (4.8 mg).
^{1}H NMR (D_2O, δ): 3.25 (m, 6H, CH_2TACN), 2.99 (m, 6H, CH_2TACN).
ESI MS *m/z*: 400 $[M]^+$.

Biological methods

Cell culture

Human cervical carcinoma cells (HeLa) were cultured in DMEM (Euroclone) supplemented with 5% fetal bovine serum (FBS, Gibco), 100 UImL^{-1} penicillin, 100 µg mL^{-1} streptomycin, 2 mM L-glutamine. The non-small-cell lung carcinoma cell line (H460M2) was grown in RPMI (Euroclone) supplemented with 5% FBS (Gibco), HEPES (Euroclone), 100 UImL-1 penicillin, 100 µg mL^{-1} streptomycin, 2 mM L-glutamine. HBL-100 non-tumorigenic epithelial cells were grown in McCoy's (Sigma) supplemented with 10% FBS (Gibco), 100 UI mL^{-1} penicillin, 100 µg mL^{-1} streptomycin, 2 mM L-glutamine. The cells were cultured at 37 °C and in 5% CO_2 humidified atmosphere.

Cell phototoxicity

Cells were sown at 10000 per well on 96-well plates and allowed to grow 24 h. Then they were incubated for 24 h with 0.1–100 µM solutions of each compound, obtained by serial dilutions of stock solutions (freshly prepared in DMSO at a concentration of 10-2M) with complete medium. Maximum DMSO concentration in the cell incubation medium was <_0.3% v/v. Thereafter, the media containing compounds were replaced with drug-free medium and cells were irradiated at λ = 650 nm at a fluence rate of 14

mW cm^{-2} for a time such that the total light dose was either 1, 5, or 10 J cm^{-2} (71 s; 5 min, 57 s; or 11 min, 54 s). The illumination was performed with a LED board equipped with dedicated software. The LED board and software were assembled and set up by F. Armani and G. Verona (A.P.L. Laboratory of the Department of Engineering and Architecture at the University of Trieste). The LED board is equipped with 96 red LEDs (L-53SRC-E, Kingbright) arranged in order to fit with the 96 wells of the cell culture plates. The emitted power (mW) at the end of the optical fiber was measured with an Ophir NOVA Laser Measurement power meter. Control experiments performed in the absence of any photosensitizer indicated that light doses up to 10 Jcm^{-2} cause no evident cell damage. A plate similarly treated, but not exposed to light was used as reference for dark cytotoxicity under the same experimental conditions. Analysis of cell phototoxicity by MTT assay was performed after further 24 h of incubation and compared with the values of control cells without light irradiation. Briefly, MTT dissolved in phosphate-buffered saline (PBS, 5 mg mL^{-1}) was added (10 µL per 100 µL medium) to all wells, and the plates were then incubated at 37 °C with 5% CO_2 and 100% relative humidity for 4 h. After this time, the medium was discarded, and 200 µL DMSO were added to each well according to the method of Alley et al.[99] Absorbance units were measured at λ = 570 nm on a SpectraCount Packard instrument (Meriden, CT, USA). IC_{50} values were calculated from dose–effect curves and are the mean +_SD of at least three separate experiments. The fitting procedure applied is a nonlinear regression performed with GraphPad Prism version 6 for Mac OS X version 6.0b (GraphPad Software, San Diego, CA, USA). Experiments were conducted in quadruplicate and repeated thrice.

Statistical analysis

Data obtained in the experiments were subjected to statistical analysis of variance (ANOVA) and Tukey–Kramer post-test, or to unpaired t test performed using GraphPad InStat version 3.06 for Windows (GraphPad Software, San Diego, CA, USA).

Singlet oxygen production

The quantum yield (Φ_Δ) of singlet oxygen generated by compounds **9**, **16**, **20**, **21** upon photoexcitation was measured using 9,10-dimethylanthracene (DMA) as substrate. Typically, 3 mL of 0.133 mM $CHCl_3$ solution of DMA and 0.4 µL solution of the porphyrin (0.4 A at Soret band maximum, ≈ 10 mM) in DMSO were placed in a luminescence quartz cuvette of 1 cm optical path and irradiated in a RPR100 Rayonet

Chamber Reactor (Southern New England Ultraviolet Company) complete with two lamps of λ = 420 nm light for different periods of time. The fluence rate was 2.57 mW cm^{-2}. The first-order rate constant of the photo oxidation of DMA by $^1O_2$ was obtained by plotting A_0-A as a function of the irradiation time t, in which A_0 and A represent the absorbance intensity at time 0 and at time t, respectively. The rate constant was then converted into $^1O_2$ quantum yield by comparison with the rate constant for DMA photo-oxidation sensitized by TPP, (for which Φ_Δ was shown to be 0.55) and with the absorbance correction factor $I=I_0*(1-10-A\lambda)$, where I_0 is the light intensity of the irradiation source in the irradiation interval, and A is the absorbance of the sample at wavelength λ.

Fluorescence microscopy

Cells were grown on 18 mm Menzel glass coverslips (Menzel, Germany) at a density of 2.5 x 10^5 cells mL^{-1} and incubated with the indicated compound. Upon 2 h treatment, cells were fixed for 15 min at room temperature in 4% formaldehyde solution (4% formaldehyde (w/v) in 1 x PBS) and mounted on microscopy slides. Fixed cells were examined with a CLSM Leica SP5 confocal microscope (DAPI λ_{ex}= 405 nm, λ_{em} = 430–500 nm; porphyrin λ_{ex} = 514 nm, λ_{em} = 600–700 nm) using 63 x 1.20 oil-immersion lenses.

DNA preparation

All oligonucleotides, namely Myc22 (5'-TGA GGG TGG GTA GGG TGG GTA A-3'), H-telo (5'-AGG GTT AGG GTT AGG GTT AGG G-3'), and ds-26 (5'-CAA TCG GAT CGA ATT CGA TCC GAT TG-3') were purchased from Eurogentec and used without further purification. ct-DNA was purchased from Sigma–Aldrich and used as received. The oligonucleotides (for both emission and CD spectroscopic studies) were dissolved in Milli-Q water to yield 1 mM stock solution which was stored at – 20 °C and defrosted on the day when a given experiment was carried out. The 1 mm oligonucleotide stock solution was further diluted using appropriate buffer to the desired concentration on the day of the experiment. The concentration of oligonucleotides was determined by UV-Vis spectroscopy using appropriate extinction coefficients at λ = 260 nm. For the emission titrations, concentration of the compound being studied was kept constant (at 5 μm); the concentration of DNA added during the titrations (after appropriate dilutions from the stock solution) ranged between 0 and 40 μm. For the variable-temperature CD

spectroscopic studies the final concentrations of DNA and compound were 5 and 10 µm, respectively.

Compound preparation for DNA binding studies

Compounds were dissolved in Milli-Q water to yield 1 mM solutions (except for 2, which was dissolved in DMSO). These solutions were diluted with the buffer to give a final concentration of 5 µm for the emission titrations and 10 µm variable-temperature CD studies. Unless stated otherwise, all measurements were performed in Tris・HCl (50 mM) buffer containing 100 mm KCl (pH 7.4). Emission and excitation spectra were recorded on Varian Cary Eclipse Spectrometer. Circular dichroism measurements were carried out using a Jasco J-715 Spectropolarimeter.

DNA photocleavage

DNA photocleavage experiments were performed according to a method reported recently by Gasser's group [100]. More specifically, supercoiled pUC18 plasmid (0.20 µg) was incubated with 1–4 at increasing concentrations in buffer (50 mM Tris・HCl, 18 mM NaCl, pH 7.2) and at λ = 420 nm for 22 min (10 J cm^{-2}) in a RPR100 Rayonet Chamber Reactor (Southern New England Ultraviolet Company). A series of negative controls of the plasmid treated with the highest concentrations of 1–4 in the dark was used for comparative purposes. After irradiation the samples were added with loading buffer (250 mg xylene cyanol in 33 mL 150 mM Tris・HCl buffer, pH 7.6) and analyzed by electrophoresis in agarose 0.8% in 1_TBE (diluted from a 10_ solution of 108 g Tris・HCl, and 55 g of H3BO3 in 900 mL H2O) at 70 V (BioRad Power Pack 1000) for 1.5 h. The gel was pre-stained with GelRed (1:10 000, Biotium), photographed and quantified with an AlphaDigiDoc 1000 CCD camera (Buchner Biotec AG) and AlphaImager software (version 1.3.0.7.).

3.

SYNTHESIS OF PEPTIDE-PHOTOSENSITERS TO TARGET PROSTATE CANCER CELLS

This work is in collaboration with the research group of Professor Gilles Gasser – Department of Chemistry, University of Zurich

3.1. TARGETING CANCER CELLS

Targeted drug delivery methods have been explored to improve drug efficacy and reduce side effects by directing the drug to a specific cell type. Many molecules have been studied to target drugs such as monoclonal antibodies, nanoparticles, folate ligands and peptides. The concept of drug-carriers conjugates is illustrated in Figure 40 [101].

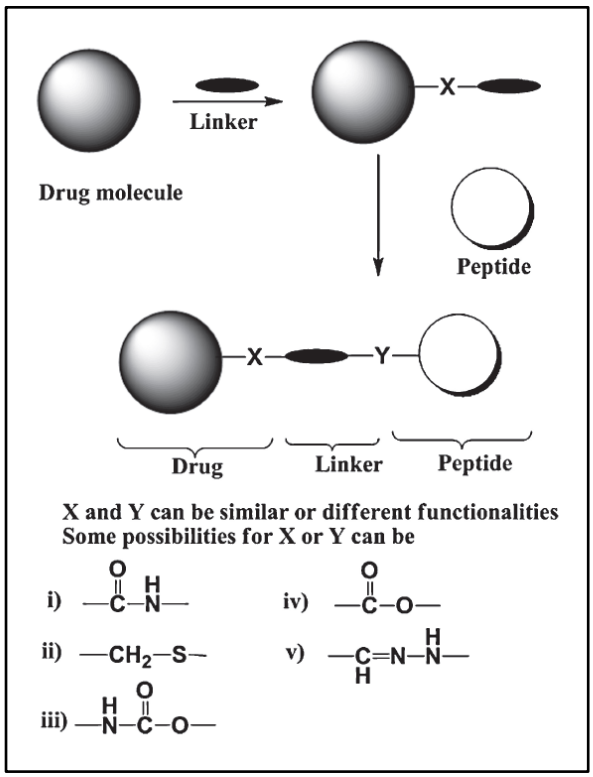

Figure 40: The structure of a drug-linker-peptide conjugate [101]

Peptides are deeply investigated since they have advantages that make them excellent candidates for drug targeting such as: *i*) increased tissue permeability; *ii*) rapid internalization capacity; *iii*) effective receptor binding; *iv*) rapid clearance; *v*) very mild antigenicity [102]. Peptides present also negative factors such as short biological half-life and loss of binding affinity upon coupling with a chelator that can be minimized by inserting a spacer between the binding sequence and the chelating moiety [103]. The treatment of cancer has been enhanced with targeting drug delivery methods exploiting for example specific targets receptors overexpressed in tumor cells [104]. Focusing on photodynamic therapy (PDT), a third generation of PSs is being investigated to

enhance the tumor selectivity by using additional molecular entities capable to address the PSs to a specific target [105]. In this way PDT can overcome the low tumor selectivity of the clinically used PSs. Since porphyrins are preferentially but not selectively accumulated in tumor tissues, Vicente and coworkers synthetized several peptides-porphyrins to increase the tumor selectivity. The selective accumulation of these porphyrin-peptides depends on the type of targeting peptide bound to the porphyrin. For example the cell-penetrating peptides (CPPs) increase the penetration of the porphyrin into the cell; instead the mitochondrial localization signals (MLSs) increase the accumulation in the mitochondria [106-109]. The CPP-conjugate, reported in Figure 41 is more selective for prostate tumor than hematoporphyrin derivative (HPD) [110].

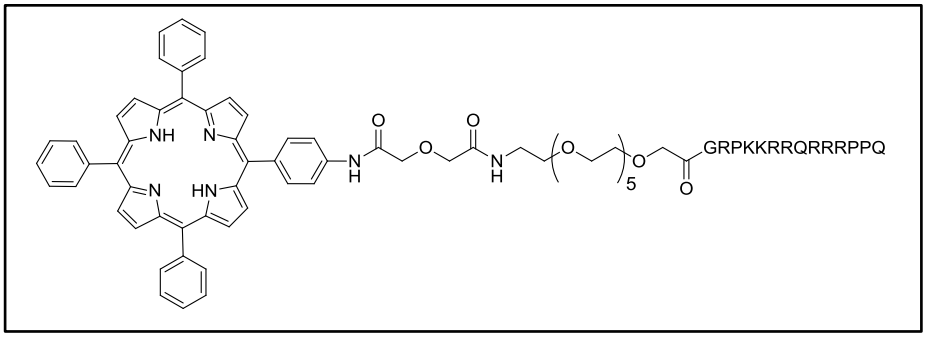

Figure 41: Vicente's porphyrins containing a peptide sequence CPP based on the HIV-1 Tat sequence

Besides CPPs also the membrane translocation sequences (MTSs) are used to target the tumor cells. CPPs and MTSs are peptides with a maximum of 30 amino acids that are able to translocate across the biological cell membranes. Their cell membrane penetration mechanism is not fully understood. However it seems to depend on the type of peptide and it is probably an endocytic mechanism [111, 112]. Instead the synthetic peptides containing a nuclear localization signal sequence (NLS) are peptides that bind DNA after cell penetration via receptor-mediated endocytosis. The resulting DNA–NLS complex can be recognized by specific intracellular receptor and proteins [113]. Peptides that target the vascular system are also studied to increase the selectivity of the PS. Also the second generation of radiopharmaceuticals is based on targeted drug delivery methods. Several researches focused on the development of new tumor specific peptide based radiopharmaceuticals [103, 114]. To be clinically useful for tumor imagining, a radiolabeled peptide should have: *i*) high affinity for the target receptor; *ii*) ease of preparation; *iii*) high stability in vivo; *iv*) high specific uptake and retention in tumors [103, 114]. The structure of a targeting peptide radiopharmaceutical is illustrated in Figure 42.

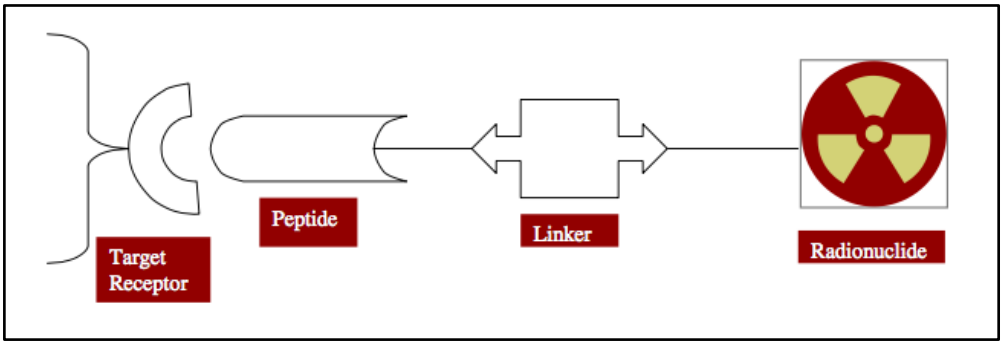

Figure 42: A general strategy to target a receptor with a peptide radiopharmaceutical [103]

An important example of targeting peptide, especially in the field of radiopharmaceutical, is represented by bombesin (BN), a 14-amino acid neuropeptide isolated from the skin of the *Bombina orientalis* frog. Its structure (a COOH terminus ending in Gly-His-Leu-Met-NH_2) is well known and is reported in Figure 43 [115].

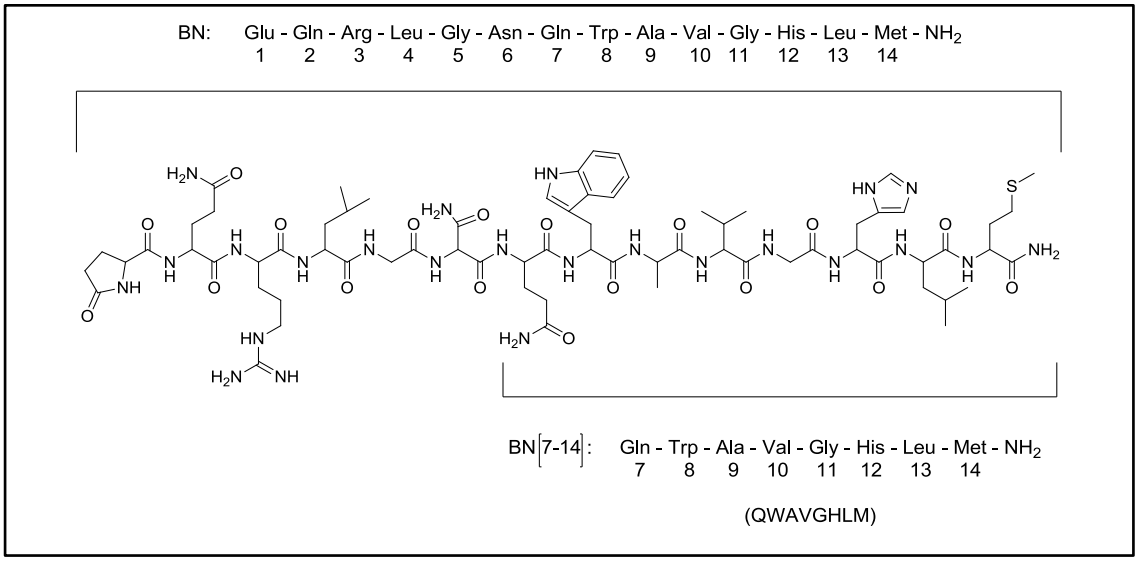

Figure 43: Peptide sequence of bombesin BN and BN[7-14]

Two related peptides, the gastrin-releasing peptide (GRP) and the neuromedin-B (NMB), are present in humans [114]. GRP is made of 27 amino acids and shares with BN the seven COOH terminal amino acids; instead NMB is made of 10 amino acids and present a COOH terminus ending in Gly-His-Phe-Met-NH_2. To date, three mammalian BN/GRP receptor subtypes were characterized for these peptides: *i*) GRP-R or BB2-R (GRP-preferring receptor); *ii*) NMB-R or BB1-R (NMB-preferring receptor) and *iii*) an orphan receptor called BRS-3 or BB3-R. These are heptahelic G protein-coupled membrane receptors, which stimulate many signals; in particular they activate phospholipase C and MAP kinase, stimulate tyrosine phosphorylation and rarely adenylate cyclase [116, 117]. After activation, they undergo a number of receptors

modifications including phosphorylation, internalization and recycling, down regulation and desensitization. Researchers are interested in two signals cascades especially in tumor tissues: the tyrosine kinase cascades and the epidermal growth factor receptor (EGFR) (Figure 44) [118].

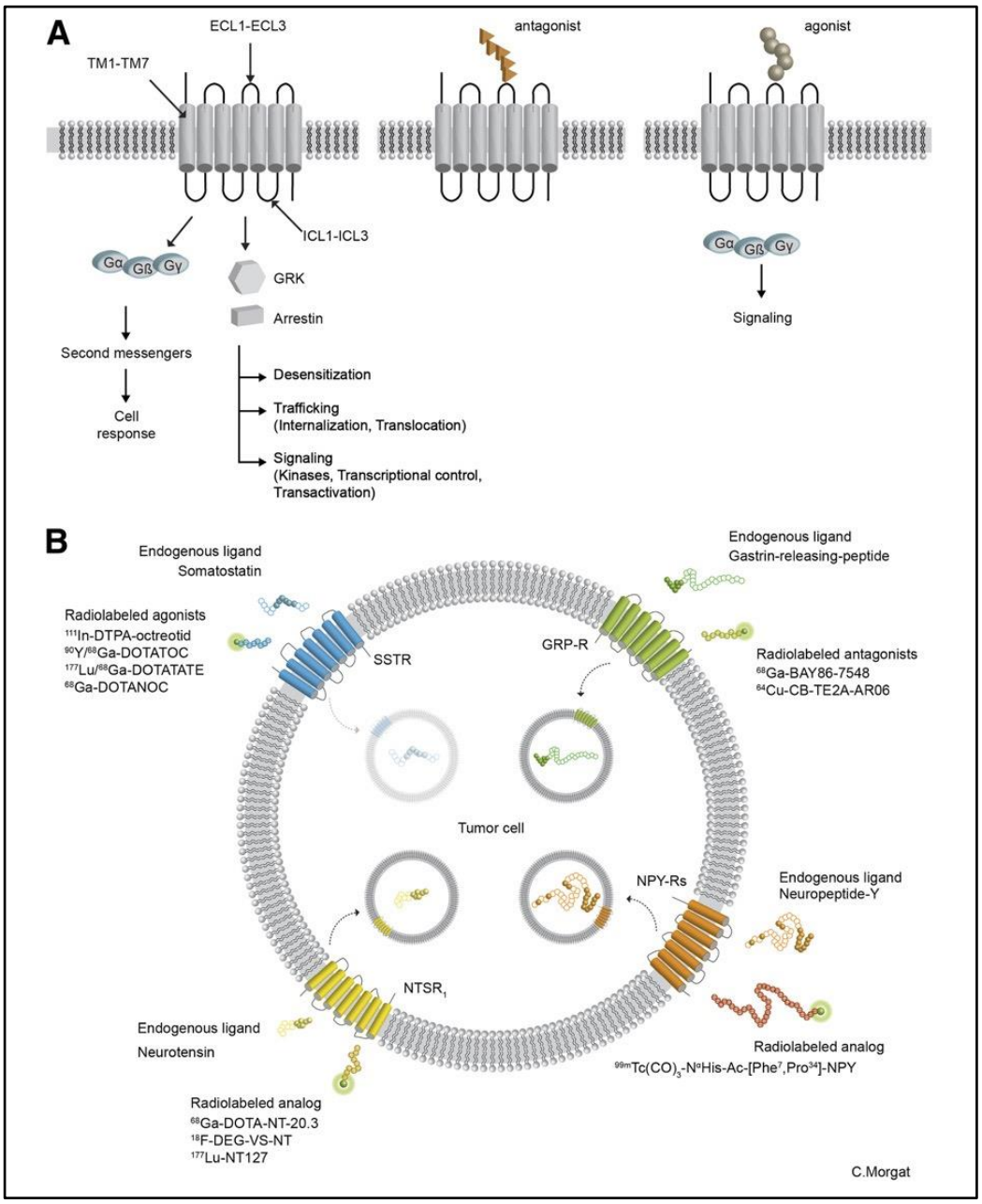

Figure 44: General transduction of G-protein-coupled receptors GPCRs (A) and BN receptors (B) [114]

GRP and NMB are distributed in both central and peripheral nervous system of mammals; indeed they are involved in several physiological processes such as circadian rhythm, TSH release, behavior control, thermoregulation, satiety, and in the urogenital, respiratory and immune systems. They are important especially in the

gastrointestinal (GI) tract where they stimulate the gastrin release and regulate gastric acid secretion and enteric motor function. Furthermore, since these receptors are overexpressed in several tumors, GRP and NMB stimulate the growth and the differentiation of tumors such as colon, prostate, lung, head and neck, CNS, pancreatic and some gynecologic tumors. These peptides have effect also in the premalignant cells of prostate, gastric and lung cancers [119]. For such a reason, their receptors are promising targets for the cancer therapy and BN-like peptides are excellent molecules to deliver drugs into tumor cells [120]. Going into detail about the structure-activity relationship (SAR) of the BN-like peptides, the C terminus of BN is required for high affinity binding and its BN[7-14] fragment is the minimum sequence required to stimulate the receptor activity (Figure 43). More specifically GH(L/F)M-NH_2 are the amino acids of the carboxylic terminus of bombesin, GRP and NMB required for the activity [121, 122]. Concerning the receptor, four amino acids of the gastrin releasing peptide receptor were proposed by Battery and co-workers as important for a high binding affinity: Gln-121, Arg-288, Ala-308 and Pro-199 [122]. With the aim to treat the tumors already cited, BN and GRP agonists are used, and recently also their antagonists were taken into account since they can provide antitumor effect [114, 123]. Although antagonists are not internalized into tumor cells after binding to the receptors, they offer excellent targeting properties. BN[7-14] was studied to evaluate the transport of metals such as ruthenium into tumor cells [124], and the same peptide was conjugate with radioactive metals such as ^{105}Rh, ^{99m}Tc, ^{111}In, ^{177}Lu, ^{18}F, ^{64}Cu showing promising results as tumor localizing agent [118]. For example the bombesin analogues ^{177}Lu-AMBA and $Re(CO)_3$/$^{99m}Tc(CO)_3$ BBS-II were synthesized and evaluated in vitro in PC-3 cell cultures (Figure 45) and ^{177}Lu-AMBA showed high affinity and specificity for the GRP-R and it bounds this receptor with a nanomolar affinity.

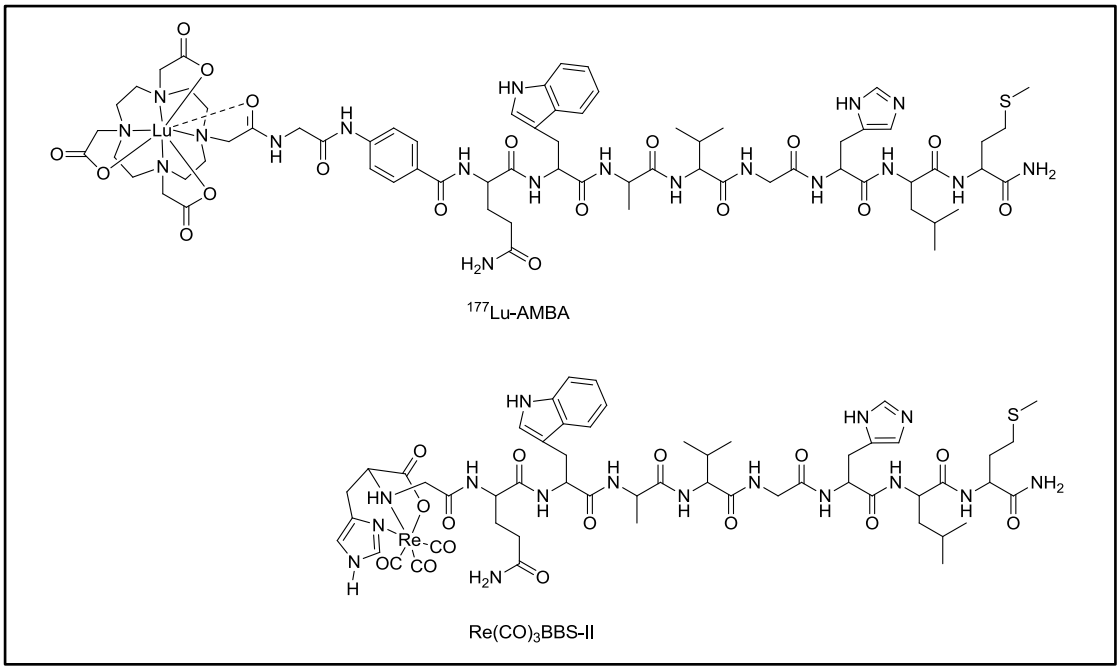

Figure 45: ^{177}Lu-AMBA and Re(CO)$_3$BBS-II structures

3.2. STRATEGIES FOR THE DEVELOPMENT OF NEW PHOTOSENSITIZERS

For all the reasons detailed above we designed a new tumor-specific PS, according to the synthetic strategy showed in Figure 46. The structure is formed of several parts bound together by covalent bonds. The main portions are a porphyrin, a targeting peptide sequence and a chelator suitable for metal coordination.

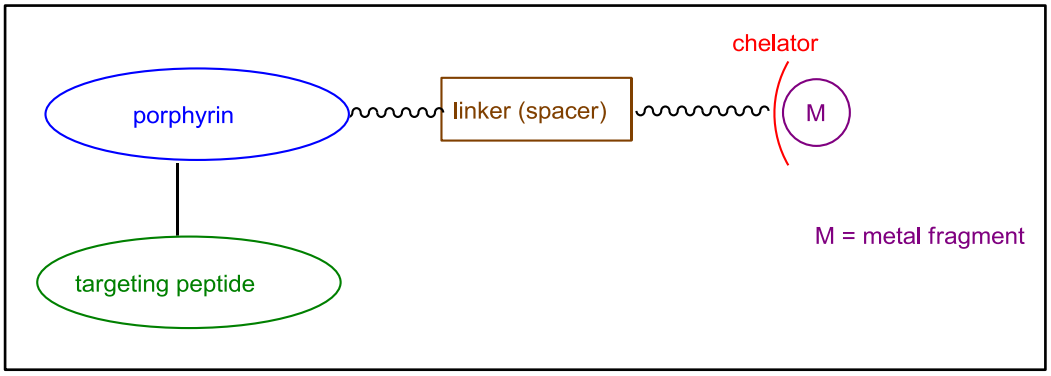

Figure 46: Schematic structure of the designed molecule

Porphyrin **14** (Scheme 9) was chosen since it is water soluble and it can easily bind a chelator unit in one peripheral position. The tridentate chelator unit is the functionalized TACN **4** (Scheme 9) that can coordinate $Re^{I}/^{99m}Tc^{I}$ fragments, such as $\{Re/^{99m}Tc(CO)_3\}^{+}$. Bombesin BN[7-14] (Scheme 9) was chosen as a targeting peptide for three reasons: *i*) it can target prostate cancer cells, a tumor already treated with PDT in clinical practice; *ii*) its coupling with a functionalized chelator (NOTA) is described [125]; *iii*) it is in clinical trials for prostate cancer [126]. Consequently, this very challenging molecule might act as a PS, be selectively targeted to prostate cancer cells and be able to coordinate both cold Re and hot ^{99m}Tc in order to have a potential application also in the diagnostic field. Two different synthetic approaches based on click chemistry and coupling reaction are described in the following sections.

3.3. CLICK CHEMISTRY APPROACH FOR THE SYNTHESIS OF BN [7-14]- PORPHYRIN

3.3.1. FIRST STRATEGY FOR THE SYNTHESIS OF THE FINAL MOLECULE

The first synthetic approach to bind the three parts of the molecule (porphyrin, peptide and chelator) was planned by using a click chemistry reaction. The key molecule of the synthesis is the commercially available Boc-propargyl-Gly-OH. This compound has either *i*) a carboxylic group, that can react with the amino group of porphyrin **14**; *ii*) an amino group, that can form an amide bond with the carboxylic group of the functionalized TACN **4**; and *iii*) an alkyne suitable to the click reaction. An azido function was introduced on the BN[7-14] by reacting 5-azidopentanoic acid with the amino group of the glutamine in position 7 of the peptide sequence, thus making possible the click chemistry reaction between the peptide and the porphyrin (Scheme 9).

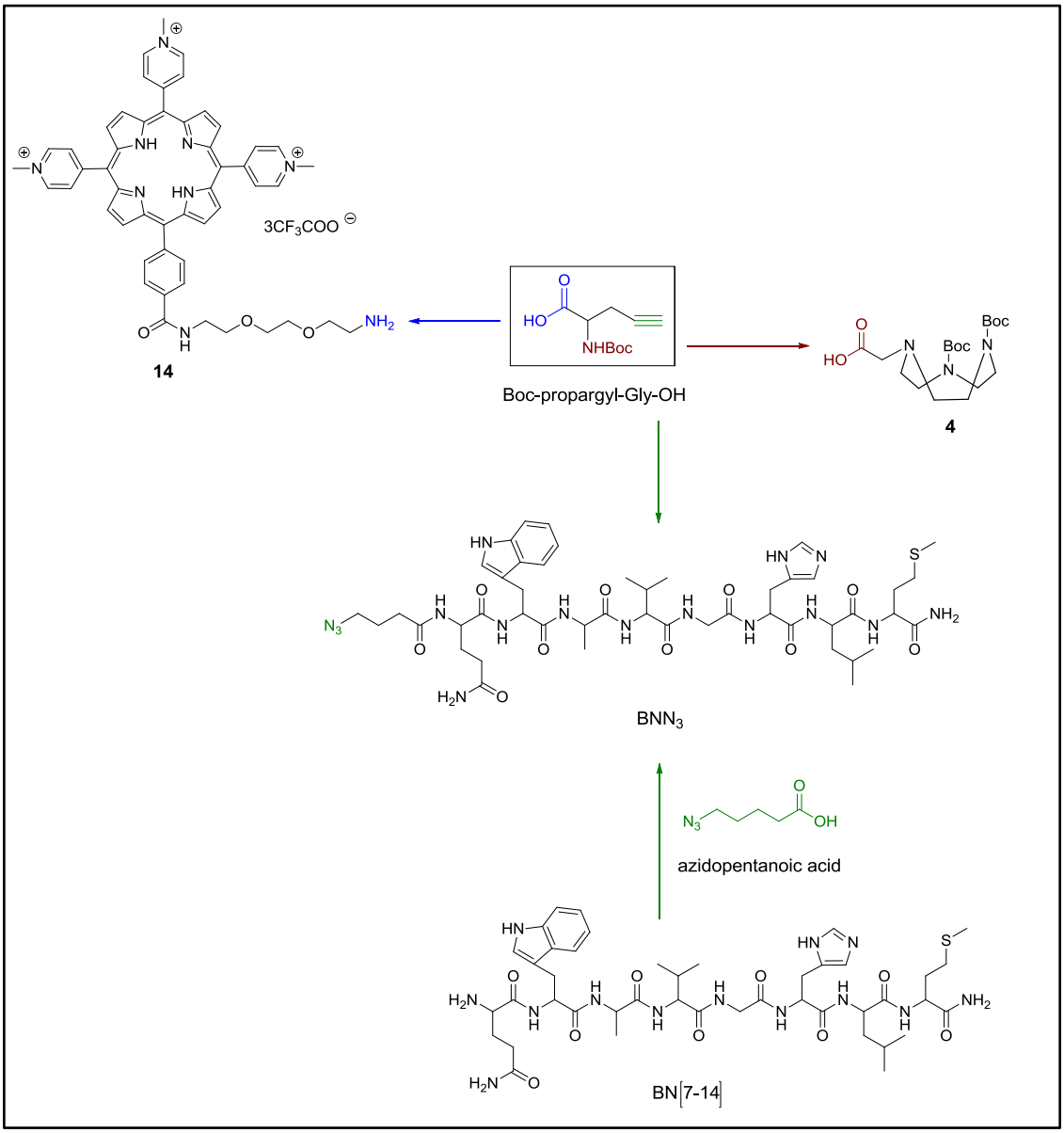

Scheme 9: Synthetic strategy to connect **14**, **4** and BN[7-14] using Boc-propargyl-Gly-OH

3.3.2. SYNTHESIS OF THE ALKYNE-PORPHYRIN AND THE AZIDO PEPTIDE

Porphyrin **14** was first coupled with the Boc-propargyl-Gly-OH and then with the functionalized TACN **4** following the procedure showed in Scheme 10.

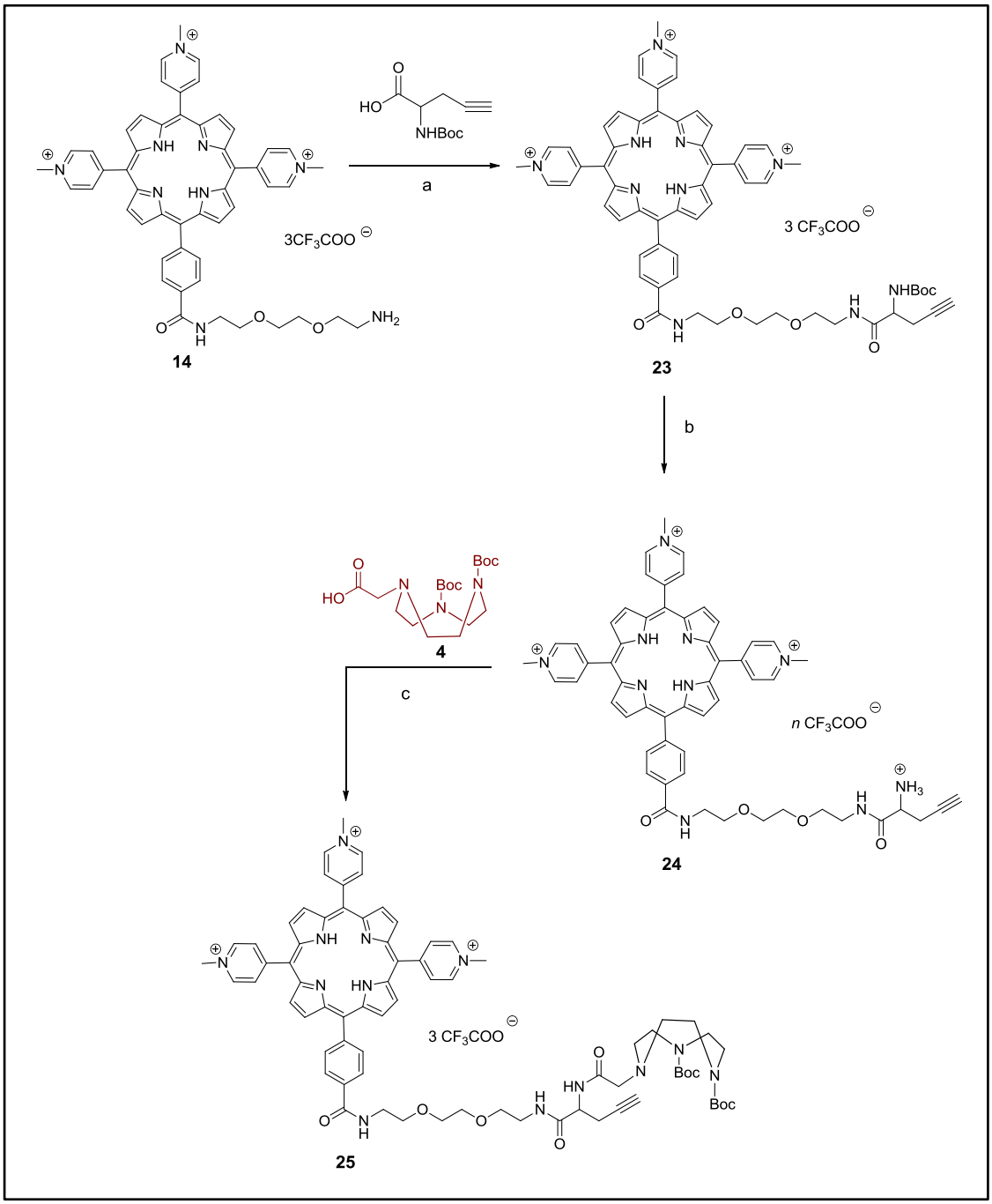

Scheme 10: Synthetic route for **22**-**24**. *Reagents and conditions*: a) DMAP, EDCI, HOBt, DMF, overnight, rt, 69%; b) TFA, CH_2Cl_2, 4h, rt; c) DMAP, EDCI, HOBt, DMF, overnight, rt, 70%

The first coupling reaction between the amino group of porphyrin **14** and the carboxylic group of Boc-propargyl-Gly-OH was performed using EDCI, HOBt and DMAP in DMF at room temperature overnight. After the purification by repeated precipitations

(CH_3OH/Et_2O) and extensive washes with Et_2O and CH_2Cl_2, the product was obtained in high yield. The amino group of the Boc-propargyl-Gly-OH was deprotected using TFA in CH_2Cl_2 and porphyrin **24** was obtained as TFA salt and then directly reacted with the carboxylic group of the chelator. After the usual workup of precipitations and washes, porphyrin **25** was obtained and characterized by RP-UPLC-MS, ^1H and HSQC NMR. The downfield region of the ^1H NMR spectrum (Figure 47) shows the pyridine protons at δ 9.39 (2,6py) and 8.97 (3,5py) (cross peaks in the HSQC spectrum at δ 145 and δ 133), and the 4H of the phenyl ring at δ 8.30 (cross peaks at δ 126 and 135 in the HSQC spectrum). In the upfield region the resonance of the CH_3 protons bound to the pyridines (δ 4.80, cross peak at δ 48 in the HSQC spectrum) is superimposed on the H_2O resonance. The protons of the spacer resonate as a cluster of multiples between δ 3.41 and 3.82 (cross peaks at δ 70 for the protons bound to an oxygen atom and δ 40 for the ones bound to a nitrogen atom in the HSQC spectrum) (Figure 48). The protons in position 2' and 5' of the glycine resonate at δ 4.51 (cross peak at δ 52 in the HSQC spectrum) and at δ 2.36 (cross peak at δ 72 in the HSQC spectrum) respectively. The protons in position 3' of the glycine overlap with Ha of TACN and resonate as a multiplet. This assignment was confirmed by the HSQC spectrum that showed two cross peaks at δ 54, for the Ha protons of the chelator, and at δ 22 for the 3' protons of the glycine. Between δ 3.5 and 3.1 the spectrum shows the multiplets of Hb, Hc and Hd protons of TACN and the protons of a CH_2 bound to a nitrogen atom of the spacer.

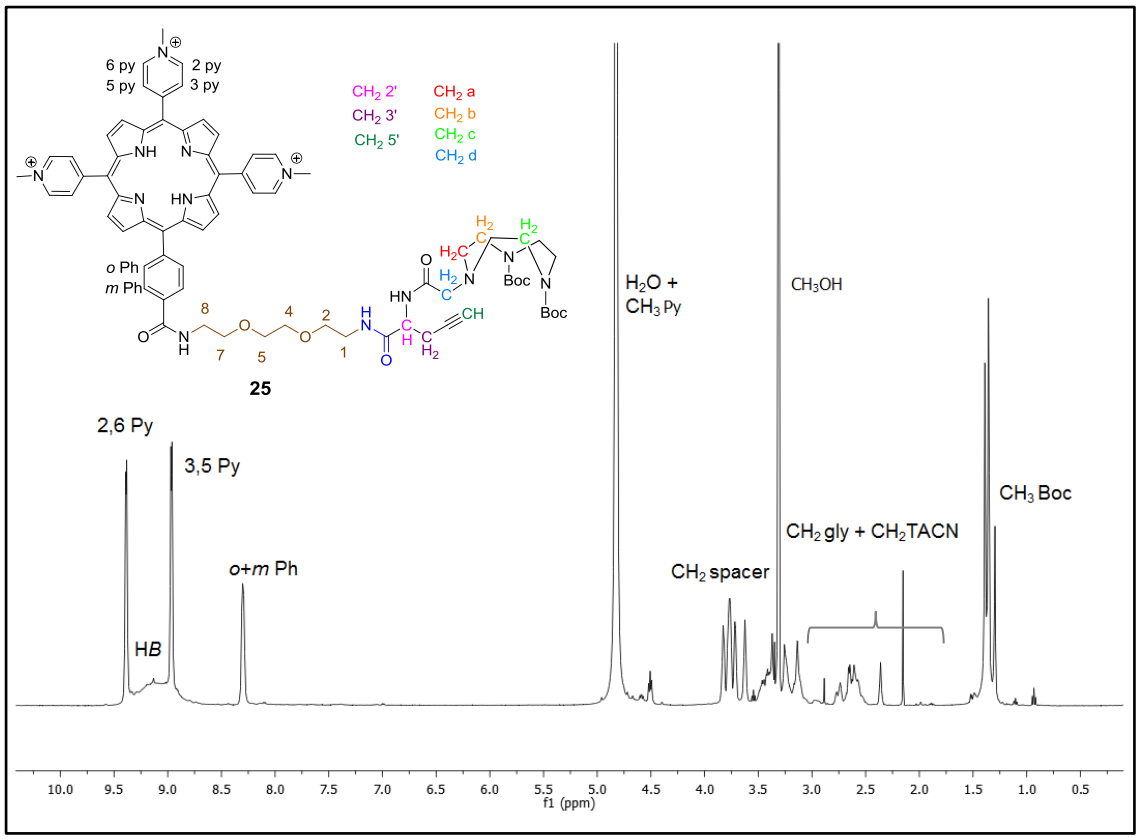

Figure 47: ^{1}H NMR (CD_3OD) of **25**

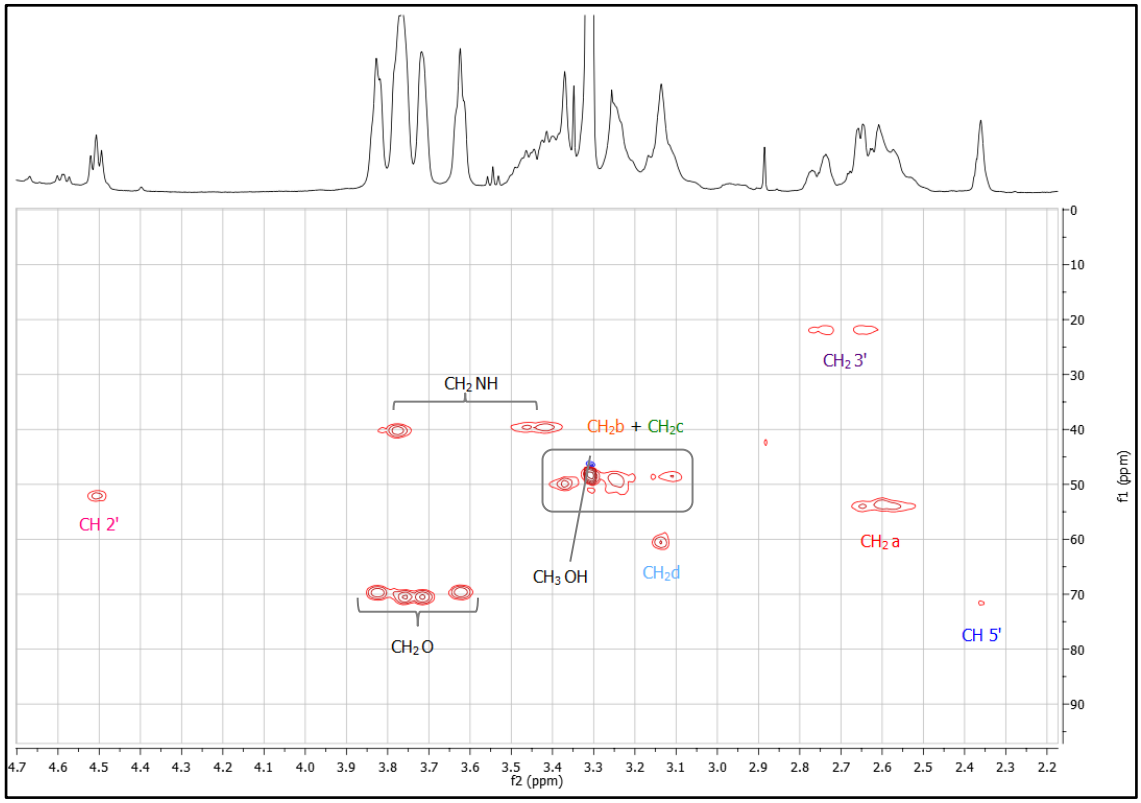

Figure 48: HSQC (CD_3OD) of **25**

The azido-peptide BNN_3 (Scheme 15) was synthesized by solid-phase peptide synthesis (SPPS). Tentagel-S-RAM was used to build up the peptide sequence BN[7-14]. This is a low cross-linked polystyrene resin on which a poly(ethylene glycol) is grafted via an ether bond, which has high stability towards acid treatment and minimizes PEG leaching (Figure 49). Thanks to the PEG chains the resin solubilizes both hydrophobic and hydrophilic compounds and it is stable to pressure [127].

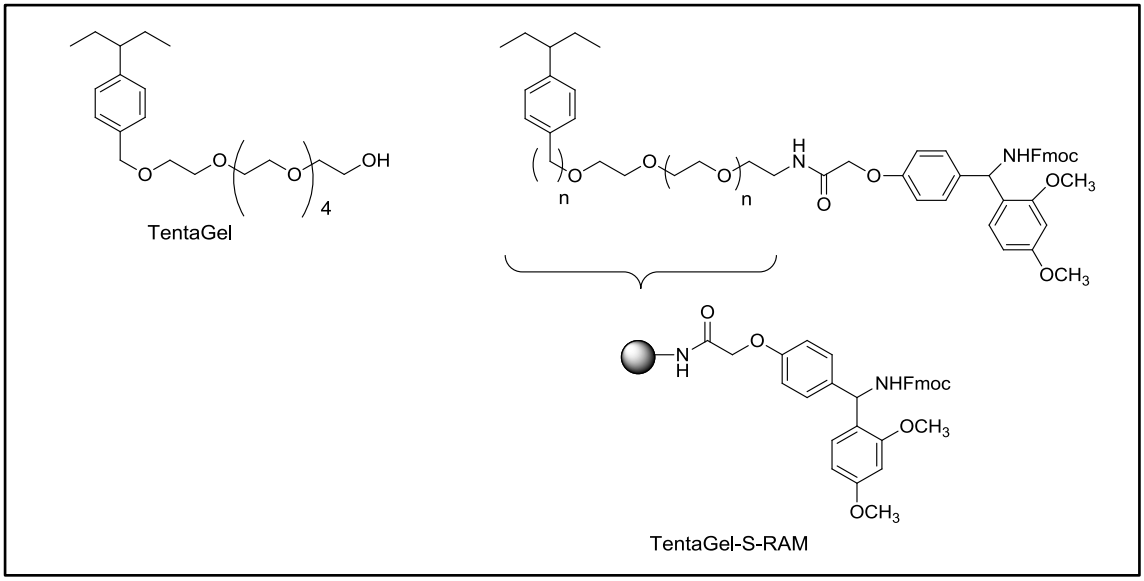

Figure 49: TentaGel and Tentagel-S-RAM resins

The peptide was synthesized following these steps:

1) Swelling of the resin

The resin was left shaking in DMF for at least 1 h before use in order to open the resin beads and to allow the Fmoc amino groups of the resin to be available for the coupling reaction with the first amino acid (methionine). After filtration, the resin was ready for the second step.

2) Deprotection of the NHFmoc

The Fmoc deprotection was performed with piperidine in DMF [128].

3) Activation of the carboxylic group and coupling reaction

The activation of the carboxylic group of the first amino acid was performed using a large excess of TBTU in DMF [128-132].

4) Reaction control

A Kaiser test was performed to evaluate the reaction completion. A positive result (yellow Kaiser test solution) indicated that no free amino group was present on the resin. Steps 2 and 3 were repeated for the second amino acid of the sequence and so on for the other amino acids of the target peptide. A negative result (dark blue Kaiser test solution) indicated that Fmoc amino groups were still present on the resin, and step 2 and 3 were repeated for the same amino acid.

5) Cleavage reaction

This step was performed both to check the coupling reaction before performing other reactions in solid phase (SP) and to completely release the peptide from the resin in order to carry out other reactions in solution. After the peptide synthesis completion, the peptide was cleaved from the resin using a cleavage solution made of TFA, TIPS and H_2O. The TFA was used both to release the peptide from the solid support and to remove the protecting groups of the side chains of the amino acids (Scheme 11). It is convenient that the protecting groups of the side chains are released with the same reagent (TFA) used to release the peptide from the solid support [133]. Secondary reactions can occur during the deprotection and cleavage steps, since the carbocations that are formed during the reaction can react with the side chains of the peptide. For this reason TIPS is usually added as scavenger to the cleavage solution. The filtrate containing the deprotected and cleaved peptide was evaporated and the peptide was precipitated and washed several times with cold Et_2O. The peptide was purified by HPLC and characterized by RP-UPLC-MS and analytical HPLC.

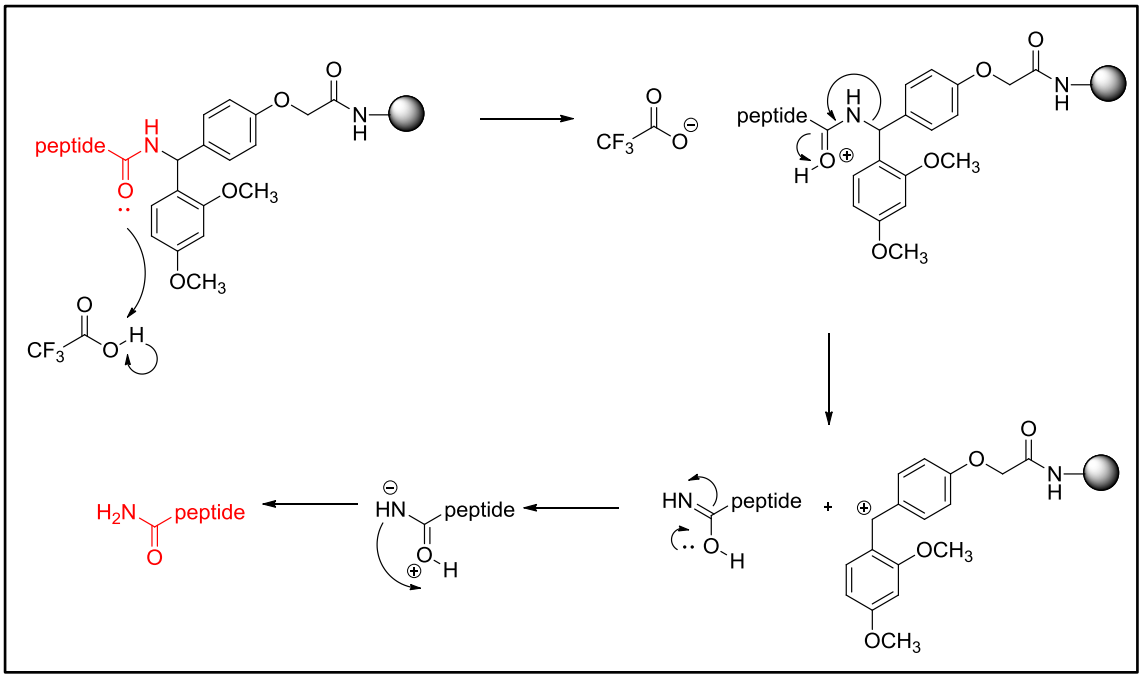

Scheme 11: Cleavage reaction of the peptide

The whole peptide BN[7-14] synthesis is reported in Scheme 12. A large excess of each amino acid was used and after every coupling reaction the peptide was purified simply by filtration, increasing the yield and reducing the reaction time.

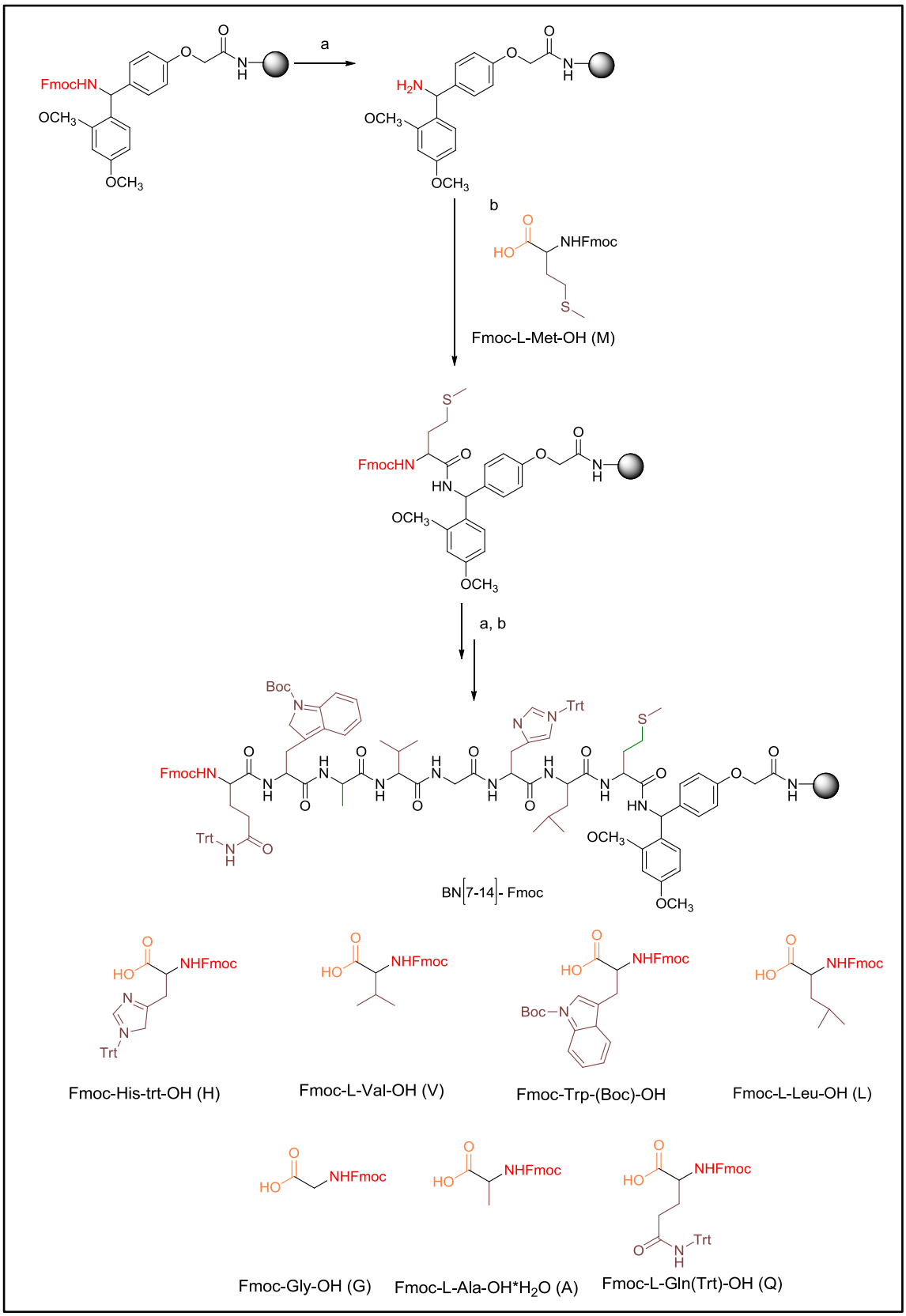

Scheme 12: Synthesis of BN[7-14]. *Reagents and conditions*: a) piperidine, DMF, 2'+10'; b) TBTU, DIPEA, 2,6-lutidine, DMF, amino acid, 1h, rt.

The following step was the SP coupling reaction between the TBTU-activated carboxylic group of the azido pentanoic acid and the amino group of the glutamine of BN[7-14] that was previously deprotected (Scheme 13).

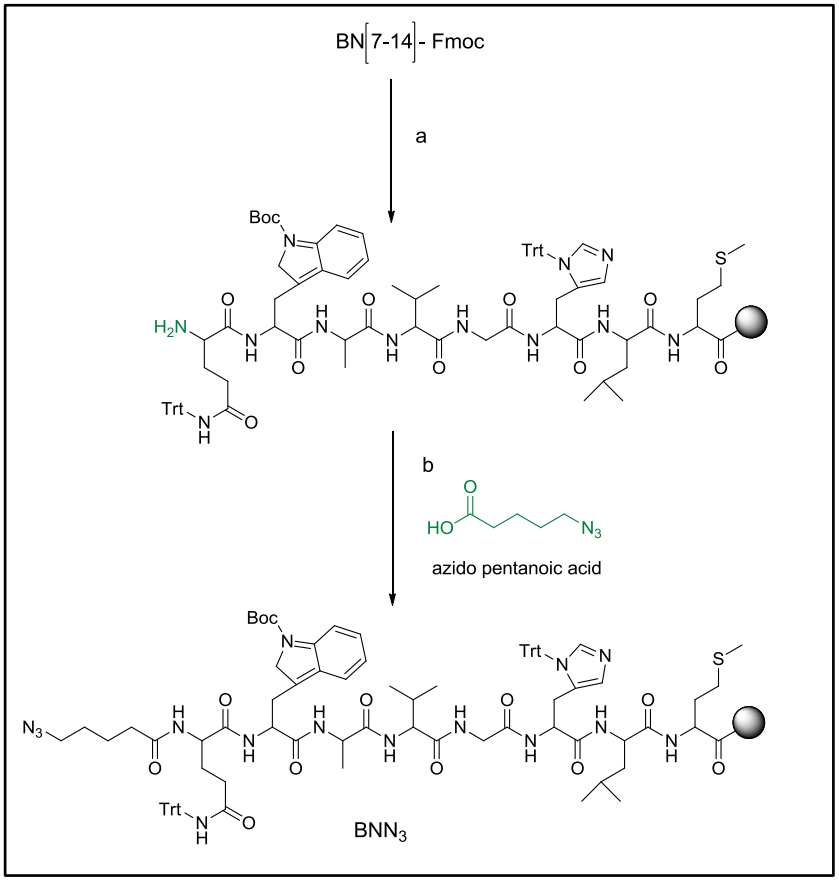

Scheme 13: Synthesis of BNN_3. *Reagents and conditions*: a) piperidine, DMF, 2'+10'; b) TBTU, DIPEA, 2,6-lutidine, DMF, 1h, rt

Both BNN_3 and the correspondent BNN_3 with methionine oxidized ($BNN_{3\ OX}$) were observed in RP-UPLC-MS chromatogram (Figure 50).

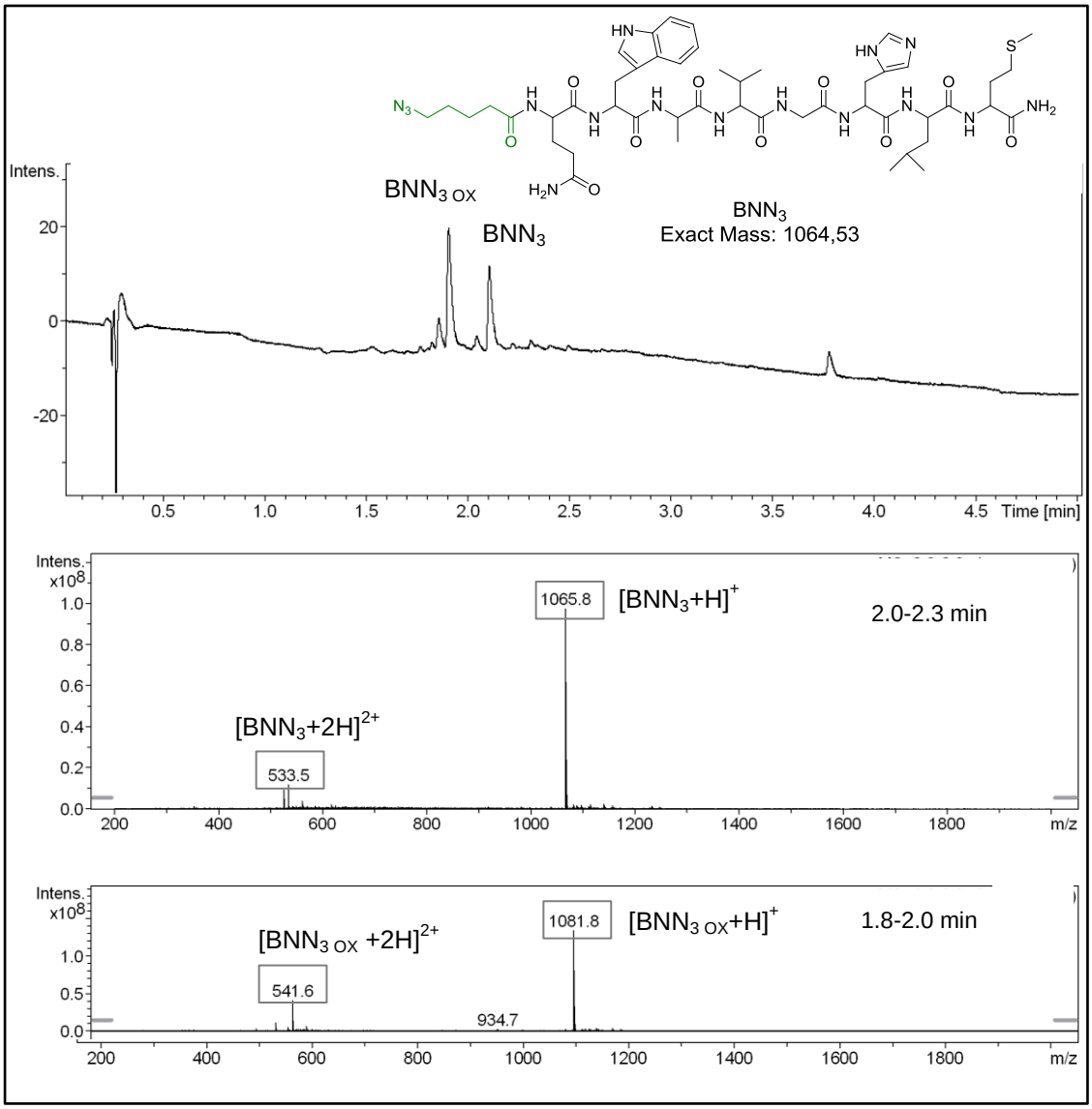

Figure 50: RP-UPLC-MS (H_2O/ACN) of BNN_3, 290 nm

The oxidation of methionine to sulfoxide (Figure 51) is a reaction that can occur during extraction and storage, in the presence of biological oxidants (NAD) and also in an acidic environment. In fact oxygen-exchange reactions can occur in strong acids or in the presence of copper or iron ions that are biological species [134-136].

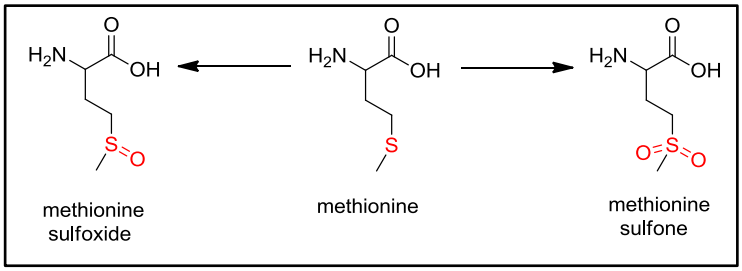

Figure 51: Oxidized forms of methionine

3.3.3. CLICK CHEMISTRY REACTION

A click chemistry reaction must meet the several requirements. It should: *i*) start from few small molecules; *ii*) use easily removed and environmentally friendly solvents such as water; *iii*) give high yield and *iv*) give products that can be purified with easier methods than chromatography [137]. The copper catalyzed azide-alkyne cycloaddition reaction (CuAAC) perfectly satisfies the requirements of this synthetic approach [138]. Thanks to the copper catalysis, the reaction occurs at room temperature in water and a single product is formed in high purity. A simplified mechanism of the CuAAC is reported in Scheme 14. The electrons of the Cu(I) coordinate the ones of the alkyne, then the azide can easily attack the alkyne, giving the triazole ring.

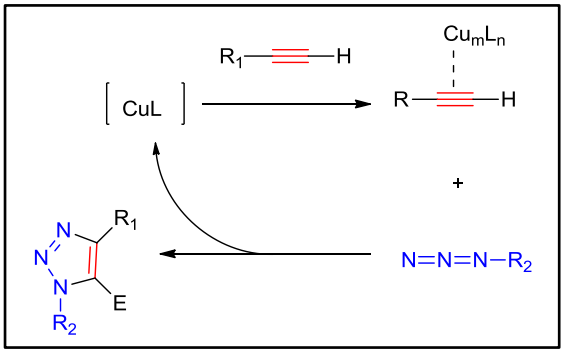

Scheme 14: Simplified mechanisms of the CuAAC reaction

The most critical aspect of this reaction is to maintain a high amount of Cu(I) during the whole reaction, as Cu(I) is easily oxidized to Cu(II). For this reason it is convenient to use a source of Cu(II) (for example copper sulfate) and to generate Cu(I) in situ by a reducing agent (for example sodium ascorbate).

The reaction between porphyrin **25** and BNN_3 was performed in different experimental conditions (Table 3). All the reactions were performed under a nitrogen atmosphere to avoid copper oxidation. In trials 1 and 2 porphyrin **25** was used in SP and the resin was washed with a solution 0.1 M of EDTA that should remove the copper that was possibly inserted into the porphyrin ring [139]. Trial 3 was performed in solution using porphyrin **25**, since $[Cu(CH_3CN)_4]PF_6$ should avoid the insertion of the copper into the porphyrin ring [140]. Trial 4 was performed in solution using the zinc porphyrin **26**.

Trial number	Type of synthesis	Reactive	Conditions	Mass values from RP-UPLC-MS
1	SP	**25**, CuI, TBTA [141]	DMF, overnight, rt	BNN_3, $BNN_{3\ ox}$
2	SP	**25**, CuI, DIPEA [142]	DMF, overnight, rt	BNN_3, $BNN_{3\ ox}$
3	solution	**25**,$[Cu(CH_3CN)_4]PF_6$,TBTA[143]	H_2O/tBuOH, 48 h, rt	Cu-**25**
4	solution	**26**, Na ascorbate, $CuSO_4$	H_2O/tBuOH, 64 h, rt	**26**,BNN_3,BNN_{3ox}

Table 3: Trials for the click chemistry reaction between porphyrin **25** or **26** and BNN_3. When the reaction was performed in solution, the mmol of BNN_3 were calculated from the law of Lambert-Beer, using the ε value of the tryptophan in aqueous solution: 5690 $cm^{-1}M^{-1}$ [144].

The insertion of zinc ensures that the porphyrin **25** will not coordinate the copper during the reaction. Furthermore, zinc should not reduce the efficacy of the molecule as PS since several zinc-porphyrins revealed good photoactive properties [145]. Porphyrin **25** was reacted with a large excess of zinc acetate dihydrate for 2 hours at room temperature to give porphyrin **26** (Scheme 15).

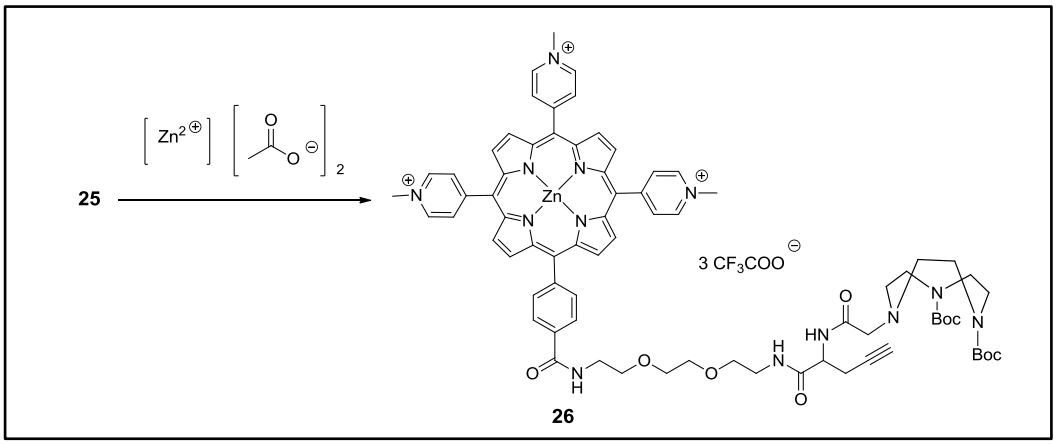

Scheme 15: Synthetic route for **26**. *Reagents and conditions*: CH_3OH, 2h, rt

The reaction was monitored by UV-vis since after metal insertion only two Q bands are observed between 500 and 700 nm (Figure 52).

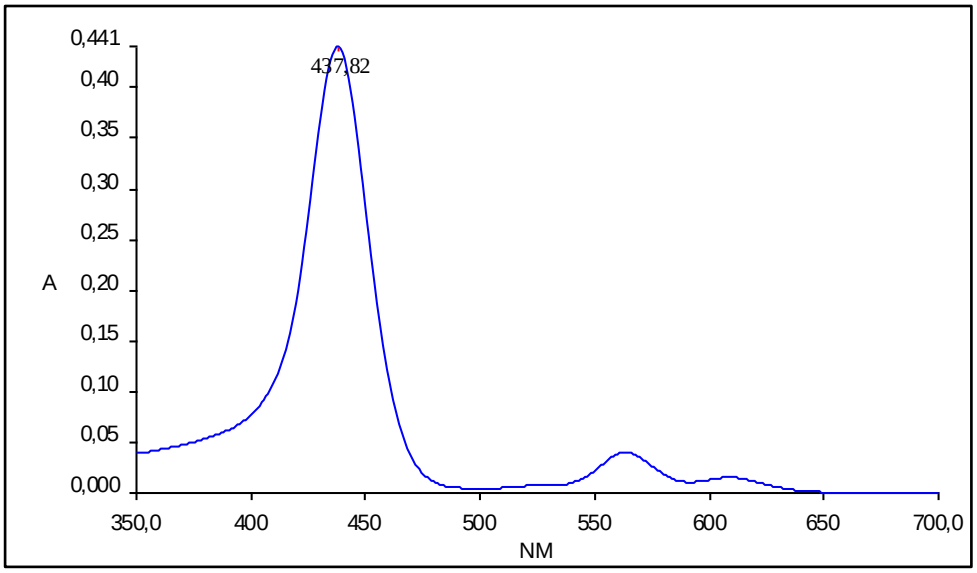

Figure 52: UV-vis (CH_3OH) of **25**

As the product **26** is water soluble, it was not possible to purify it from the excess of zinc acetate which however should not interfere with the following click chemistry reaction. The RP-UPLC-MS analysis showed that the product was substantially pure (Figure 53).

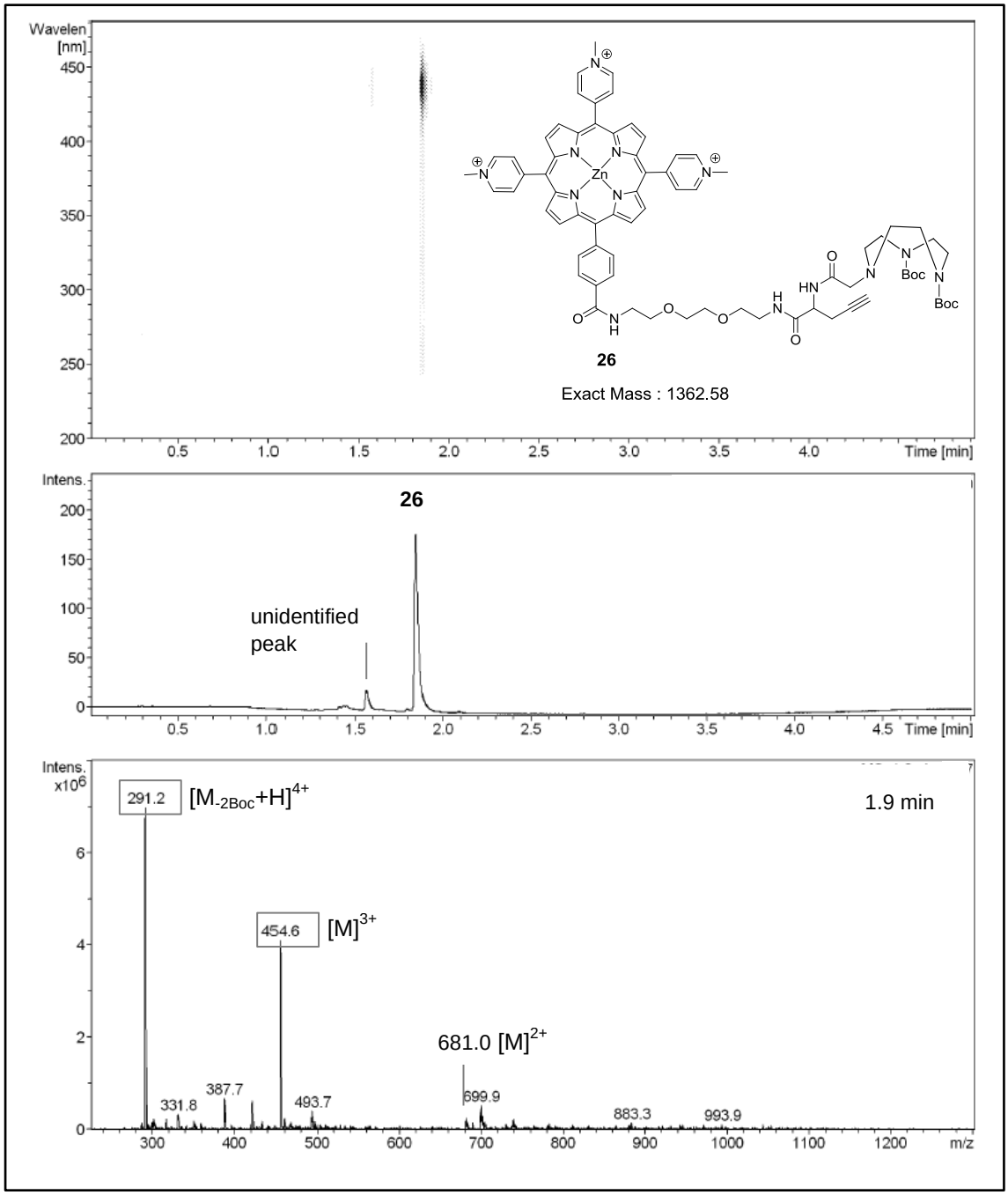

Figure 53: RP-UPLC-MS (CH_3OH) of **26**, 440 nm

Since the attempts of click chemistry between the porphyrin **25** or **26** and BNN_3 in SP and in solution were unsuccessful, we studied a model reaction between zinc porphyrin **26** and the azido pentanoic acid in solution (Scheme 16) [146, 147].

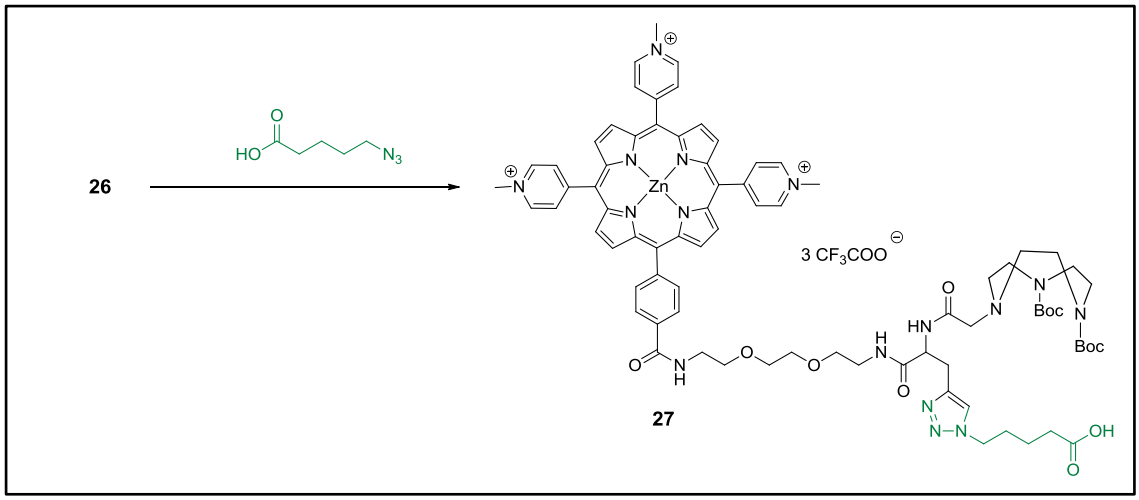

Scheme 16: Synthetic route for **27**. *Reaction conditions*: $CuSO_4$, Na ascorbate, H_2O/tBu, 22h, rt; then 30' 85 °C MW

26 was reacted in solution with 2.6 equivalents of azido pentanoic acid in the presence of 2 equivalents of sodium ascorbate, 0.6 equivalents of copper sulphate in 1:2 H_2O/tBu and the solution was left stirring at room temperature shielded from light. The reaction was monitored by TLC (CH_3CN/KNO_3 sat/H_2O 4:0.3:1) and RP-UPLC-MS. After 22 hours of reaction product **27** and the unreacted **26** were observed from the RP-UPLC-MS analysis (Figure 54).

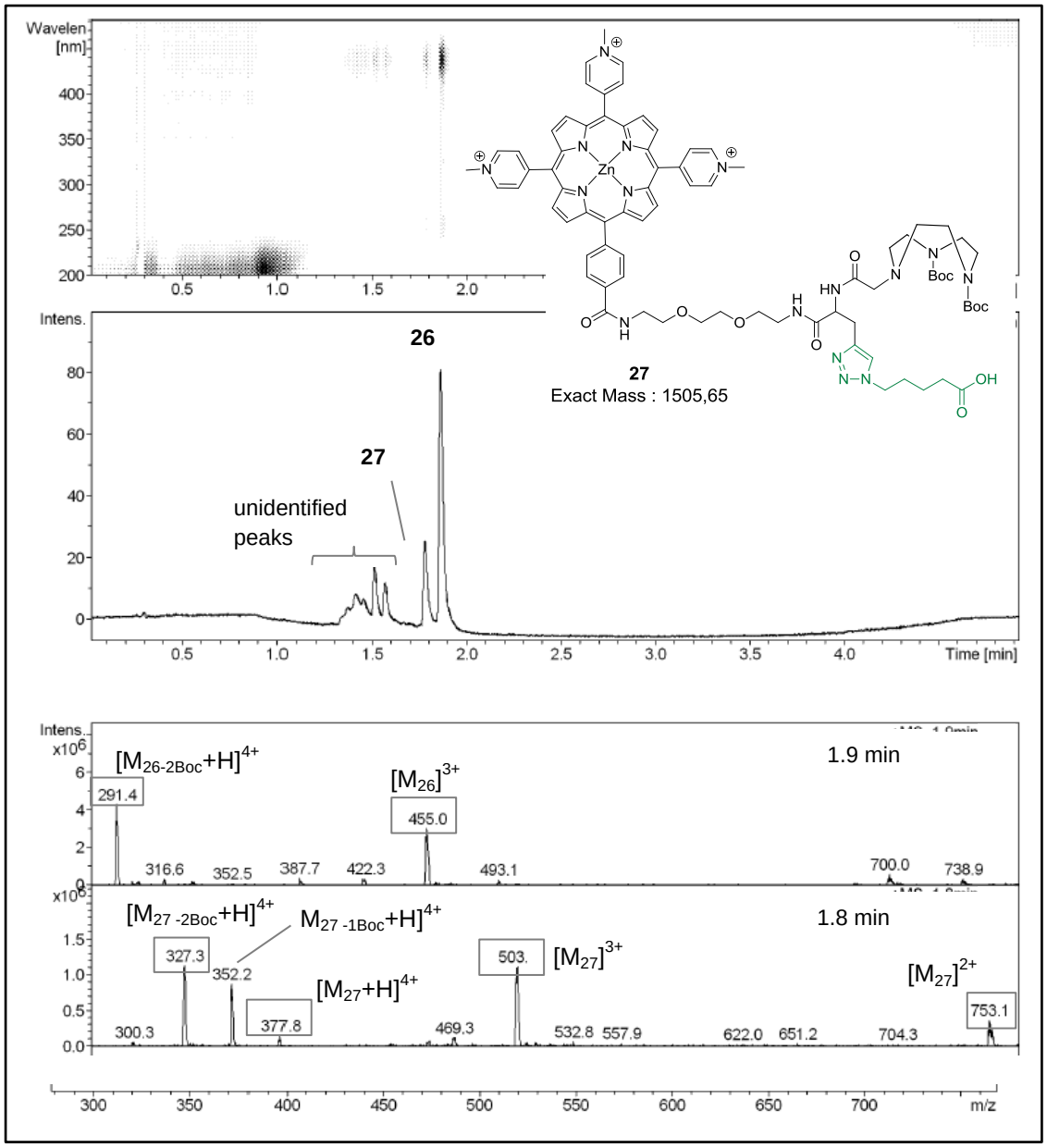

Figure 54: RP-UPLC-MS (H_2O/ACN) of **27** after 22h of reaction, 446 nm

In order to improve the yield of **27**, the reaction mixture was heated in a microwave reactor for 30 minutes at 85 °C [148]. A large excess of the azide was used to bring the reaction to completion. As it can be observed from the RP-UPLC-MS in Figure 55, the chromatogram shows the peak of **27** at 1.9 minutes of retention time and no starting material was observed.

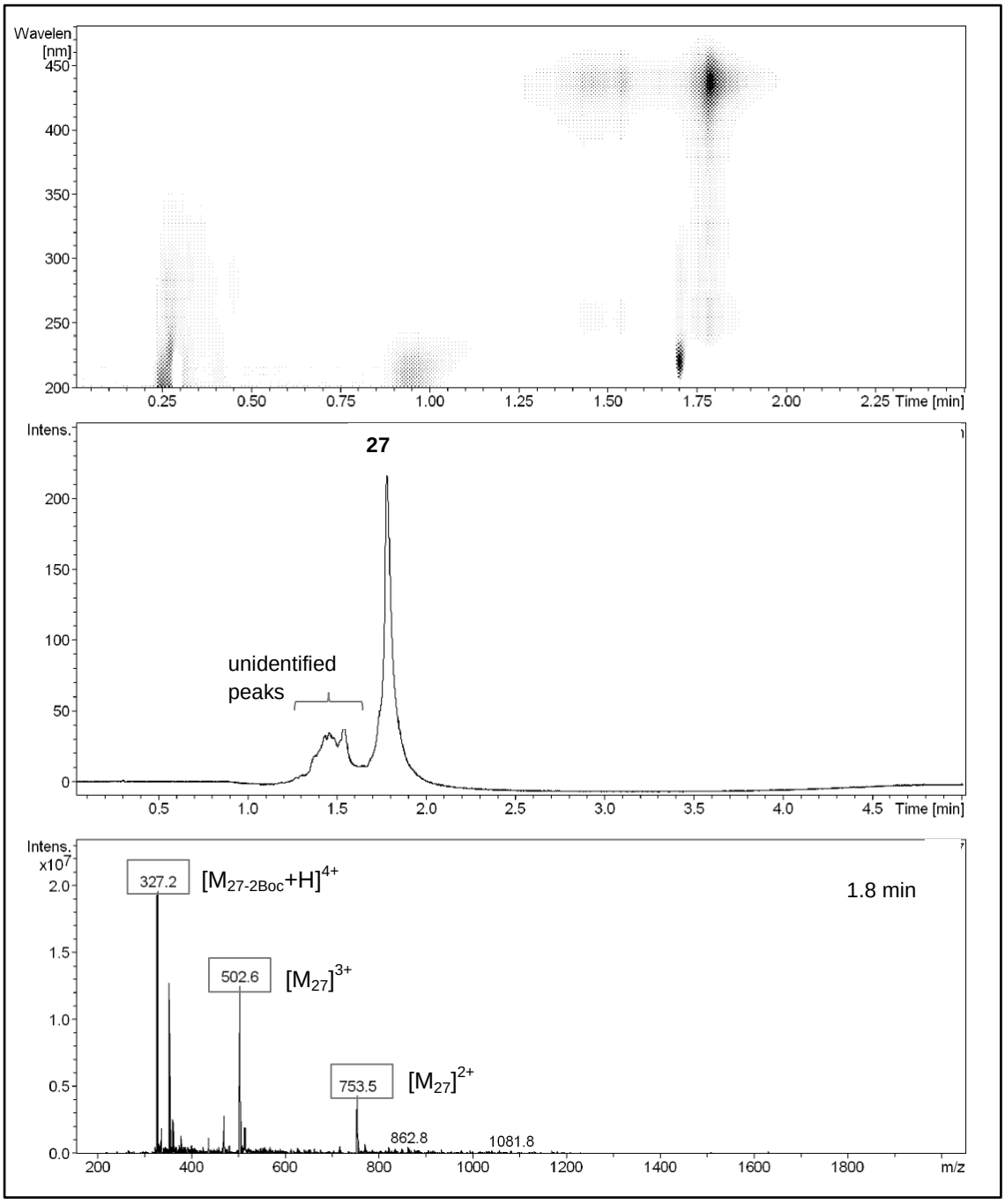

Figure 55: RP-UPLC-MS (H_2O/ACN) of **27** after 22 h + 30' MW, 436 nm

As the formation of **27** was observed in the model reaction, the click chemistry reaction between porphyrin **26** and BNN_3 was performed in solution using microwave irradiation. The experimental conditions (reaction time and equivalents) used for the synthesis of **27** were optimized for the synthesis of **28**. A solution of zinc porphyrin **26**, BNN_3, a large excess of copper sulfate and sodium ascorbate in 1:2 H_2O/tBu was directly heated in a microvave reactor at 85 °C for 1h obtaining a precipitate and a green solution (Scheme 17).

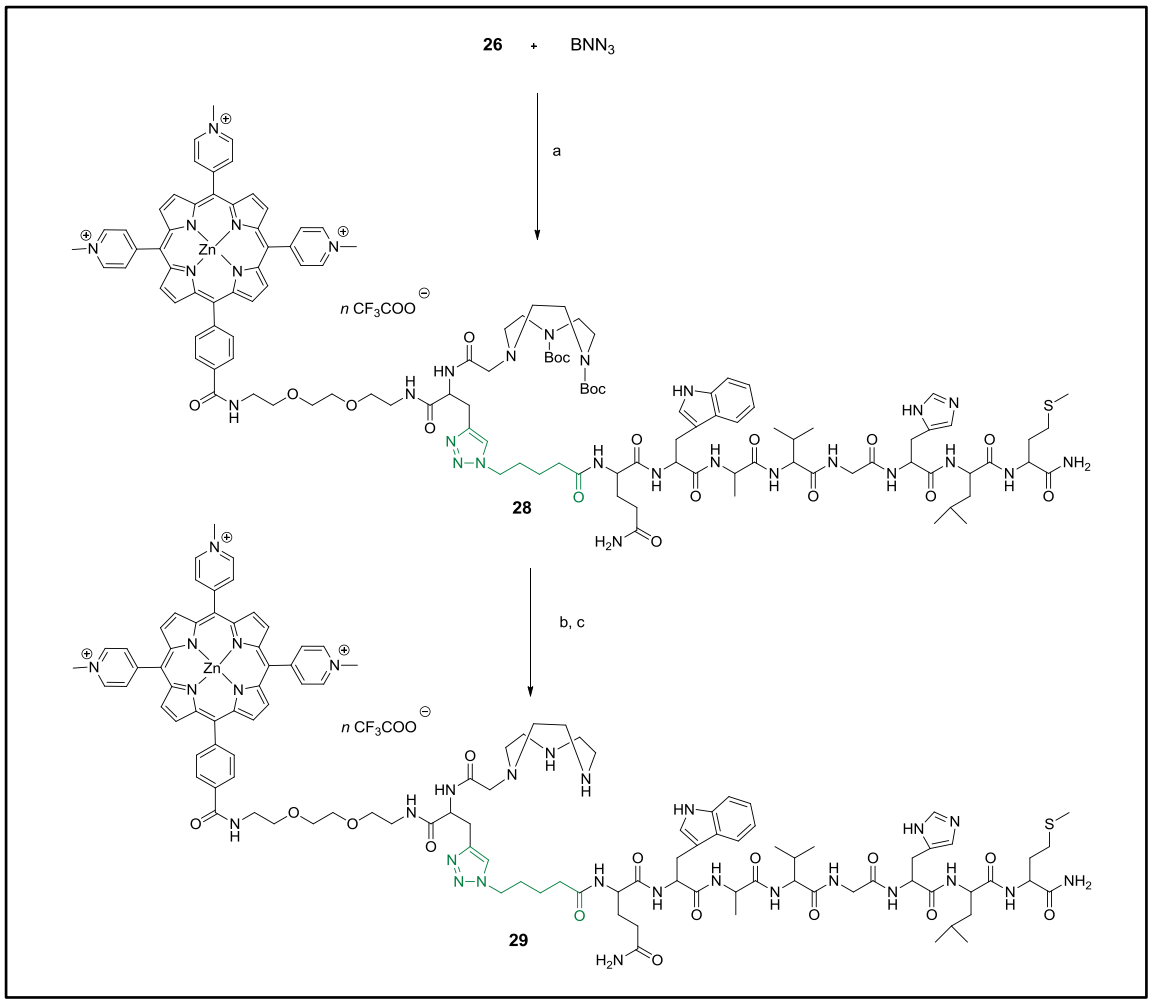

Scheme 17: Synthetic route for **28** and **29**. *Reaction conditions*: a) $CuSO_4$, Na ascorbate,1:2 H_2O/tBu, 1 h MW; b) TFA, 2h, rt; c) TEA, CH_3OH

From the RP-UPLC-MS analysis a mixture of **28** and unreacted BNN_3 was observed along with the correspondent oxidated forms. The RP-UPLC-MS analysis of the reaction mixuture presents two broad peaks at retention time 1.8 minutes and 1.9 minutes. The first one is a superimposition of $BNN_{3\ 2\ OX}$ (azido peptide with the sulfur oxidated to sulfon) with **28** $_{OX}$, and the second one is a superimposition of $BNN_{3\ OX}$ with **28**. The peak at retention time 2.1 min is related only to BNN_3 and for this reason the UV absorption was observed only at 275 nm (Figure 56).

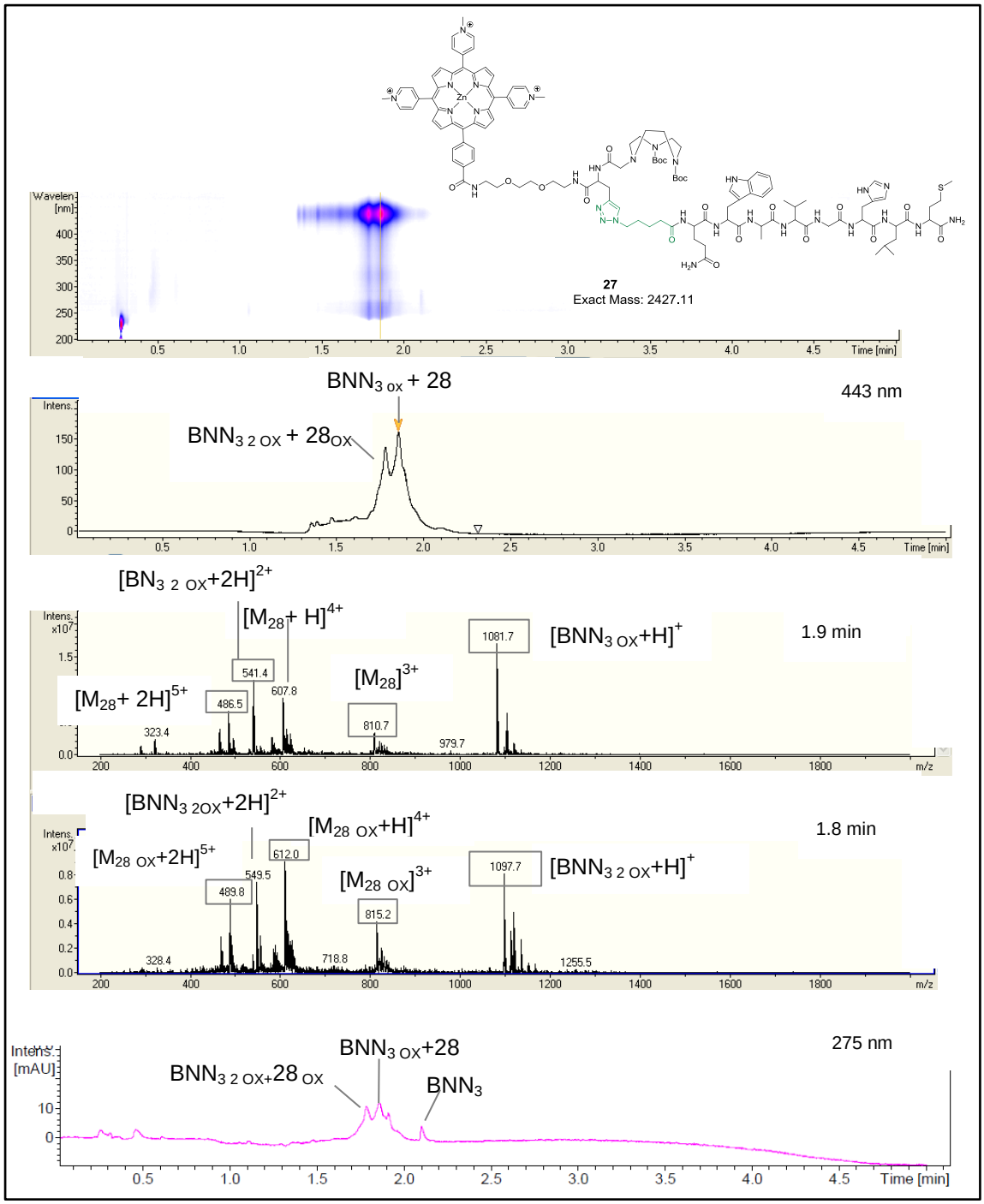

Figure 56: RP-UPLC-MS (H_2O/ACN) of **28**, 443 nm and 275 nm

The solvent was evaporated and **28** was treated with TFA for 2 hours at room temperature, then the TFA was evaporated and the solid was treated with TEA (Scheme 16). The crude product was purified by semipreparative HPLC and the most consistent and pail purple peak absorbing at 400 nm was collected. From the RP-

UPLC-MS analysis the product **29** $_{2\ OX}$ was observed with an acceptable degree of purity (Figure 57).

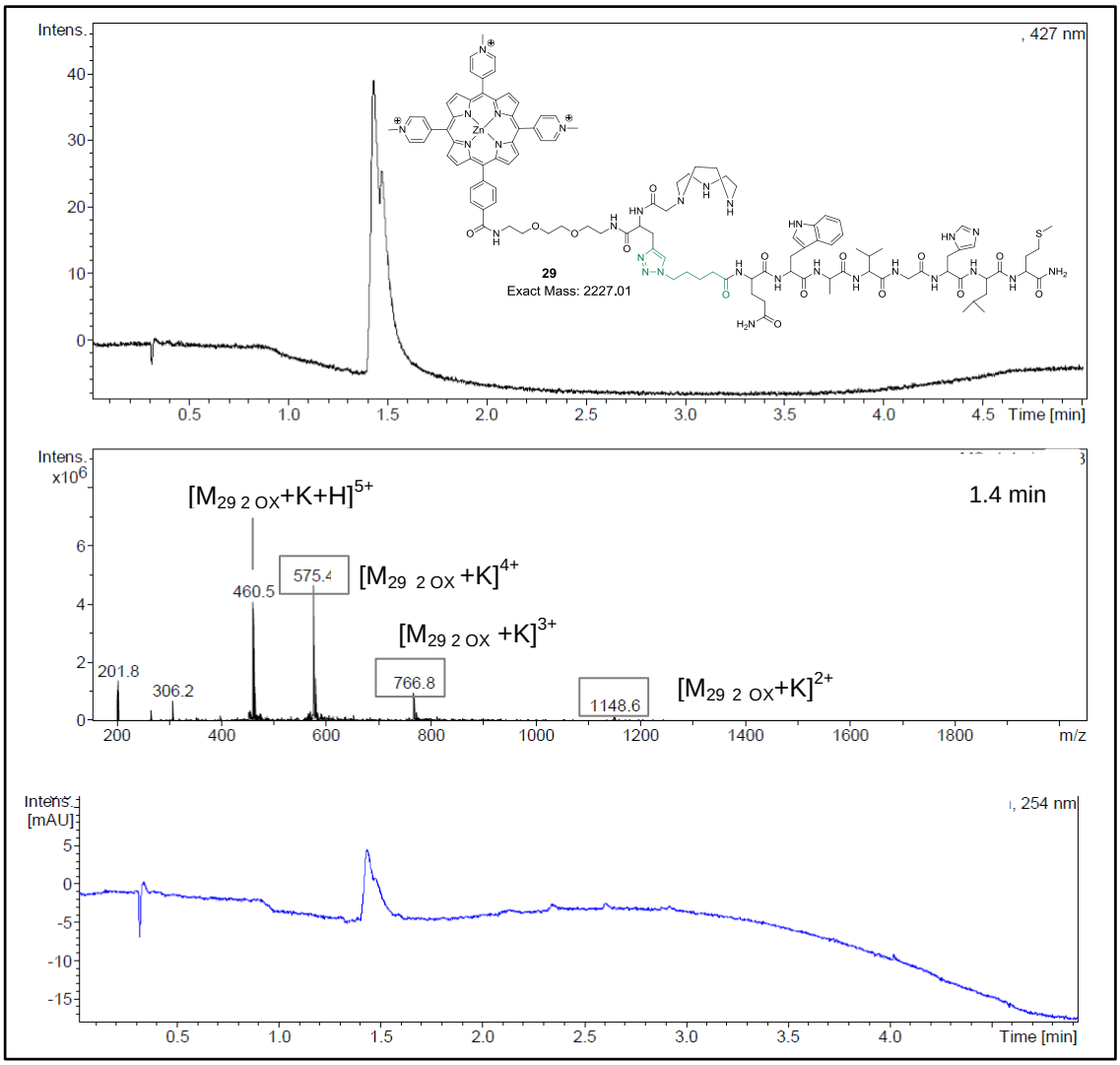

Figure 57: RP-UPLC-MS (H_2O/ACN) of the purified **29**, 427 and 254 nm

Due to the difficulty of the HPLC purification a very low quantity of the product was obtained. This is in agreement with the crowded RP-UPLC chromatograms of both the crude **28** and **29**. For this reasons a different synthetic route was explored.

3.4. COUPLING REACTION APPROACH FOR THE SYNTHESIS OF THE BN[7-14]- PORPHYRIN

3.4.1. SECOND STRATEGY FOR THE SYNTHESIS OF THE FINAL MOLECULE

In this synthetic strategy Fmoc-Lys(Mtt)-OH was used as key molecule to connect BN[7-14], porphyrin **14** and the chelator **4** by using conventional coupling reactions. The commercially available Fmoc-Lys(Mtt)-OH was chosen since it has three functional groups, a carboxylic group and two differently protected amino groups, namely a NHFomc in α position and a NH-4'methyltrilyl (NHMtt) in ε position (Scheme 18). As the two amino groups are deprotected in different environments (basic for the NHFomc and acidic for the NHMtt), a different coupling reaction can be performed on each amine. In peptide chemistry the Mtt group is used as it can be selectively removed to allow further modifications of the amino acid side chains of the peptide, such as lysine [98]. According to the synthetic strategy, the carboxylic group of the Fmoc-Lys(Mtt)-OH was coupled to the glutamine of the BN[7-14] sequence and, after a first deprotection step, the amino group in ε position was coupled to the functionalized TACN **4**. After the deprotection, the α-amine was coupled with porphyrin **14** through an anhydride link. A spacer (Fmoc-AEEA-OH) was inserted between BN[7-14] and the lysine in order to increase both the solubility in water and the distance between the peptide and the porphyrin. All the reactions were performed on solid phase following the general procedure already described, unless otherwise specified.

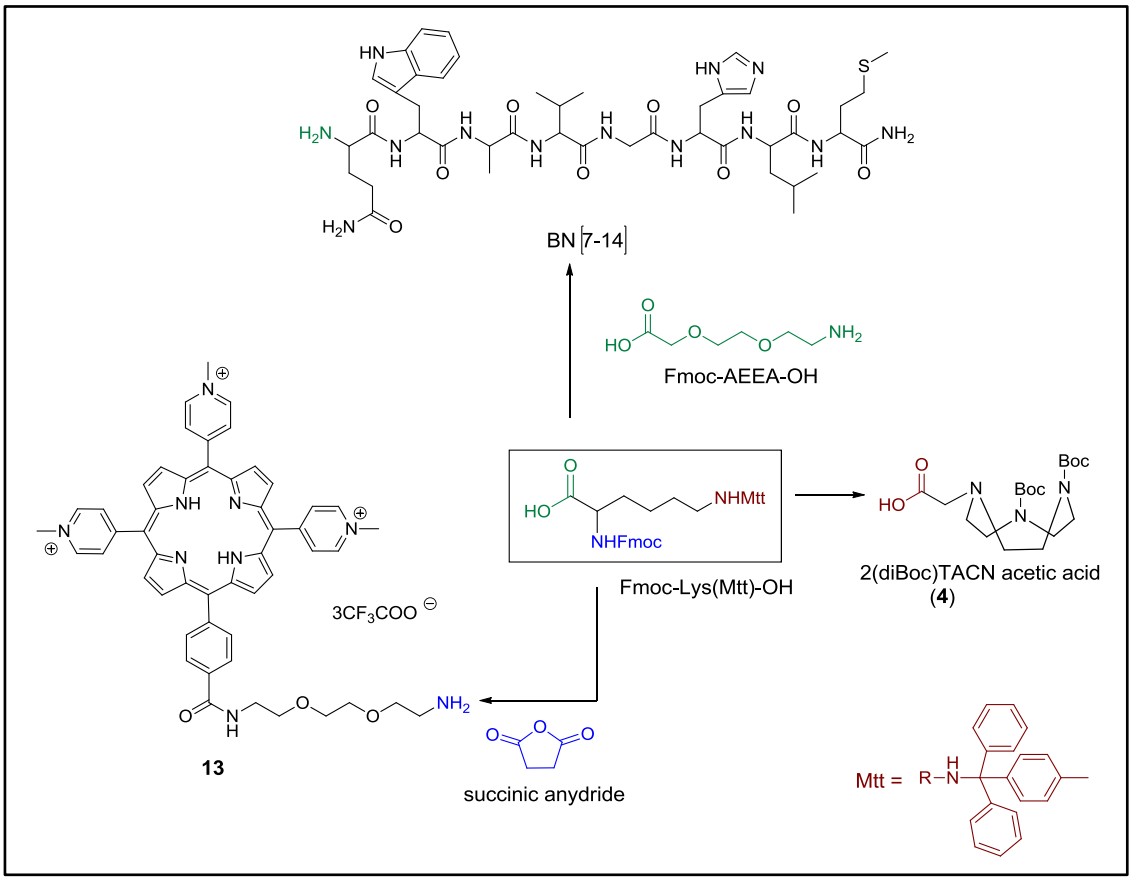

Scheme 18: Synthetic strategy using Fmoc-Lys(Mtt)-OH

3.4.2. SYNTHESIS OF THE BN[7-14]-PORPHYRIN

The first two coupling reactions in SP involved the spacer (Fmoc-AEEA-OH), and the Fmoc-Lys(Mtt)-OH. These compounds are commercially available and have been previously used in solid phase synthesis [149]. The coupling reactions showed in Scheme 19 were successfully completed. More in detail, the NHFmoc of the glutammine of BN[7-14] sequence was deprotected and reacted with the carboxylic group of the PEG chain. When the coupling reaction was complete, the NHFmoc of the PEG chain was deprotected and coupled with the carboxylic group of the Fmoc-Lys(Mtt)-OH to give BNPL-Fmoc-Mtt.

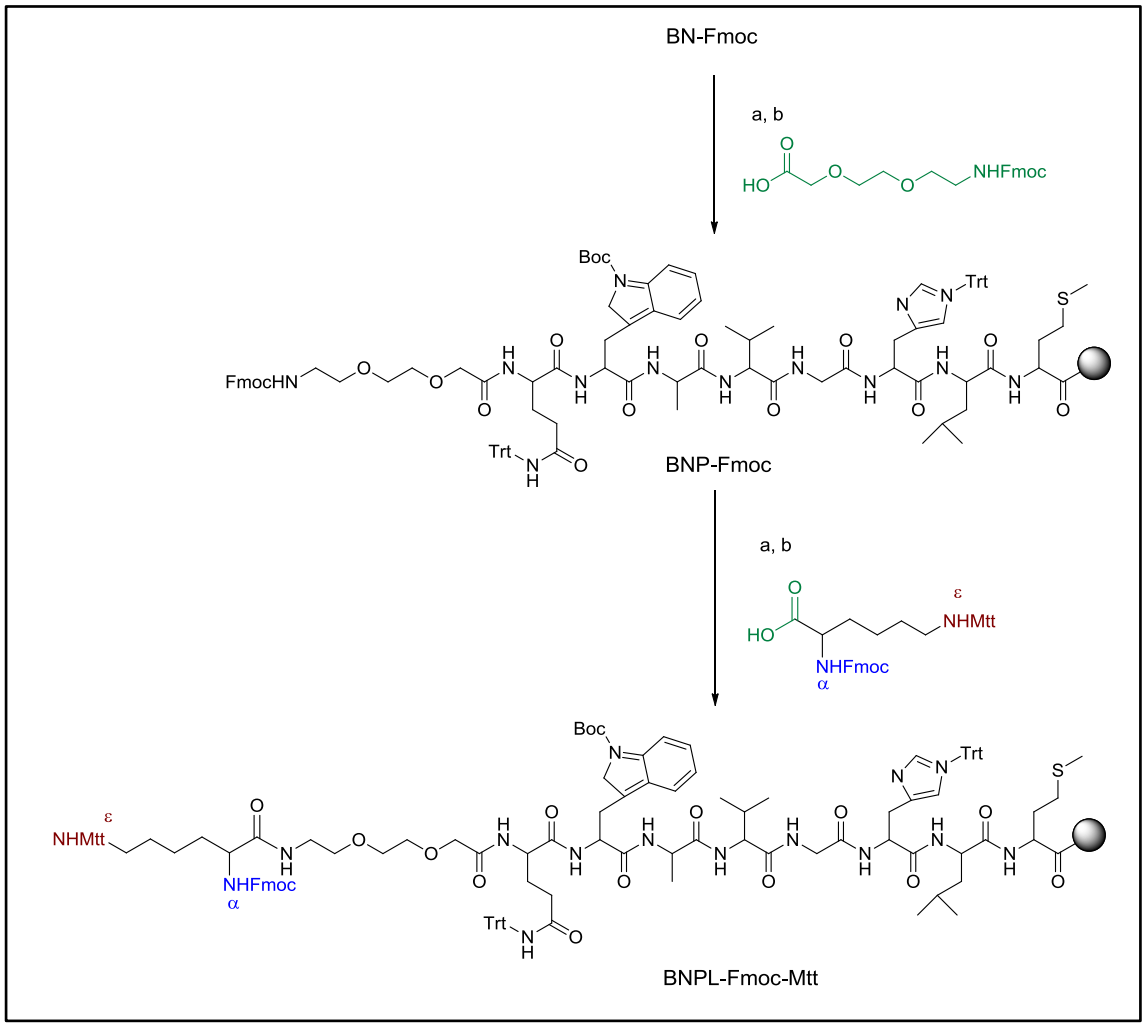

Scheme 19: Synthetic rote for BNPL-Fmoc-Mtt. *Reagents and conditions*: a) piperidine, DMF, 2'+10'; b) TBTU, DIPEA,2,6 lutidine, DMF, 1h, rt

In order to check the purity of these intermediate, a small amount of BNPL-Fmoc-Mtt was cleaved and an RP-UPLC-MS analysis was performed. Since the Mtt group was released during the cleavage reaction, BNPL-Fmoc and the oxidized BNPL-Fmoc $_{OX}$ were observed in the RP-UPLC-MS chromatogram (Figure 58).

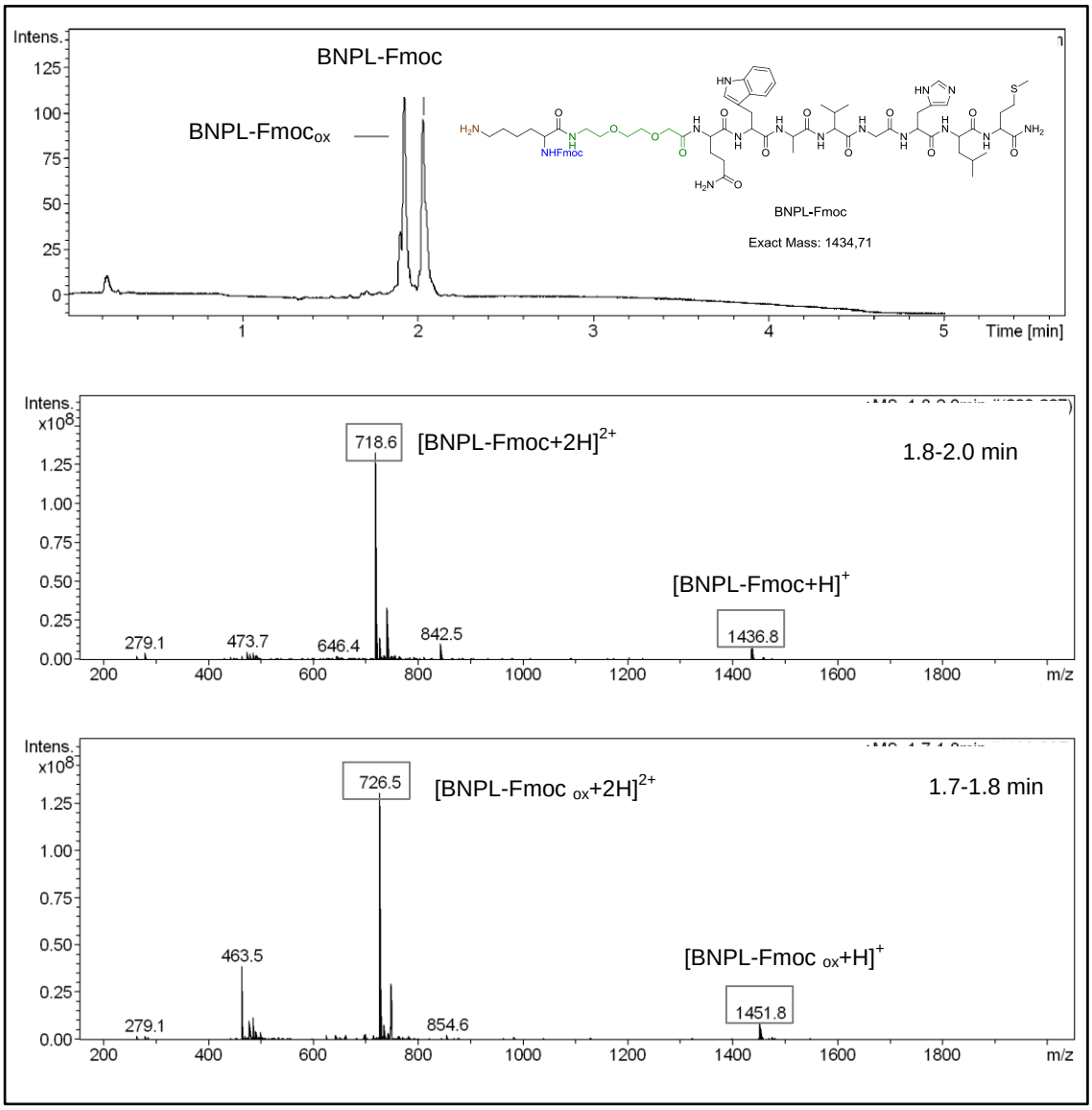

Figure 58: RP-UPLC-MS (ACN/H_2O) of BNPL-Fmoc, 276 nm

The Mtt protecting group was released from BNPL-Fmoc-Mtt in order to couple the ε-amino group with the carboxylic group of the functionalized TACN **4**. This deprotection leaves untouched the other acid-labile protecting groups of the peptide sequence such as Trt and Boc. The choice of the acid for this purpose depends on the type of resin used in SP. Usually TFA in CH_2Cl_2 containing TIPS (to prevent the reattachment of the trityl cations) or with TES in HFIP and TFE are used on hydrophilic resin and the mixture AcOH and TFE in CH_2Cl_2 is used on hydrophobic resin [150]. The Mtt deprotection had to be quantitative, but only a small amount of acid was used to avoid the cleavage of the peptide from the resin. Furthermore this deprotection could not be monitored either by Kaiser test and RP-UPLC-MS. In fact the Mtt groups were released during the RP-UPLC-MS analysis. A solution made of 92:5:3 CH_2Cl_2/TIPS/TFA was

used to wash the resin containing BNPL-Fmoc-Mtt several times before the Mtt removal and then the resin was left shaking twice for 10 minutes with a 94:5:1 CH_2Cl_2/TIPS/TFA solution. The resin changed color both during the washes and the deprotection steps [150-152]. Another test was performed to evaluate the presence of still protected amino groups: a small sample of resin was collect and 1-2 drops of TFA were added and the non-immediate orange TFA color indicated that all the Mtt groups were correctly removed [102]. Before proceeding with the coupling reaction with **4**, a model reaction with a simple amino acid (Fmoc-Gly-OH) was performed in order to evaluate if both the Mtt deprotection and the following coupling were quantitative (Scheme 20). After the deprotection of the α-Fmoc amino group of the glycine, the RP-UPLC-MS analysis showed BNPLG and the correspondent $BNPLG_{OX}$ without any trace of the starting material.

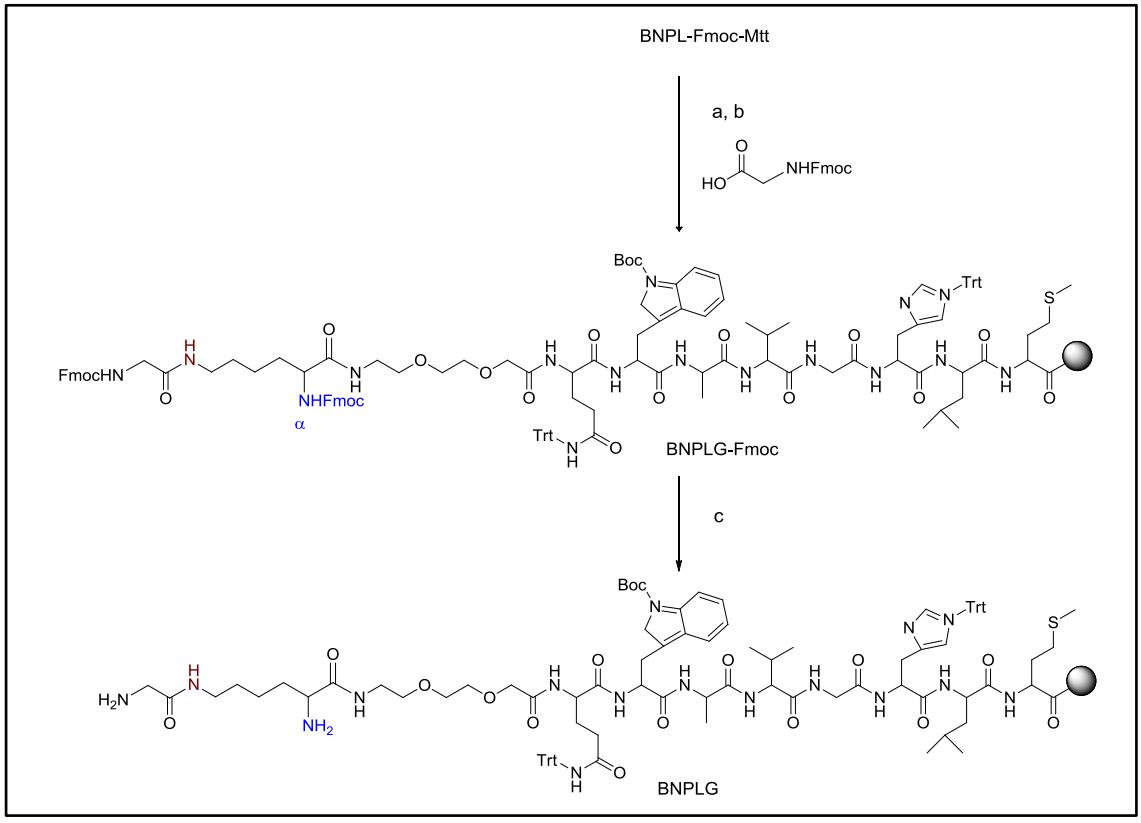

Scheme 20: Synthetic rote for BNPLG. *Reagents and conditions*: a) 92:5:3 CH_2Cl_2/TIPS/TFA 10'x2; b) TBTU, DIPEA, 2,6 lutidine, DMF, 1h, rt c) piperidine, DMF, 2'+10'

After the Mtt deprotection, the coupling between the BNPLFmoc and chelator **4** was carried out in a quantitative yield (Scheme 21). The reaction lasted overnight and 4 equivalents of **4** were required. The α-Fmoc amino group was deprotected in a basic environment affording the pure BNPLT.

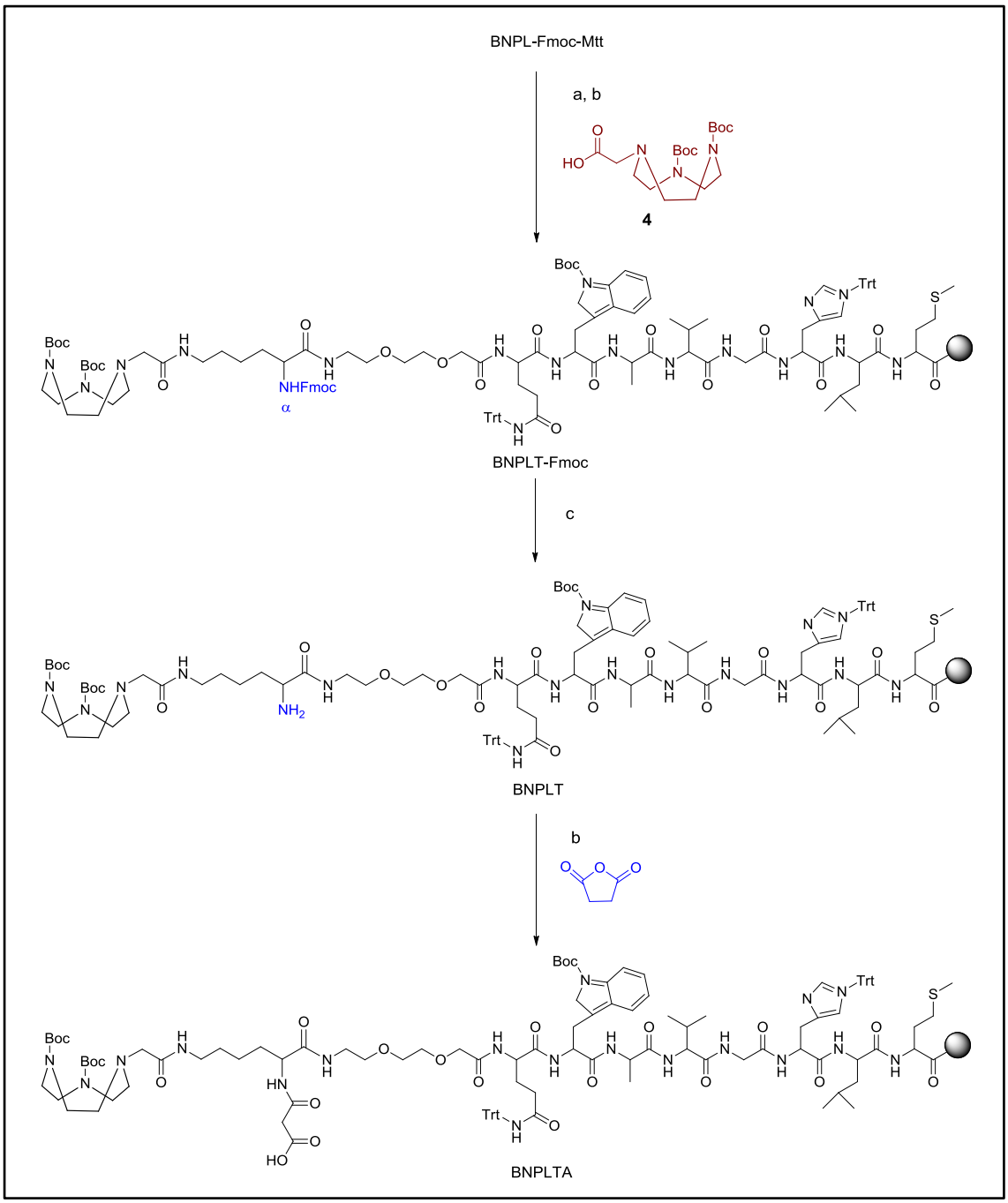

Scheme 21: Synthetic rote for BNPLFmoc, BNPLT and BNPLTA. *Reagents and conditions*: a) 92:5:3 CH_2Cl_2/TIPS/TFA 10'x2, b) TBTU, DIPEA, 2,6-lutidine, DMF, overnight, rt c) piperidine, DMF, 2'+10'

At this stage the oxidation of the methionine was investigated. Indeed the main side reaction is the acid catalyzed oxidation of methionine that can occur during the cleavage and deprotection reactions. It is to note that scavengers such as DTE, EDT, 2-mercaptoethanol or ethyl methyl sulfide should be added to the cleavage solution in order to prevent this oxidation [153]. In order to reduce the oxidation, in the following steps TIPS was replaced with 2-mercaptoethanol in the cleavage solution. From the

RP-UPLC-MS of BNPLT the peak of $BNPLT_{OX}$ is less intense than the peak of BNPLTA (Figure 59).

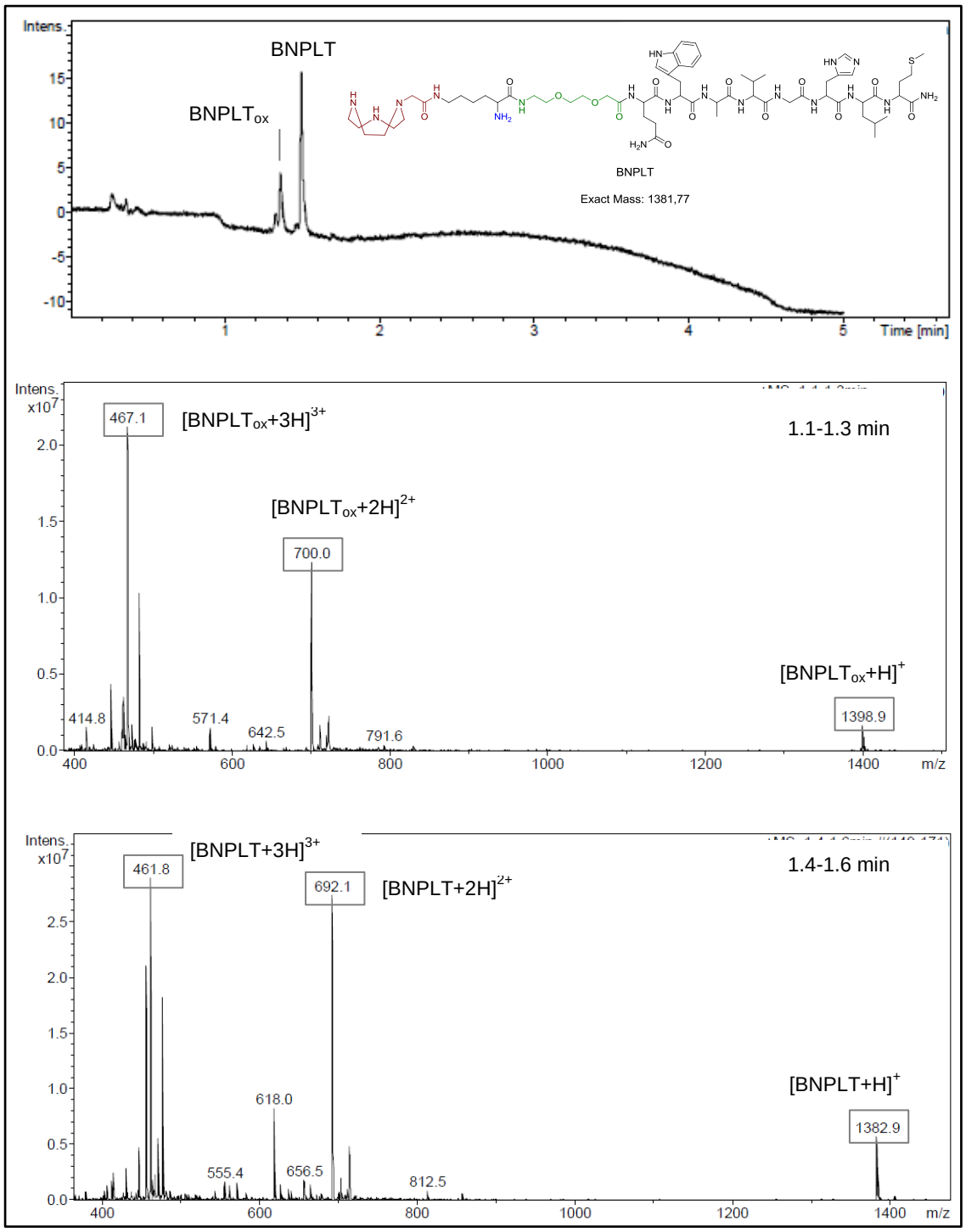

Figure 59: RP-UPLC-MS (ACN/H_2O) of BNPLT

Then the α-amino group of the lysine of BNPLT was reacted with a large excess of succinic anhydride (Scheme 21). The resin was left shaking overnight in order to obtain

BNPLTA in a quantitative yield. Before performing the coupling reaction with the porphyrin **14**, the carboxylic group of BNPLTA was coupled to the amine of the benzylamine as model reaction in order to evaluate its reactivity. The product was obtained with a good grade of purity after 1.5 hours of reaction using 4 equivalents of benzylamine in the presence of TBTU, DIPEA, 2,6-lutidine in DMF. Following a similar procedure, the coupling reaction between porphyrin **14** and BNPLTA was performed: the carboxylic group of the resin was activated both with TBTU and HOBt in base solution, and 3 equivalents of the porphyrin **14** were used (Table 4 and Scheme 22) [154].

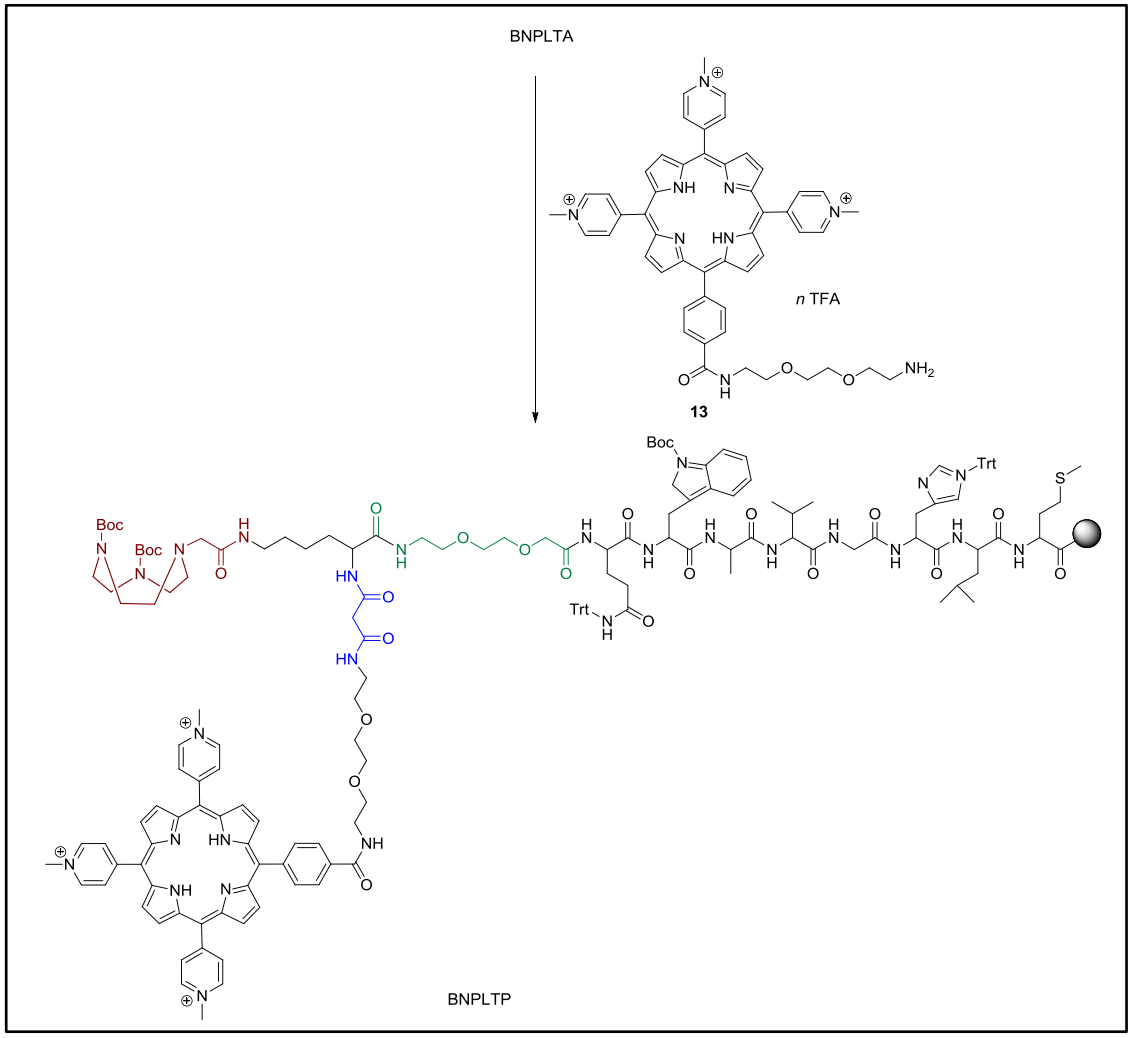

Scheme 22: Synthetic rote for BNPLTAP. *Reagents and conditions*: TBTU, HOBt, DIPEA, 2,6 lutidine, DMF, overnight, N_2, rt

The RP-UPLC-MS analysis of the crude solid obtained after the cleavage reaction showed a superposition of BNPLTA and a side product (sp) with *m/z* 1509.9. Also the mass value of the correspondent sp_{OX} was observed (*m/z* 1524.9). The product

BNPLTAP could only be observed from MALDI-Tof spectrum where a mixture of $BNPLTAP_{OX}$ (with the methionine oxidized to sulfoxide) and $BNPLTAP_{2\ OX}$ (with the methionine oxidized to sulfur) were observed (Figure 60).

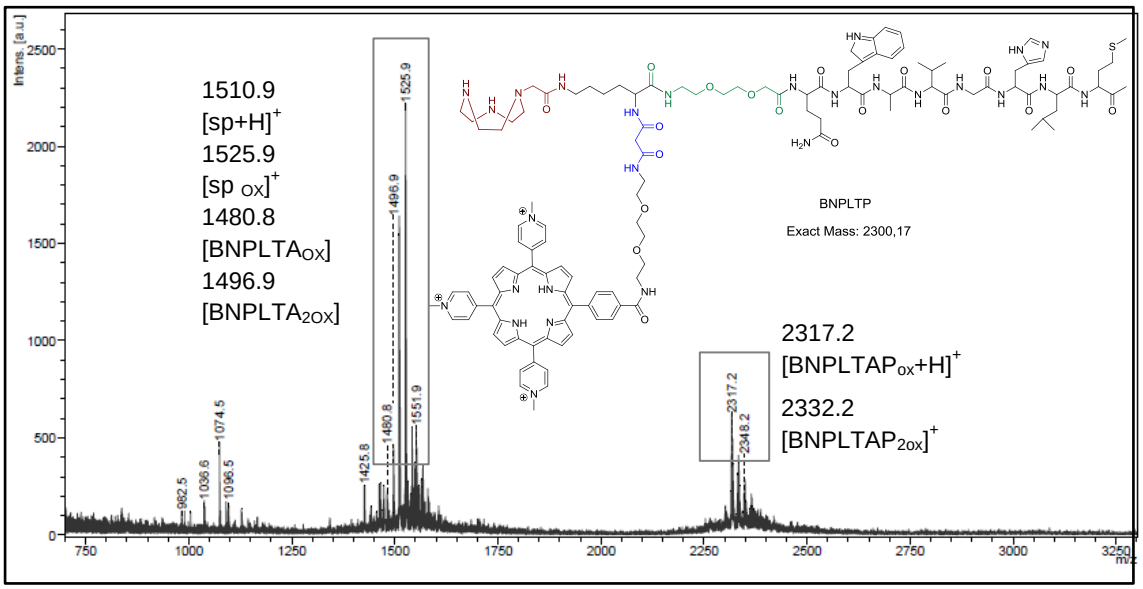

Figure 60: MALDI-Tof of the crude BNPLTAP

In order to increase the reaction yield, the coupling reaction between BNPLTA and porphyrin **14** was performed in different conditions (Table 4) but a mixture of BNPLTA, sp and BNPLTAP was always obtained.

Trial number	Type of synthesis	Reactives	Conditions	Porphyrin's equivalents
1	SPPS	TBTU, DIPEA, 2,6 Lutidine	DMF, 24 h, rt	2
2	SPPS	TBTU, DIPEA, 2,6 Lutidine, HOBt	DMF, 24 h, rt	3
3	SPPS	TBTU, DIPEA, HOBt, 2,6 Lutidine, Rodamine(4.9 equiv)	DMF, 24 h, rt	3
4	SPPS	TBTU, DIPEA, HOBt, 2,6 Lutidine, PPh_3	DMF, 24 h, rt	3
5	SPPS	TBTU, DIPEA, HOBt, 2,6 Lutidine [155]	MW (60°C,10')	3
6	solution	TBTU, HOBt, DIPEA, 2,6 Lutidine	DMF, 24 h, rt	0.5

Table 4: trials for the synthesis of BNPLTAP. The fluorine dye (rhodamine) was left shaking with the resin for 1 h before performing the coupling reaction with porphyrin **14** in order to prevent the stacking of the porphyrin to the resin. The rhodamine should stack into the resin and all the equivalents of the porphyrin should be free to react with the carboxylic group. The coupling reaction was also performed in a microwave reactor but degradation of the product was observed from RP-UPLC-MS.

Since the yield of the coupling reaction could not be improved, an analytical method was studied in order to purify the product. In the analytical HPLC (linear gradient from 0 to 100% of CH_3CN over 30 minutes) a peak was observed at 420 nm (blu arrow, Figure 61 A). This peak splits into two peaks at 275 nm (red arrows, Figure 61 B). The peak indicated with the blue arrow was collected and its MALDI-Tof spectrum showed the simultaneous presence of BNPLTA, BNPLTAP and sp.

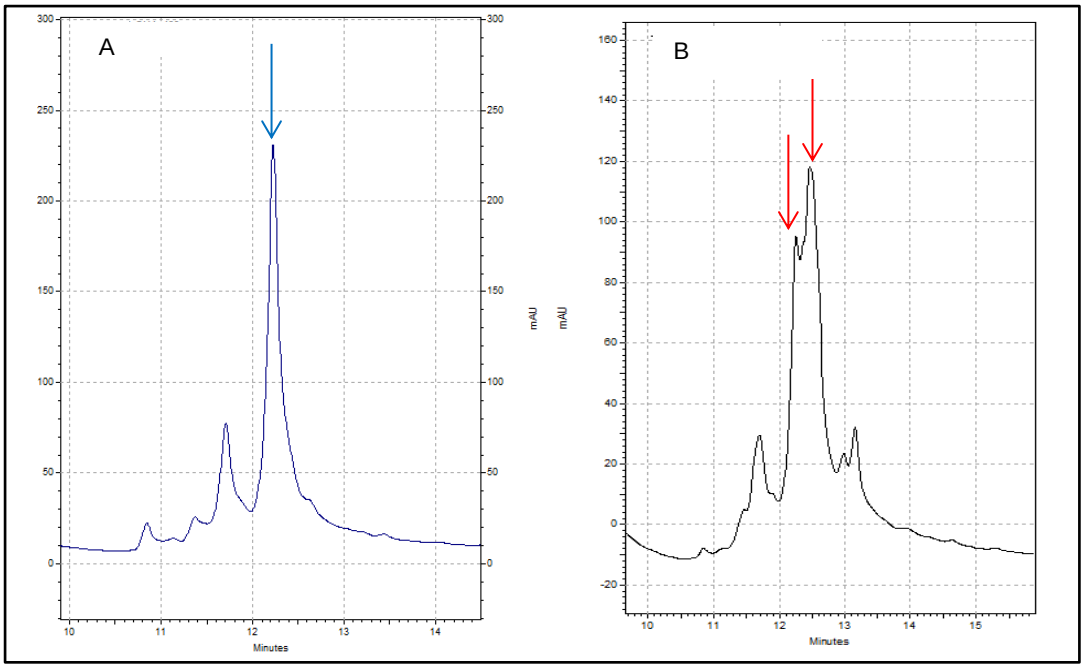

Figure 61: Analytical HPLC chromatogram of the crude BNPLTAP, zoom at 400 nm (A) and at 275 nm (B), zorbax column.

A successful separation of the crude BNPLTAP was obtained using a slower gradient (from 0 to 50% of CH_3CN over 55 minutes). In this way BNPLTAP, BNPLTA and sp could be separated (Figure 62). Indeed, the peak at retention time 31.7 min corresponds to BNPLTA. Since the peak at the retention time 38.0 min absorbs both at 275 nm and 400 nm, it was attributed to BNPLTAP. The peak at the retention time 32.7 min was collected and analyzed by RP-UPLC-MS, and the sp (*m/z* 1509.9) was observed. The peaks at retention time 27.0 and 36.5 min might correspond respectively to $BNPLTA_{OX}$ and $BNPLTAP_{OX}$.

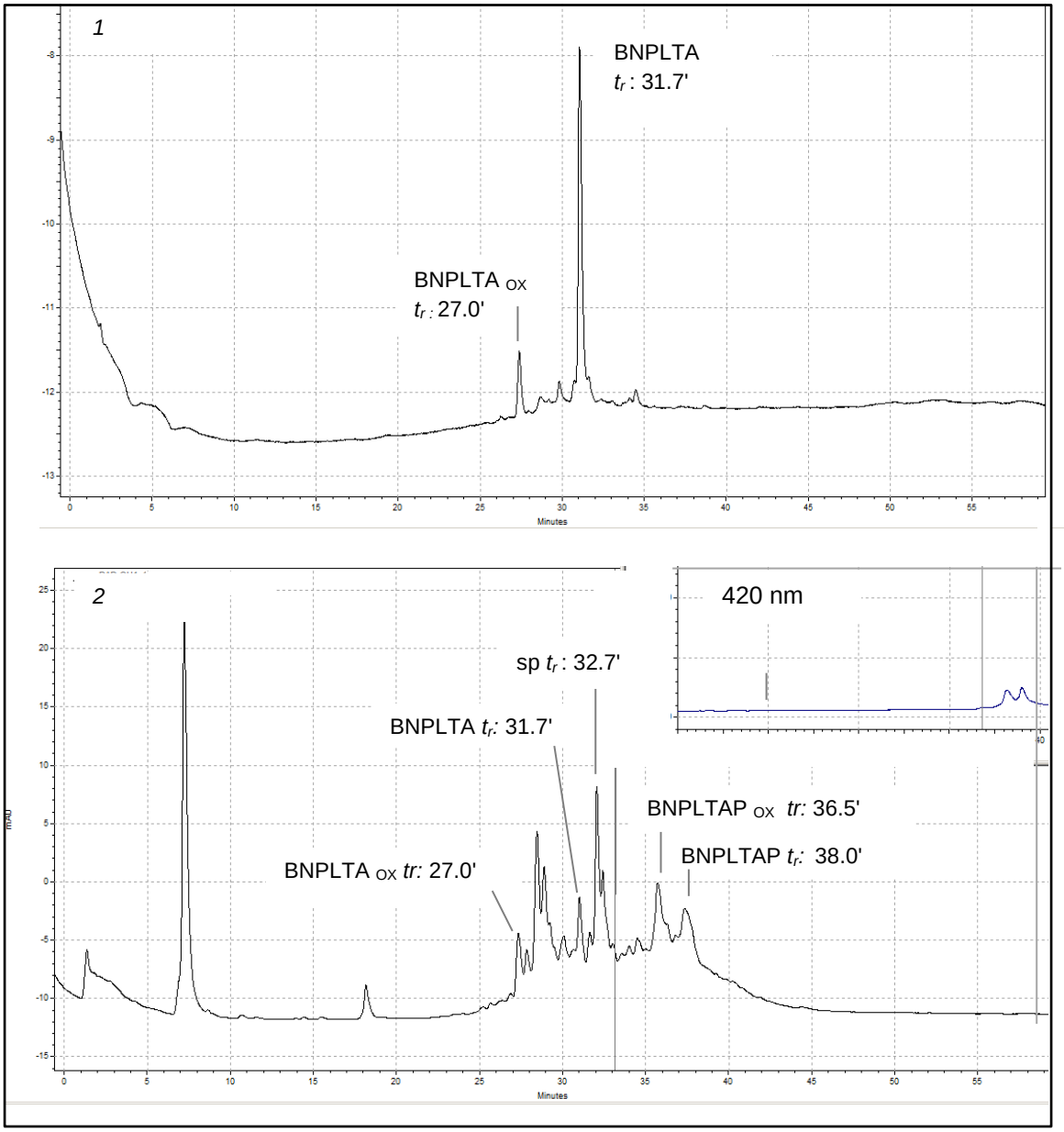

Figure 62: analytical HPLC chromatogram of BNPLTA (1) and BNPLTAP (2), 275 nm

After a scale up of the reaction, the crude product was purified by preparative HPLC adapting this analytical method. The pail purple fraction was isolated and the MALDI-Tof spectrum showed the pure BNPLTAP in different oxidation states (Figure 63). Unfortunately, only 0.3 mg of the purified product were obtained. BNPLTAP was soluble in water soluble, as well as all the intermediates of this synthetic route.

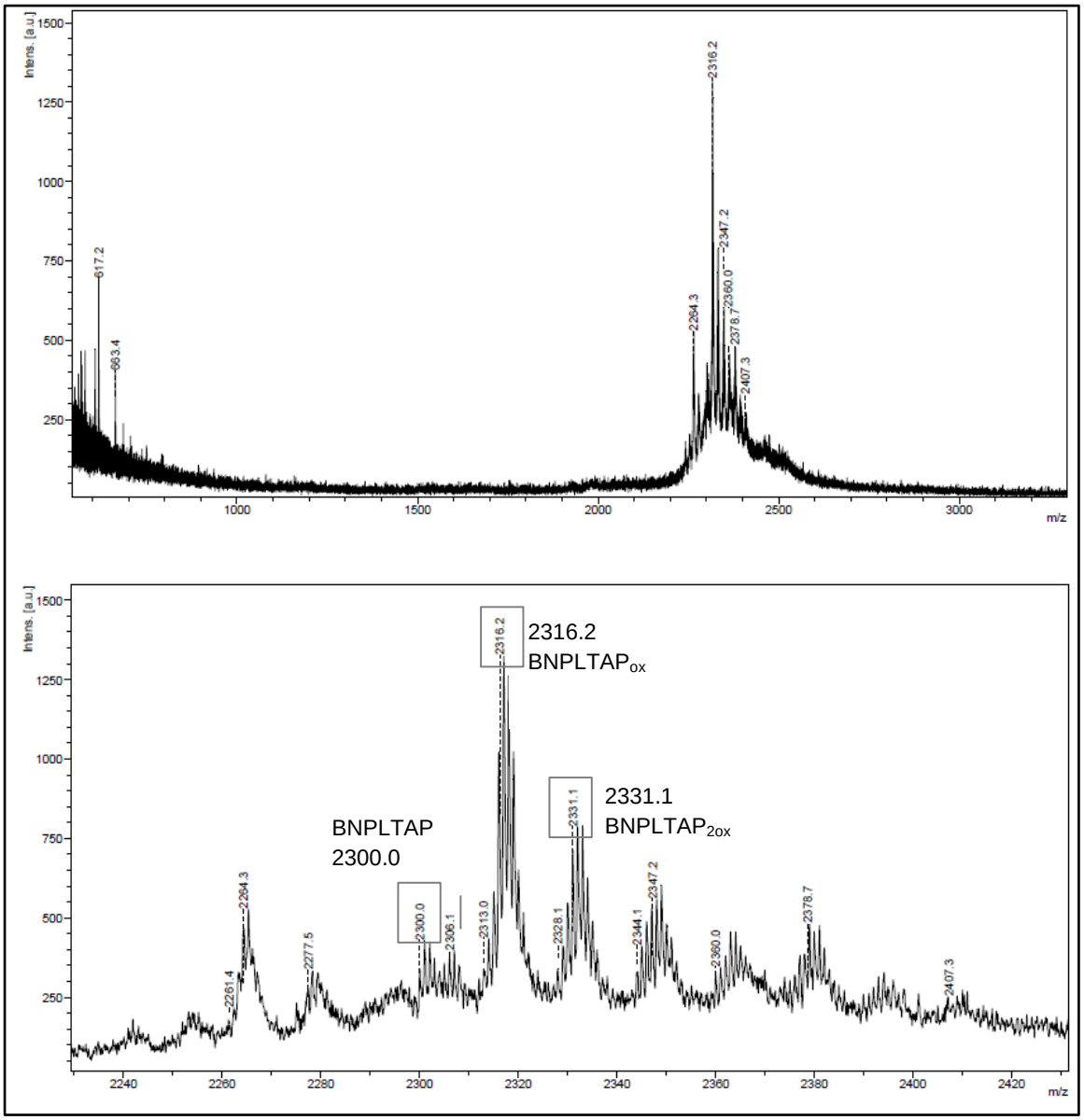

Figure 63: MALDI-Tof spectrum of the pure BNPLTAP

Due to the low quantity of BNPLTAP isolated, the reaction of coordination with Re(I) could not be performed. Since only the last coupling reaction gave a complex mixture of products (Figure 63, compare the analytical HPLC of BNPLTA and BNPLTAP) we decided to choose a functionalized fullerene for the reaction with BNPLTA.

3.4.3. SYNTHESIS OF A BN[7-14]-FULLERENE

This work was performed in collaboration with professor Tatiana Da Ros

Fullerene C60 is a carbon nanomaterial with a soccer-ball shape that is biocompatible and non-toxic. Fullerene presents interesting applications such as in, antibacterial, anti-HIV, radiopharmaceuticals and drug delivery fields. This carbon material can also act as a photosensitizer in PDT since it generates singlet oxygen after irradiation, and some fullerene derivative are in vivo preclinical stage for this treatment [155]. Fullerene absorbs in the visible region thanks to its extended π-conjugated system, and after irradiation (532 nm) produces reactive oxygen species (ROS). Unfortunately C60 present also several limitations as: *i*) it is very hydrophobic and its application in the biomedical field are limited; ii) it aggregates in polar solvents; *iii*) it absorbs in the blue-green visible light at wavelengths not ideal for PDT. However a lot of research is ongoing to overcome these problems and allow a possible use in the biomedical field, especially in PDT [156-160].

Therefore a coupling reaction between BNPLTA and a functionalized fullerene was performed on solid phase (Scheme 23). To assure that fullerene was completely solubilized during the reaction, high volumes of a base solution made of DIPEA and 2,6-lutidine in 1:1 dioxane/NMP were used (1 mg/3 mL) and the solution of the fullerene was added in portion (5 x 6 mL) over 72 hours. Then the resin was left shaking for additional 72 hours at room temperature shielded from light.

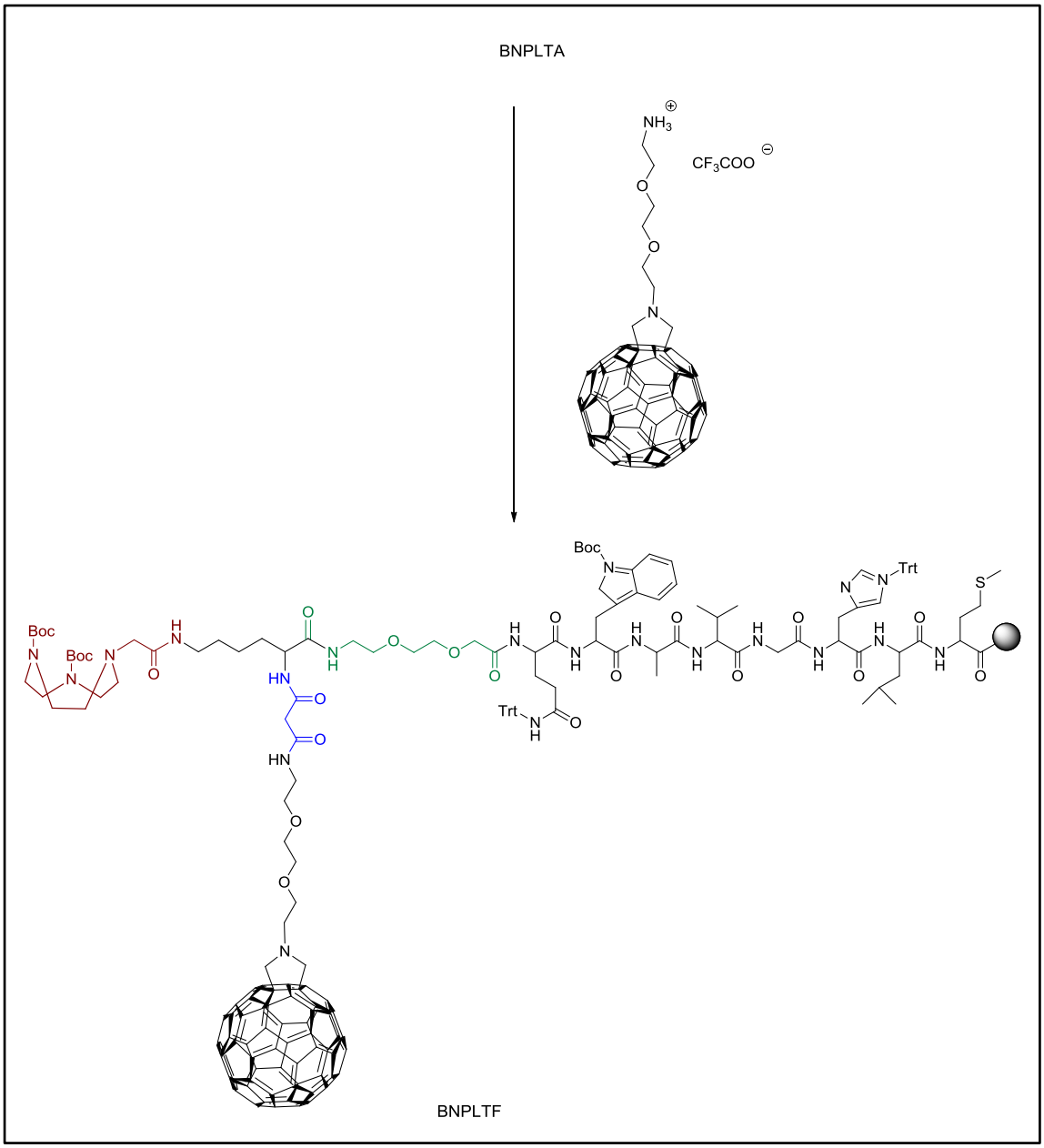

Scheme 23: Synthetic rote for BNPLTAF. *Reagents and conditions*: TBTU, DIPEA, 2,6-lutidine in DMF, 1:1 dioxane/NMP, 6 days, rt

After the cleavage reaction (TFA, H_2O, TIPS) 8.27 mg of a water soluble brown solid were obtained. As for BNPLTAP also the RP-UPLC-MS of BNPLTAF showed the presence of BNPLTA and some side products with retention times close to the one of BNPLTA. In the MALDI-Tof spectrum the molecular peak of BNPLTAF plus water was observed (Figure 64). The HPLC purification of the crude BNPLTAF did not afford the pure product, for this reason no further reaction could be performed.

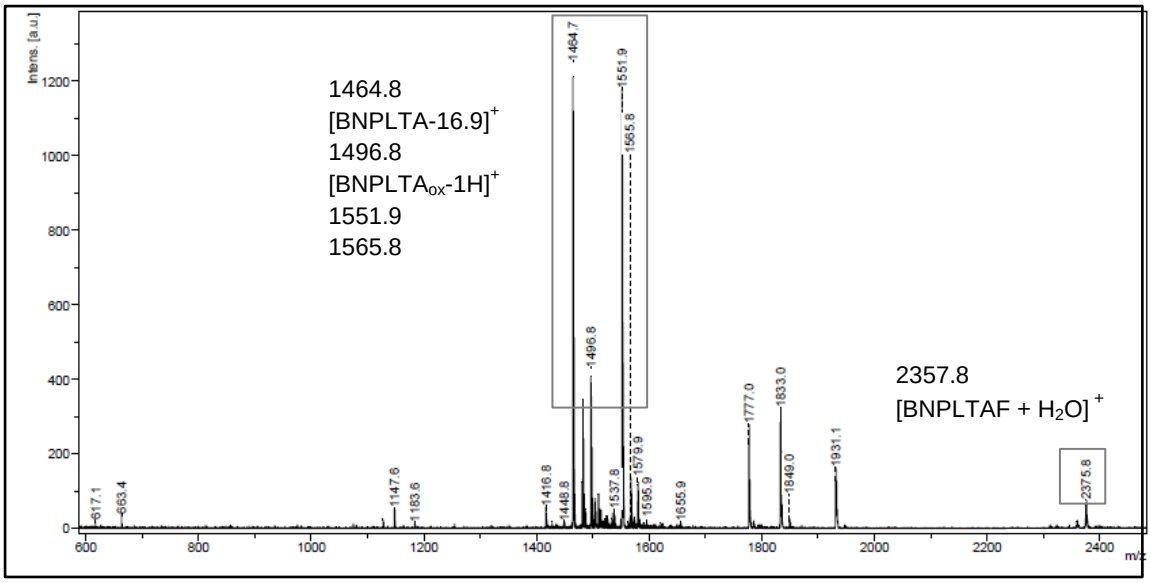

Figure 64: MALDI-Tof of BNPLTAF

3.5. CONCLUSIONS

The peptide BN[7-14] was successfully connected to the porphyrin **14** together with a functionalized chelator TACN **4** using either click chemistry or a coupling reaction approach. The peptide BN[7-14] was also connected to a functionalized fullerene together with a functionalized chelator TACN **4**. Unfortunately in both cases the products were obtained in a very small amount, and the coordination reaction with rhenium for both the porphyrin-peptide and the fullerene-peptide was not feasible.

3.6. EXPERIMENTAL PART

Mono and bidimensional (HSQC) NMR spectra were recorded on a 500 MHz Bruker spectrometer. All the spectra were run at ambient temperature and chemical shifts were referenced to the peak of residual non deuterated solvent (δ = 3.31 for CD_3OD). The UV-Vis spectra were performed at ambient temperature on a Varian Cary 100 spectrophotometer. The RP-UPLC-MS were performed using a Bruker Daltonics HCT 6000 mass spectrometer. RP-UPLC-MS were recorded with a Waters Acquity™ system equipped with a PDA detector and auto-sampler using an Acquity UPLC BEH C18 column (21.50 x 1.7 mm). RP-UPLC-MS were performed by using a Bruker Daltonics HCT 6000 mass spectrometer. RP-UPLC-MS was performed at a flow rate of 0.6 mL min^{-1} with a linear gradient of A (double-distilled water containing 0.1% v/v formic acid) and B (acetonitrile): t =0 min, 0, 5% B; t = 0.25 min, 5% B; t = 4.5 min, 100% B; t = 5.0 min, 100% B. The matrix-assisted laser desorption/ionization time of fight mass spectrometry (MALDI-Tof) mass spectra were measured on a Bruker Daltonics Autofex. The experiments were performed in reflector (RP) or linear (LP) mode with positive polarity using acyano-4-hydroxy-cinnamic acid on a Prespotted AnchorChip (PAC HCCA) or sinapinic acid (SA) as the matrix. Microwave reactions were perfomed using a Biotage Initiator+ Robot Eight instrument. Preparative HPLC purification was carried out with a Varian ProStar system and an Agilent Zorbax 300 SB-C18 prep column (5 µm particle size, 300 Å pore size, 15021.2 mm, flow rate: 20 mL min^{-1}) using a method which depends on the type of compound to be purified. Semipreparative HPLC was carried out Merck Hitachi system (interface D-7000, diode array detector L-7455, pump L-7100) and an Agilent Zorbax 300 SB-C18 colunm (5 um particle size, 300 A pore size, 250x9.4 mm). Analytical HPLC was performed with a VWR Hitachi Chromaster system with a 5110 pump, 5210 auto-sampler, 5310 column oven and 5430 diode array detector with a Macherey-Nagel nucleosil 100-5 C18 column (5 µm particle size, 100 Å pore size, 250 x 3 mm, flow rate: 0.75 mL min^{-1}) or with an Agilent Zorbax 300 SB-C18 analytical column (3.5 µm particle size, 300 Å pore size, 150 x 4.6 mm, flow rate: 0.75 mL min^{-1}). The analytical runs were performed with a method which depended on the type of compound to be purified. The TLC was performed using silica gel/UV TLC, 0.25 mm, aluminum support. Chemicals and solvents were of reagent grade or better and purchased from commercial suppliers and were used without further purification unless otherwise specified. The peptide synthesis was performed according to a procedure reported by Metzler-Note [161]. The peptides

were prepared manually in one-way polypropylene syringes (5, 10 or 100 mL) equipped with a frit using a standard solid-phase peptide synthesis procedure. All the reactions were carried out using a mechanical shaker. The synthetic steps related to the porphyrin were characterized with mono, bidimensional spactra and RP-UPLC-MS. Each step of the SPPS was characterized by RP-UPLC-MS.

Porphyrin 23

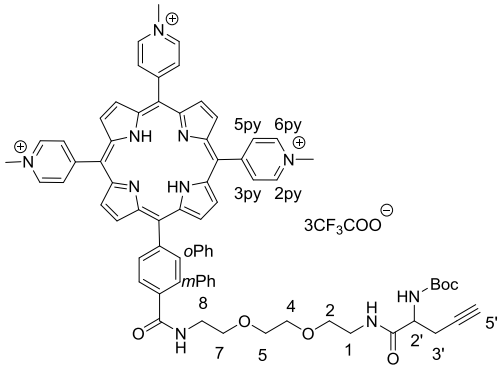

To a solution of Boc-L-2-propargylglycine (5.03 mg, 0.0237 mmol, 1.4 equiv) in anhydrous DMF (0.5 mL) HOBt (5.38 mg, 0.0398 mmol, 2.4 equiv) and EDCI (7.30 mg, 0.0382 mmol, 2.3 equiv) were added and the resulting solution was stirred for 30 min. To this solution a purple solution of the porphyrin **13** (19.5 mg, 0.0166 mmol) and DMAP (5.45 mg, 0.0446 mmol, 2.7 equiv) in anhydrous DMF (2.5 mL) was added. The resulting solution was stirred shielded from light for 20 h at rt. The reaction was monitored by TLC (CH_3CN/KNO_3sat/H_2O 4:0.3:1, R_f = 0.55). The charged porphyrin was purified by repeated precipitation (CH_3OH/Et_2O) and extensive washed with Et_2O and CH_2Cl_2 to remove the excess of the reagents and of the Boc-L-2-propargylglycine.

Yield: 69% (15.7 mg).

^{1}H NMR (CD_3,OD): δ=9.38 (d, 6H, 2,6py, *J*=6.1 Hz), 9.38-8.96 (br s, 8H, βH), 8.96 (d, 6H, 3,5py, *J*=5.9 Hz), 8.32 (m, 4H, *o*Ph+*m*Ph), 4.80 (s, 9H, CH_3py), 4.22 (m, 1H, CH 2'), 3.84 (t, 2H, CH_2O, *J*=5.2 Hz), 3.79 (m, 4H, CH_2O+CH_2NH), 3.73 (m, 2H, CH_2O), 3.63 (t, 2H, CH_2O, *J*=5.6 Hz), 3.45 (m, 2H, CH_2NH), 2.62 (ddd, 1H, CH_2 3', *J*=2.6, 6.0, 16.8 Hz), 2.58 (ddd, 1H, CH_2 3', *J*=2.7, 7.4, 16.9 Hz), 10.0, 6.7, 2.7), 2.32 (s, 1H, CH_2 5'), 1.32 ppm (s, 9H, CH_3Boc)

ESI-MS m/z: 515.5 $[M]^{2+}$, 344.1 $[M]^{3+}$, 310.8 $[M_{\text{-Boc}}]^{3+}$.

RP-UPLC-MS (sample dissolved in CH_3OH) t_r: 0.9 min

Porphyrin 24

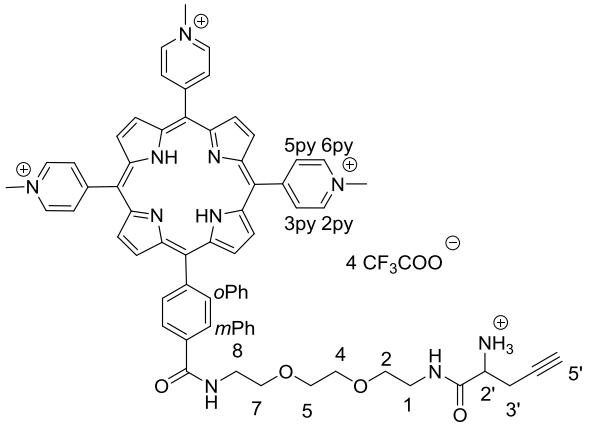

To a solution of porphyrin **23** (15.70 mg, 0.0114 mmol) in CH_2Cl_2 (2 mL) TFA (2 mL) was added. The solution was stirred at rt for 4 h shielded from light, then the solvent was removed under reduced pressure until the complete elimination of the excess of TFA, to give the product as TFA salt. The reaction was quantitative and the product was used in the following step without further purification. TLC: $CH_3CN/KNO_3sat/H_2O$ 4:0.3:1, R_f = 0.35.

Porphyrin 25

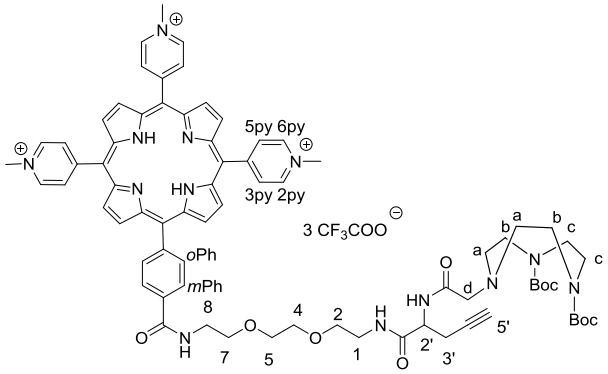

To a solution of **4** (6.87 mg, 0.0177 mmol, 1.5 equiv) in anhydrous DMF (1 mL) HOBt (4.30 mg, 0.0318 mmol, 2.8 equiv) and EDCI (6.09 mg, 0.0318 mmol, 2.8 equiv) were added and the resulting solution was stirred for 45 min. To this solution a purple solution of the porphyrin **24** (0.0114 mmol) and DMAP (3.32 mg, 0.0272 mmol, 2.4 equiv) in DMF (1.5 mL) was added. The reaction was left under stirring at rt for 21 h. The reaction was monitored by TLC ($CH_3CN/KNO_3sat/H_2O$ 4:0.3:1, R_f = 0.55). The charged porphyrin was purified by repeated precipitation (CH_3OH/Et_2O) and extensive washes with Et_2O and CH_2Cl_2 to remove the excess both of the reagents and of the ligand.

Yield: 69.52% (13 mg).

^{1}H NMR (CD_3,OD): δ=9.39 (d, 6H, 2,6py, *J*=5.1 Hz), 8.97 (m, 6H, 3,5py, *J*=5.5 Hz), 9.39-8.97 (br s, 8H, βH), 8.30 (m, 4H, *o*Ph+*m*Ph), 4.80 (s, 9H, CH_3py), 4.51 (t, 1H, CH 2'), 3.82 (m, 2H, CH_2O), 3.77 (m, 4H, CH_2O+CH_2NH), 3.72 (m, 2H, CH_2O), 3.62 (m, 2H, CH_2O), 3.52-3.34 (m, CH_2NH+CH_2 c/b, 6H), 3.25 (m, CH_2 c/b, 4H), 3.14 (m, CH_2 c/b, CH_2 d, 4H) 2.67 (m, 6H, CH_2 a + CH_2 3'), 2.36 (m/s, 1H, CH 5'), 1.39-1.36-1.30 ppm (3s, 18H, CH_3Boc).

ESI-MS *m/z*: 650.1 $[M]^{2+}$, 433.8 $[M]^{3+}$, 367.1 $[M_{-2Boc}]^{3+}$, 275.6 $[M_{-2Boc}+H]^{4+}$

RP-UPLC-MS (sample dissolved in CH_3OH) t_r: 1 min

Porphyrin 26

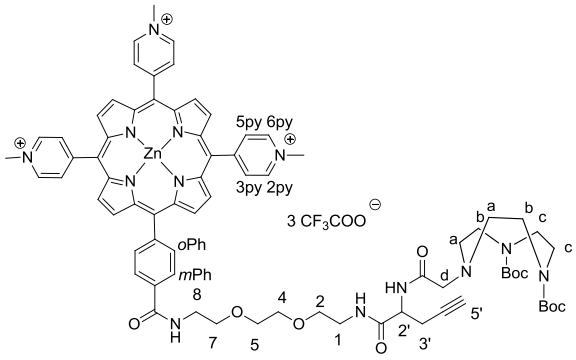

Porphyrin **25** (3 mg) and zinc acetate dihydrate (2.5 mg, 0.0114 mmol, 6 equiv) were dissolved in methanol (3 mL) obtaining a deep green-brown solution. The reaction was left under stirring at rt for 2 h and was monitored by TLC (CH_3CN/KNO_3sat/H_2O 4:0.3:1, R_f = 0.32) and UV-Vis. Then the solvent was removed under reduce pressure. The reaction is quantitative and the product was used in the following step without further purification to remove the excess of zinc acetate.

ESI MS *m/z*: 681 $[M]^{2+}$, 454.6 $[M]^{3+}$, 291.2 $[M_{-2Boc}+H]^{4+}$

RP-UPLC-MS t_r: 1.85 min.

Porphyrin 26

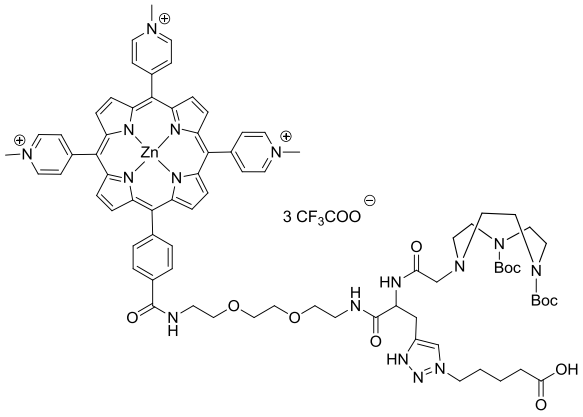

To porphyrin **25** (0.00061 mmol), 35 µL (0,00122 mmol, 2 equiv) of a solution 0.035 mM of sodium ascorbate in 1:2 H_2O/*t*BuOH, 43 µL (0.00037 mmol, 0.6 equiv) of a solution 0.0086 mM of copper sulfate in the 1:2 mixture H_2O/*t*BuOH and 16 µL (0.0016 mmol, 2.6 equiv) of a solution 0.1 mM of the azido acid pentanoic in the mixture 1:2 H_2O/*t*BuOH were added. 200 µL of a mixture made of 1:2 H_2O/*t*BuOH were added to this solution. The solution was left under stirring at rt and the reaction was monitored by TLC (CH_3CN/KNO_3 sat/H_2O 4:0.3:1, R_f = 0.27) and RP-UPLC. After 22 h less than 50% of the product was obtained. Then the reaction yield was increased in a microwave reactor at 85 °C for 17 min. The reaction was complete after adding 2, 0.83 and 6.5 equivalents of sodium ascorbate, copper sulfate and azido acid pentanoic respectively in 1:2 H_2O/*t*BuOH and heating for further 10 min at 85 °C.

ESI MS *m/z*: 753.5 $[M]^{2+}$, 502.6 $[M]^{3+}$, 327.2 $[M_{-2Boc}+H]^{4+}$

RP-UPLC-MS t_r: 1.9 min.

Porphyrin 28

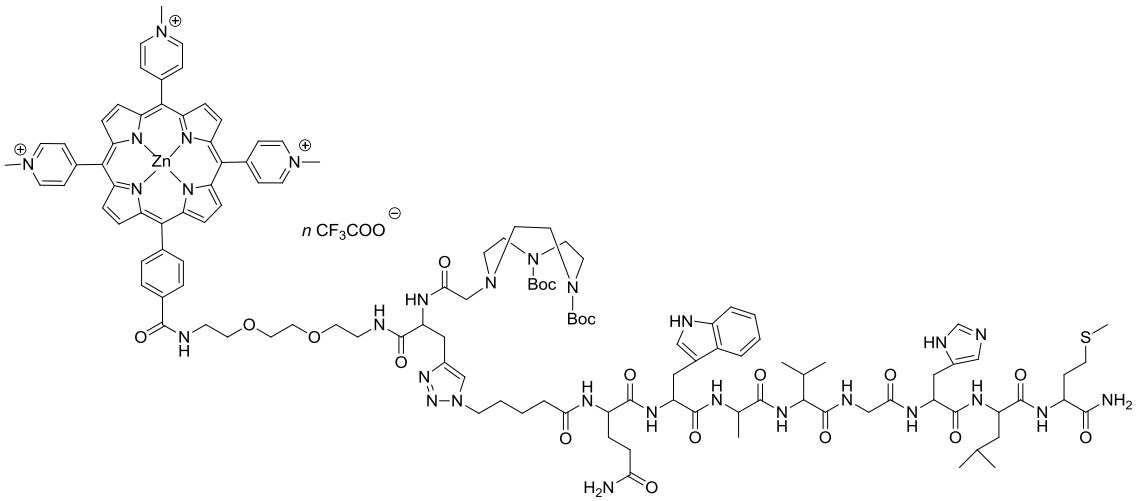

To 5.05 mg of porphyrin **26** (0.00196 mmol), copper sulphate (1.33 mg, 0.0084 mmol, 4.3 equiv), sodium ascorbate (3.47 mg, 0.0175 mmol, 8.9 equiv) were dissolved in 6 mL of 1:2 mixture H_2O/*t*BuOH and the solution was heated in a microwave reactor at 85 °C for 1 h obtaining a precipitate and a green solution. The reaction was checked by RP-UPLC-MS and then the solvent was evaporated. The product was obtained in a mixture with the oxidized product.

ESI MS *m/z*: 1097.7 $[BNN_{3\ 2\ OX}+H]^+$, 1081.7 $[BNN_{3\ OX}+H]^+$, 815.2 $[M_{OX}]^{3+}$, 810.7 $[M]^{3+}$, 612.0 $[M_{OX}+H]^{4+}$, 607.8 $[M+H]^{4+}$, 549.5 $[BNN_{3\ OX}+2H]^{2+}$, 541.4 $[BNN_{3\ 2\ OX}+2H]^{2+}$, 489.9 $[M_{OX}+2H]^{5+}$, 486.5 $[M+2H]^{5+}$.

RP-UPLC-MS t_r: 1.90 min (M_{OX}+ $BNN_{3\ ox}$) 1.80 min (M + $BNN_{3\ 2\ ox}$).

Porphyrin 29

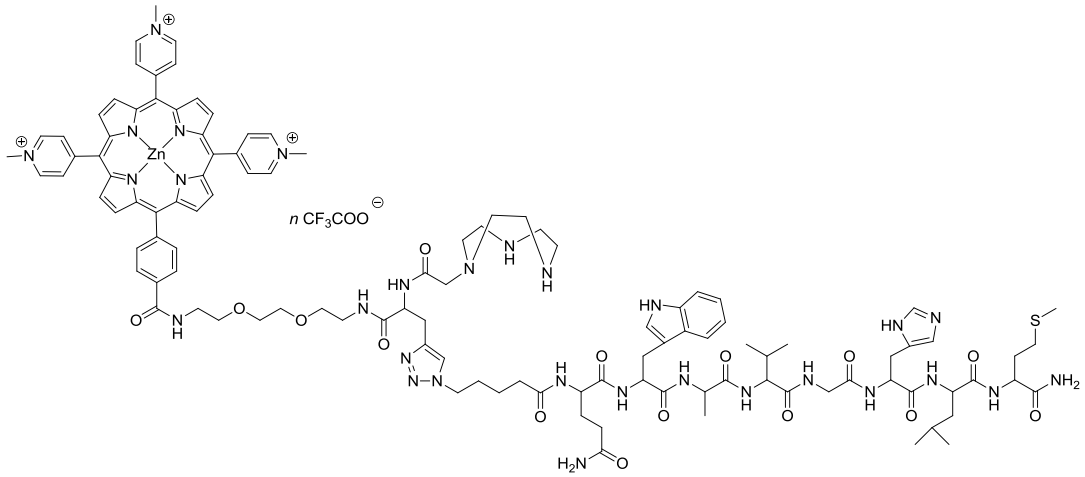

Porphyrin **28** was dissolved in TFA (1.5 mL) and the solution was stirred for 2 h shielded from light, then the solvent was removed under reduced of pressure and the product was suspended in CH_3OH. 100 µL of TEA were added to precipitate product precipitated and s washed several times with Et_2O. The product was purified by 3 semipreparative HPLC.

Semipreparative HPLC, flow rate = 4mL/min, linear gradient of A (double distilled H_2O containing 0.1% v/v TFA) and B (ACN, Sigma-Aldrich HPLC-grade), *t* = 0 min, 10% B; *t* = 3 min, 10% B; *t* = 45 min, 50% B; *t* = 47 min, *t* =95% B; *t*= 49 min, *t*= 95%, t_r: 17.5 min ESI MS *m/z*: 1148.6 $[M_{2\ OX}+K]^{2+}$, 766.8 $[M_{2\ OX}+K]^{3+}$, 575.4 $[M_{2\ OX}+K]^{4+}$, 460.5 $[M_{2\ OX}+K+H]^{5+}$.

RP-UPLC-MS t_r: 1.5 min.

General procedure for the synthesis of peptides on solid phase

Polystyrene resin beds of TentaGel S RAM (capacity 0.24 mmol g^{-1} or 0.26 mmol g^{-1}) were inserted into a polypropylene syringe equipped with a frit swollen in DMF for at least 1 h before use. The resin was deprotected with piperidine (20% v/v in DMF) first for 2 min and then for 10 min. Either after 2 and 10 min the resin was washed with DMF (5 mL × 5), CH_2Cl_2 (5 mL × 5) and DMF (5 mL × 5). A first Fmoc-protected amino acid (4.5 equiv) was first pre-activated using TBTU (4 equiv) and base solution (3.8%v/v DIPEA, 3.8% v/v 2,6 lutidine in DMF, usually 3 mL for 1 g of resin) for 5 min and then reacted with the resin for 1h. Afterwards, the resin beads were washed with DMF (5 mL × 5) and CH_2Cl_2 (5 mL ×5), and a Kaiser test was performed to check if the coupling was complete. Then the resin beads were washed with DMF (5 mL × 5). The amino group of the first amino acid was deprotected with piperidine (20% v/v in DMF) for 2

min and then for 10 min. Either after 2 and 10 min the resin was washed with DMF (5 mL × 5), CH_2Cl_2 (5 mL × 5) and DMF (5 mL × 5). The second Fmoc-protected amino acid was added following the same procedure for the first one. When the whole peptide sequence was synthesized, the peptide was cleaved from the resin, checked and eventually purified.

General procedure for the cleavage of the product from the resin

After the Fmoc deprotection of the last amino acid the resin was shrunk in CH_3OH and dried under vacuum for at least 30 min. A small amount of the product was cleaved using 4 mL of a mixture 38:1:1 v/v/v TFA:H_2O:TIPS for 4 h at rt. The resin was filtrate and the filtrate was evaporated under vacuum. The peptide was precipitated and washed with cold Et_2O and dried under vacuum. The purity of the compound was check by RP-UPLC-MS and analytical HPLC and then eventually purified by preparative HPLC. For BNPLT, BNPLTA and BNPLTAP TIPS was replaced with 2-mercapthoetanol.

BN[7-14]

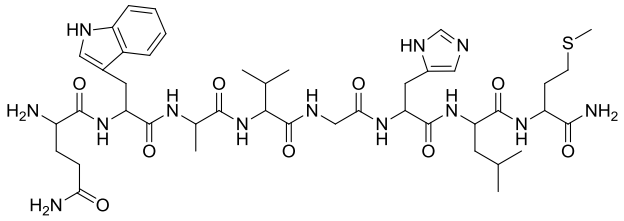

The peptide was synthetized on solid phase following the general procedures described for the synthesis of peptides on solid phase.

ESI MS *m/z*: 940.6 $[M+H]^+$, 470.8 $[M+2H]^{2+}$, 956.6 $[M_{OX}+H]^+$, 478.8 $[M_{OX}+2H]^{+2}$, 978.5 $[M_{OX}+Na]^+$

RP-UPLC-MS t_r: 1.45 min (M_{OX}), 1.65 min (M).

Analytical HPLC, Zorbax column, linear gradient of A (double distilled H_2O containing 0.1% v/v TFA) and B (ACN, Sigma-Aldrich HPLC-grade), t = 0 min, 5% B; t = 3 min, 5% B; t = 20 min, 80% B; t = 22 min, 100% B; t = 23 min, 100 % B; t_r: 10.2 min (M_{OX}), 10.7 min (M).

BNN_3

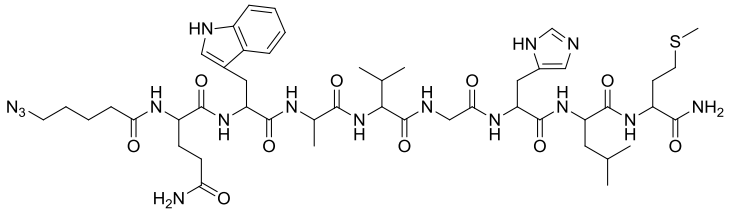

52 mg of BN[7-14] (0.01352 mmol) were used to couple the azidopentanoic acid (8.71 mg, 0.06084 mmol, 4.5 equiv) using TBTU (17.7 mg, 0.05512, 4 equiv) and base solution (2 mL) following the general procedure described for the SPPS. After the cleavage the product was purified by preparative HPLC.

ESI MS *m/z*: 1065.8 $[M+H]^+$, 533.5 $[M+2H]^{2+}$, 1081.8 $[M_{OX}+H]^+$, 541.6 $[M_{OX}+2H]^{+2}$.

RP-UPLC-MS t_r: 1.90 min (M_{OX}), 2.15 min (M).

Preparative HPLC, linear gradient of A (double distilled H_2O containing 0.1% v/v TFA) and B (ACN, Sigma-Aldrich HPLC-grade), *t* = 0 min, 5% B; *t* = 23 min, 100% B; *t* = 30 min, 100% B; *t* = 32 min, 5% B; t_r: 16 min.

BNPL-Fmoc-Mtt

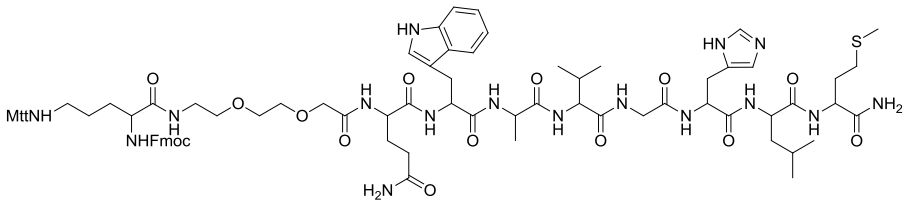

129.6 mg of peptide BN7-14 (0.0312 mmol) were used to couple first Fmoc-AEEA-OH (54.11 mg, 0.1404 mmol, 4.5 equiv) and then Fmoc-Lys (Mtt) (87.72 mg, 0.1404 mmol, 4.5 equiv) using TBTU (40.1 mg, 0.1249 mmol, 4 equiv for the first coupling, 54.11 mg, 0.1404 mmol, 4.5 equiv for the second coupling) and 3.5 mL of base solution for each coupling reaction, following the general procedure described for the synthesis of peptides on solid phase. Both coupling reactions last over an hour.

ESI MS *m/z*: 1436.8 $[M_{(-Mtt)}+H]^+$, 718.6 $[M_{(-Mtt)}+2H]^{2+}$, 1451.8 $[M_{(-Mtt)OX}+H]^+$, 726.5 $[M_{(-Mtt)OX}+2H]^{+2}$.

RP-UPLC-MS t_r: 1.95 min (M_{OX}) 2.05 min (M).

BNPL

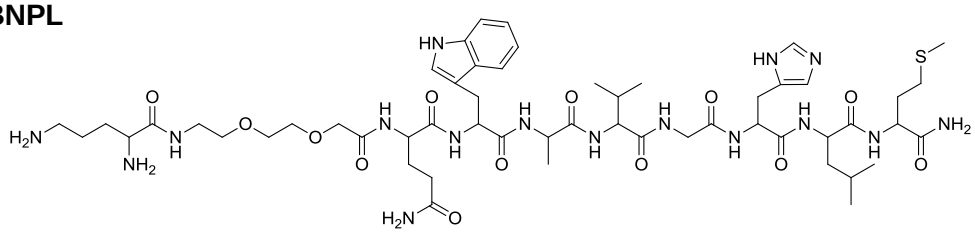

ESI MS *m/z*: 1213.8 $[M+H]^+$, 607.5 $[M+2H]^{2+}$, 1229.7 $[M_{OX}+H]^+$, 615.5 $[M_{OX}+2H]^{2+}$, 410.7 $[M_{OX}+3H]^{3+}$,

RP-UPLC-MS t_r: 1.35 min (M_{OX}) 1.5 min (M).

BNPL-Fmoc

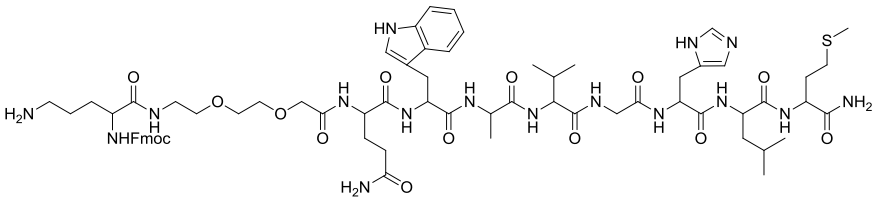

To remove the Mtt protecting group the resin with the peptide BNPL-Fmoc-Mtt (10 mg, 0.0024 mmol) was washed several times with a solution 92:3:5 CH_2Cl_2/TFA/TIPS or with a solution 94:5:1 CH_2Cl_2/TIPS/TFA. Then the resin was left shaking for 10 min with 1 mL of the fresh solution 92:3:5 CH_2Cl_2/TIPS/TFA for two times or for 30 min with 2 mL of the fresh solution 94:5:1 CH_2Cl_2/TIPS/TFA. During the washes the solution becomes deep yellow and then transparent. The resin was then washed with DMF (5 mL x 5) and CH_2Cl_2 (5 mL x 5) and a Kaiser test was performed. The resin was finally washed with DMF (5 mL x 5). As from RP-UPLC-MS the starting material could not be detected, this intermediate was used for the following coupling reaction without further characterization.

BNPLG

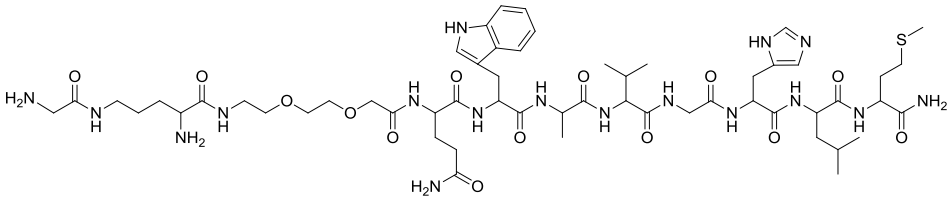

10 mg of peptide BNPLFmocMtt (0.0024 mmol) were used to couple Fmoc-glycine (3.21 mg, 0.0108 mmol, 4.5 equiv) using TBTU (3.08 mg, 0.0096 mmol, 4 equiv) and 1mL of base solution, following the general procedure described for the synthesis of peptides on solid phase. The RP-UPLC-MS analysis was performed after the Fmoc deprotection.

ESI MS *m/z*: 1270.8 $[M+H]^+$, 636.0 $[M+2H]^{2+}$, 1286.8 $[M_{OX}+H]^+$, 644.0 $[M_{OX}+2H]^{2+}$.

RP-UPLC-MS t_r: 1.25 min (M_{OX}), 1.4 min (M).

BNPLT

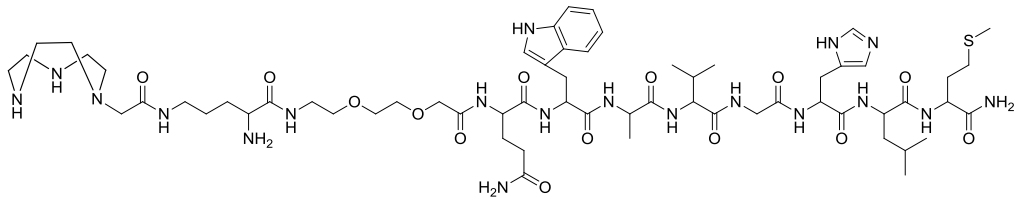

129.6 mg of peptide BNPL-Fmoc-Mtt (0.0312 mmol) were used to couple the chelator (44 mg, 0.1135 mmol, 3.6 equiv) using TBTU (40.1 mg, 0.1217 mmol, 4 equiv.) and 2 mL of base solution, following the general procedure described for the synthesis of peptides on solid phase. The resin was left shaking overnight. The RP-UPLC-MS analysis was performed after the Fmoc deprotection.

ESI MS *m/z*: 1382.9 $[M+H]^+$, 692.1 $[M+2H]^{2+}$, 461.8 $[M+3H]^{3+}$, 1398.9 $[M_{OX}+H]^+$, 700.0 $[M_{OX}+2H]^{+2}$, 467.1 $[M_{OX}+3H]^{3+}$.

RP-UPLC-MS t_r: 1.25 min (M_{OX}), 1.35 min (M).

BNPLTA

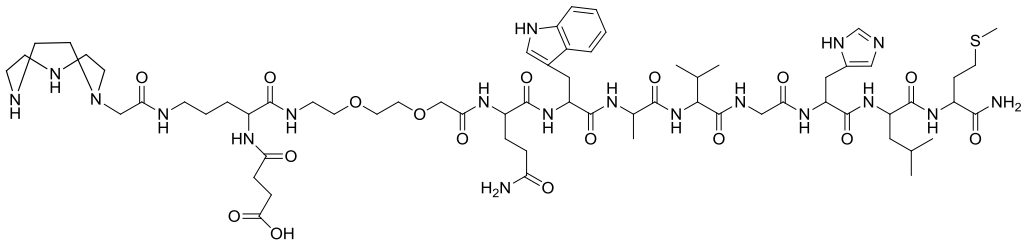

The resin with the peptide BNPLFT (129.6 mg, 0.0312 mmol of BN[7-14]) was reacted with the anhydride (14.04 mg, 0.1404 mmol, 4.5 equivalents) dissolved in base solution (2 mL) overnight.

ESI MS *m/z*: 1483.9 $[M+2H]^{+}$, 742.1 $[M+2H]^{2+}$, 1498.9 $[M_{OX}+H]^{+}$, 750.1 $[M_{OX}+2H]^{+2}$.

RP-UPLC-MS t_r: 1.3 min (M_{OX}), 1.45 min (M).

Analytical HPLC, Zorbax column, linear gradient of A (double distilled water containing 0.1% v/v TFA) and B (ACN, Sigma-Aldrich HPLC-grade), *t* = 0 min, 5% B; *t* = 3 min, 5% B; *t* = 20 min, 80% B; *t* = 22 min, 100% B; *t* = 23 min, 100 % B; t_r: 11.25 min (M_{OX}) 12.2 min (M).

Analytical HPLC, nucleosil column, linear gradient of A (double distilled water containing 0.1% v/v TFA) and B (ACN, Sigma-Aldrich HPLC-grade), *t* = 0, 2% B; *t* = 2, 2% B; *t* = 55, 50% B; *t* = 58, 50% B; *t* = 58.1, 100% B; t_r: 28.0 min (M_{OX}) 31.7 min (M).

BNPLTAB

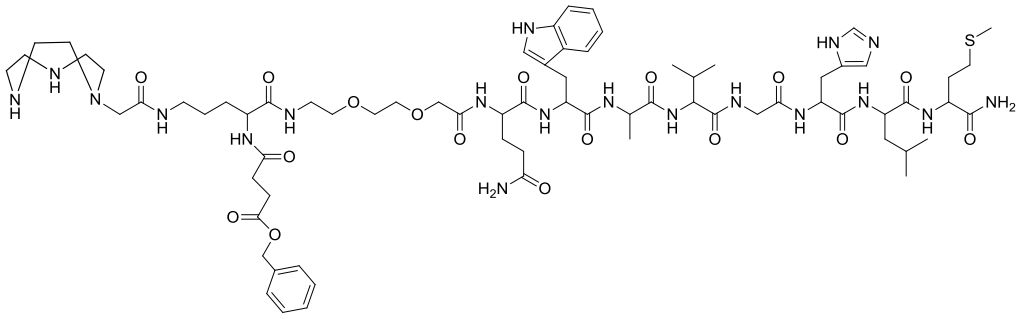

The resin with the peptide BNPLFTA (5 mg, 0.0012 mmol) was first pre-activated using TBTU (1.54 mg, 0.0048 mmol, 4 equiv) in base solution (300 µL) for 10 min. Then a solution of benzylamine (590 µL, 0.5787 mmol, 4.5 equiv) in base solution (300 µL) was added and then the resin was left shaking for over an hour.

ESI MS *m/z*: 1571.9 $[M]^{+}$, 786.7 $[M+2H]^{2+}$, 525 $[M+3H]^{3+}$, 1588.0 $[M_{OX}]^{+}$.

RP-UPLC-MS t_r: 1.45 min (M_{OX}), 1.6 min (M).

BNPLTAP

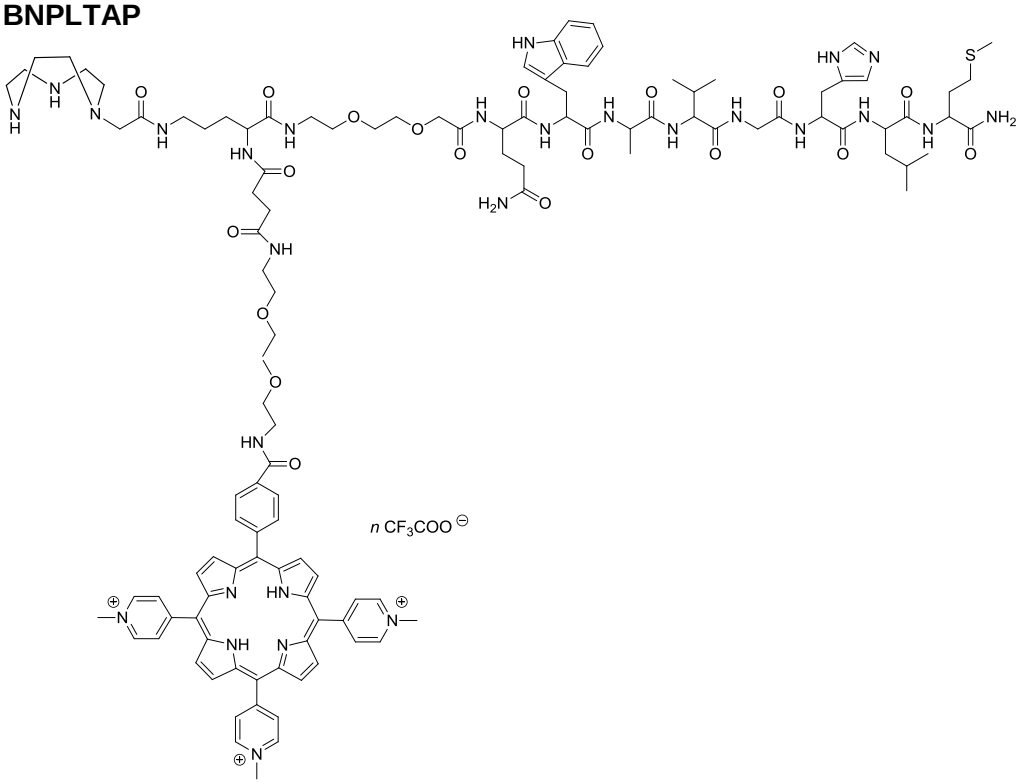

18.3 mg of resin with the peptide BNPLFTA (0.0044 mmol) were first pre-activated using TBTU (7.4 mg, 0.0230 mmol, 5.2 equiv) and HOBt (3.2 mg, 0.0237 mmol, 5.4 equiv) in anhydrous base solution (1.5 mL) for 15 min. Then a solution of porphyrin (15.6 mg, 0.0133 mmol, 3 equiv) in anhydrous base solution (1.5 mL) was added and the resin was left shaking for 20 h under a nitrogen atmosphere. Afterwards, the resin beads were washed with DMF (5 mL × 5), CH_2Cl_2 and DMF (5 mL × 5). The product was cleaved from the resin using a cleavage solution made of 38:1:1 v/v/v TFA:H_2O:2-mercaptoethanol obtaining 21.3 and 47.11 mg of crude product respectively from the first and second cleavage. The product was dissolved in 20 mL of distilled H_2O containing 0.1% v/v TFA and two preparative HPLC were performed. The product was checked by RP-UPLC-MS, analytical HPLC and MALDI. Overall 0.30 mg of pure product were obtained.

RP-UPLC-MS t_r: 1.5 min.

Preparative HPLC, method A, linear gradient of A (double distilled H_2O containing 0.1% v/v TFA) and B (ACN, Sigma-Aldrich HPLC-grade), t = 5 min, 5% B; t = 130 min, 34% B; t = 135 min, 34% B; t = 145 min, 50% B; t = 150 min, 90 % B; t = 155 min, 5% B; t_r: 87 min.

Preparative HPLC, method B, linear gradient of A (double distilled H_2O containing 0.1% v/v TFA) and B (ACN, Sigma-Aldrich HPLC-grade), t = 5 min, 5% B; t = 130 min, 26%

B; *t* = 140 min, 35% B; *t* = 145 min, 50% B; *t* = 150 min, 100 % B; *t* = 160 min, 100% B; *t* = 165 min, 5% B; t_r: 110 min.

Analytical HPLC, Zorbax column, flow rate = 0.75 mL/min, inject volume= 100μL, linear gradient of A (double distilled H_2O containing 0.1% v/v TFA) and B (ACN, Sigma-Aldrich HPLC-grade), *t* = 0 min, 5% B; *t* = 3 min, 5% B; *t* = 20 min, 80% B; *t* = 22 min, 100% B; *t* = 23 min, 100 % B; t_r:12.3

Analytical HPLC, nucleosil column, linear gradient of A (double distilled water containing 0.1% v/v TFA) and B (ACN, Sigma-Aldrich HPLC-grade), *t* = 0, 2% B; *t* = 2, 2% B; *t* = 55, 50% B; *t* = 58, 50% B; *t* = 58.1, 100% B; t_r: 36.1 min (M_{OX}) 37.9 min (M). t_r: 11.7 min (M_{OX}) 12.2 min (M).

MALDI-Tof *m/z*: 2301.2 $[M+H]^+$, 2317.2 $[M_{OX}+H]^+$, 2333.2 $[M_{2\,OX}+H]^+$.

BNPLTAF

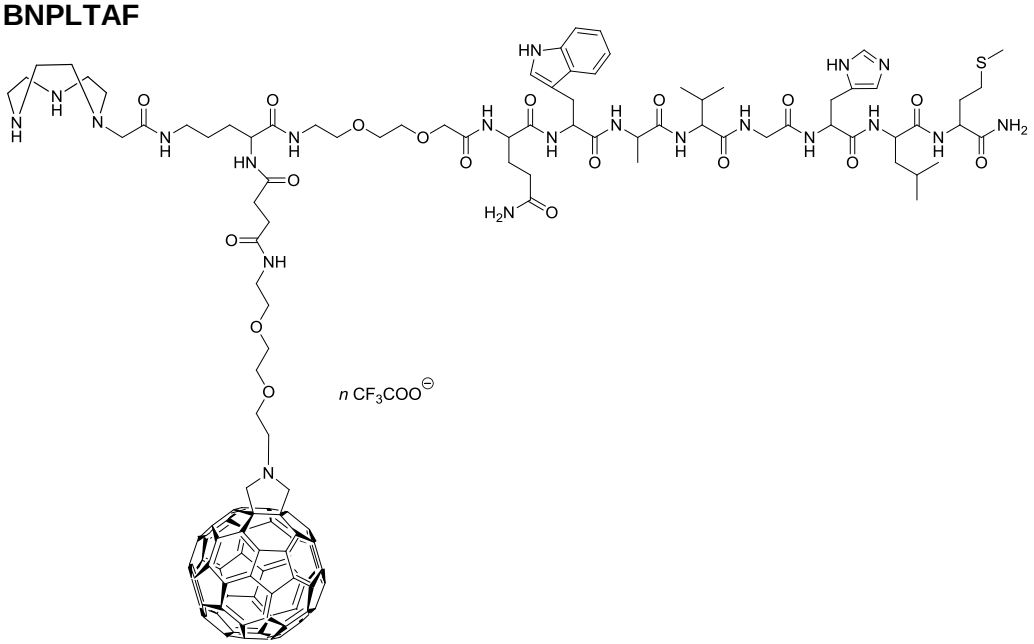

70.14 mg (0.017 mmol) of resin with the peptide BNPLFTA was divided in three 100 mL syringes, the functionalized fullerene (65.35 mg, 0.0648 mmol, 3.81 equiv) was divided in 15 equal portions and each portion was dissolved in 10 mL of a base solution made of DIPEA, 2,6-lutidine in dioxane and NMP 1:1. 5 portions were added in 3 days for each syringe. Before each addition of the fullerene, the resin was pre-activated using 4.5 equiv TBTU (128.51 mg, 0.4002 mmol, 23.54 equiv) in DMF (10 mL total) for 15 min. The resin was then left shaking for other 3 days at rt. The solution was then filtered and the resin was then washed several times with DMF, CH_2Cl_2, CH_3OH, dioxane and NMP. After the cleavage of the product from the resin the product was

characterized with RP-UPLC-MS and MALDI. 8.27 mg of impure product were obtained.

RP-UPLC-MS t_r: 1.55 min.

MALDI-Tof *m/z*: 2375.8 [M+H_2O].

4.

BIBLIOGRAPHY

[1] Ethirajan M., Chen Y., Joshi P., Pandey R. K., *Chem. Soc. Rev*. **2011**, 40, 340-362

[2] Dougherty T. J., Grindey G. B., Fiel R., Weishaupt K. R., Boyle D. G., *J. Natl. Cancer Inst.*, **1975**, 55, 115-121.

[3] (a) Dougherty T. J., *J. Clin. Laser Med. Surg*., **2002**, 20, 3-7 (b) Oleinik N. L., Evans H. H., *Radiat. Res.*, **1998**,*150*, 146-156.

[4] (a) Pass H. I., *J. Natl. Cancer Inst.*, **1993**, *85*, 6, 443-456 (b) Henderson B. W., Dougherty T. J., *J.Photochem. Photobiol.*, **1992**, *55*, 145-157.

[5] Allison R. R., Downie G. H., Cuenca R., Hu X.-H., Childs C. J. H, Sibata C. H., *Photodiagnosis and Photodynamic Therapy*, **2004**, *1*, 27-42

[6] Dhaneshwar S., Patil K., Bulbule M., Kinjawadekar V., Joshi D., Joshi V., *Int. J. Pharm. Sci. Rev. Res.*, **2014**, *27*, 2, 125-141

[7] Pizova K., Tomankova K., Daskova A., Binder S., Bajgar R., Kolarova H., *Biomed Pap Med Fac. Univ. Palacky Olomocuc Czech Repub*, **2012**, *156*, 2, 93-102

[8] Dougherty T. J., Gomer C. J., Henderson B. W., Jori G., Kessel D., Korbelik M., Moan J., Peng Q., *J. Natl. Cancer. Inst.*, **1998**, *90*, 889-905.

[9] Engbreht B. W., Menon, C., Kahur A. V., Hahn S. M., Fraker, D. L., *Cancer Res.*, **1999**, *59*, 4334-4342.

[10] Kruk M. M., Starukhin A. S., Maes W., *Macroheterocycles*, **2011**, *4,* 2, 69-79

[11] Majumdar P., Nomula R., Zhao J., *J. Mater. Chem. C*, **2014**, *2*, 5982-5997

[12] De Rosa M. C., Crutchley R. J., *Coordination Chemistry Reviews*, **2002**, 233-234, 351-371

[13] Yakubovskaya R. I., Morozova N. B., Pankratov A. A., Kazachkina N. I., Plyutinskaya A. D., Karmakova T. A., Andreeva T. A., Venediktova Y. B., Plotnikova E. A., Nemtsova E. R., Sokolov V. V., Filonenko E. V., Chissov V. I., Kogan B. Ya., Butenin A. V., Feofanov A. V., and Strakhovskaya M. G., *Russian Journal of General Chemistry*, **2015**, *85*, 1, 217-239

[14] Baeumler W., *Comprehensive Series in Photoscience*, **2001**, 1st ed., *2*, Elsevier, 83–98.

[15] Szaciowski K., Macyk W., Drzewiecka-Matuszek A., Brindell M., Stochel G., *Chem. Rev.*, **2005**, *105*, 2647-2694

[16] Mang T. S., *Photodiagnosis and Photodynamic Therapy*, **2004**, *1*, 43-48

[17] Voon S. H., Kiew L. V., Boon Lee H., Lim S. H., Noordin M. I., Kamkaew A., Burgess K., Chug L. Y., *Small*, **2014**, *24*, 4993-5013

[18] Brancaleon L., Moseley H., *Laser Med. Sci.,* **2002**, *17*, 173-186

[19] Defu C., Huang Z., Zhyong H., Lin H., Ke Z., Xie S., Li B., Chen D., *International Journal of Photoenergy*, **2012**, *2012*, ID 920671, 6 pages, doi:10.1155/2012/920671

[20] Mathias O., Senge Dr.rer.nat., FTCD, Radomski M. W., *Photodiagnosis and Photodynamic Therapy*, **2013**, *10*, 1-16

[21] Malik Z., *Photon Lasers Med*, **2015**, *4, 1*, 19-26

[22] Tetard M.C., Vermandel M., Mordon S., Lejeune J.P., Reyns N., *Photodiagnosis and Photodynamic Therapy*, **2014**, *11*, 319-330

[23] Nokes B., Apel M., Jones C., Brown G., Lang J.E., FACS, *Journal of Surgical Research*, **2013**, *181*, 262-271

[24] Detty M.R., Gibson S.L., Wagner S.J., *Journal of Medicinal Chemistry*, **2004**, *47*, 16, 3897-3915

[25] Paszko E., Ehrhardt C., Senge M. O., FTCD, Kelleher D. P., Reynolds J. V., *Photodiagnosis and Photodynamic Therapy*, **2011**, *8*, 14-29

[26] Bhuyan J., *Dalton Trans.*, **2015**, *44*, 15742-15756

[27] Castano A. P., Demidova T. N., Hamblin M. R., *Photodiagnosis Photodyn Ther*., 2004, *1,* 4, 279–293.

[28] Rezazgui O., Trouillas P., Qui S., Siegler B., Gierschner J., Leory-Lhez S., *New Journal of Chemistry*, **2016**, DOI: 10.1039/c5nj02901e

[29] Kadish K. M., Smith K. M., R. Guilard, *The Porphyrin Handbook*, **2003**, *18*, 63-249

[30] Kadish K. M., Smith K. M., R. Guilard, *The Porphyrin Handbook*, **2003**, *6*, 233

[31] Jori G., Reddi E., *Int. J. Biochem*., **1993**, *25*, 1369-1375

[32] Vicente M. G. H., *Curr. Med. Chem*., **2001**, *1*, 175-194

[33] Jori G., Beltramini M., Reddi E., Salvato B., Pagnan A., Ziron L., Tomio L., Tasnov T., *Cancer Lett*., **1984**, *24*, 291-297

[34] Candide C., Morliere P., Marziere J. C., Goldstein S., Santus R., Dubertret L., Reyftmann J. P., Polanovski J., FEBS *Lett*., **1986**, *207*, 133-138

[35] Kessel D., *Cancer Lett*. **1986**, *33*, 183-188

[36] Berg K., Western A., Bommer J. C., Moan J., *Photochem. Photobiol.*, **1990**, *52*, 481-487.

[37] Woodburn K. W., Vardaxis N. J., Hill J. S., Kaye A. H., Philips D. R., *Photochem. Photobiol*., **1991**, *54*, 725-732

[38] Kessel D., *Photochem. Photobiol*., **1993**, *58*, 623-626

[39] Almeida R.D., Manadas B.J., Carvalho A.P., Duarte C.B., *Biochim, Biophys.Acta*, **2004**, *1704*, 59-86

[40] Bonnet R., *Chem. Soc. Rev*., **1995**, *24*, 19-33

[41] Jori G., Galiazzo G., Scoffone E., **1969**, *8*, 7, 2868-2875

[42] Ben-hur E., Bubbleman T.M.A.R., *J. Photochem. Photobiol. B*, **1993**, *58*, 890

[43] Gibson S.L., Murant R. S., Hilf R., *Cancer Research*., **1988**, *48*, 3360-3366

[44] K. F. Ferri, G. Kroemer, *Nat. Cell Biol.*, **2001**, *3*, 255-263

[45] Kessel D., Luo Y., *J. Photochem. Photobiol. B*, **1998**, *42*, 89-95

[46] Granville D. J., Carthy C. M., Jiang H., Shore G. C., Mcmanus B. M., Hunt D. W., *FEBS Lett.*, **1998**, *437*, 1-2, *5*-10

[47] Moan J., Berg K., *J. Photochem. Photobiol.*, **1992**, *55*, 931-948

[48] Krystona T.B., Georgieva A. B., Pissis P., Georgakilas A. G., *Mutation Res.*, **2011**, *711*, 193-201

[49] Korbelik M., *J. Clin. Laser. Med. Surg*., **1996**, *14*, 329-334

[50] Chester A. N., Martellucci S., Verga A. M., *Laser Systems for Photobiology and Photomedicine*, **1991**, Plenum Press, New York

[51] Celli J. P., Spring B .Q., Rizvi L., Evans C. L., Samkoe K. S., Verma S., Pogue B. W., Hasan T., *Chem. Rev*., **2010**, *110*, 2795-2838

[52] Lovell J. F., Liu T. W. B., Chen J., Zheng G., *Chem. Rev*, **2010**, *110*, 2839-2857

[53] Leonidova A., Gasser G., *ACS Chem. Biol*., **2014**, *9*, 2180−2193

[54] Collery P., Bastian G., Santoni F., Mohsen A., Ming W., Collery M., Tomas T., Desmaele A., D'Angelo D., *Anticancer Res.,* **2014**, *34*, 1679–1690.

[55] Kitanovic I., Can S., Alborzinia H., Kitanovic A, Pierroz V., Leonidova A., Pinto A., Molteni R., Spingler B., Ferrari S., Steffen A., Metzler-Nolte N., Wölfl S., Gasser G., *J. Chem. Eur.*, **2014**, *20*, 2496–2507

[56] Leonidova A., *ACS Chemical Biology,* **2014**, *9*, 10, 2180-2193

[57] Suzuki K., Shimmura N., Thipyapong K., Uehara T., Akizawa H., Arano Y., *Inorg. Chem*., **2008**, *47*, 2593-2600

[58] Abram U., Alberto R., *J. Braz. Chem. Soc.*, **2006**, *17,* 8, 1486-1500

[59] Arano Y., *Annals of Nuclear Medicine*, **2002**, *16*, 2, 79-93

[60] Liu S., *Adv. Drug Delivery Rev*., **2008**, *60*, 1347-1370

[61] Yeh W. M., Sherman D. G., Meares C. F., *Anal. Biochem.*, **1979**, *100*, 152-159

[62] Hnatowich D. J., Mardirossian G., Rusckowki M., Fogarasi M., Virzi F., Winnard P., *J. Nucl. Med.*, **1993**, *34*, 109-119

[63] Liu S., *Chem. Soc. Rev*., **2004**, *33*, 445-461

[64] Alberto, R. Alessio, E., **2011**, 253-282 Wiley-VCH Verlag GmbH&Co. KGaA, Weinheim, Germany

[65] Spagnul C., Alberto R., Gasser G., Ferrari S., Pierroz V., Bergamo A., Gianferrara T., Alessio E., *J. Inorg. Biochem*., **2013**, *122*, 57–65.

[66] Gianferrara T., Spagnul C., Alberto R., Gasser G., Ferrari S., Pierroz V., Bergamo A., Alessio E., *ChemMedChem*, **2014**, *9*, 1231–1237.

[67] Naik A., Rubbiani R., Gasser G., Spingler B., *Angew. Chem. Int. Ed*., **2014**, *53*, 6938–6941.

[68] Fiel R. J. J., *Biomol. Struc. Dyn*., **1989**, *6*, 1259–1274.

[69] Pasternack R. F., Gibbs E., *J. Met. Ions Biol. Syst.,* **1996**, *33*, 367–397.

[70] Pratviel G., Bernadou J., Meunier B., *Met. Ions Biol. Syst.*, **1996**, *33*, 399-426.

[71] Marzilli L. G., *New. J. Chem*., **1990**, *14*, 409-420

[72] Field R., Jenkins B., Alderfer J., *The 23rd Jerusalem Symposium in Quantum Chemistry and Biochemistry*, Kluwer Accademic Publishers, Netherlands, **1990**, *23*, 385-399

[73] Field R. J., Datta-Gupta N., Mark E. H., Howard J. C., *Cancer Res*, **1981**, *41*, 3543-3545

[74] (a) Han H., Langley D. R., Rangan, A., Hurley L. H., *J. Am. Chem. Soc.*, **2001**, *123*, 8902–8913 (b) Seenisamy J., Bashyam S., Gokhale V., Vankayalapati H., Sun D., Siddiqui-Jain, A., Streiner N., Shin-Ya K., White E., Wilson W. D., Hurley L. H., *J. Am. Chem. Soc*., **2005**, *127*, 2944–2959.

[75] (a) Martino L., Pagano B., Fotticchia I., Neidle S., Giancola C., *J. Phys. Chem. B*, **2009**, *113*, 14779–14786 (b) Cummaro A., Fotticchia I., Franceschin M., Giancola C., Petraccone L., *Biochimie*, **2011**, *93*, 1392–1400

[76] (a) Dixon I. M., Lopez F., Tejera A. M., Estève J. P., Blasco M. A., Pratviel G., *J. Am. Chem. Soc*., **2007**, *129*, 1502–1503 (b) Romera C., Bombarde O., Bonnet R., Gomez D., Dumy P., Calsou P., Gwan J. F., Lin J. H., Defrancq E., Pratviel G., *Biochimie,* **2011**, *93*, 1310–1317

[77] (a) Shi D. F., Wheelhouse R. T., Sun D., Hurley L. H., *J. Med. Chem.,* **2001**, *44*, 4509–4523 (b) Cohn E. P., Wu K. L., Pettus T. R., Reich N. O., *J. Med. Chem*., **2012**, *55*, 3678–3686

[78] (a) Siddiqui-Jain A., Grand C. L., Bearss D. J., Hurley L. H., *Proc. Natl. Acad. Sci. USA*, **2002**, *99*, 11593–11598 (b) Grand C. L., Han H., Muñoz R. M., Weitman S., Von Hoff D. D., Hurley L. H., Bearss D., *J. Mol. Cancer Ther*., **2002**, *1*, 565–573.

[79] Dixon I. M., Lopez F., Esteve J.-P., Tejera A. M., Blasco M. A., Pratviel G., Meunier B., *ChemBioChem*, **2005**, *6*, 123–132.

[80] Balasubramanian S., Neidle S., *Chem. Biol.*, **2009**, *13*, 345–353.

[81] Balasubramanian S., Hurley L. H., Neidle S., *Nat. Rev.Drug Discovery,* **2011**, *10*, 261–275.

[82] Collie G. W., Parkinson G. N., *Chem. Soc. Rev*., **2011**, *40*, 5867–5892

[83] Duchler M., *J. Drug Targeting*, **2012**, *20*, 389–400

[84] (a) Alberto R., Herrmann W. A., Kiprof P., Baumgartner F., *Inorg. Chem.,* **1992**, *31*, 895–899 (b) Braband H., Imstepf S., Benz M., Spingler B., Alberto R., *Inorg. Chem*., **2012**, *51*, 4051−4057

[85] Pomp C., Drueke S., Kuppers H. J., Wieghardt K., Kruger C., Nuber B., Weiss J., *Chem. Sci.,* **1988**, *43*, 299–305

[86] Benniston A. C., Gunning P., Peacock R .D., *J. Org. Chem*., **2005**, *70*, 115-123

[87] (a) Kimura S., Bill E., Bothe E., Weyhermuller T., Wieghardt K., *J. Am. Chem. Soc*., **2001**, *123*, 6025-6039 (b) Zobi F., Alberto R., *J. Chem. Eur.*, **2010**, *16*, 2710-2713 (c) Braband H., Tooyama Y., Fox T., Simms R., Forbes J., Valliant J. F., Alberto R., J*. Chem. Eur.,* **2011**, *17*, 12967 – 12974

[88] (a) Benniston A. C., Gunning P., Peacock R .D., *J. Org. Chem*., **2005**, *70*, 115-123 (b) S. Kimura, E. Bill, E. Bothe, T. Weyhermuller, K. Wieghardt, *J. Am. Chem. Soc*., **2001**, *123*, 6025-6039

[89] Gianferrara T., Giust D., Bratsos I., Alessio E., *Tetrahedron*, **2007**, *63*, 5006-5013

[90] Lidstrom P., Tierny J., Wathey B., Westman J., *Thetrahedron*, **2001**, *57*, 9225

[91] Schmitt F., Govindaswamy P., Zava O., Suss-Fink G., Juillerat-Jeanneret L., B. Therrien, *J. Biol.Inorg.Chem*., **2009**, *14*, 101-109

[92] Davia K., King D., Hong Y., Swavey S., *Inorg. Chem. Commun*., **2008**, *11*, 584–586

[93] Poon C.-T., Chan P.-S., Man C., Jiang F.-L., Wong R. N.S., Mak N.-K., Kwong D. W. J., Tsao S.-W., Wong W.-K., *J. Inorg. Biochem*., **2010**, *104*, 62–70

[94] Zhang J.-X., Zhou J.-W., Chan C.-F., Lau T. C.-K., Kwong D. W. J., Tam H.-L., Mak N.-K., Wong K.-L., Wong W.-K., *Bioconjugate Chem*., **2012**, *23*, 1623−1638

[95] De Rosa F. S., Bentley M. V. L. B., *Pharm. Res*., **2000**, *17*, 1447–1455

[96] Delaey E., Van Laar F., De Vos D., Kamuhabwa A., Jacobs P., De Witte P. A., *J. Photochem. Photobiol. B: Biol*., **2000**, *55*, 27–36

[97] Ochsner M., *J. Photochem. Photobiol. B*, **1997**, *39*, 1–18

[98] Casanova M., Zangrando E., Munini F., Iengo E., Alessio E., *Dalton Trans.*, **2006**, *42*, 5033-5045

[99] Alley M. C., Scudiero D. A, Moks A., Hursey M. L., Czerwinski M. J., Fine D. L., Abbott B. J., Mayo J. G., Schoemaker R. H., Boyd M. R., *Cancer Res*., **1988**, *48*, 589-601

[100] Mari C., Pierroz V., Rubbiani R., Patra M., Hess J., Springler B., Oehninger L., Schur J., Ott I., Salassa L., Ferrari S., Gasser G., *J. Chem. Eur,* **2014**, *20*, 14421-14436

[101] Majumdar S., Siabaan J., *Medicinal Research Reviews*, **2012**, *32*, 3, 637-658

[102] Olivo M., Bhuvaneswari R., Lucky S. S., Dendukuri N., Thong P. S., *Pharmaceuticals,* **2010**, *3*, 1507-1529

[103] Okarvi S. M., *Cancer Teatment Reviews*, **2008**, *34*, 13-26

[104] Jamous M., Haberkorn U., Mier W., *Molecules*, **2013**, *18*, 3379-3409

[105] N Shirasu., Nam S. O., Kuroki M., *Anticancer Research*, **2013**, *33*, 2823-2832

[106] Sibrian-Vazquez M., Jensen T. J., Hammer R. P., Vicente M. G. H., *J. Med. Chem.*, **2006**, *49*, 1364-1372

[107] Sibrian-Vazquez M., Nesterova I. V., Jensen T. J., Vicente M. G. H., *Bioconjugate Chem*., **2008**, *19*, 705–713

[108] Sibrian-Vazquez M., Ortiz J., Nesterova I. V., Lazaro F., Sastre-Santos A., Soper S. A., Vicente M. G. H., *Bioconjugate Chem*., **2007**, *18*, 410-420

[109] Sibrian-Vazquez M., Hao E., Jensen T. J., Vicente M. G. H., *Bioconjugate Chem*., **2006**, *17*, 928-934

[110] Sehgal I., Sibrian-Vazquez M., Vicente M. G. H., *J. Med. Chem.,* **2008,** *51,* 6014–6020

[111] Regberg J., Srimanee A., Langel Ü., *Pharmaceuticals*, **2012**, *5*, 991-1007

[112] Lundberg P., Langel U¨., *J. Mol. Recognit*, **2003**; *16*, 227–233

[113] Cartier R., Reszka R., *Gene Therapy*, **2002**, *9*, 157–167

[114] Morgat C., Mishra A.K., Varshney R., Allard M., Fernandez P., Hindie E., *The Journal of Nuclear Medicine*, **2014**, *55*,10,1650-1657

[115] Williamson R.T., Màrquez B.L., Gerwick W.H, **1999**, *55*, 2881-2888

[116] Gonzalez N., Moody T. W., Igarashi H., Ito T., Jensen R. T., *Curr Opin Endocrinol Diabetes Obes,* **2008**, *15*, 1, 58–64

[117] Gastrointestinal Endocrinology, George Greeley, Springer Science Business Media New York

[118] Ramos-Alvarez I., Moreno P., Mantey S. A., Nakamura T., Nunche-Berenguer B., Moody T. W., Coy D. H., Jensen R. T., *Peptides*, **2015**, *72*, 128-144

[119] Sancho V., Di Florio A., Moody T. W., Jensen R., *Current Drug Delivery*, **2011**, *8*, 79-134

[120] Hosta-Rigau L., Olmedo I., Arbiol J., Cruz L. J., Kogan M. J., Albericio F., *Bioconjugate Chem*., **2010**, *21*, 1070-1078

[121] Knight M., Takahashi K., Chandrasekhar B., Geblaoui A. Z., Jensen R. T., Strader D., Moody T.W., *Peptides*, **1995**, *16*, 6, 1109-1115

[122] Akeson M., Sainz E., Mantey S. A., Jensen R. T., Battey J. F., *J. Biol. Chem.*, **1997**, *272*, 17405-17409

[123] (a) Schwartsmann G., Di Leone L. P., Horowitz M., Schunemann, Cancella A., Pereira A.S., Richter M., Souza F., Brondani A., Da Rocha N., Souza F. H., Poholmann P., De Nucci G., *Invest New Drugs*, **2006**, *24*, 403-412 (b) Xu Y., Jiang Y., Wu B., *The Journal of International Medical Research*, **2012**, *40*, 1217-1226

[124] Joshi T., Pierroz V., Ferrari S., Gasser G., *ChemMedChem.,* **2014**, *9*, 7, 1419-27

[125] Engel J., Schally A.V, Halmos G., Baker B., Nagy A., Keller G., *Endocrine-Related Cancer*, **2005**, *12*, 999–1009

[125] Dijkgraaf I., Franssen G. M., McBride W. J., D'Souza C. A., Laverman P., Smith C. J., Goldenberg D. M., Oyen W. J. G., Boerman O. C., *J. of Nuclear Medicine*, **2012**, *53*, 6, 946-952

[126] (a) Lantry L. E, Cappelletti E., Maddalena M. E., Fox J. S., Feng W., Chen J., Thomas R., Eaton S. M., Bogdan N. J., Arunachalam T., Reubi J. C., Rsju N., Metcalfe E. C., Lattuada L., Linder K.E., Swenson R. E., Tweedle M. F., Nunn A. D., *J. Nucl Med*, **2006**, *47*, 7, 1144-1152 (b) Cappelletti E., Maddalena M. E., Fox J. S., Chen J, Feng W., A. Cagnolini, Linder K.E, Tweedle M. F. Nunn A. D Lantry L. E, *J. Nucl. Med*., **2009**, *50*, 12, 2017-2024

[127] Sucholeiki I., *Molecular Diversity*, **1999**, *4*, 25–30

[128] Arantes D., Pires T., Bemquerer M., Nascimento C., *Int. J. Pept. Res. Ther.,* **2014**, *20*, 53-69

[129] Al-Warhi T. I., Al-Hazimi H., El-Faham A., *J. Saudi Chemical Society*, **2012**, *16*, 97–116

[130] El-Faham A., Albericio F., *Chem. Rev*., **2011**, *111*, 6557–6602

[131] Valeur E., Bradley M., *Chem. Soc. Rev*., **2009**, *38*, 606–631

[132] Han S., Kim Y., *Tetrahedron*, **2004***, 60*, 2447–2467

[133] Alsina J., Albericio F., Wiley Periodicals, *Inc. Biopolymers (Pept. Sci.),* **2003**, *71*, 454–477

[134] Shechter Y., *J. Biological Chemists*, **1986**, *261*, 1, 66-70

[135] Tam J. P., Heath W .F., Merrifield R. B., *J. Am. Chem. Soc*., **1983**, *105*, 6442-6455

[136] Vogt W., *Free Radic. Biology Med.*, **1995**, *18*, 1, 93-105

[137] Kumar A., Kumar P., Joshi H., *Int. J. of Current Research and Review*, **2012**, *4*, 17

[138] Hein C. D., Liu X., Wang D., *Pharmaceutical Research*, **2008***, 25*, 10, 2216-2230

[139] Kadish K. M., Smith K. M., R. Guilard, *The Porphyrin Handbook*, **2003**, *3*, 116-191

[140] Umezawa N., Matsumoto N., Iwama S., Kato N., Higuchi T., *Bioorg. Med. Chem*., **2010**, *18*, 6340–6350

[141] Chan T. R., Hilgraf R., Sharpless K. B., Fokin V. V., *Org. Lett*., **2014**, *6*, 17

[142] Gasser G., Husken N., Koster S. D., Metzler-Nolte N., *Chem. Commun*., **2008**, 3675–3677

[143] Umezawa N., Matsumoto N., Iwama S., Kato N., Higuchi T., *Bioorg. Med. Chem*., **2010**, *18*, 6340–635

[144] Pace C. N., Vajodos F., Fee L., Grimsley G., Gray T., *Protein Science*, **1995**, *4*, 2411-2423

[145] Siibrian-Vazquez M., Ortiz J., Nestrerova I. V., Fernandez-Lazaro F., Sastre-Santos A., Soper S. A., M. Vicente G. H., *Bioconjugate Chem*., **2007**, *18*, 410-420

[146] Mindt T. L., Struthers H., Brans L., Anguelov T., Schweinsberg C., Maes V., Tourwe´D., Schibli R., *J. Am. Chem. Soc*., **2006**, *128*, 15096-15097

[147] Ogasawara Y., Murai Y., Sakihama Y., Hashidoko Y., Hashimoto M., *Int. J. of Organic Chemistry*, **2012**, *2*, 302-304

[148] Bakleh M.E., Sol V., Estieu-Gionnet K., Granet R., Déléris G., Krausz P., *Tetrahedron*, **2009**, *65*, 7385–7392

[149] (a) Aletras A., Barlos K., Gatos D., Koutsogianni S., Mamos P., *Int. J. Peptide Protein Res.*, **1995**, *45*, 488-496 (b) Bourel L., Bourel L., Carion O., Gras-Masse H., Melnyj O., *J. Peptide Science*, **2000**, *6,* 264-270 (c) Hoogerhout P., Stittelaar K. J., Brugghe H. F., Timmermans J. A. M., Ten Hove G. J., Jiskoot W., Hoekman J. H. G., Roholl P. J. M., *J. Peptide Res*., **1999**, *54*, 436-443 (d) Park C., Burgess K., *J. Comb. Chem,* **2001**, *3*, 257-266

[150] Arantes D., Pires T., Bemquerer M., Nascimento C., *Int. J. Pept. Res. Ther.*, **2014**, *20*, 53-69

[151] *aapptec technical support information bulletin,* 1181

[152] Li D., Elbert D.L., *J. Pept. Res*., **2002**, *60*, 300-3

[153] Guide to selection of building blocks, Millipore, a division of Merck

[154] Vazquez M.S.V., Jensen T. J., Hammer R. P., Vicente M. G. H., *J. Med. Chem.*, **2006**, *49*, 1364-1372

[155] Pedersen S.L., Tofteng A.P., Malik L., Jensen K.J., *Chem. Soc. Rev.,* **2012**, *41*, 1826-1844

[156] Biju V., *Chem. Soc. Rev.*, **2014**, *43*, 3, 737-962

[157] Ayane Debele T., Peng S., Tsai H-C., *Int. J. Mol. Sci*, **2015**, *16*, 22094-22136

[158] Wang S., Gao R., Zhou F., Selke M., *J. Mater. Chem.*, **2004**, *14*, 487 – 493

[159] Bartelmess J., Quinnb S. J., Giordani S., *Chem. Soc. Rev.*, **2015***, 44*, 4672-4698

[160] Montellano A., Lopez, Alonsobc A., Prato M., *J. Mater. Chem*., **2011**, *21*, 1305–131

[161] Raszeja L., Maghnouj A., Hahn S., Metzler-Nolte N., *ChemBioChem*, **2011**, *12*, 371-376

ACKNOWLEDGMENTS

First of all I would like to heartfelt thank my supervisor, Dr. T. Gianferrara, for welcome me in her laboratory and for all her help during these three years. She accompanied me until the end of this beautiful journey supported me and passed me her knowledge.

I would like to heartfelt thank Professor G. Gasser for welcome me in his research group for two periods and for all his help for the project.

I would like to thank Professor T. Da Ros especially for her contribution in the fullerene part, Professors E. Alessio, B. Milani, E. Iengo and their research groups for their help with the NMR experiments.

Thanks to Professors A. Bargamo, R. Vilar and their research groups for the collaboration and F. Hollan for the ESI-MS analysis performed in Trieste.

Thanks Dr. Federico and Sara, for the time spent together in the laboratory.

Thanks to all our master students for all their hard work: Alessandra, Gloria, Manuela, Francesco and Sara.

Thanks to all Prato's group, in particular to Adrian, Marco and my "PhD colleagues" Tanja, Valentina, Agnesca, Ana and Maria, for their support, help but mostly for their precious friendship!

Thanks to all Gasser's research group: Cristina, Anna, Jeannine, Riccardo, Philipp, Anita, Angelo, Vanessa, Sandra, Seraina, Giuseppe, Lea, Konstantis and Loganathan. I would like to thank them for all the things that they thought me. In particular I would like to thank Cristina, Anna and Jeanine, for helping me in my research, and for the UPLC that they have performed for me. Thanks to Marjory, Lukas for the UPLC.

Thanks to my friends Costantin, Jenny, Flavia and Sara. Thanks mum and dad for supporting and for being always present. Thanks to Paolo, Marina, and Marco, for being like a family. Finally I would like to thank my brother, my sister and Andrea that occupy my heart.